الجمهورية الجزائرية الديمقراطية الشعبية

People's Democtratic Republic of Algeria

وزارة التعليم العالي و البحث العلمي

Ministry of Higher Education and Scientific Research

**Mohamed Khider University – Biskra**

**Faculty of Science and Technology**

**Departmenet of Electrical Engineering**

**Ref : ……..**



جامعة محمد خيضر - بسكرة

كلية العلوم و التكنولوجيا

قسم الهندسة الكهربائية

المرجع : .....

Thesis presented with a view to
obtaining the diploma of :

## LMD Doctorate in Electrical Engineering

Speciality: Electrical Engineering

Option: Electrical Machines

Entitled:

# "Supplementary techniques for the diagnosis of the induction machine without a priory model"
# " Compléments de techniques de diagnostic de la machine asynchrone sans modèle à priori"

**Presented by :**

## Bentrad Moutaz Bellah

**Publicly defended on : 09/04/2026**

**In front of the jury composed of**

| | | | |
|---|---|---|---|
| **President:** | **Pr. ZOUZOU Salah Eddine** | **Prof** | **University of Biskra** |
| **Supervisor:** | **Pr. GHOGGAL Adel** | **Prof** | **University of Biskra** |
| **Co-supervisor:** | **Pr. BAHI Tahar** | **Prof** | **University of Annaba** |
| **Examiner** | **Pr. SAHRAOUI Mohamed** | **Prof** | **University of Biskra** |
| **Examiner:** | **Dr. LOUZ Lamri** | **MCA** | **University of Constantine** |

# Acknowledgments

First and foremost, I would like to express my deepest gratitude to my thesis advisor, **Professor Ghoggal Adel**, for his invaluable guidance, continuous support, and insightful feedback throughout the course of this research. His impressive scientific expertise and commitment were instrumental in shaping the direction and quality of this work.

I would also like to sincerely thank my co-advisor, **Professor Bahi Tahar**, for his thoughtful supervision, constructive remarks, and constant encouragement. His scientific rigor and availability greatly contributed to the success of this thesis.

A special word of appreciation goes to the **LGEB Laboratory** for providing a stimulating research environment and the necessary resources to carry out this work. The support and collaboration within the laboratory have been essential to the completion of this study.

I would like to extend a warm thanks to the members of the jury for accepting to assess our research

To all those who contributed, directly or indirectly, to this research, please accept my heartfelt thanks.

# Dedications

First and foremost, I thank **Allah** for granting me the strength, patience, and perseverance to complete this work.

With all my love and gratitude, I warmly dedicate this work to my **dear parents**, for their unconditional support—both emotional and financial—and for always believing in me.

To my **brothers**, thank you for standing by my side with encouragement and care.

To my **beloved wife**, your unwavering support, love, and constant motivation have been a pillar of strength—I am deeply grateful.

A heartfelt thanks also to my **friends**, the **QLF group**, and my **colleagues**, whose presence, encouragement, and companionship have made this path more enjoyable and fulfilling.

This achievement is as much yours as it is mine.

Abstract

With the great demand of the industry on electrical machines due to their pivitol role in the industrial chain, it became highly important to anticipate any faillure and to prevent sudden breakdowns, traditional methods that count on developing a dynamical model of the machine are becoming more challenging since the command techniques and fault intricacies are growing more and more which emplores us to intigrate more efficient and reliable approach which is a non model based, and that is AI that proved its reliability in fault detection in the induction machine which represents a promising approach to help us in decision making.

Key words: electrical machines, induction machine, non model based, Artificial Intelligence, fault detection.

Résumé

Avec la forte demande de l'industrie sur les machines électriques, en raison de leur rôle central dans la chaîne industrielle, il est devenu crucial d'anticiper toute défaillance et d'éviter les arrêts soudains. Les méthodes traditionnelles, qui reposent sur l'élaboration d'un modèle dynamique de la machine, deviennent de plus en plus complexes en raison de l'évolution des techniques de commande et de la complexité croissante des défauts. Cela nous incite à intégrer une approche plus efficace et plus fiable : l'approche **non basée sur un modèle**, incarnée par **l'intelligence artificielle**. Cette dernière a prouvé sa fiabilité dans la détection des défauts des machines asynchrones, représentant ainsi une solution prometteuse pour assister la prise de décision.

**Mots-clés :** machines électriques, machine asynchrone, approche non basée sur un modèle, intelligence artificielle, détection des défauts.

ملخص

مع الطلب المتزايد من طرف الصناعة على الآلات الكهربائية نظرًا لدورها المحوري في السلسلة الصناعية، أصبح من الضروري جدًا التنبؤ بالأعطال المحتملة وتفادي التوقفات المفاجئة. إن الطرق التقليدية التي تعتمد على تطوير نموذج ديناميكي للآلة أصبحت أكثر تعقيدًا، وذلك بسبب تطور تقنيات القيادة وتعقيد الأعطال بشكل متزايد، مما يدفعنا إلى اعتماد منهج أكثر كفاءة وموثوقية، ألا وهو النهج غير المعتمد على النمذجة، والمتمثل في الذكاء الاصطناعي. لقد أثبت الذكاء الاصطناعي فعاليته في كشف الأعطال في آلة التيار غير المتزامن، مما يجعله منهجًا واعدًا لدعم اتخاذ القرار.

**الكلمات المفتاحية :**الآلات الكهربائية، آلة التيار غير المتزامن، منهج غير معتمد على النمذجة، الذكاء الاصطناعي، كشف الأعطال.

# Summary

# Summary

General introduction 1

Chapter 1: State of the art : Diagnosis of the Induction Machine

1.1 Introduction 2
1.2. Conceptual definitions and terminology of Maintenance 2
1.2.1 Maintenance 3
1.2.2 System state terminology 3
1.3. Conceptual definitions and terminology of Diagnostics 3
1.3.1 Monitoring 3
1.3.2 Detection 4
1.3.3 Diagnosis 4
1.4 Constitutional components of the induction machine 4
1.4.1 Stator 4
1.4.2 Rotor 5
1.4.3 Winding 6
1.4.4 Air gap 7
1.5 Fault natures and sources of induction machine 7
1.6 Overview of induction machines faults 8
1.6.1. Stator faults 9
1.6.2. Rotor faults 12
1.7. Diagnostic approaches 16
1.7.1. Condition monitoring techniques 16
1.7.2. Model-Based approaches 17
1.7.3. Non-Model-Based approaches 23
1.8 Conclusion 24

Chapter 2: An overview of Non Model Based Approaches : Signal Processing and Artificial intelligence techniques

2.1 Introduction 25
2.2 Signal processing 26
2.2.1 Signal notion 26
2.3 Signal processing approaches 27
2.3.1 Fourier Transform 27
2.3.1.1 Window Function 29
2.3.1.2 The Short-Time Fourier Transform (Sliding window) 30
2.3.1.3 Discrete Fourier Transform 32
2.3.1.4 Fast Fourier Transform 32
2.3.2 Wavelet Transform 32
2.3.2.1 Definition 33
2.3.2.2 Mother wavelet 33
2.3.2.3 Continuous Wavelet Transform 33
2.3.2.4 Discrete Wavelet Transform 35
2.3.2.5 Multiresolution Wavelet Analysis (MRA) 35
2.4 Artificial Intelligence 37
2.4.1 Machine Learning 37

2.4.1.1 Definition 37
2.4.1.2 overview 37
2.4.2 Types of machine learning 37
2.4.2.1 supervised learning 37
2.4.2.2 unsupervised learning 37
2.4.2.3 Semi-supervised learning 38
2.4.2.4 Reinforcement Learning 38
2.4.2.5 Transfer Learning 38
2.4.3 Supervised learning techniques 38
2.4.3.1 Classification techniques 38
2.4.3.2 Regression technique 52
2.4.3.3 Model performance score 52
2.4.3.4 overfitting 54
2.5 Conclusion 55

Chapter 3: Squirrel cage induction machine modelling dedicated to fault diagnosis

3.1 Introduction 56
3.2 State model of the machine 56
3.2.1 Multi-winding model 56
3.2.2 Voltage equations 57
3.2.3 Mechanical equations 61
3.2.4 System of state equations 62
3.3 Faulty machine modelling 63
3.3.1 Eccentricity types 63
3.3.1.1 Air gap eccentricity model 66
3.3.2 Broken rotor bars 67
3.4 Calculation of Inductances 68
3.4.1 Stator part 68
3.4.2 Rotor part 70
3.4.3 Mutual inductance between statror and rotor 71
3.5 Simulation Results 73
3.5.1 Healthy machine variables 73
3.5.1.1 Healthy machine variables by varying load conditions 74
3.5.2 Faulty machine variables 75
3.5.2.1 Eccentricity fault 75
3.5.2.2 Eccentricity fault by varying load conditions 76
3.5.2.3 Eccentricity fault types 77
3.5.2.4 Eccentricity fault under various fault severity degrees 78
3.5.2.5 Broken rotor bars fault 81
3.5.2.6 Broken rotor bars fault by varying load conditions 83
3.5.2.7 Broken rotor bars fault under various fault severity scenarios 83
3.6 Conclusion 85

Chapter 4: Proposed Diagnostic Methodology and Artificial intelligence techniques application

4.1 Introduction 86
4.2 Classic MCSA approaches 86
4.2.1 Frequency domain analysis 86
4.2.1.1 Frequency domain analysis under variable load conditions for eccentricity 86
4.2.1.2 Frequency domain analysis under weak loads 87

4.2.1.3 Frequency domain analysis under heavy loads 89
4.2.1.4 Frequency domain analysis under various fault types 90
4.2.1.5 Frequency domain analysis under various fault types at weak loads 90
4.2.1.6 Frequency domain analysis under various fault types at heavy loads 92
4.2.1.7 Frequency domain analysis under variable load conditions for broken rotor bars 93
4.2.1.8 under weak load conditions 94
4.2.1.9 under heavy load conditions 95
4.2.2 time-frequency domain analysis 97
4.3 AI-based approaches 102
4.3.1 without signal processing 102
4.3.2 with signal processing 105
4.4 Artificial neural networks 110
4.4.2 Model evaluation 112
4.5 Classification and regression 114
4.5.1 Classification 114
4.5.2 Multi-class classification technique 117
4.6 Ensemble Methods in fault detection 120
4.6.1 Ensemble Methods: boosting 123
4.6.2 LightGBM 123
4.7 Machine learning-signal processing combination 129
4.7.1 Models evaluation 131
4.8 Conclusion 132
General conclusion 134

# Figures list


| | | |
|---|---|---|
| Figure 1.1 | General constitution of the induction machine | 4 |
| Figure 1.2 | Stator of the induction machine | 5 |
| Figure 1.3 | Rotor of the induction machine | 6 |
| Figure 1.4 | Star and Delta connection | 7 |
| Figure 1.5 | categories of IM faults | 8 |
| Figure 1.6 | (a) Induction machine frequent faults,(b) Induction machine fault classes. | 9 |
| Figure 1.7 | Different types of short circuit faults | 10 |
| Figure 1.8 | Inter turn short-circuit | 11 |
| Figure 1.9 | Phase-to-Phase Short Circuit fault | 11 |
| Figure 1.10 | Rotor bar fault types | 12 |
| Figure 1.11 | Air gap eccentricity types | 14 |
| Figure 1.12 | parallel and angular misalignment faults between the motor and load shaft | 15 |
| Figure 1.13 | Bearing fault in induction machine | 15 |
| Figure 1.14 | Pictures of different bearing fault types | 16 |
| Figure 1.15 | Fault detection methods | 17 |
| Figure 1.16 | Model based diagnostic process. | 18 |
| Figure 1.17 | Principle of the Observer-Based Diagnostic Method | 18 |
| Figure 1.18 | Observer bank architecture. | 19 |
| Figure 1.19 | Observer principal functioning diagram. | 20 |
| Figure 1.20 | Kalman filter architecture | 21 |
| Figure 1.21 | Adaptive observer principal. | 22 |
| Figure 2.1 | Stationary signal sample | 26 |
| Figure 2.2 | non-stationary signal sample | 27 |
| Figure 2.3 | Time and Frequency domain presentation | 28 |
| Figure 2.4 | Rectangular window function | 29 |
| Figure 2.5 | Most frequent window functions | 30 |
| Figure 2.6 | Principle of the Short-Time Fourier Transform | 31 |
| Figure 2.7 | a- time domain signal, b-spectrogram | 32 |
| Figure 2.8 | Translation of a window in frequency via modulation. | 34 |
| Figure 2.9 | Frequency translation of the Mexican Hat function via scaling (dilation) : time domain. | 34 |
| Figure 2.10 | Three level decomposition of a signal. | 36 |
| Figure 2.11 | Classification concept | 39 |
| Figure 2.12 | Support vectors in classification | 40 |
| Figure 2.13 | K-NN classification concept | 41 |
| Figure 2.14 | Ensemble classifiers combination | 44 |
| Figure 2.15 | Parallel classifiers employment (Bagging) | 45 |
| Figure 2.16 | Sequential classifiers employment (Boosting) | 46 |
| Figure 2.17 | Perceptron Model representation | 48 |
| Figure 2.18 | Simple Multi-layer Perceptron representation | 49 |
| Figure 2.19 | Deep Learning network architecture | 50 |
| Figure 2.20 | Simplified Graph Neural Network architecture. | 51 |
| Figure 2.21 | Linear and nonlinear regression | 52 |

| | | |
|---|---|---|
| Figure 2.22 | Example of overfitting against unseen data. | 55 |
| Figure 3.1 | Equivalent electrical circuit of the squirrel cage rotor based on the multi-winding structure. | 57 |
| Figure 3.2 | Equivalent circuit for the rotor mesh | 58 |
| Figure 3.3 | Star connection with connected neutral (left) and floating neutral (right). | 61 |
| Figure 3.4 | Relative motion of rotation centers in the case of eccentricity | 63 |
| Figure 3.5 | Illustration of radial eccentricity | 64 |
| Figure 3.6 | Terms illustration of *Lst* and *Ldy* that characterize axial eccentricity | 64 |
| Figure 3.7 | Axial eccentricity illustration | 65 |
| Figure 3.8 | Equivalent circuit of a healthy rotor cage | 67 |
| Figure 3.9 | Equivalent circuit of a rotor cage in case of one broken rotor bar. | 67 |
| Figure 3.10 | Magnetic induction produced by a rotor loop. | 70 |
| Figure 3.11 | Mutual flux (stator phase- rotor loop) | 72 |
| Figure 3.12 | Healthy machine variables | 74 |
| Figure 3.13 | Healthy machine stator current | 75 |
| Figure 3.14 | Faulty machine variables | 76 |
| Figure 3.15 | Faulty machine stator current | 77 |
| Figure 3.16 | Eccentricity fault types | 78 |
| Figure 3.17 | static eccentricity influence on stator current | 79 |
| Figure 3.18 | Dynamic eccentricity influence on stator current | 80 |
| Figure 3.19 | Mixed eccentricity influence on stator current | 80 |
| Figure 3.20 | Faulty machine variables | 82 |
| Figure 3.21 | Faulty machine stator current | 83 |
| Figure 3.22 | Broken rotor bars fault signature | 84 |
| Figure 4.1 | Current spectral analysis under weak loads | 88 |
| Figure 4.2 | Current spectral analysis under heavy loads | 90 |
| Figure 4.3 | Current spectral analysis various fault types weak loads | 92 |
| Figure 4.4 | Current spectral analysis various fault types heavy loads | 93 |
| Figure 4.5 | Current spectral analysis under weak loads | 95 |
| Figure 4.6 | Current spectral analysis under heavy loads | 97 |
| Figure 4.7 | DWT signal decomposition and reconstruction. | 98 |
| Figure 4.8 | Full decomposition of stator current | 100 |
| Figure 4.9 | Energy distribution analysis | 101 |
| Figure 4.10 | AI algorithm integration in fault detection | 103 |
| Figure 4.11 | AI algorithm combination with signal processing in fault detection | 106 |
| Figure 4.12 | Detail decomposition levels 4, 5 and 6. | 107 |
| Figure 4.13 | Energy distribution analysis under various conditions for air gap types | 109 |
| Figure 4.14 | Results of the machine's health condition classification. | 107 |
| Figure 4.15 | Results of the machine's fault nature classification. | 111 |
| Figure 4.16 | Results of the machine's load condition classification. | 112 |
| Figure 4.17 | Results of the machine's current phase classification. | 112 |
| Figure 4.18 | Loss curve results after 100 epochs | 113 |
| Figure 4.19 | Confusion matrix results | 115 |
| Figure 4.20 | Results of the machine's health prediction | 118 |
| Figure 4.21 | Results of the machine's fault type | 119 |
| Figure 4.22 | Results of the machine's load condition | 119 |
| Figure 4.23 | Results of the machine's phase localization | 119 |
| Figure 4.24 | Overall comparison of classification models. | 120 |

| | | |
|---|---|---|
| Figure 4.25 | Performance results for fault detection | 122 |
| Figure 4.26 | Performance results of fault type | 122 |
| Figure 4.27 | Performance results of fault severity | 122 |
| Figure 4.28 | Classifiers accuracy results comparison | 123 |
| Figure 4.29 | LightGBM learning curve for overfitting evaluation | 124 |
| Figure 4.30 | Comparative Learning curve for overfitting evaluation for GB, DT and LightGBM | 125 |
| Figure 4.31 | Speed prediction test | 125 |
| Figure 4.32 | Confusion matrix results of multi-class classification. | 126 |
| Figure 4.33 | classification of adjacent broken rotor bars | 127 |
| Figure 4.34 | classification of seperated borken rotor bars | 127 |
| Figure 4.35 | ROC values one vs rest | 128 |
| Figure 4.36 | Performance comparison of LightGBM vs Ensemble Methods | 129 |
| Figure 4.37 | SVM confusion matrix results | 130 |
| Figure 4.35 | DT multi-class classification | 131 |


## Tables list


| | | |
|---|---|---|
| Table 2.1 | Most frequent activation functions | 50 |
| Table 4.1 | Output dataset denotation | 104 |
| Table 4.2 | Energy levels of decomposition levels. | 109 |
| Table 4.3 | Train/test loss curve values | 114 |
| Table 4.4 | Different classifier models of the classification task. | 116 |
| Table 4.5 | Multi-class classification models performance | 118 |
| Table 4.6 | XGBoost model architecture. | 121 |
| Table 4.7 | Performance evaluation of xgboost | 121 |
| Table 4.8 | LightGBM hyperparameters. | 124 |
| Table 4.9 | LightGBM model evaluation against original models. | 126 |
| Table 4.10 | LightGBM performance evaluation against Ensemble Methods models | 128 |
| Table 4.11 | SVM architecture | 129 |
| Table 4.12 | SVM multi-class classification performance | 130 |
| Table 4.13 | DT architecture | 131 |
| Table 4.14 | Global approachs evaluation | 132 |

# Notations and symbols

| | |
|---|---|
| $f_V$ | viscosity friction coefficient (Kg/m.s) |
| $f_s$ | Fundamental frequency |
| $f_r$ | rotational frequency |
| $f_{se}$ | static eccentricity frequency |
| $f_{de}$ | dynamic eccentricity frequency |
| $f_{me}$ | mixed eccentricity frequency |
| $n_d$ | harmonic order |
| $I_{bk}$ | current of the bar k (A) |
| $I_{rk}$ | current of the rotoric loop k (A) |
| $I_r$ | current of rotor current loop (A) |
| $J$ | index of rotor current loop; |
| $J_T$ | total moment of inertia (Kg.m$^2$) |
| $h^*$ | mother window |
| $L_b$ | leakage inductance of a rotor bar (H) |
| $L_e$ | leakage inductance of a short-circuit portion (H) |
| $L_{sc}$ | stator cyclic inductance (H) |
| $L_{sr}$ | the mutual inductances between the stator phases and the rotor meshes (H) |
| $L_{st}$ | axial position of concentric section in static eccentricity |
| $L_{dy}$ | axial position of concentric section in dynamic eccentricity |
| $N_r$ | number of rotor bars |
| $r$ | residual |
| $R_b$ | rotor bar resistance (Ω) |
| $R_e$ | short-circuit ring resistance (Ω) |
| $S_r$ | resistance of a stator phase |
| $T_e$ | electromagnetic torque (N.m) |
| $T_r$ | load torque (N.m) |
| $V_r$ | rotor circuit voltage (V) |
| $V_s$ | stator circuit voltage (V) |
| $\psi_r$ | total flux through rotor winding (Wb) |
| $\psi_s$ | total flux through stator winding (Wb) |
| $\psi$ (t) | mother wavelet |
| $\Omega_r$ | mechanical speed |
| $\theta_r$ | mechanical position of the rotor |
| $\delta(z)$ | total eccentricity degree |
| $\varphi$ | angular opening |
| $\delta_s$ | static eccentricity |
| $\delta_d$ | dynamic eccentricity |
| $g_0$ | air gap thickness (mm) |
| $I_s$ | current of one stator phase (A) |

Notations and symbols

| | |
|---|---|
| $\mu_0$ | void magnetic permeability ($H.m^{-1}$) |
| $\psi_{sp}$ | main flux of the stator winding |
| $\psi_{fs}$ | leakage flux |
| $M_{rr}$ | mutual inductance between non-adjacent (disjoint) rotor loops |
| $\psi_{srlk}$ | induction produced by the stator coil of rotor loop k |
| $M_{rkm}$ | mutual inductance between phase "n" of the stator and the *k-th* rotor loop |
| $\alpha_m$ | classifier weight |
| $K_m$ | prediction error |
| $h_m$ | weak classifiers |
| HAG | healthy air gap |
| HLC | heavy load condition; |
| MBM | model-based methods; |
| ME | mixed eccentricity |
| ML | machine learning |
| MLC | medium load condition |
| MWM | multi-winding model |
| NMBM | non-model-based methods |
| MCSA | motor current signature analysis |
| FFT | fast fourier transform |
| STFT | short-time fourier transform |
| DFT | discrete fourier transform |
| WT | wavelet transform |
| CWT | continuous wavelet transform |
| DWT | discrete wavelet transform |
| SVM | support vector machines |
| KNN | k-nearest neighbors |
| DT | decision trees |
| RF | random forest |
| EM | ensemble methods |
| AdaBoost | adaptive boosting |
| XGBoost | extreme gradient boosting |
| ANN | artificial neural networks |
| MLP | multi layer perceptron |
| GNN | graph neural networks |
| CNN | convulotional neural network |
| ROC | receiver operating characteristic |
| MSE | mean squared error |
| RMSE | root mean square error |
| MAE | mean absolute error |

# General Introduction

Many faults can be modeled using mathematical-physical equations, notably Maxwell's equations, as a starting point in the field of predictive diagnostics and condition-based maintenance of electrical machines and their associated systems. However, for detailed studies, complex faults, interference between phenomena, as well as the coexistence and combination of multiple defects, modeling becomes increasingly challenging. Moreover, the resulting simulations and experiments require more time and impose greater demands on hardware and instrumentation.

Therefore, the adoption of new diagnostic methods—or redundant approaches that can complement and strengthen the outcomes—is always welcome. In this thesis, we aim to use deterministic and algebraic approaches traditionally employed in automatic control for diagnostic purposes. These methods do not require a prior physical model; instead, they rely on analyzing the system's output signals (i.e., the machine's response) following excitation by control signals (inputs), without the need to consider the system's classical parameters.

In addition, decision support approaches based on artificial intelligence and/or statistical studies can complement this task by estimating fault severity and localization. Artificial intelligence has proven to be a powerful and promising tool in this context. Its ability to learn from data, identify complex patterns, and generalize across varying operating conditions makes it particularly effective in diagnosing faults that are difficult to model analytically. AI-driven methods can not only enhance diagnostic accuracy but also significantly speed up the decision-making process, offering real-time or near-real-time insights into machine health. As a result, AI contributes to more informed, faster, and more reliable decisions in maintenance planning and operational safety—thereby increasing system availability and reducing unplanned downtimes.

These are the goals and perspectives we aim to develop in order to overcome the limitations of classical model-based methods.

# Chapter 1
# State of the art : Diagnosis of the Induction Machine

## 1.1. Introduction

In today's industrial landscape, three-phase Induction Motors (IMs) dominate, accounting for over 85% of all electric motors utilization [1–4]. Their widespread adoption stems from their reliability, ease of design, high performance, and ability to handle heavy loads, making them suitable for various applications across manufacturing, processing, power systems, transportation, and more. Despite their benefits, IMs operate in challenging mechanical and electrical environments, rendering them susceptible to multiple stator and/or rotor faults.

In recent years, the interest in on-line Fault Detection and Diagnosis (FDD) of engineering systems came to the attention of researchers as a crucial concern in industrial and control applications [5]. Furthermore, automated fault diagnostics and condition monitoring are important parts of most of the world's industrial and control processes [6]. Induction motors are far more widespread than other electric machines in industry. The total number of operating electrical machines in the world was around 16.1 billion in 2011, with a growth rate of about 50% in the last five years [7]. According to several surveys, these machines demand around 40%−50%of the total energy generated in any given developed country [8].

Fault diagnosis in IMs is a complex decision-making process due to the complexity of the involved processes, as well as the possibility of occurrence of multiple faults. Moreover, experimental data depend on many factors, including fault type, location and operating conditions [9, 10].

Fault detection is enabled by maintenance, therefore, in this context, machine maintenance mainly falls in one of the two categories preventive and predictive maintenance . Preventive maintenance is scheduled in advance and requires the motor to shut down during maintenance. In predictive-or condition-based maintenance monitoring is done while the motor is in operation and it has been established in order to cope with lost production time and unnecessary maintenance. Maintenance scheduling is done based on the fault identification decision output. Early fault detection methods in Squirrel Cage Induction Machine (SCIM) included vibration or thermal monitoring [11-13].

## 1.2. Conceptual definitions and terminology of Maintenance

Maintenance of systems involves a set of actions that allow maintaining or restoring an asset to a specified state or ensuring it can provide a determined service" [14,15].

Terminologies related to maintenance and diagnostics are defined as follows:

### 1.2.1 Maintenance

System maintenance can be [16,17]:

***Corrective***: performed in the event of a system failure .

***Preventive***: carried out at predetermined intervals or according to specified criteria, aimed at reducing the probability of failure or degradation in the performance of an entity, and it branches out to :

***Conditional*** : related to system diagnostics, initiating repair actions only if a failure is detected. It is defined as maintenance conducted "based on a predefined event that indicates asset degradation (sensor information, wear measurement, etc.). It aims to offset the costs of corrective maintenance by minimizing system downtime. Preventive maintenance has become the most effective strategy, as scientific research in diagnostics has advanced alongside technological progress .

***Systematic*** : is a strategy where maintenance tasks are performed at fixed time intervals or based on defined units of use (such as hours of operation or mileage), regardless of the actual condition of the machine

### 1.2.2 System state terminology

**Anomaly**: a deviation from what is expected. An anomaly justifies an investigation that may lead to the identification of a non-conformity or a defect.

**Failure**: the deterioration or loss of an asset's ability to perform a required function.

**Defect**: the discrepancy between an entity's actual characteristic and its nominal characteristic. A defect in the system generally does not affect the system's ability to perform a required function. Therefore, a defect does not always lead to a failure. Consequently, a defect is viewed as an opinion on proper functioning. In contrast, a failure invariably leads to a defect.

**Breakdown**: the inability of an entity to perform a required function or to provide the appropriate service due to a failure.

## 1.3. Conceptual definitions and terminology of diagnostics

Machine monitoring and diagnostics allow verifying the condition of the device to manage system uncertainties during the operational phase. The terms used in the field of fault diagnostics can be categorized into three main concepts: monitoring, detection, and diagnostics [18].

### 1.3.1 Monitoring

In industry, machine monitoring aims to replace systematic preventive maintenance. The objective is to equip these devices with a decision-support system that alerts the operator to a defect before it causes damage and then aids in diagnosing it by pinpointing the faulty components and identifying root causes.

### 1.3.2 Detection

The knowledge gained in the first step provides information on the system's behavior in the event of a fault, its most likely critical failures, and indicators of their occurrence. To detect one or more system faults, successive direct or indirect measurements of parameters related to the system in operation must be performed. Detection is the stage where any variation in the system is identified. This requires the ability to classify observed situations as either normal or abnormal.

### 1.3.3 Diagnosis

The term diagnosis can have various interpretations depending on the context and field of application. In industrial processes, the objective of the diagnostic function is to determine the probable causes and locate a fault or defect. This function is divided into two basic components: localization, which identifies the malfunctioning subsystem, and identification, which determines the reasons behind the abnormal condition.

## 1.4 Constitutional components of the induction machine

figure 1.1 illustrates a general view of an induction machine (IM), detailing its various constituent parts.

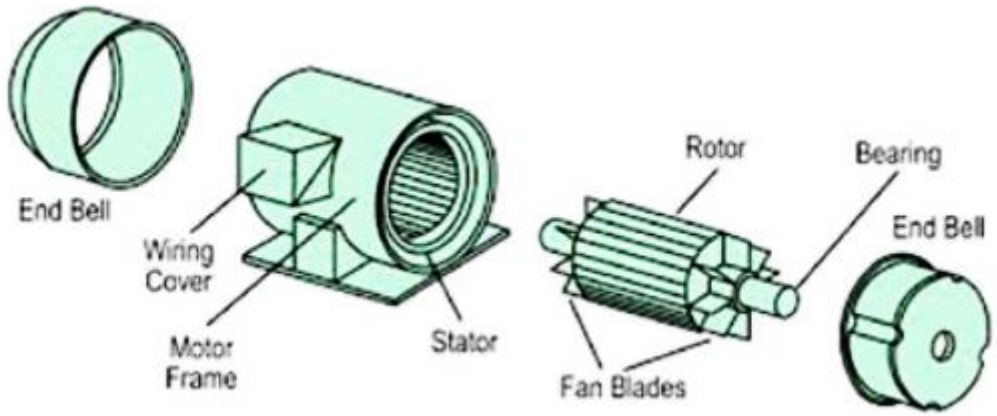



Figure 1.1.General constitution of the induction machine [19]

The asynchronous machine, often called an induction motor, consists of a stator and a rotor, both made of silicon steel laminations with slots that hold the windings. The stator is stationary and contains the windings connected to the power source. The rotor is mounted on a rotating shaft. Depending on whether the rotor windings are externally accessible or permanently short-circuited, two types of rotors are defined: wound rotor and squirrel-cage rotor. However, we assume it to be electrically equivalent to a wound rotor with short-circuited windings. In this work, we focus on the asynchronous machine.

### 1.4.1 Stator

It consists of a wound winding distributed in the slots of the magnetic circuit. This magnetic circuit is made up of a stack of laminations with parallel slots cut along the machine's axis (see

figure 1.2). The stator winding can be divided into two parts: the slot conductors and the coil heads. The slot conductors create the magnetic field in the air gap that is responsible for electromagnetic conversion. The coil heads, on the other hand, close the currents by judiciously organizing the flow of currents from one slot conductor to another. The goal is to achieve as sinusoidal a current distribution as possible at the surface of the air gap to minimize the ripples in the electromagnetic torque [20].

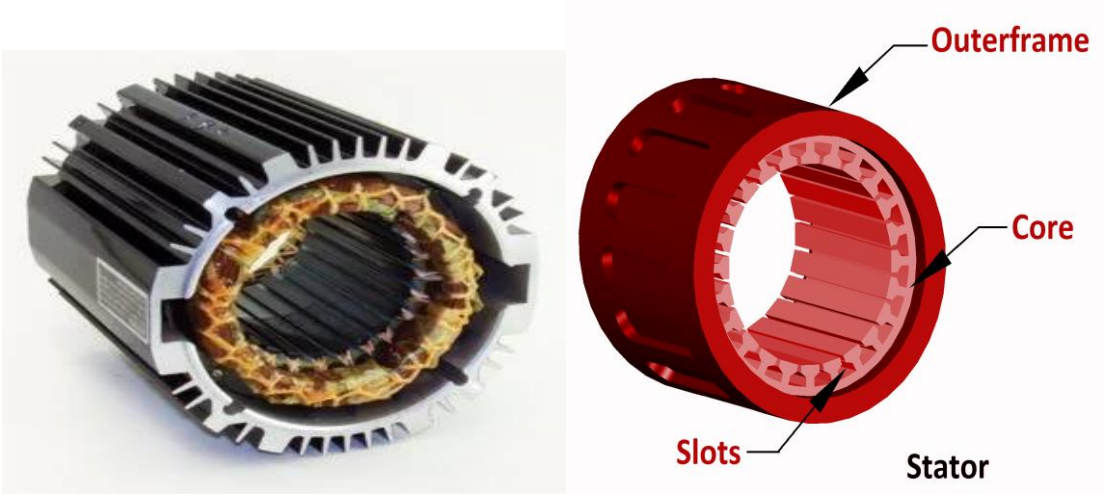
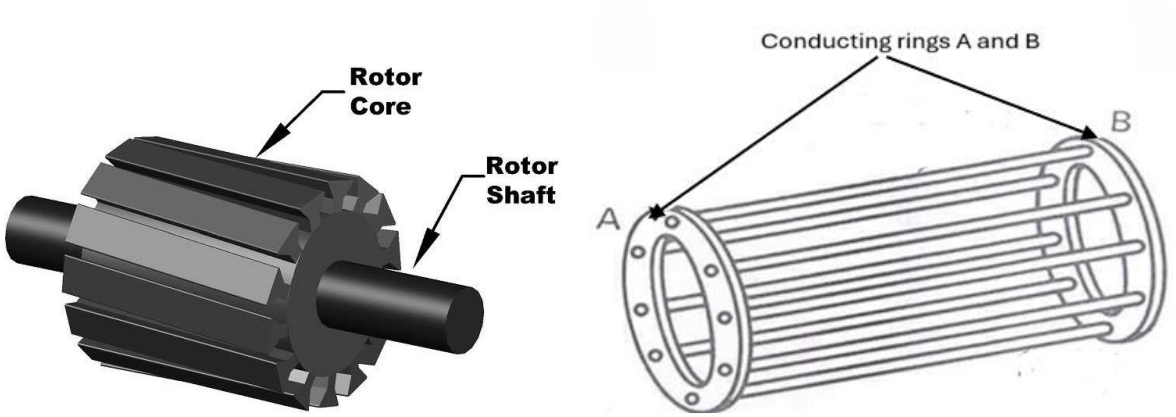



Figure. 1.2. Stator of the induction machine

### 1.4.2. Rotor

In the squirrel-cage rotor, the short-circuit rings allow for the circulation of currents from one slot conductor (rotor bar) to another. These conductive bars are evenly distributed and form the rotor circuit (see Figure 1.3). The cage is placed inside a magnetic circuit made up of stacked discs on the machine's shaft, similar to that of a wound rotor motor. In the case of the squirrel-cage rotor, the conductors are made by casting an aluminum alloy or by using solid pre-formed copper bars that are wedged into the rotor laminations. There is generally little to no insulation between the rotor bars and the magnetic laminations, but their resistance is sufficiently low to make leakage currents in the laminations negligible, except in cases of broken bars [21].The rotor slots are inclined relative to the longitudinal axis to reduce higher space harmonics and minimize the reactance associated with the rotor/stator angular variation position.




(a) rotor and the shaft (b) squirrel cage

Figure 1.3 Rotor of the induction machine

### 1.4.3. Winding

The three coils (one winding per phase) are identical and offset from one another by 120° and are supplied with three-phase voltages. They produce a rotating magnetic field at the rotational frequency.

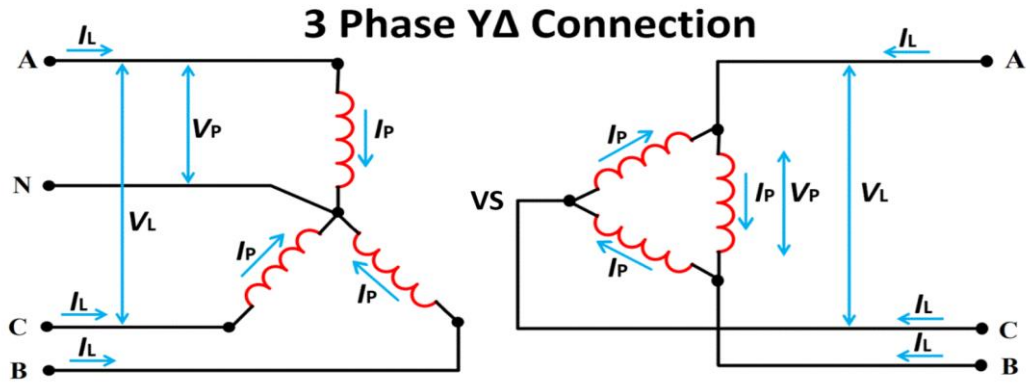
there are two types of winding connections, namely star and delta connection (see figure 1.4) :

- ***Star Connection***

Star connection is one type of three-phase AC circuit, denoted by 'Y'. It consists of four wires: three phase wires that carry current and one neutral wire. This neutral wire helps prevent electrical equipment from experiencing overcurrent and voltage issues. Star connection can be implemented using either three or four wires. If only three phase wires are used, it is referred to as a three-phase, three-wire system. If both three phase wires and one neutral wire are used, it is known as a three-phase, four-wire system.

- ***Delta Connection***

Delta connection is another type of three-phase AC circuit, denoted by 'Δ'. It is also known as a mesh connection. The delta connection consists solely of three phase wires, with no neutral wire utilized. Because there is no neutral wire, the delta connection cannot prevent the circuit from overcurrent. Therefore, it is primarily used for applications over short distances and in distributed networks.




(a) Star connection (b) Delta connection

Figure 1.4. Star and Delta connection

### 1.4.4 Air gap

The air gap in an induction machine, such as an induction motor or generator, is the small physical space between the rotor and stator. It's essential for the proper magnetic coupling between these two parts, as it allows the magnetic field generated in the stator to induce currents in the rotor, creating the torque necessary for rotation. Typical air gap values in induction machines are very small (usually between 0.2 mm to 2 mm for small to medium-sized machines). In an ideal induction machine, the air gap between the stator and the rotor is the same for the complete circular path. But in reality, the air gap is not completely uniform, even in a newly manufactured machine.

## 1.5 Fault natures and sources of induction machine

The operating modes of the induction machine are susceptible to various undesirable conditions, making it vulnerable to different types of faults. The causes of failures in rotating electrical machines stem from design, manufacturing tolerances, assembly, installation, working environment, load nature, and maintenance schedule. Typically, faults arise from a combination of one or more of these factors. In this regard, faults in the machine can be classified into three categories [22]: electrical, mechanical and environment related faults.

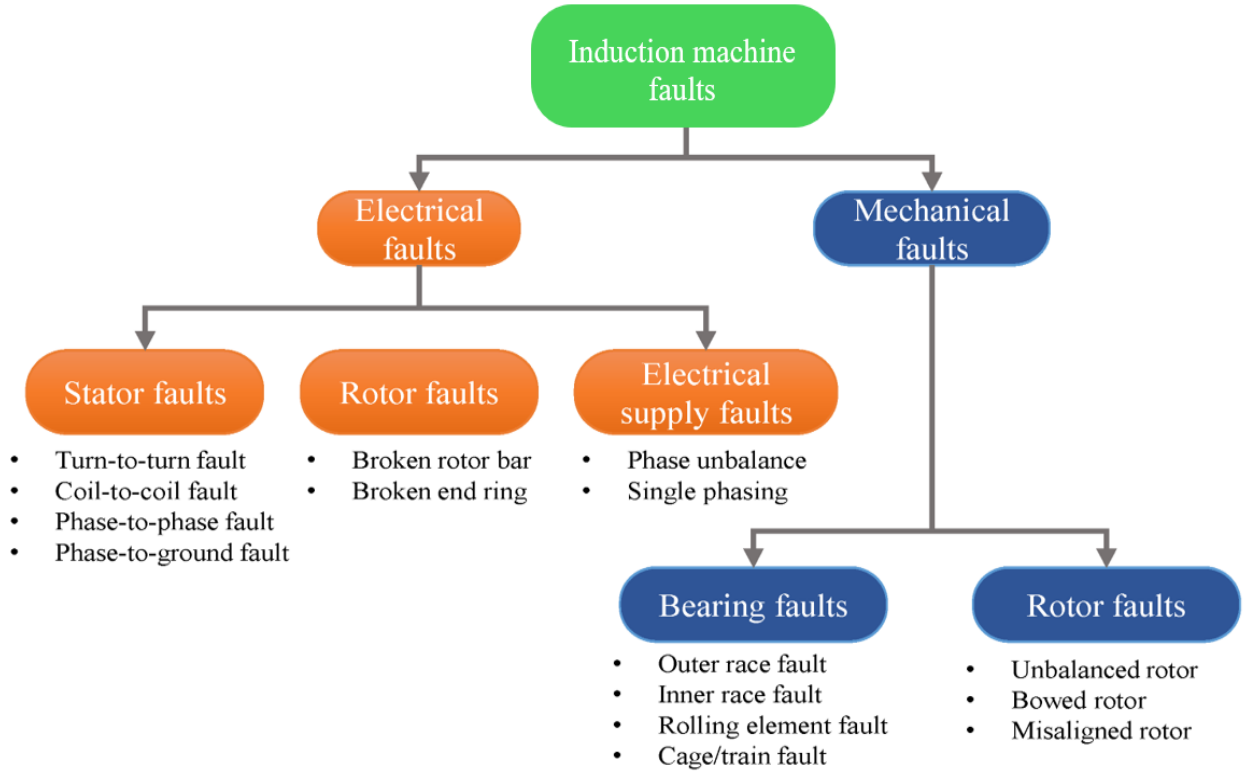
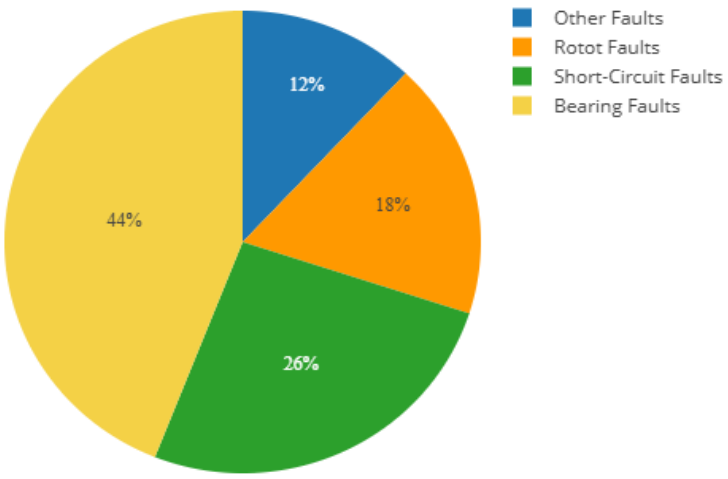



Figure 1.5. categories of IM faults [23]

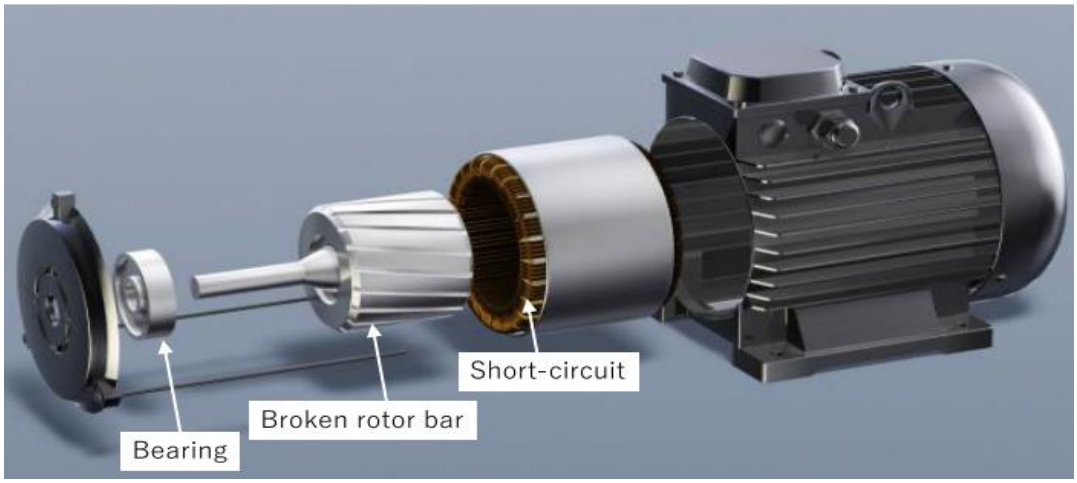
## 1.6. Overview of induction machines faults

Induction machine, although robust and efficient, is prone to various faults that lead to failure, in case of late detection or ill diagnosis it may cause total breakdown.

figure 1.5 illustrates the most frequent faults in IM ;




(a)




(b)

Figure 1.6.(a) Induction machine frequent faults,(b) Induction machine fault classes.

Among the possible classes of faults of IMs, bearing faults (44%) has the highest occurrence percentage, followed by short-circuit stator winding faults (26%), rotor faults (18%), and other kinds of faults (12%) [24]. The main causes of bearing faults are environmental conditions, voltage fluctuations, contamination, and insufficient lubrication [25]. Meanwhile, short-circuit faults are caused by the frequent start/stop of IMs, thermal deterioration due to high temperatures, temperature rise through dust attachment to the cooling fan, moisture absorption, and contact of rotor iron and stator winding. In the case of broken rotor bars, the reason is primarily overheating due to the continuous operation of a motor. From the above three major faults, the common point stands to be the continuous operation of IMs, and considering its fatal impact, these faults should be identified at slight fault stages. However, we cannot practically forecast the fault that may occur. Thus, a common diagnosis method is in demand for distinguishing the various types of slight faults.

### 1.6.1. Stator faults

There are two types of defecrts in the statoric part of IM:

- ***(a) Short-circuit faults***

These faults originate in the stator, where the stationary winding generates a rotating magnetic field to drive the rotor.

The stator is made up of three main parts: the stator outer frame, the stator core, and

the insulated stator windings.

The majority of stator faults are located in the stator windings. These faults include

insulation defects, open circuit faults, and short-circuit faults (interturn, phase to phase, phase to ground), figure 1.7 shows various possible short-circuit faults.

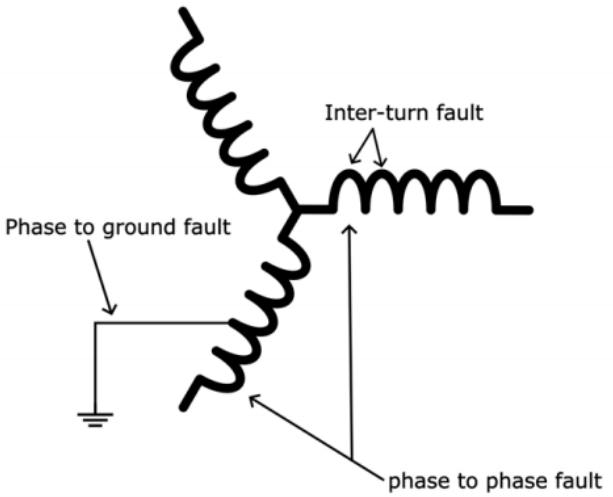



Figure 1.7. Different types of short circuit faults

The stress factors that can cause failures in the stator are as follows [26]:

- Thermal (overheating, etc.),
- electrical (dielectric breakdown, etc.), voltage variations, and imbalances in the power supply, frequent startups, etc. Mechanical (movement of rotor windings, etc.).
- Environmental (restricted ventilation, ambient temperature, mold, exposure to harsh conditions, etc.).

The faults generated in the stator as a result of these different stress factors are typically short-circuits, which are discussed in detail below.

- ***(b) Inter turn short circuit***

There is an apparent relationship between the lifespan of winding insulation and the stresses caused by voltage on insulating materials. It is also evident that some materials have greater endurance against voltage stress than others. The consequences of insulation deterioration include short-circuiting between windings, either within the same phase or between the phase and ground. If the insulation system is not sealed against environmental exposure, an avalanche phenomenon may occur within the winding. This situation is typically triggered by a small hole or leak between the copper wire of the stator winding and the open environment (air). A combination of external debris and humidity creates a high-resistance bridge between the wire and ground. Due to the potential difference, a small current flows to the ground, causing minor sparks within the insulation system. As this condition progresses, the insulation deteriorates to the point where a phase-to-ground failure occurs.

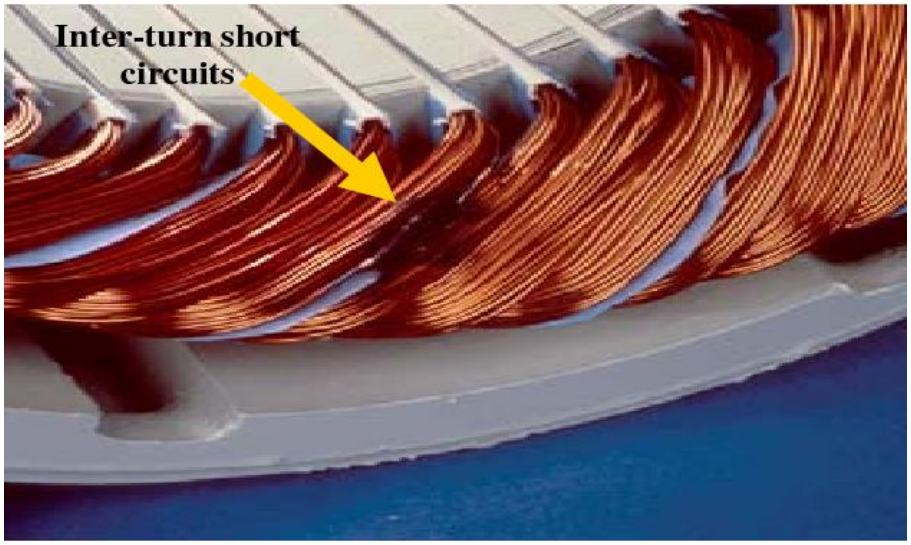



Figure 1.8. Inter turn short-circuit

- *(c) Phase-to-Phase Short Circuit*

This type of fault can occur at any point within the winding, though the repercussions vary depending on the location. This characteristic makes it challenging to analyze the fault's impact on the system. If a short circuit occurs near the power supply between phases, it can generate very high currents, potentially leading to the melting of supply conductors and/or tripping of protective devices.

Conversely, a short circuit near the neutral between two phases causes an imbalance without melting the conductors. The stator currents become entirely unbalanced, and this imbalance is proportional to the severity of the fault. The currents in both the rotor bars and the end rings increase with the onset of this fault. Detecting this type of fault can rely on observing the imbalance in phase currents [27].

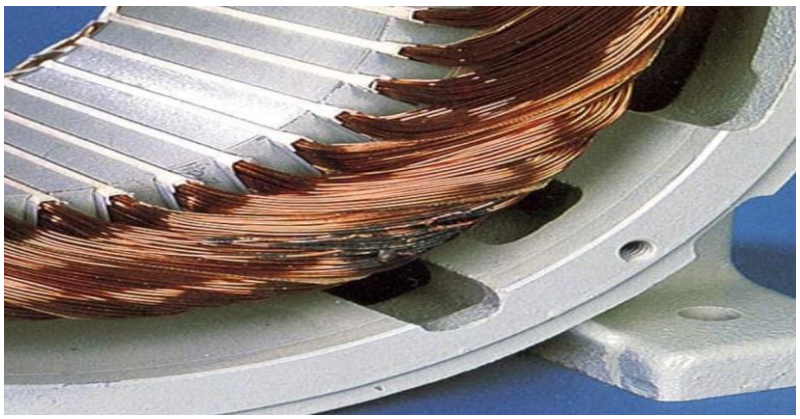


Figure 1.9. Phase-to-Phase Short Circuit fault

- *(d) Phase to ground short circuit*

The frame generally has a floating potential, but it is often grounded due to mechanical connections. If the potential is floating, a short circuit between the winding and the frame is not a concern from a material perspective, except for capacitive effects, as the frame assumes the potential of the winding at the short-circuit location, potentially causing insulation faults within

the winding. Moreover, this fault will generate a specific component. However, from a safety standpoint, this type of fault can be highly dangerous, requiring the installation of protective devices (such as differential circuit breakers).

In the presence of this fault, the voltage in the affected phase remains unchanged. However, the current flowing in this phase increases due to the reduction in resistance and inductance. This current increase results in a rise in homopolar temperature, leading to the appearance of a pulsating torque. Measuring the leakage current could be a method to detect this type of fault .

### 1.6.2. Rotor faults

A wound rotor can be affected by the same faults as the stator. For a squirrel-cage rotor, however, faults are limited to broken bars or broken end rings.

- ***(a) Broken rotor bars***

A broken or cracked bar is one of the most common faults in a rotor. It can occur either along the bar's slot or at the end where it connects to the rotor ring. Deterioration of the bars reduces the average value of the electromagnetic torque and increases the oscillation amplitude, which in turn leads to rotational speed oscillations. This generates mechanical vibrations, resulting in abnormal machine operation. The large amplitude of these oscillations accelerates machine deterioration. Consequently, the torque significantly decreases with the number of broken bars, creating a cumulative effect of the fault. The impact of a broken bar escalates rapidly as more bars are affected.

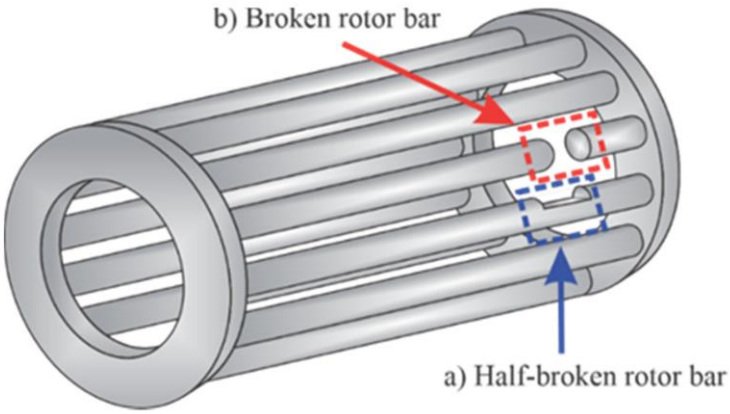



Figure 1.10. Rotor bar fault types [28].

Bar or ring segment breaks can be caused by factors such as mechanical overload (frequent startups, etc.), excessive localized heating, or manufacturing defects (such as air bubbles or poor welds) [29]. Such faults lead to oscillations in currents and electromagnetic torque, which become more apparent with higher inertia (constant speed). When the drive system has lower inertia, oscillations appear in the mechanical speed and in the amplitude of stator currents.

Ring segment breaks are as common as bar breaks. These breaks are often due to casting voids or differential expansion between bars and rings, especially since the short-circuit ring segments carry larger currents than the rotor bars. Consequently, poor ring design, deteriorated operating conditions, or torque overloads can lead to ring breaks.

A bar breakage doesn't immediately halt the machine, as the current through the broken bar is redistributed to adjacent bars. However, these bars become overloaded, which can lead to further breaks. This cycle continues until enough bars fail to stop the machine entirely. Given the variety of potential faults and their impacts, monitoring techniques have become essential for electric machine users and are increasingly gaining interest among machine designers.

- ***(b) Rotor air gap eccentricity***

In a fault-free machine, the rotor is center aligned in the stator bore that results in a uniform air gap between the stator and rotor. In fault-free electrical machines, the rotation center of the rotor is the same as the geometric center of the stator bore. As a result, the rotor symmetrical axis , stator symmetrical axis , and rotor rotational axis coincide with each other,and thus the magnetic forces are balanced in opposite directions. Rotor eccentricity, displacement of the rotor from its centered position in the stator bore, generates an asymmetric air gap between the stator and rotor [30]. The rotor eccentricity also produces unbalanced magnetic pull (UMP), which is a radial magnetic force on the rotor shaft. The UMP also pulls away the rotor from the stator bore center, thus causing excessive stress on the electrical machine [31,32]. Eccentricity commonly presents in rotating electrical machines, and the maximum permissible level of eccentricity is defined, which is 5 or 10% of the air-gap length [33]. If eccentricity exceeds the permissible level, it will increasingly damage the winding, stator core and rotor core in the motor due to rubbing of the stator with the rotor. Three different types of eccentricity occur in an electrical machine: *static eccentricity, dynamic eccentricity, and mix eccentricity*. As an example, static eccentricity is explained next.

Static eccentricity in electrical machines occurs when the rotor symmetrical axis is concentric with the rotor rotational axis; however, they are dislocated with respect to the stator symmetrical axis; hence, the position of minimum radial air-gap length is fixed. In this state, the mutual inductances across the stator and rotor as well as the self- and mutual inductances among the rotor phases are related to the angular position of the rotor [34]. Static eccentricity can be due to numerous motives such as elliptical stator core, wrong placement of the rotor or stator at the setup or subsequent of maintenance, incorrect bearing positioning, bearing deterioration, shaft deflection, housing imperfection, end-shield misalignment, excessive tolerance, and rotor weight or pressure of interlocking ribbon [35–37]. Static eccentricity leads to second failures which cause drastic harm to the rotor, stator core and windings. The radial forces in the static eccentricity condition produce a steady UMP in the radial route across the motor because the reluctance of the magnetic flux path decreases with the transmission of flux on the side of a tiny air gap [38]. Albeit, the winding current induces more magnetic flux that causes a stronger pull and leads to the expansion of the air gap on the opposite side where the reluctance increases, thereby decreasing the flux and magnetic side pull.Therefore, the UMP compels the rotor to move toward the area of the narrowest air-gap length. During abrasion, the stator core subsequently generates abnormal vibration and severely damages the rotor, windings and the stator [39]. Air gap eccentricity principle difference is depicted in figure 1.10:

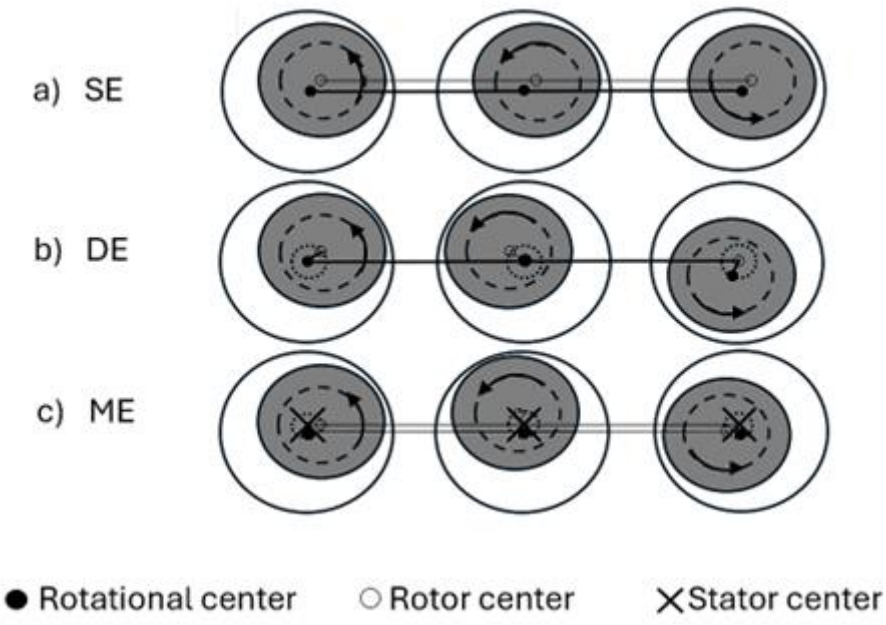



Figure 1.11. Air gap eccentricity types : a)- Static, b)- Dynamic and c)- Mixed.

- ***(c) Rotor Bow***

Any irregular thermal variation (heating or cooling) and unfavorable thermal distribution of the rotor during operation of electrical machines may bow the rotor. The bow created in the rotor prevents sufficient alignment in the motor and generally produces a preload on the bearings. Bend locations in the rotor cause major failures in other parts of the motor. The bow in the rotor is classified as local and extended. When an asymmetrical heating is confined to a part of the rotor, a local bow is generated. For example, rotor-to-stator rubbing can generate a local asymmetric thermal distribution, which causes the local bow. When an asymmetrical heating extends along the rotor, an extended bow is generated. Long-lasting gravity effects on off-line machines generate a rotor bow classified as an extended bow, when an unsuitable rotor straightening turning system is not used. Since the rotor is limited by two bearings, an extended bow commonly causes a shaft bow [40,41].

- ***(d) Misalignment Faults***

Misalignment is the result of an incorrect coupling of the motor and load shafts during

assembly, or it can be the result of motor overload. Three types of misalignments can be seen: parallel misalignment, angular misalignment, and combined misalignment. figure 1.12 illustrates both parallel and angular misalignments.

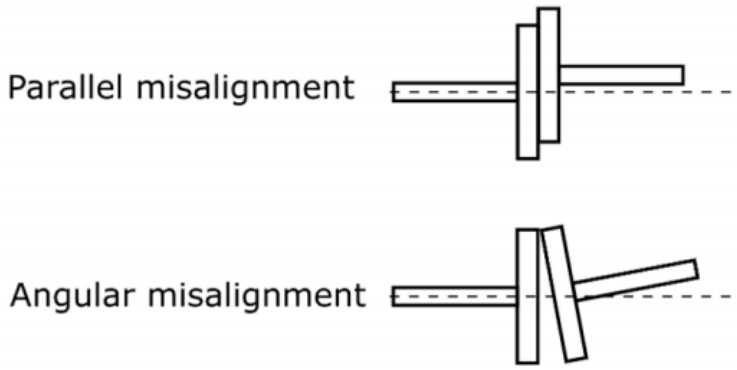


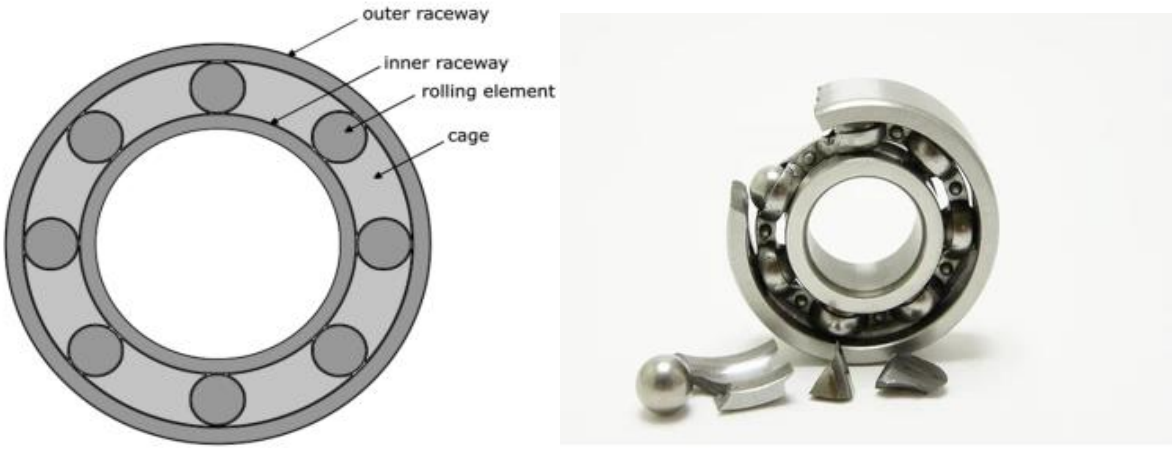

Figure 1.12. parallel and angular misalignment faults between the motor and load shaft [42]

Misalignment can cause vibrations in the machine, which is the origin of other rotor and bearing faults.

- ***(e) Bearing fault***

Bearings are mechanical devices mounted on the rotor shaft of an IM to minimize friction during its rotation. They are located on either side of the machine rotor. An example of ball bearings and the different bearing elements are shown in figure 1.12.

In general, bearing wear involves spalling defects on the internal and external contact surfaces. Wear mechanisms never occur in isolation; instead, a combination of mechanisms leads to bearing degradation and a reduction in its lifespan. This refers to a decrease in the number of rotations it can perform, under a specific load, before exhibiting defects. Numerous external factors influence bearing lifespan: excessive mechanical loads, installation defects, electric current flow, corrosion, contaminants within the bearing, lubrication quality, and operating temperature.




(a) (b)

Figure 1.13. Bearing fault in induction machine: a- types of bearing defect, b- damaged bearing.

Different types of bearing faults exist, and they are classified according to their location: in the outer raceway, in the inner raceway, in the cage, or on the rolling element. In these cases, the fault is called a “localized fault”. figure 1.14 shows three types of localized bearing faults: the first one is the outer raceway of the bearing. The second one is in the inner raceway and the third one can be seen in the rolling element (outlined by the red box) A bearing fault can also be “distributed”, in which case it represents a series of irregularities in the geometry of the bearing.

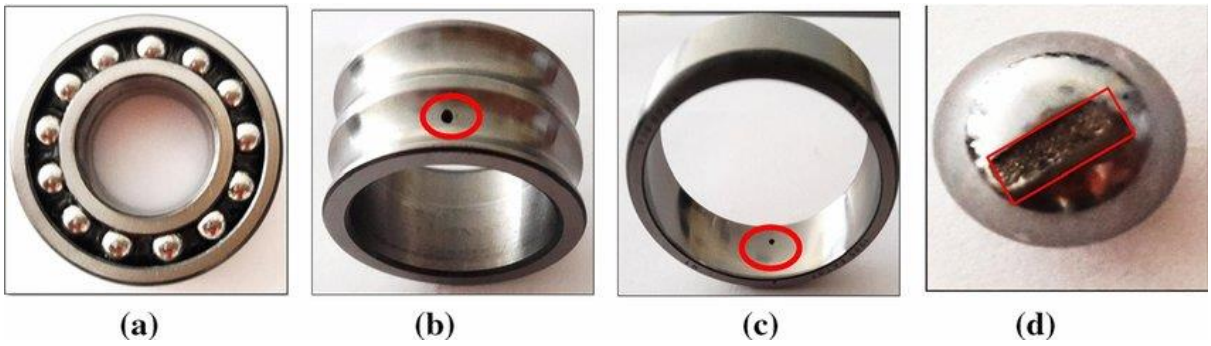



Figure 1.14. Pictures of different bearing fault types : a- Healthy, b-Outer race, c- Inner race, d- Ball [43].

## 1.7. Diagnostic approaches

### 1.7.1. Condition monitoring techniques

Condition monitoring programme which can predict a failure in electrical machines has received considerable attention for many years. Successful detection of any failure in electrical machines is achieved by using suitable condition monitoring. When a failure occurs, some machine parameters are exposed to changes that depend upon the fault degree. Any irregularity in the rotor of electrical machines presents with variation distributed in the rotor currents. The feedback of these currents to the air-gap field produces specific signatures of fault in the spectrum of speed, torque, current, and power. Reliable condition monitoring techniques depend on the best understanding of the mechanical and electrical characteristics of the electrical machines in both fault-free and faulty situations. Researchers have used different condition monitoring techniques that can be categorized as follows [44-50]:

• Acoustic emission

• Air-gap torque

• Current

• Electromagnetic field monitoring

• Induced voltage

• Instantaneous angular speed

• Motor circuit analysis

• Power

• Surge testing

• Vibration

• Voltage

Model-based and non-model-based (Data-driven) approaches for diagnosing induction machine faults differ in reliance on machine-specific information. figure 1.15 regroups the most frequent techniques used for both of these approaches:

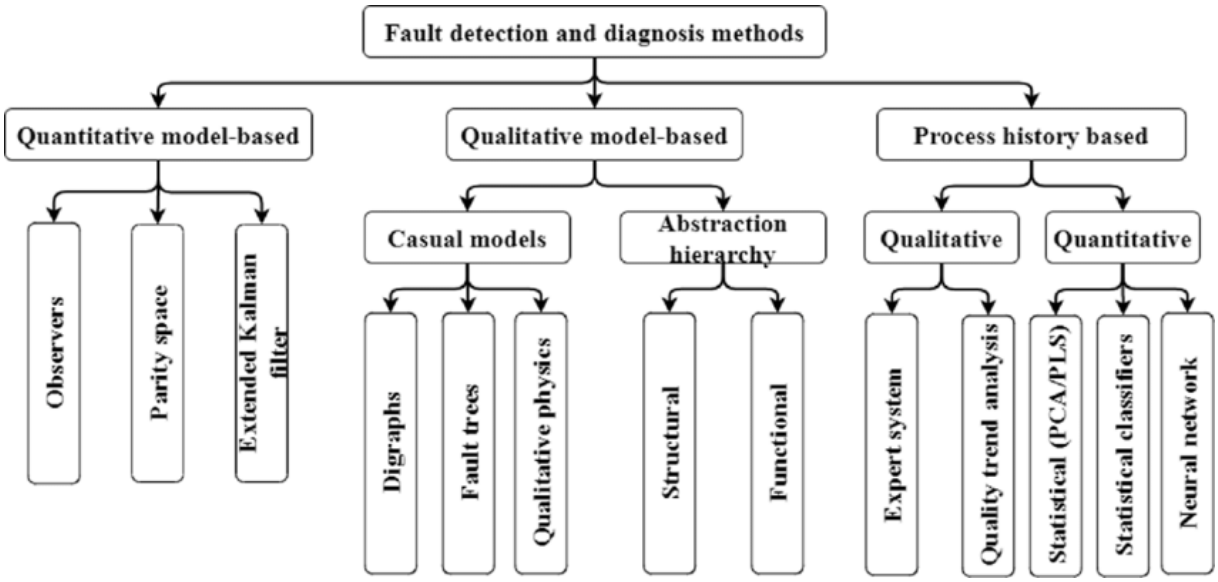



figure 1.15 Fault detection methods

### 1.7.2. Model-Based approaches

These diagnostic methods are typically based on the physical modeling of the machine. They involve comparing the evolution of the model with that of the actual physical process. In this approach, the asynchronous machine is treated as an experimental process, with the objective of identifying the corresponding behavioral model at each moment or sampling interval. figure 1.15 illustrates this procedure.This method is based on estimating unmeasured signals or tracking parameters during operation [51]. It assumes an in-depth understanding of the process in the form of a numerical model. For an induction machine, modeling in a three-phase or equivalent two-phase reference frame is necessary. Signals or parameters from these models are measured or estimated to create a fault signature. The consistency between measurements and estimates is assessed using characteristic quantities of the process state, known as residuals.The residual vector, which is zero during normal operation,is compared online to fault signatures. According to this diagnostic mechanism, we distinguish [52]:

- Diagnosis using observers [53].
- Diagnosis through analytical redundancy (parity space).
- Diagnosis through parameter estimation [54].

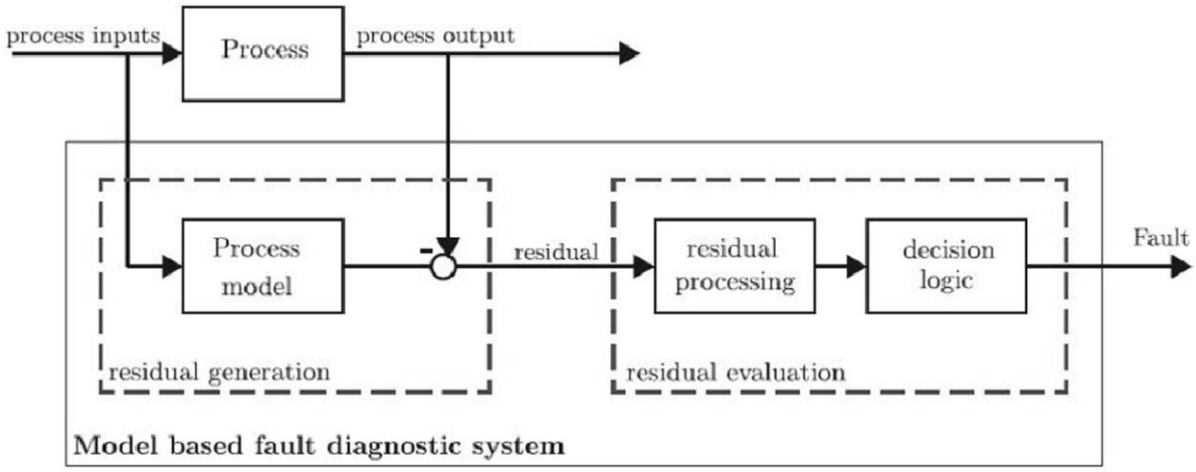



Figure 1.16. Model based diagnostic process.

- ***Observer-based approaches***

The use of observers for fault detection relies on the complete or partial reconstruction of the state vector using measurements from the monitored system. The difference between reconstructed and measured variables generates residuals (see Figure 1.16). Here, input signals that indicate faults are assumed to remain zero in normal operation. When a fault occurs, these inputs become non-zero. The observer's role is to rapidly indicate fault presence, and it must also be resilient to disturbances. Various solutions have been proposed for this purpose. In linear systems, a well-chosen observer gain matrix can address this issue. A particular class of observers generates directional residuals, known as fault detection filters introduced in [55]. Another approach is based on direct or indirect decoupling methods [56].The unknown-input observer with linear or nonlinear decoupling has been proposed to achieve this goal [57-60]. The main idea is to use a state transformation $z = T(x)$ to obtain part of the state vector, $z$, whose dynamics are decoupled from the unknown inputs $d$ . This process requires two steps:

- Generation of the decoupled state
- Observer synthesis and residual generation

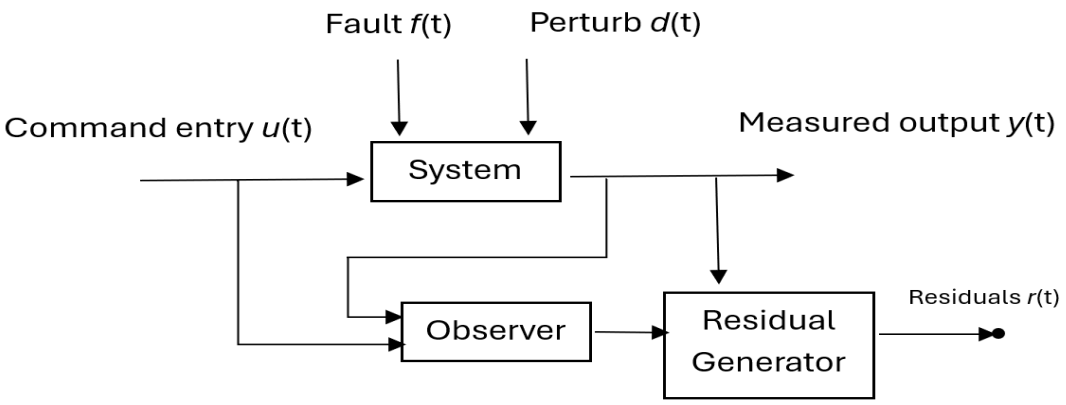



Figure 1.17. Principle of the Observer-Based Diagnostic Method

- ***Fault detection and localization***

*(a) Fault detection*

Fault detection is the process of identifying the occurrence and timing of a fault. This is achieved by using the residual r(t) , generated by comparing the behavior of the system model to that of the actual system. Ideally, the residual remains zero when the system operates under normal conditions.In observer-based diagnostic methods, the residual r(t) is typically generated by comparing the measured outputs with the estimated outputs: $r(t) = y(t) - \hat{y}(t)$

The residual vector r(t) enables the detection of a fault $f(t)$ . In real situations, the residual r(t) has a zero mean in the absence of faults due to noise. To detect a fault, the residual r(t) is compared to a threshold $J$ , which is defined based on modeling errors. The following decision logic is applied:

$$r(t) < J_s(t) \text{ No fault detected}$$

$$r(t) > J_s(t) \text{ Fault detected}$$

*(b) Fault localization*

After detecting a fault in the system, it is essential to identify the exact affected component, a step known as fault localization. This process often relies on generating residuals so that a set of these residuals is sensitive to certain faults and insensitive to others. Another method for fault localization involves using a bank of observers, where the number of observers included depends on the number of faults to be detected and localized.

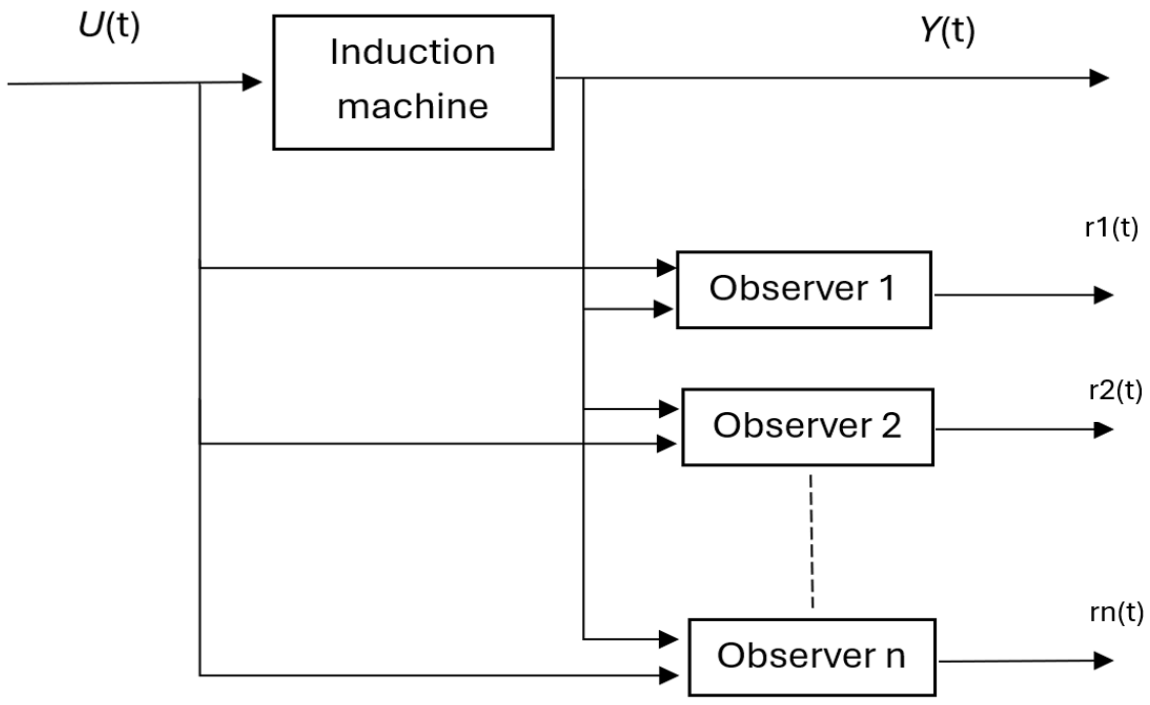



Figure 1.18. Observer bank architecture.

Comparison between open-loop and closed-loop residual generation

The goal is to highlight the influence of control on the residuals and, consequently, its impact on diagnostic quality. This approach involves comparing the residuals generated from the open-loop system with those from the same system within a control loop.

*(a) Observers Types*

The observer is a system designed to reconstruct unmeasurable or inaccessible quantities of the asynchronous motor from the accessible and measurable variables of the system. The following figure illustrates the principle of a state observer.

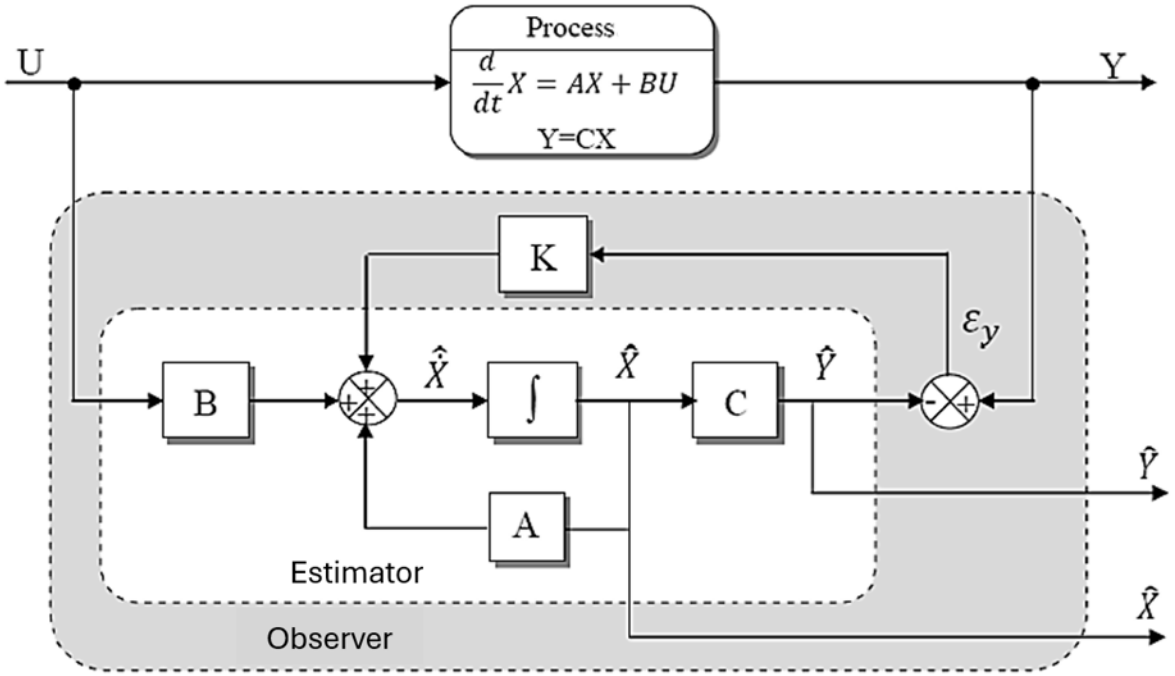



Figure 1.19. Observer principal functioning diagram.

*(b) Deterministic observers*

This type of observer does not account for measurement noise or random fluctuations in state variables. In this category, there are several observers, such as the Kubota observer and the adaptive observer.

*(c) Stochastic observers*

These observers provide an optimal estimation of states based on stochastic criteria. They account for the presence of state and output noise within the system. This family includes, for example, the Kalman filter (see Figure 1.20).

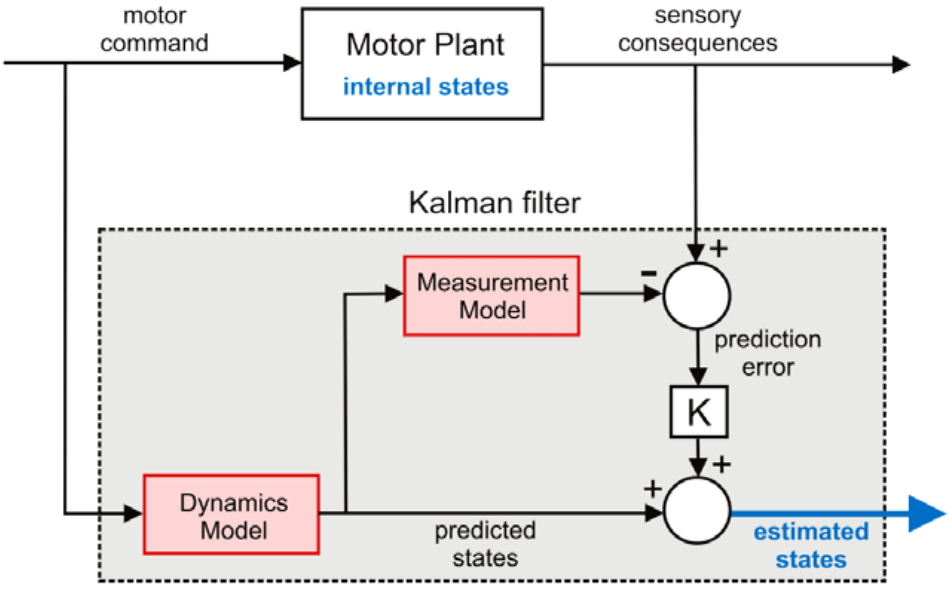



Figure 1.20. Kalman filter architecture [61].

*(d) Linear observers*

These are observers whose gain construction is based on a system matrix A that is linear and time-invariant. Luenberger observers and the Kalman filter are examples that rely on this approach.

*(e) Non linear observers*

These are observers used for monitoring nonlinear systems, such as electric machines. There are two main development approaches for these observers:

- Linearization around the operating point: The extended Kalman filter operates with this approach.

- Gain construction based on the system's nonlinearity: This includes high-gain observers and the nonlinear Kalman filter, where observers are synthesized considering the system's nonlinear modeling.

*(f) Adaptive observer*

The Model Reference Adaptive System (MRAS) method relies on choosing two models to represent a system. The first is called the "reference model," while the second is termed the "adaptive model." The reference model should not explicitly depend on the variable to be estimated, whereas the adaptive model does depend on it. An adaptation mechanism, typically a PI controller, aligns the behavior of the adaptive model to match that of the reference model, as illustrated in Figure 1.20.

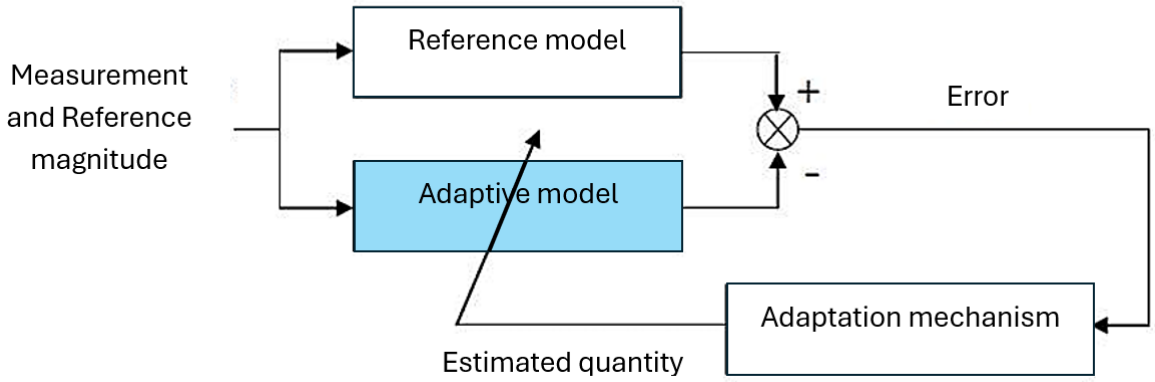



Figure 1.21. Adaptive observer principal.

To implement our observer, we need to select the quantities of the system. In the case of vector control of the induction machine, we assume that:

- The model parameters are known and invariant (in the healthy state).
- The stator currents are measured, as well as the stator voltages.
- The rotor fluxes are estimated.
- The rotor speed is estimated.

- ***Parameter Estimation-Based Approach***

Identification methods are widely used to determine the parameters of a physical system by measuring input-output signals, assuming that the basic structure of the model is known. The defect detection method based on parametric models relies on the assumption that faults are reflected in the physical parameters of the system.

In this context, a parameter vector is estimated, and any variation outside a reference range indicates the occurrence of a fault in the monitored system (or more precisely, signifies a change in the characteristics of the process). This variation can then be detected using a decision test in the parametric space.

Let's consider a system described by its state and output equations. Here, $\theta$ represents the vector of unknown parameters.

$$\dot{x} = f(x, u, \theta)$$
$$y = h(x, u, \theta) \quad (1.1)$$

We consider a set of $N$ measured data acquired with a sampling period $T_0$. The problem is to estimate the model that best explains these data, thus determining the parameter vector $\theta$. The

residual is defined as the difference between the estimated value of the parameter vector, $\widehat{\theta_k}$, and its nominal value $\theta_0$:

$$r(k) = \widehat{\theta_k} - \theta_0 \quad (1.2)$$

Or, by considering the measured and estimated outputs

$$r(k) = y(k) - h(\hat{\theta}_{k-1}, u(k)) \quad (1.3)$$

Parametric estimation methods require optimizing a performance criterion and must meet two closely linked, restrictive constraints: persistence of excitation and a limited number of parameters to estimate. Additionally, the performance criterion is minimized using numerical techniques, which significantly increases computational demands, generally making real-time application infeasible. These constraints limit their implementation. However, they are well-suited for detecting multiplicative faults[62].

- ***Parity Space Approach***

The principle of this approach is to transform the model equations to obtain relationships known as analytical redundancy relations (ARR). These relationships only utilize known quantities. The offline generation of the ARR is a general problem of variable elimination in a system of equations. In the linear case, elimination is achieved by projection into the parity space. In the nonlinear case, formal elimination techniques can be implemented [63-64].

When the model is linear, the generation of the residual uses the analytical redundancy relations (ARR) in which the influence of the inputs and the unknown state has been canceled out. The effect of the inputs is directly subtracted since these inputs are known along with their action matrix. As the interaction matrix of the state on the output (the observability matrix) is known, the influence of the state is canceled by projecting onto the orthogonal space of this interaction matrix. In the absence of faults, the resulting residual reflects only the action of random noise. If a fault affects the system and its direction is not collinear with that of the state, its influence will manifest as a change in the mean of the residual. The residual is then structured to localize the fault.

### 1.7.3. Non-Model-Based approaches

The foundation of any reliable diagnostic system is understanding the electrical, magnetic, and mechanical behavior of the asynchronous machine (ASM) in both healthy and faulty conditions. The so-called "model-free" methods rely on the analysis of acquired signals. They have the advantage of being independent of the analysis concerning the internal fluctuations of the system. Moreover, the information contained in the signals, not being filtered by modeling, remains intact.

Some methods are widely used in the industry and include: the so-called Park vector method, Motor Current Signature Analysis (MCSA), instantaneous power analysis, estimated or measured electromagnetic torque analysis, and vibration and acoustic noise analysis [65,66].

These methods apply classical approaches to signal processing, as well as more modern techniques such as wavelet transforms and Hilbert transforms, to extract the spectral content

related to various faults [67]. Other, more recent techniques leverage artificial intelligence tools to develop databases derived from the extraction of characteristics of faults based on their origins. They collect accessible signals (stator currents, leakage flux, vibrations), process them, and apply heuristic techniques for classification aimed at diagnosing faults. However [68], these methods are dependent on issues related to sensor placement and the conditioning of measured signals. Furthermore, they do not exploit information from the rotor with a squirrel cage, as this component is inaccessible.

Non model based techniques will be discussed thoroughly in the upcoming chapter.

## 1.8 Conclusion

In this chapter, a state-of-the-art overview of the different diagnostic methods has been presented. First, the terminology related to maintenance and diagnostics used in this field is provided. The various components of the induction machine are briefly described. Subsequently, the different faults that can affect the induction machine are presented, highlighting that the short-circuiting of stator windings is predominant in the induction machine; its occurrence can very quickly generate a cascading effect that can be fatal. Finally, a classification of diagnostic methods for the induction machine is given based on the type of description of the monitored induction machine, with or without an analytical model.

# Chapter 2

# An overview of Non Model Based Approaches : Signal Processing and Artificial intelligence techniques

## 2.1 Introduction

There are already a large number of publications and extensive reviews in the research field of fault detection and diagnosis in induction motors and other machine types [69–72]. The selection of suitable measurement quantities is central to the implementation of monitoring. The three phase currents of the electrical machine are often used for further evaluation [71]. Alternatively, measured data on the mechanical vibrations can also be recorded and analyzed using a vibration or acceleration sensor [72,73]. These respective measurement quantities have their own advantages and disadvantages [74]. Other options for fault detection and diagnosis involve the use of a supplementary sensor to monitor the magnetic flux in the inner or outer area of the machine [75,76] and the use of infrared cameras for thermal monitoring [77,78] or microphones to record acoustic signals [79,80]. However, like the measurement of mechanical vibrations, these approaches require the installation of a special sensor, which is associated with additional effort and costs. Monitoring based on stator currents, on the other hand, has the advantage that the corresponding sensors are generally inexpensive, easy to install and easily scalable. Current sensors are often already integrated in existing motors and can therefore be used immediately.

There are generally different techniques for the fault detection and diagnosis of induction motors [70,81]. In model-based methods, detection is performed via the deviation between the real systems and the modeling used. Kalman filters, for instance, can be used for this purpose [82,83]. In addition, physical modeling in different variations such as simplified models [84,85], multiple coupled circuit models [86,87] or FEM models [88,89] are also widely applied. Another aspect is signal processing techniques, which work on the basis of an evaluation and analysis of measurements by extracting specific characteristics for individual fault cases from the recorded data. With the help of existing prior knowledge about the characteristics in the healthy and faulty states, it is then possible to evaluate the condition of the electrical machine. Frequency-based methods such as motor current signature analysis (MCSA) [90,91] or methods from the time–frequency domain such as discrete wavelet transform (DWT) [92,93], the Hilbert–Huang transformation (HHT) [94] or the Wigner–Ville distribution (WVD) [95] are frequently used for this purpose. Data-based approaches, on the other hand, only use

data sets for fault detection and diagnosis. No additional prior knowledge of individual fault cases is required. Common approaches from the field of machine learning (ML) are the support vector machine (SVM) or the k-Nearest Neighbors (kNN) [96-99] algorithm. The use of neural networks in a wide variety of designs is also very widespread. These include feed-forward neural networks (FFNNs) [100–104], recurrent neural networks (RNNs) [105,106], convolutional neural networks (CNNs), deep belief networks (DBNs), self-organizing maps (SOMs) [107-110] and autoencoders (AEs) [111-114]. A combination of both signal-based and data-based methods is also usual, with the signal-based approaches used for extracting known fault features [94,97,101]. The isolated features are in turn used by algorithms to differentiate between conditions.

In this chapter, we will introduce Non-Model Based approaches, more specifically Signal Processing techniques and we will discuss their limitations. Later, we will introduce Artificial Intelligence and their various techniques with a focus on supervised learning as it suits our fault diagnosis problem, several algorithms that fall into this category will be defined in detail.

## 2.2 Signal processing

Signal processing is the discipline that develops and studies techniques for processing, analyzing, and interpreting signals. It extensively draws on concepts from probability, statistics, and various other fields of applied mathematics.

### 2.2.1 Signal notion

The concept of a signal is very broad. It arises from the observation of a phenomenon, involving certain quantities that depend on time, space, frequency, or other factors. These measurable quantities are referred to as signals [115].

A one-dimensional signal is a function that propagates in a single direction and depends on a single parameter (e.g., a sound signal), whereas a two-dimensional signal is a function that depends on two parameters (e.g., an image). There are various types of signals [116] :

- Stationary signal : A stationary signal is one whose statistical properties do not depend on time, such as white noise. While it may exhibit unexpected events, the probabilities of these events occurring are known in advance (unpredictable events are statistically foreseeable). Figure 2.1 illustrates an example of a stationary signal.

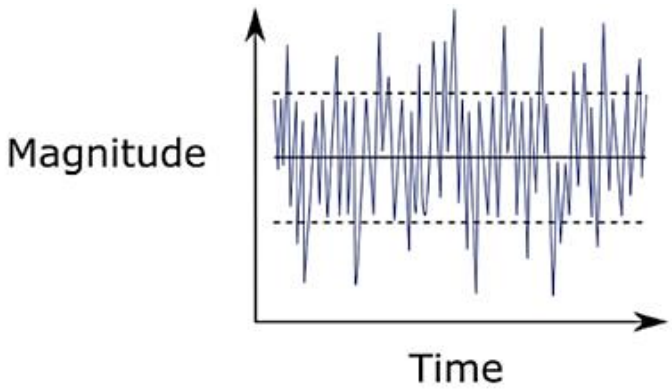



Figure 2.1 Stationary signal sample

- A non-stationary signal is one in which transient events occur that cannot be statistically predicted based on past data. Figure 2.2 illustrates an example of a non-stationary signal.

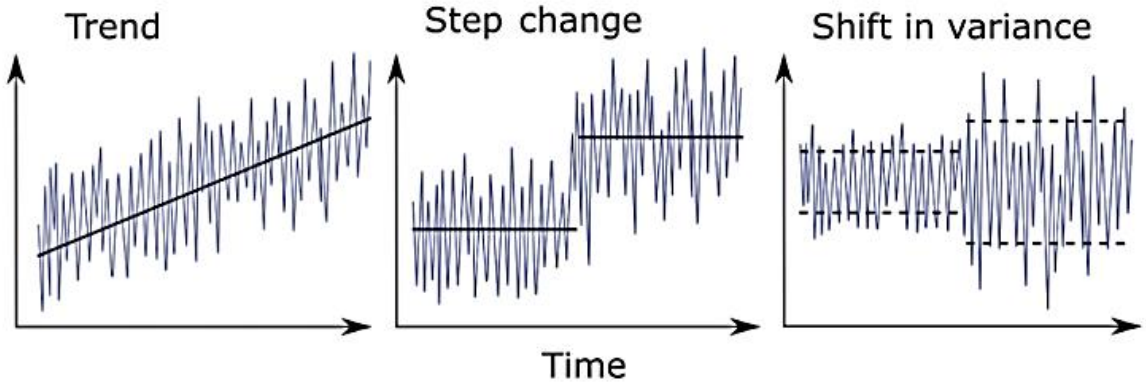



Figure 2.2 non-stationary signal sample

## 2.3 Signal processing approaches

### 2.3.1 Fourier Transform

The Fourier transform is a mathematical method used to study a signal and extract information about its frequency behavior and properties [117]. To accomplish this, the signal is decomposed into a sum of simple components called elementary functions. The elementary functions in Fourier analysis are sinusoidal functions, which depend on a single parameter: frequency [118].Based on the work of French physicist Jean-Baptiste Joseph Fourier, it enables the transition between time and frequency domains through the integral that bears his name. For a function $x(t)$, it is expressed as :

$$X(f) = \int_{-\infty}^{+\infty} x(t) e^{-i2\pi ft} dt \qquad (2.1)$$

It can be shown that, conversely, $x(t)$ can generally be obtained from $X(f)$ using the so-called inverse Fourier transform:

$$x(t) = \frac{1}{2\pi} \int_{-\infty}^{+\infty} X(f) e^{i2\pi ft} df \qquad (2.2)$$

This analysis allows us to describe the distribution of a signal's frequency components without providing information about the timing of their occurrence. The squared magnitude of the Fourier Transform, ($|X(f)|^2$) is known as the power spectral density. For stationary signals, it offers a simple and easily interpretable characterization. Figure 2.3 illustrates the time-domain representation (Figure 2.3.a) and the Frequency-domain represention (Figure 2.3.b) of the signal $x(t)$,

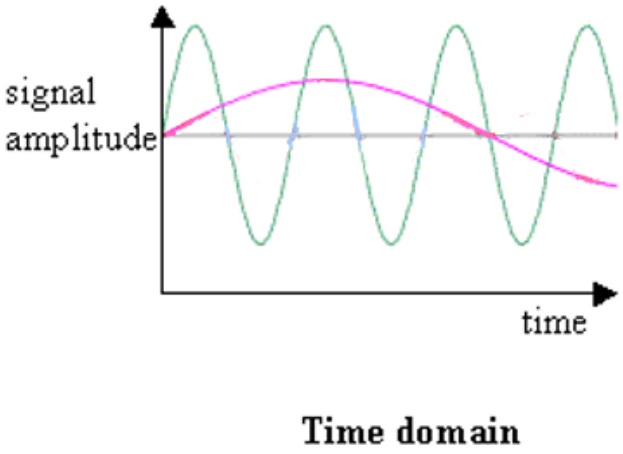



Figure 2.3.a Time domain representation

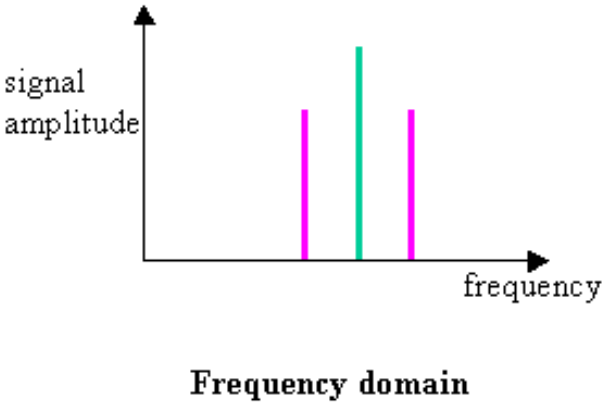



Figure 2.3.b Frequency domain representation

Despite its immense success, this technique has two major drawbacks [119] :

- Lack of temporal localization : Fourier analysis provides information about the different frequencies present in a signal, i.e., its spectrum, but it does not reveal when these frequencies were emitted. This analysis gives global, not local, information because the analysis functions used are sinusoids that oscillate indefinitely without damping. This loss of locality is not a problem for analyzing stationary signals, but it becomes an issue for non-stationary signals.

- The Fourier transform is not suited for studying signals whose frequency varies over time. Such signals require the implementation of a time-frequency analysis, which enables the localization of periodicities in time and thus indicates whether the period changes continuously.

### 2.3.1.1 Window Function

A window is a regular function that changes slowly and is well localized, meaning it is zero outside a certain region, called its support. To study the local spectral behavior of a signal, it is necessary to work with time segments by multiplying the signal by a window that is zero outside the desired interval. The simplest window function is the rectangular function (Figure 2.4), which has a fixed amplitude.

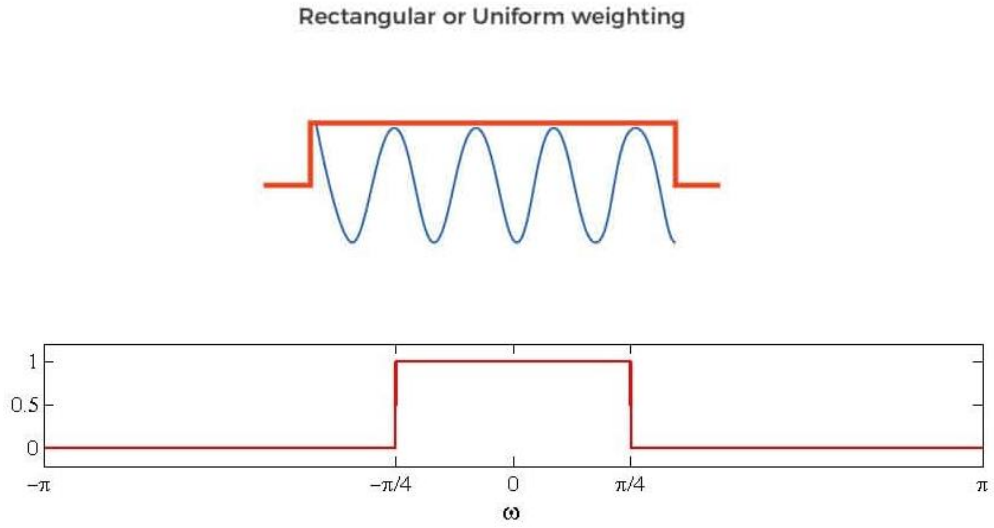



Figure 2.4 Rectangular window function

From the previous figure, we can define the following equation:

$$w(t) = \begin{cases} 1, & t \in \left[-N - \frac{T}{2}, N - T/2\right] \\ 0 \end{cases}$$

By varying the parameter *N*. it will be possible to move the window along the axis to analyze the local behavior of the signal over different intervals. Two important factors for a window function are its center and its length. Figure 2.5 illustrates the most used window functions.

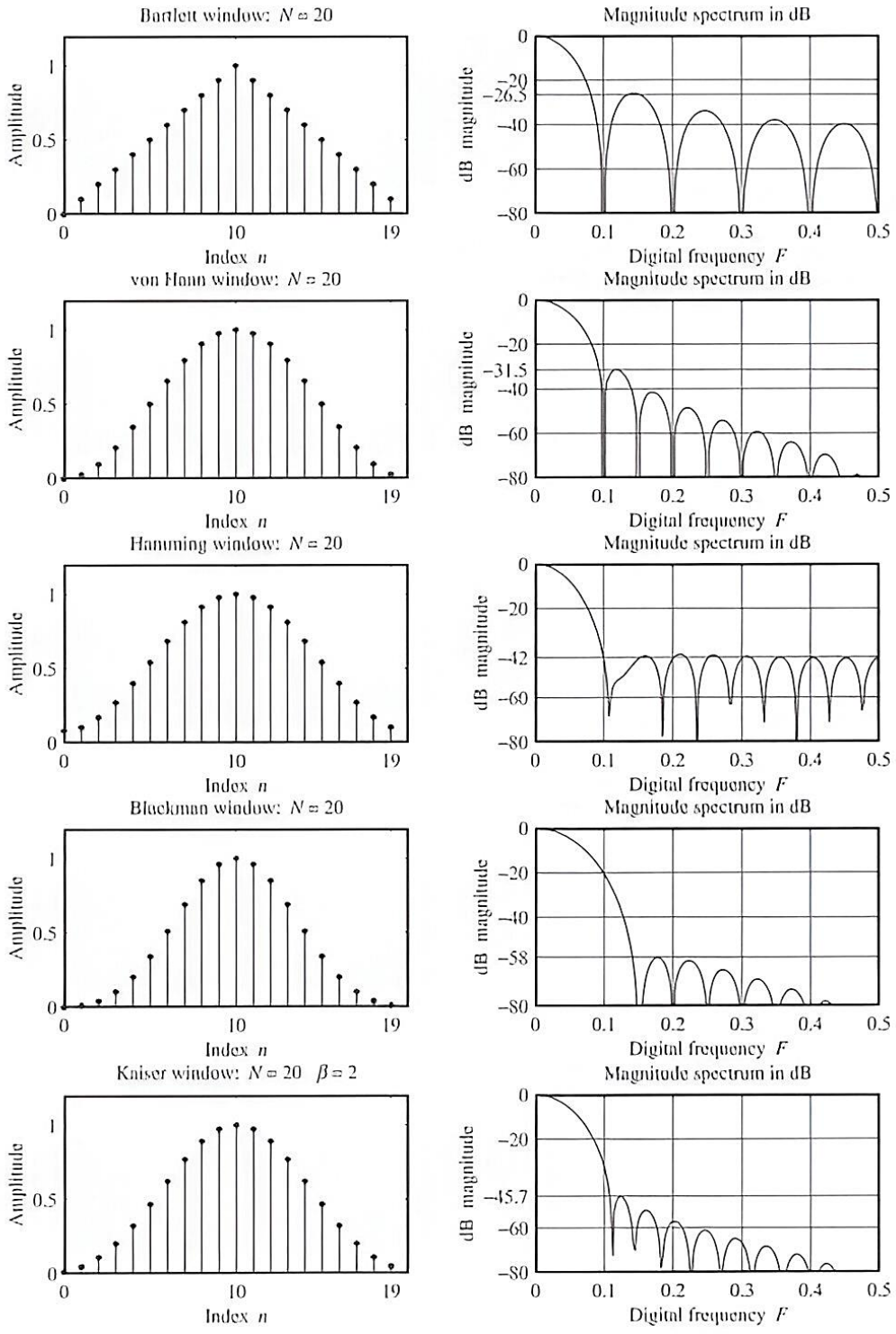



Figure 2.5 most frequent window functions

### 2.3.1.2 The Short-Time Fourier Transform (Sliding window)

To avoid the disadvantage of the global nature of the Fourier transform, an idea introduced by Gabor [119] in 1946 is to "truncate" the signal. The basic concept is to divide the signal into regular intervals or windows and perform a Fourier analysis on each of them. This provides information about the frequencies contained in the signal, as well as the position of the time

intervals to which these frequencies belong. Figure 2.6 illustrates the principle of the Short-Time Fourier Transform (STFT) :

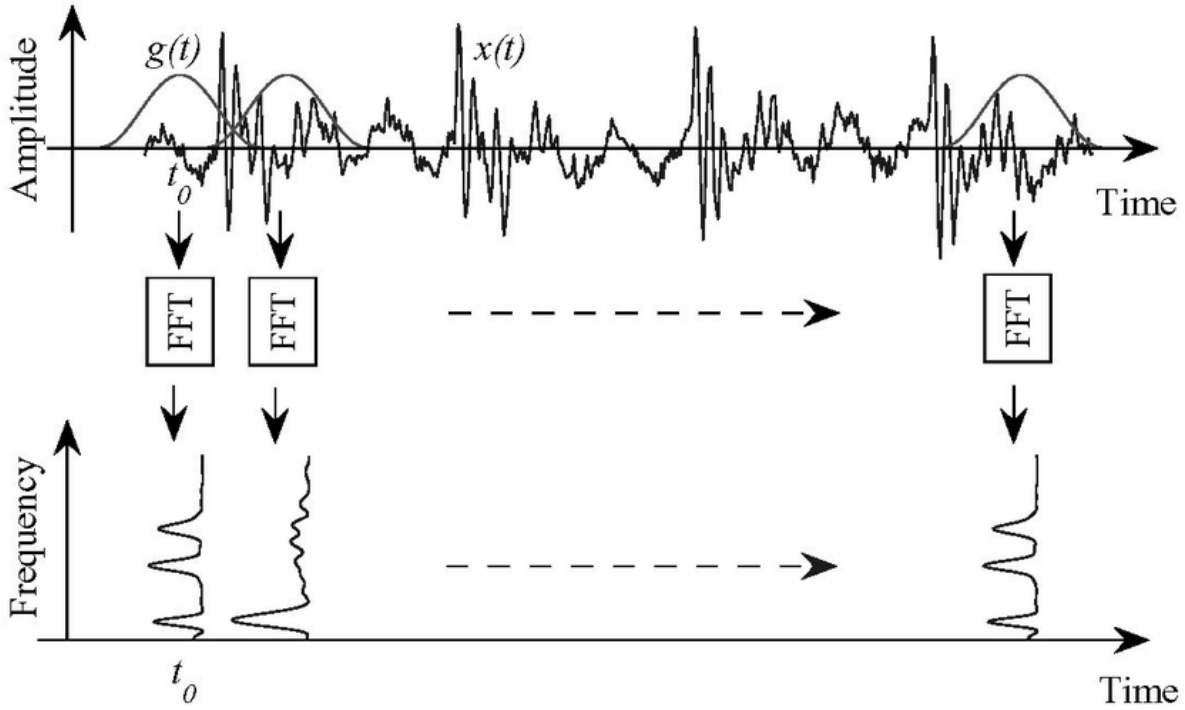


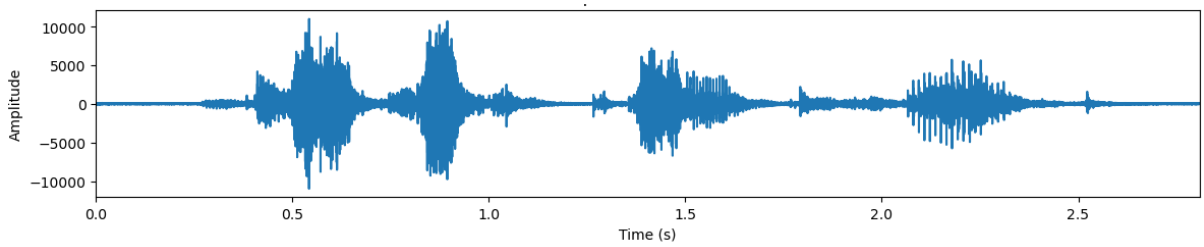

Figure 2.6 Principle of the Short-Time Fourier Transform

From a mathematical perspective, the STFT can be interpreted as the Fourier analysis of successive segments weighted by a time window. This principle is equivalent to approximating the signal by a set of elementary functions that are semi-localized simultaneously in both time and frequency.

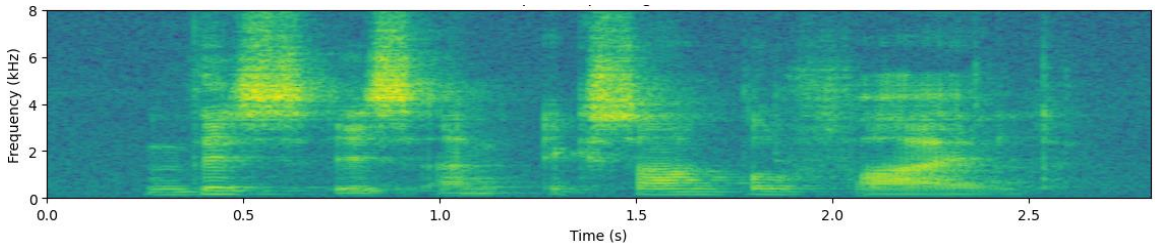
$$G_x(t,v) = \int x(\tau)h^*(\tau)d\tau = \int x(\tau)h^*(\tau - t)e^{-j2\pi v\tau}d\tau \qquad (2.3)$$

The signal is characterized by x(τ), and $h^*(\tau)$ is a windowing function centered around *t*. To obtain the spectral representation around *t*, it is sufficient to translate the window $h^*(\tau)$ and perform a Fourier transform on the windowed signal. The mother window $h^*(\tau)$ can be chosen arbitrarily, with the simplest being the rectangular function (a box function) over an analysis duration *T*. However, it is also advisable to choose a function that has both good time-frequency localization and good regularity (rapid decay, and differentiability up to n times) [120]. The square of the magnitude of the STFT is generally referred to as the spectrogram.

$$S_x(t,v) = |G_x(t,v)|^2 \qquad (2.4)$$



(a)




(b)

Figure 2.7 a- time domain signal, b-spectrogram

However, one major drawback of the Short-Time Fourier Transform (STFT) method should be noted. Indeed, the window size is fixed, which is a significant limitation when dealing with signals whose variations can span a wide range of magnitudes.

### 2.3.1.3 Discrete Fourier Transform

The Fourier transform performed on a sampled signal is called the Discrete Fourier Transform (DFT). The DFT of a sequence of $N_e$ terms $x(0)$, $x(1),\ldots,x(N_e-1)$ is the sequence of $N_e$ terms $X(0),X(1),\ldots,X(N_e-1)$ defined by the following formula:

$$X(k) = \sum_{n=0}^{N_e-1} x(n) e^{-j\frac{2\pi}{N_e}kn}, k = 0,1,\ldots,N_e-1 \qquad (2.5)$$

Where :

$X(k)$: frequency domain representation of the signal ;

$x(n)$: time domain samples ;

$N_e$ : number of samples ;

$k$ : index corresponding to the frequency bin ;

$j$: imaginary unit ($j^2 = -1$).

### 2.3.1.4 Fast Fourier Transform

The Fast Fourier Transform (FFT) is simply an algorithm designed to reduce the number of operations, particularly the number of multiplications, required to compute the DFT. This reduction in computational time is crucial for implementing digital systems in real-time.

### 2.3.2 Wavelet Transform

We previously saw that both the Fourier transform and the STFT have major drawbacks. The Fourier transform is a global transformation, while the STFT is local, but both have fixed time resolution. The wavelet transform allows us to overcome this limitation. It is indeed necessary to have a tool that adapts its resolution to the size of the object or detail being analyzed.

#### 2.3.2.1 Definition

A wavelet is a wave function that has a zero mean and a limited duration. The wavelet transform (WT) is a mathematical tool that decomposes a signal into frequencies while preserving its temporal localization. The original signal is projected onto a set of basic functions that vary in both frequency and time. The window has a constant surface area, but its size varies depending on the frequency being analyzed.

#### 2.3.2.2 Mother wavelet

Wavelet analysis is performed using a function $\psi$ (t) (called the mother wavelet), which specifies the characteristics of the signal that we want to detect. WT allows a signal to be represented by a set of wavelets, which are simply dilated and translated versions of the mother wavelet, as given by :

$$\psi_b^a(t) = \left|\frac{1}{\sqrt{a}}\right| \psi\left(\frac{t-b}{a}\right) \qquad (2.6)$$

$\psi\left(\frac{t-b}{a}\right)$ represents daughter wavelet ;

$b$ : translation factor ;

$a$ : translation scale ;

$\psi$ (t) : mother wavelet ;

$\left|\frac{1}{\sqrt{a}}\right|$ : energy normalization factor (to ensure that the transformed signal has the same energy at all scales).

The WT has the ability to change the size of the window at different time-frequency resolutions. Through scaling, the wavelet basis functions can be stretched or compressed within the analysis window. This helps isolate signal discontinuities because short basis functions are used for detailed frequency information, while long basis functions are used to capture the approximate frequency information of the signal. Translation is the operation of sliding the wavelet across the signal. This technique is similar to the one used in the STFT.

#### 2.3.2.3 Continuous Wavelet Transform

The Continuous Wavelet Transform (CWT) is a time-frequency, or more correctly, a time-scale representation We can define CWT. Suppose that $\psi$ (t) is a mother wavelet, meeting the admissibility condition, and that $s(t)$ is a finite energy signal. The CWT of $s(t)$ is the function of two variables, a> 0 and b, defined by

$$CWT(a,b)\frac{1}{\sqrt{a}}\int_{-\infty}^{\infty} s(t)\psi*\left(\frac{t-b}{a}\right)dt \qquad (2.7)$$

CWT can be viewed as a filtering of the signal by a dilated version of the mother wavelet, defined and denoted by $\psi_a(t) = 1/\sqrt{a}\psi(-t/a)$., the frequency translation is effected by dilation and contraction rather than by modulation. Figure 2.9 illustrates the dilate wavelets for

different values of the so-called scaling variable a. As can be seen, for a > 1, the dilated wavelet expands in time ; for a < 1, the dilated wavelet contracts in time. Regarding the wavelet as a sort of window in time, the window width adjusts, depending on scale, widening for large-scale (low-frequency) information and narrowing for small-scale (high-frequency) content.

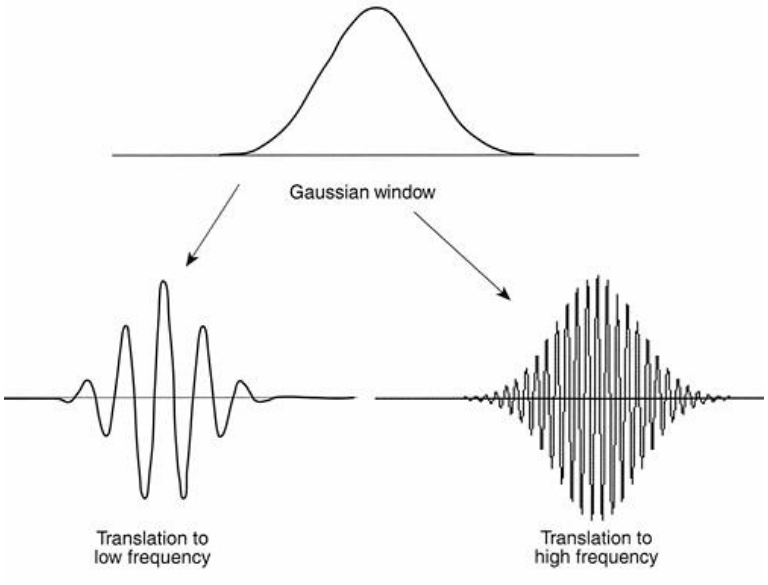



Figure 2.8 Translation of a window in frequency via modulation.

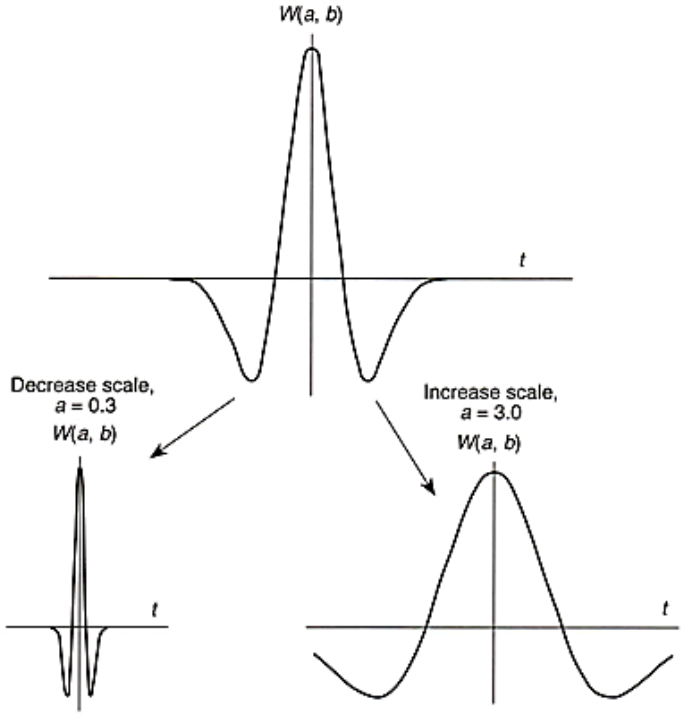



Figure 2.9 Frequency translation of the Mexican Hat function via scaling (dilation) : time domain.

### 2.3.2.4 Discrete Wavelet Transform

The Discrete Wavelet Transform (DWT) was developed to overcome the limitations of the Continuous Wavelet Transform (CWT). Indeed, it is evident that the CWT cannot be manually computed using analytical equations or integral calculus; this transformation relies on computers for its computation. Therefore, it becomes necessary to discretize the transformations [121]. Unlike the CWT, the DWT provides sufficient information for both the analysis and reconstruction of the original signal while significantly reducing computational time. The DWT translates and dilates the wavelet according to specific scale and translation factor values, as defined by :

$$a = a_0^m \text{ et } b = nb_0a_0^m \text{ où } a_0 > 1 \text{ et } b_0 > 0 \text{ avec } a_0, b_0 \in Z$$

The coefficients of the DWT are defined by :

$$DWT(m,n) = a_0^{\frac{-m}{2}} \int_{-\infty}^{+\infty} x(t)\psi\left(\frac{t - nb_0a_0^m}{a_0^m}\right) \qquad (2.8)$$

If we take $a_0$= 2 and $b_0$= 1, we are then in the case of the dyadic discrete wavelet transform.

### 2.3.2.5 Multiresolution Wavelet Analysis (MRA)

The multiresolution approach [122] using wavelets has become fundamental in signal theory. Multiresolution analysis defines linear operators that enable the analysis of a signal at different scales. Developed in late 1986 by Meyer [123] and Mallat [124], it provides a tool to view a signal "up close" or "from afar." This "zooming" is achieved using a scaling function $\Phi$, which dilates across scales. This function, along with its time-translated versions, generates a space called the approximation space. When the signal is projected onto these functions, it provides a representation of the original signal at a higher scale. The coefficients resulting from this projection form a "zoomed-out" version of the original signal, referred to as the approximation coefficients cA.

The signal is also projected onto a perpendicular space to retain all the information. The function generating this second vector space is the wavelet function $\psi$, which produces the detail coefficients (cD) and allows the recovery of information lost in the first projection.

As we will see later, the scaling function acts as a low-pass filter $g(n)$, and the wavelet function acts as a high-pass filter $h(n)$.

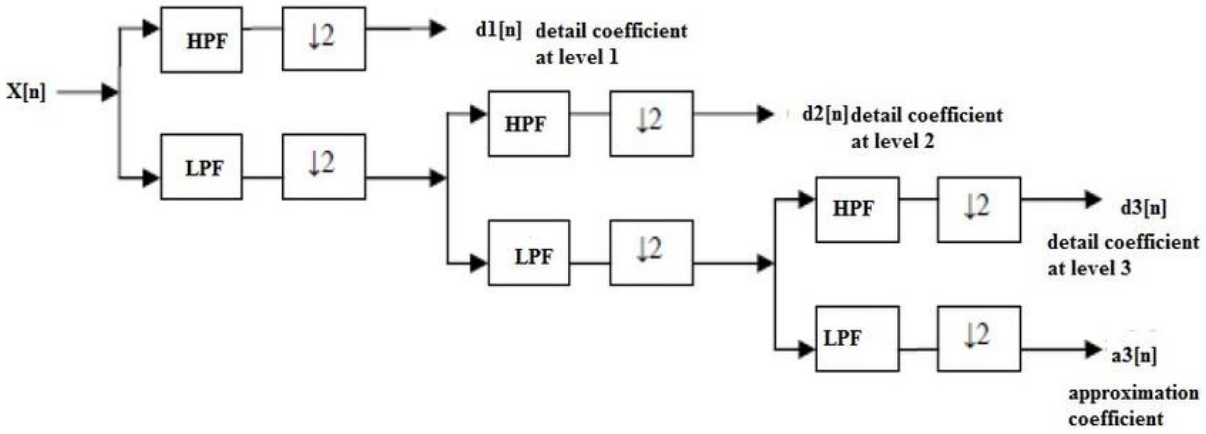



Figure 2.10 Three level decomposition of a signal.

Approximation and details coefficients at j level are expressed as follows :

$$cA_j(n) = \sum_k g(2n-k)cA_{j-1}(k);$$
$$cD_j(n) = \sum_k h(2n-k)cA_{j-1}(k).$$

Necessary decomposition level is calculated through :

$$L = \text{int}\left(\frac{\log(f_{ech}/f)}{\log(2)}\right) + 2 \qquad (2.9)$$

Where int : integer and the frequency band for each decomposition level $J$ corresponds to $[1 - \frac{f_{ech}}{2^j}]$ for the approximations and $[\frac{f_{ech}}{2^j} - \frac{f_{ech}}{2^{j-1}}]$ for the details.

By calculating the energy associated with each decomposition level, a highly effective diagnostic tool can be constructed. The energy in each frequency band is defined as :

$$E_j = \sum_{k+1}^{k=n} \left|cD_{j,k}(n)\right|^2 \qquad (2.10)$$

Where $j$ is the decomposition level. Based on energy value, we can produce a vector as follows :

$$T = \left[\frac{E_0}{E}, \frac{E_1}{E}, \frac{E_2}{E}, \dots, \frac{E_2 m_{-1}}{E}\right] \qquad (2.11)$$

Where

$$E = \sum_{j=0}^{2^m-1} \left|E_j\right|^2 \qquad (2.12)$$

## 2.4 Artificial Intelligence

### 2.4.1 Machine Learning

#### 2.4.1.1 Definition

What is Machine learning ? machine learning, also known as artificial learning or statistical learning, is a field of study within artificial intelligence that relies on mathematical and statistical approaches to enable computers to "learn" from data. This means improving their performance in solving tasks without being explicitly programmed for each specific task.

More broadly, it involves the design, analysis, optimization, development, and implementation of such methods. The term "statistical learning" is used because learning involves creating a model with the lowest possible average statistical error.

#### 2.4.1.2 overview

Three main approaches fall under the domain of machine learning : supervised learning, unsupervised learning, and reinforced learning. Of course, this classification is open to discussion, as methods like semi-supervised learning or weakly supervised learning (for example) often exist at the interfaces of these approaches.

Before diving into supervised or unsupervised learning, let us focus on the concept of data.

### 2.4.2 Types of machine learning

Several machine learning types can be counted, and each type has its specification;

#### 2.4.2.1 Supervised learning

In supervised learning, algorithms are trained using labeled data, where each input is paired with its corresponding expected output. The algorithm learns by analyzing the differences between the predicted outputs and the true outputs, adjusting the model to minimize errors. Common applications of supervised learning include classification and regression [125].

#### 2.4.2.2 unsupervised learning

Given a dataset of size $N$ consisting solely of input data $(x_1)$, $(x_2)$, …, $(x_N)$, the model must independently uncover hidden structures within the data. This type of task is often referred to as data partitioning or *clustering*. An example of an unsupervised learning algorithm is *K-means*, which outputs a set of labels. It assigns each label a reference point $x_i$ known as the centroid of cluster $k_i$. Each data group is defined by creating a centroid for that group, with the centroids serving as the core of the cluster. These centroids capture the nearest points and add them to the cluster.

Centroids are updated based on the dataset and the chosen distance metric. Other unsupervised learning algorithms include methods for dimensionality reduction, such as Principal Component Analysis (PCA) (Jolliffe, 2005) and Singular Value Decomposition (SVD) (Golub et al., 1983 ; Alter et al., 2000). Additionally, some algorithms aim to estimate the density distribution of the data, like Kernel Density Estimation (KDE) (Terrell et al., 1992).

#### 2.4.2.3 Semi-supervised learning

Given a training dataset of size $N$ consisting of partially labeled data $(x_1)$, $(x_2, y_2)$, …, $(x_{N-1})$, $(x_N, y_N)$, the model aims to uncover the underlying distribution of the examples in their feature space, either probabilistically or non- probabilistically

For instance, generative approaches based on statistical learning aim first to estimate $p(x|y)$, the distribution of data points belonging to each class. The probability $p(y|x)$, which indicates the likelihood of a point $x$ having label $y$, is then proportional to $p(x|y)p(y)$ according to Bayes' theorem. Naive Bayes classification is a straightforward probabilistic classification method based on Bayes' theorem [126].

#### 2.4.2.4 Reinforcement Learning

The model learns behavior based on observation. The algorithm's action on the environment generates a return value (reward) that guides the learning process. This reward can be positive or negative, depending on the expected outcome of the action. The algorithm aims to maximize its reward and learn from its past actions. For instance, Q-learning [127] is a model-free reinforcement learning algorithm used to learn the value of an action in a particular state.

#### 2.4.2.5 Transfer Learning

It emphasizes a system's ability to recognize and apply knowledge and skills. Starting with a model that has been trained on a previous task that is different but similar to a new desired task, it is possible to fine-tune the model and adapt it to the new task.

### 2.4.3 Supervised learning techniques

Two main supervised learning models are mentioned in the literature, classification and regression model [128], in which each model contains several algorithms that will be cited alongside the chosen algorithms in this research.

#### 2.4.3.1 Classification techniques

**Definition**

An algorithm is a set of operations followed in a precise order to solve a problem or provide new solutions, such as learning by an artificial intelligence system.

This is exactly the role of classification algorithms used in machine learning. They allow the software to autonomously learn from multiple datasets.

The idea is to classify the different elements of a dataset into several categories. These categories group the data based on their similarity. Since the data share common characteristics, it becomes easier to predict their behavior.

For example, in an e-commerce store, users who visit the site multiple times are more likely to make a purchase than those who never return. The classification algorithm segments users into different categories to help the company tailor its communication [129].

The classification algorithm is part of supervised learning methods. This means that predictions are made based on historical data.

Unlike unsupervised learning, where there are no predefined classes, supervised learning involves using labeled data to predict outcomes. The categories must be formed based on common attributes before making predictions.

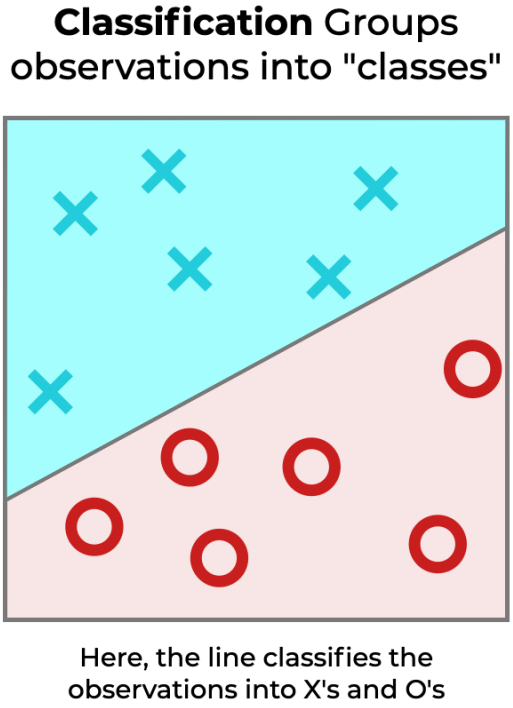



Figure 2.11 Classification concept

**(a) Support Vector Machines**

Support Vector Machines (SVM) are a set of supervised learning techniques designed to solve classification and regression problems. SVMs are a generalization of linear classifiers, as they aim to separate data in high-dimensional spaces using a hyperplane. We will detail this model as it is commonly used in literature.

SVMs were developed in the 1990s by Vladimir Vapnik based on the development of the Vapnik-Chervonenkis statistical theory [130]. SVMs were quickly adopted for their ability to work with high-dimensional data, their few hyperparameters, their theoretical guarantees, and their strong practical performance. They are particularly robust when the dataset is not excessively large.

The resolution of classification problems involves constructing a function $h$ that maps an input vector $x$ to an output $y$ : $y = h(x)$. The simplest case is a linear classification function, obtained by a linear combination of the input vector $x = (x_1, ..., x_N)^T$, with a weight vector $\omega = (w_1, ...., w_N)^T$ . For this function, the output is given by :

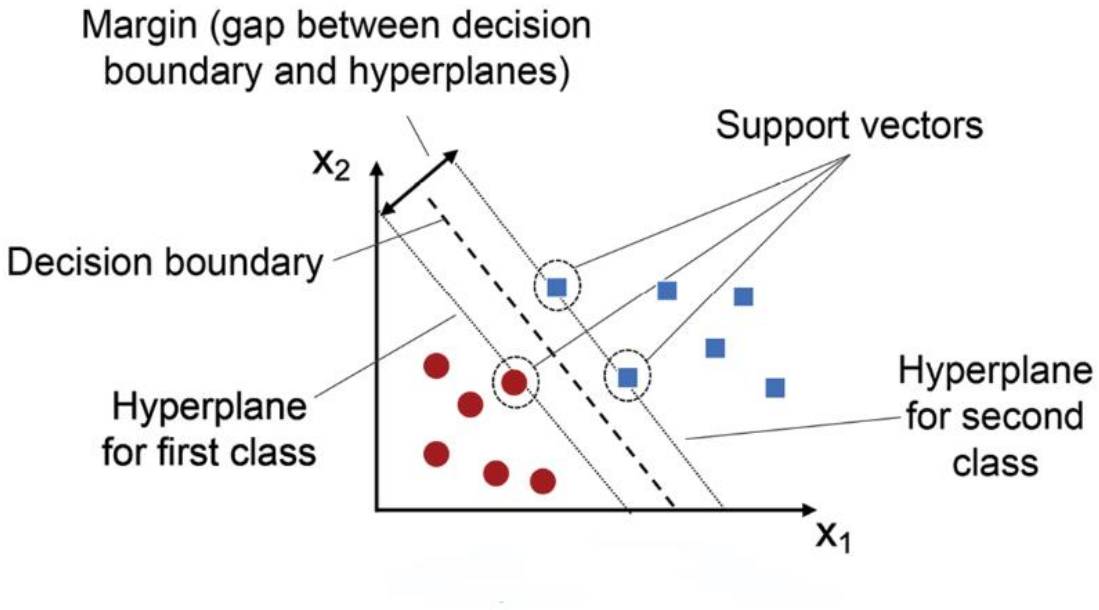
$$h(x) = w^T x + b_0 \qquad (2.13)$$

With $b_0$ being a real number that allows us to work with an affine hyperplane (bias), it is decided that $x$ is labeled as 1 if $h(x) \geq 0$ and labeled as -1 otherwise. This is a linear classifier. The decision boundary $h(x)= 0$ is a hyperplane, called the separating hyperplane. In a finite-dimensional vector space of dimension $N$, a hyperplane is a subspace of dimension $N$ - 1. Thus, in a 2-dimensional space, a hyperplane will be a line, in a 3-dimensional space, a hyperplane will be a plane, and so on.

If the problem is linearly separable, we should have :

$$l_k h(x_k) \geq 0 \text{ where } l_k(w^T x_k + b_0) \geq 0 \qquad (2.14)$$

With $p$ being the size of the training dataset, $l_k$ the label associated with the input data $x_k$ and $1 \leq k \leq p$.




2.12 Support vectors in classification

**(b) K-Nearest Neighbors**

The fundamental concept of K-Nearest Neighbors KNN is to determine the class of a test instance by considering the classes of its k nearest neighbors from the training set, under the assumption that the class of an instance is similar to that of its nearest neighbors. KNN is straightforward to implement and delivers strong predictive performance. Additionally, it is an instance-based learning algorithm, which allows for easy implementation of incremental learning. KNN does not make explicit assumptions about the data distribution. Due to these advantages, KNN has been widely used in various supervised learning tasks for classification and regression [131]. KNN is a non-parametric, lazy learner that relies on the dataset rather than a predefined model. During the training phase, only the dataset is loaded into memory for future classification calculations. The method uses a distance function to assess how far an unclassified instance is from other instances in the dataset. The k closest instances are identified,

and the majority class of these neighbors is assigned to the new instance. The two key parameters for KNN are the distance metric and the value of k used for classification [132].

To estimate a density φ at $x$, a ball $B_x$ centered at $x$ is considered, containing $K$ observations out of the total $N$ available observations, which follow the distribution φ.

According to the law of large numbers, the expected value of the indicator function of the ball $B_x$,

$$\int_{B_x} \phi(y)\mathrm{d}y \simeq \frac{K}{N} \tag{2.15}$$

If we assume that the density φ is approximately constant over the ball Bx :

$$\int_{B_x} \phi(\boldsymbol{y})\mathrm{d}\boldsymbol{y} \simeq \phi(\boldsymbol{x}) \times \mathrm{Volume}(B_{\boldsymbol{x}}) \tag{2.16}$$

So :

$$\frac{K}{N} \simeq \int_{B_x} \phi(\boldsymbol{y})\mathrm{d}\boldsymbol{y} \simeq \phi(\boldsymbol{x}) \times \mathrm{Volume}(B_x) \tag{2.17}$$

We derive the $K$ nearest neighbors estimator :

$$\phi(\boldsymbol{x}) = \frac{K}{N \times V_k(x)} \tag{2.18}$$

where $V_k(x)$is the volume of a sphere centered at $x$ containing the K-nearest neighbors of $x$, over which the density is assumed to be constant.

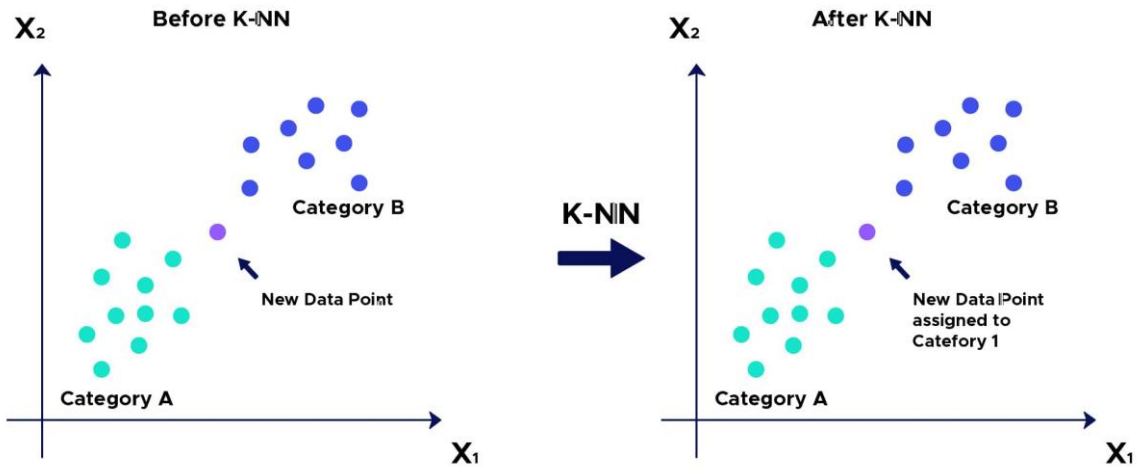



Figure 2.13 K-NN classification concept

**(c) Logistic Regression Classifier**

Logistic regression is a statistical method used to model the probability of a binary event (i.e., an event with two possible outcomes, such as success/failure, yes/no, etc.) based on one or more independent variables. Unlike linear regression, which predicts a continuous value, logistic regression predicts the probability of an event occurring.

As a classification algorithm, logistic regression is used to predict the probability that an observation belongs to a particular class. For example, it can be used to determine whether an email is spam or not, or to predict whether a patient has a particular disease based on their symptoms.

Logistic regression is particularly useful when the outcomes are binary (two possible categories). It uses a logistic function to model the relationship between the independent variables and the binary dependent variable.

$$P(Y = 1 \mid X) = \frac{1}{1 + e^{-(\beta_0 + \beta_1 X_1 + \beta_2 X_2 + \cdots + \beta_n X_n)}} \tag{2.19}$$

Where,

$P(Y = 1 \mid X)$ is the probability that the event $Y$ occurs given the variables $X$;

$\beta_0$ is the intercept;

$\beta_1, \beta_2, \ldots \beta_n$ are the coefficients of the independent variables $X_1, X_2, \ldots X_n$.

**(d) Naïve Bayes**

Naive Bayes is a family of simple, yet powerful classification algorithms based on the application of Bayes' theorem with strong (naive) independence assumptions between features. It is particularly useful for large datasets and is commonly used for text classification tasks, such as spam detection, sentiment analysis, and document categorization.

The Bayes' theorem is expressed as follows:

$$P(A \mid B) = \frac{P(B \mid A) \cdot P(A)}{P(B)} \tag{2.20}$$

$P(A \mid B)$ is the posterior probability of class $A$ given the feature $B$. It represents the probability that class $A$ is the correct class for the observed feature $B$;

$P(B \mid A)$ is the likelihood, which is the probability of observing feature $B$ given that the class is $A$;

$P(A)$ is the prior probability of class $A$, reflecting how likely class $A$ is before observing the feature $B$.

$P(B)$ is the prior probability of the feature $B$, representing the overall probability of observing feature $B$ in the dataset, regardless of the class.

**(e) Tree-Based Models**

- *Decision Trees*

This technique ranks among the most vital supervised learning methods. It is structured with branches, nodes, and leaves, making decisions from the tree's root to its leaves. Each branch culminates in a leaf that displays the resulting outcome. The intermediate nodes in the tree contain tests on specific attributes, which distribute data points among various sub-trees. The aim of the learning phase is to identify groups of examples as uniformly as possible. During test phase, new examples are assigned to the majority class of the leaf, based on a score that reflects the proportion of training examples in that leaf belonging to the same class [133].

There are algorithms available for constructing decision trees from a set of observations, such as the CART algorithm (Classification and Regression Trees), which we will describe. CART builds binary decision trees: each decision is a "yes" or "no." In graph theory terminology, this means each node of the tree has two children, except for the leaves. It is a recursive algorithm that successively constructs binary decision rules.

We assume that there is a finite set $\mathcal{S}$ of observations. Since this set is finite, each feature $x_i$ can only take a finite number of distinct values.

Since the number of training observations is finite, the algorithm eventually terminates. In algorithmic terms, this is referred to as a "greedy algorithm".

Let $p_k$ denote the proportion of observations in the current subset belonging to class $k$ ($k \in \{1, ..., K\}$ where $K$ represents the number of classes). Several segmentation criteria $C$ can be used; the most common ones include:

- Gini impurity :

$$C_{\text{Gini}} = 1 - \sum_{k=1}^{K} p_k^2 \tag{2.21}$$

Measures the impurity of a subset, with lower values indicating purer splits.

- Entropy (information gain)

$$C_{\text{Entropy}} = -\sum_{k=1}^{K} p_k \log_2(p_k) \tag{2.22}$$

Quantifies the uncertainty or disorder in a subset, often used in decision tree algorithms.

- Misclassification error

$$C_{\text{Error}} = 1 - \max_k(p_k) \tag{2.23}$$

- *Random Forests*

Decision trees are highly sensitive to variations in training observations. As a result, this type of classifier likely exhibits significant fluctuation, making the **bagging** technique particularly suitable.

As mentioned earlier, bagging is effective when weak classifiers have independent error probabilities, which justifies the use of bootstrap sampling. For decision trees, additional randomness is introduced during their construction. Instead of considering all *d* features to compute the splitting criterion, a random subset of mmm features is chosen

**(f) Ensemble Methods**

An ensemble of classifiers, also referred to as a committee, is a model built by combining several weak learners. The boosting strategy, along with classifier ensemble, involves training multiple weak classifiers and merging them, instead of focusing on creating a single strong classifier. This concept of building ensembles of classifiers has gained significant attention in recent years [134], based on the idea that it might be easier to train several simple classifiers and combine them into a more complex classifier, rather than attempting to train one intricate classifier.

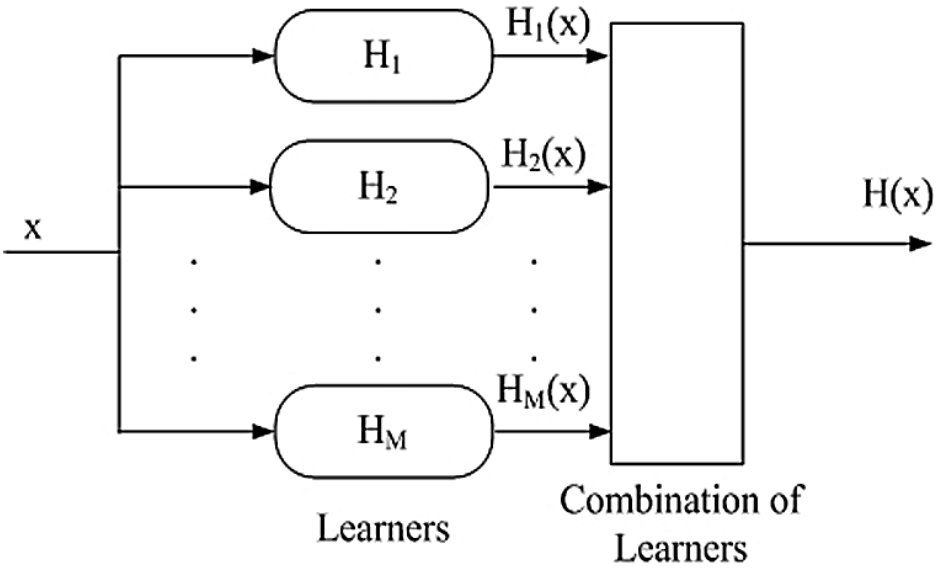



Figure 2.14 ensemble classifiers combination

The ensemble prediction function is expressed as follows :

$$H(\mathbf{x}) = \text{sign}\left(\sum_{m=1}^{M} \alpha_m H_m(\mathbf{x})\right) \qquad (2.24)$$

where

$H(\mathbf{x})$ : ensemble of classifiers ;

$H_m(\mathbf{x})$ : outputs of the weak learners, with $m \in \{1, \ldots, M\}$ ;

$\alpha_1$,..., $\alpha_M$ is a set of weights.

(g) **Bagging** :

- *Bootstrap*

In bagging techniques, weak classifiers are built by training a classifier from a given family on subsets of the original training set. These subsets are called bootstrap samples, which are created by random sampling with replacement from the initial dataset. As a result, some observations may appear multiple times in the same sample, and the bootstrap samples may share common observations. The random sampling with replacement is assumed to ensure the independence of the weak classifiers' responses, as each bootstrap sample is constructed independently of the others. Each bootstrap sample is used to construct a classifier, and then a strong classifier aggregates (combines) the predictions from these different classifiers when faced with a new observation, for example, by selecting the majority class among the predicted classes. The name "bagging" comes from Bootstrap AGGregatING.

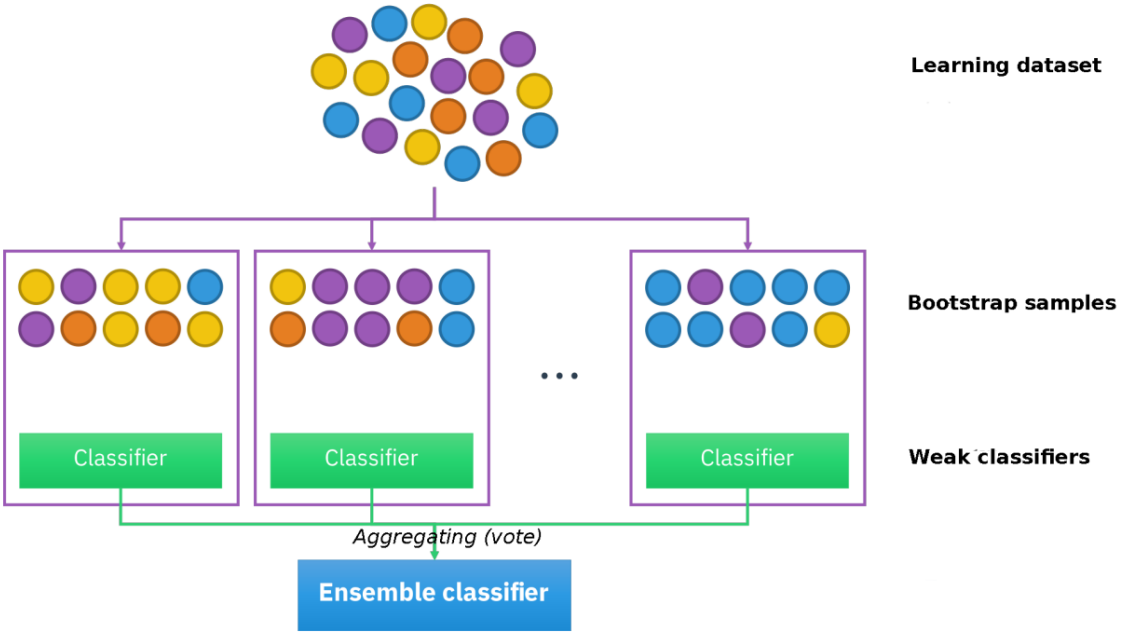



Figure 2.15 Parallel classifiers employment (Bagging)

- *Random Forest (RF)*

Random Forests is a versatile ensemble learning algorithm that combines the power of multiple decision trees to make robust predictions. It operates by constructing a multitude of decision trees during training and outputs the mode of the classes (classification) or the average prediction (regression) of the individual tree.

**(h) Boosting**

In boosting techniques, weak classifiers are built sequentially on the entire dataset. At each step, a classifier is constructed based on previous classifiers, with increased weight given to observations that were incorrectly predicted in earlier stages. This focuses the learning efforts

on difficult-to-classify instances. The boosting technique aims to improve model accuracy by reducing bias and variance over time.

In essence, each new classifier attempts to correct the mistakes made by the previous ones, adjusting the model's focus on harder cases. The key concept is the weighted emphasis on misclassified points, which allows the algorithm to gradually refine its predictions.

This idea is typically represented in a diagram, such as Figure 2.16 in certain literature, where each iteration builds upon the previous one to form a stronger overall model.

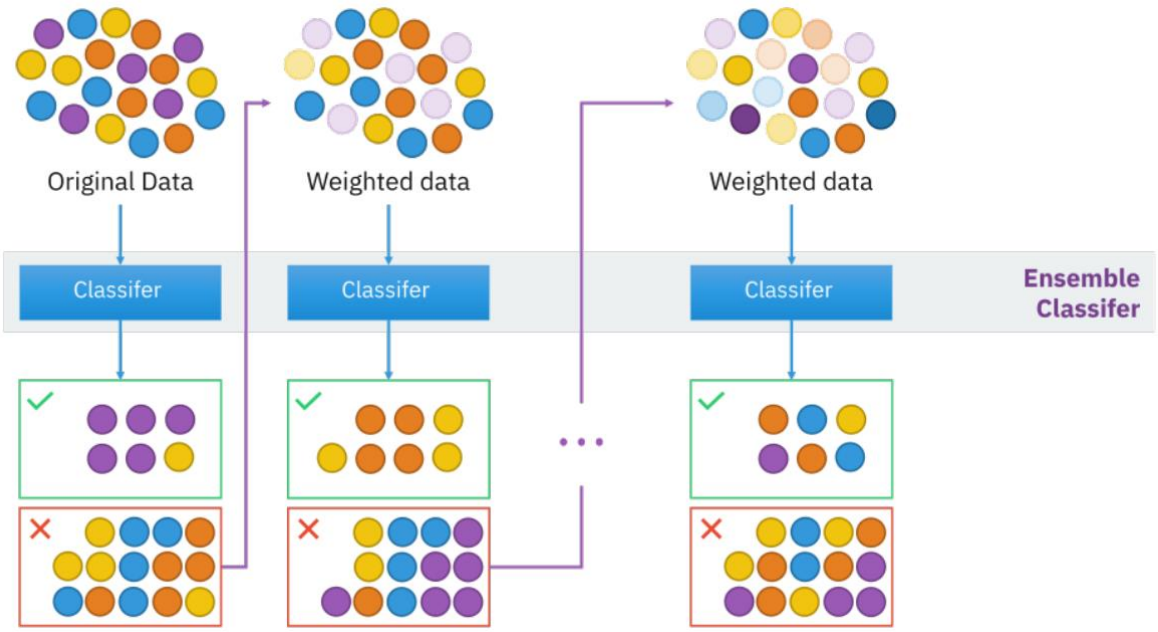



Figure 2.16 Sequential classifiers employment (Boosting)

- *AdaBoost*

The most well-known boosting method is probably AdaBoost (ADAptive BOOSTing). It is a general technique for constructing a strong classifier from weak classifiers.

We select from the set the weak classifier that minimizes the empirical risk, i.e., one that makes errors on the training set. The idea is to combine this classifier with another weak classifier that performs better on the misclassified observations. To do this, we select from the set the weak classifier that minimizes a weighted empirical risk, where the previously misclassified observations are given more weight. The new weak classifier still makes errors, and this process continues. The response of the ensemble classifier will be the sign of a weighted average of the responses from the intermediate weak classifiers.

- *Gradient boosting*

In Gradient Boosting, we generalize the concept of adaptive boosting with other loss functions supposed differentiable.

The idea is to minimize the Empirical risk $E_m$ in (2.25) to the steepest descent, a limited development to 1st order gives us in (2.26) :

$$E_m = \sum_{i=1}^{N} \ell\big(y_i, K_m(\boldsymbol{x}_i)\big) \tag{2.25}$$

Where

$\ell$ : exponential function loss;

$K_m$ : prediction error, $K_m = K_m{-}1 + \alpha_m h_m$;

$\alpha_m$ : classifier weight ;

$h_m$ : weak classifiers.

$$\begin{aligned} E_m &= \sum_{i=1}^{N} \ell\big(y_i, K_{m-1}(\boldsymbol{x}_i) + \alpha_m h_m(\boldsymbol{x}_i)\big) \\ &\simeq \sum_{i=1}^{N} \ell\big(y_i, K_{m-1}(\boldsymbol{x}_i)\big) + \alpha_m \sum_{i=1}^{N} \frac{\partial \ell}{\partial y}\big(y_i, K_{m-1}(\boldsymbol{x}_i)\big) h_m(\boldsymbol{x}_i) \\ &= E_{m-1} + \alpha_m \sum_{i=1}^{N} \frac{\partial \ell}{\partial y}\big(y_i, K_{m-1}(\boldsymbol{x}_i)\big) h_m(\boldsymbol{x}_i) \end{aligned} \tag{2.26}$$

According to the choice of loss function, gradient boosting adapts itself to problems of classification or regression.

- *eXtreme Gradient Boosting (XGBoost)*

XGBoost (eXtreme Gradient Boosting) is a highly popular machine learning algorithm known for its exceptional performance in practical applications, particularly in Kaggle competitions. It is a type of gradient boosting where the weak classifiers are decision trees or regression trees. Unlike traditional gradient boosting that uses a first-order approximation during the minimization process, XGBoost employs a second-order approximation, allowing for more accurate gradient calculations. Additionally, XGBoost includes a regularization term to prevent overfitting, which enhances its robustness and generalization abilities, making it suitable for large datasets and complex problems [135]

- *LightGBM*

LightGBM is a gradient boosting ensemble method used by tools like AutoML for training models, based on decision trees. Similar to other tree-based methods, LightGBM can be applied to both classification and regression tasks. The algorithm is optimized for high performance in distributed systems.

LightGBM builds decision trees that support leaf nodes, meaning that only one leaf is split at each given condition based on the gain. However, trees that support leaf nodes can sometimes

lead to overfitting, especially with smaller datasets. To mitigate overfitting, limiting the tree depth can be helpful.

**(i) Neural Networks**

Artificial neural networks are computer systems originally inspired by biological neural networks. These systems learn to perform tasks by analyzing examples, typically without being explicitly programmed with task-specific rules.

A neural network is a model based on a collection of interconnected units or nodes called artificial neurons, which mimic the neurons of a biological brain. Each connection, like synapses in the nervous system, can transmit information, referred to here as a signal, from one artificial neuron to another. An artificial neuron receiving a signal can process it and then transmit a signal to other connected artificial neurons.

- *Multi-Layer Perceptron (MLP)*

**Perceptron :**

The perceptron is a supervised learning algorithm designed for binary classifiers, meaning it separates data into two distinct classes. It was invented in 1957 by Frank Rosenblatt [136]. The perceptron can be considered the simplest type of neural network and functions as a linear classifier. It has an input vector $x$ consisting of $n$ attributes $x = (x_1, ..., x_n)$, and a single output $O$, defined by a specific formula:

$$O = f(x) = \begin{cases} 1 \; if \; \sum_{i=1}^{n} w_i x_i \geq \theta \\ 0 \; else \end{cases} \qquad (2.27)$$

Where $w = (w_1, \ldots, w_n)$ are n weights (or synaptic coefficients) and $\theta$ is a bias (or threshold)

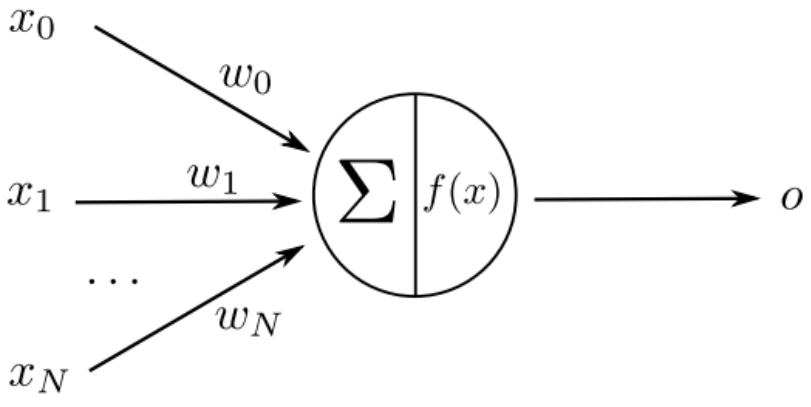



Figure 2.17 Perceptron Model representation

- Simple Multi-Layer Perceptron

In common neural network implementations, the connection between artificial neurons is represented by a real number, and the output of each artificial neuron is calculated as a nonlinear function of the sum of its inputs. The connections between artificial neurons are referred to as edges. Both artificial neurons and edges typically have a weight that adjusts during the learning process. This weight increases or decreases the intensity of the signal at a given connection.

Artificial neurons may have a threshold, meaning the signal is only transmitted if the aggregated signal surpasses this threshold. Generally, artificial neurons are grouped into layers. Each layer can perform different types of transformations on its inputs. Signals travel sequentially through these layers, starting from the input layer and moving to the output layer.

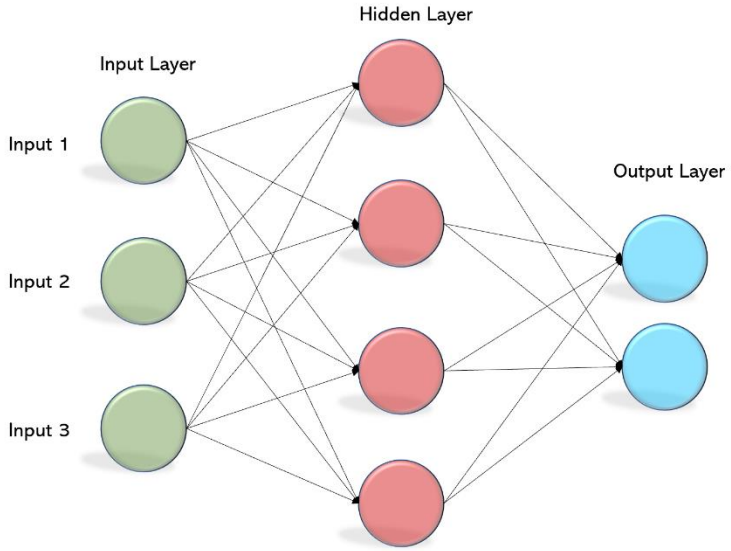


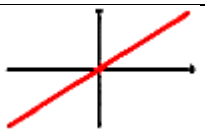
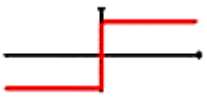
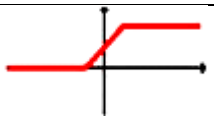
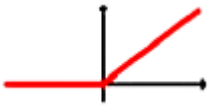

Figure 2.18 Simple Multi-layer Perceptron representation

- Activation function

The activation function is a mathematical function applied to the output signal of an artificial neuron. The term "activation function" originates from the biological concept of the activation potential of a neuron, representing the stimulation threshold that triggers a response from the neuron once exceeded.

Activation functions are often nonlinear and determine whether a neuron should activate by transforming the input signal. An example of an activation function is the Heaviside function, used by the perceptron. It outputs 1 if the input signal is positive and 0 if it is negative, as described by the related mathematical equation in (2.27)

Table 2.1 most frequent activation functions

| Activation Function | Equation | Graph |
|---|---|---|
| Linear | $\Phi(z) = z$ |  |
| Unit Step (Heaviside Function) | $\Phi(z) = \begin{cases} 0 & z < 0 \\ 1 & z > 0 \end{cases}$ |  |
| Piece-wise Linear | $\Phi(z) = \begin{cases} 0 & z \leq -1/2 \\ z + 1/2 & -1/2 \leq z \leq 1/2 \\ 1 & z \geq 1/2 \end{cases}$ |  |
| Logistic (Sigmoid) | $\Phi(z) = \frac{1}{1 + e^{-z}}$ |  |
| Hyperbolic Tangent (tanh) | $\Phi(z) = \frac{e^{z} - e^{-z}}{e^{z} + e^{-z}}$ |  |
| ReLu | $\Phi(z) = \begin{cases} 0 & z < 0 \\ z & z > 0 \end{cases}$ |  |

- Deep Learning

In deep learning, models are generally characterized by their depth, meaning the number of layers they contain. These structures are often referred to as neural networks [137]. Each layer of the network learns increasingly complex features from the data. Thus, a deep network is capable of learning complex representations of the data.

The main difference between machine learning and deep learning lies in how they approach problem-solving. While machine learning often requires human intervention to identify the appropriate features to extract from the data to solve a problem effectively, deep learning can automatically determine which features are useful for classification. This makes the learning process much more autonomous and efficient [138].

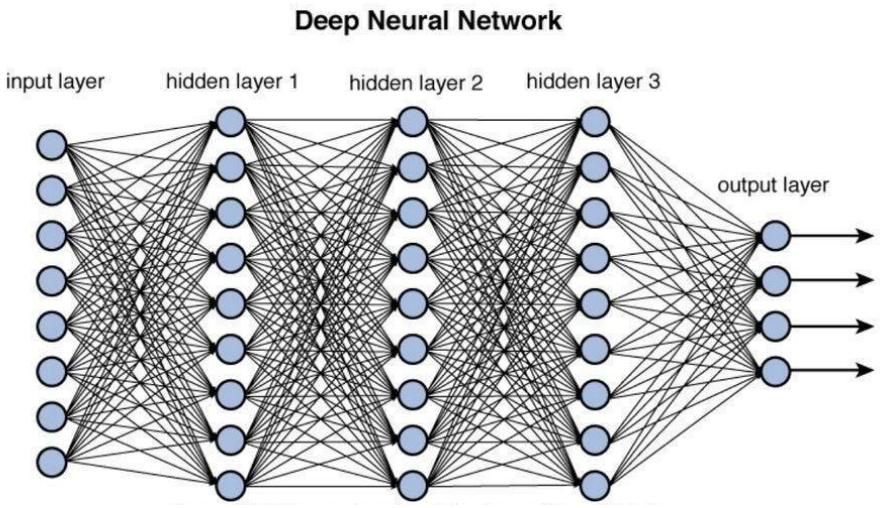



Figure 2.19 Deep Learning network architecture

- *Graph Neural Networks (GNNs)*

One of the major application areas of neural networks is computer vision, thanks in particular to the introduction of a new type of neural network : convolutional neural networks (CNNs) [139]. These networks are composed of two types of layers: convolutional layers and pooling layers. The former retrieves local information, allowing the model to consider not just a single pixel but a pixel and its neighbors, thereby accounting for the structure of the data. This is followed by a pooling step, which aggregates the results from the convolutional layer. By combining these small sub-steps, it becomes possible to create networks capable of recognizing complex patterns.

However, these techniques are only applicable to data that adheres to a Euclidean geometry, such as 1D signals, 2D images, and 3D videos or volumes. Graph data, on the other hand, does not follow this structure, requiring adaptations of these techniques to be used in this context. This led to the emergence of Graph Neural Networks (GNNs) [140], which can provide predictions at the graph level or for each node within the graph.

Following the same logic of utilizing information from neighboring pixels, GNN seeks to leverage information from neighboring nodes. To achieve this, it uses a step called message passing.

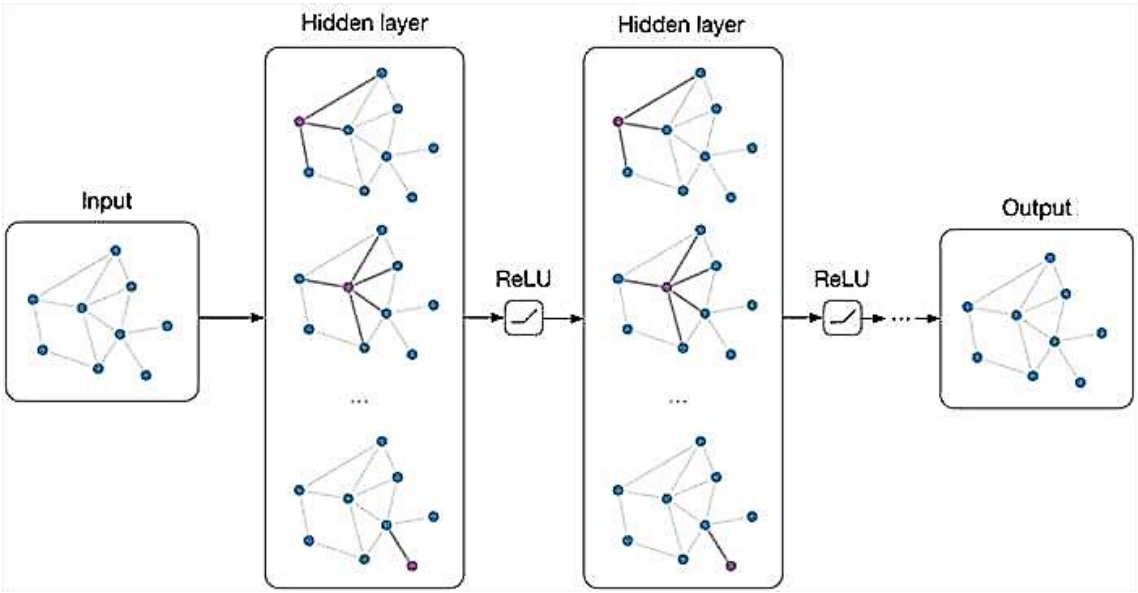



Figure 2.20 Simplified Graph Neural Network architecture.

### 2.4.3.2 Regression technique

The principle of regression models is to approximate $Y$ by a function $m(.)$ of the variable $X$, and then use $m$ for purposes such as description, evaluation of the contributions of different explanatory variables, or prediction of the response variable for new values of the explanatory variables. For example, this could involve predicting the concentration of pollutants in each area based on meteorological indices, determining if an email is spam based on the presence of specific words or characters, or identifying explanatory factors for defects in printed circuit boards based on temperature and pressure conditions in the manufacturing process.

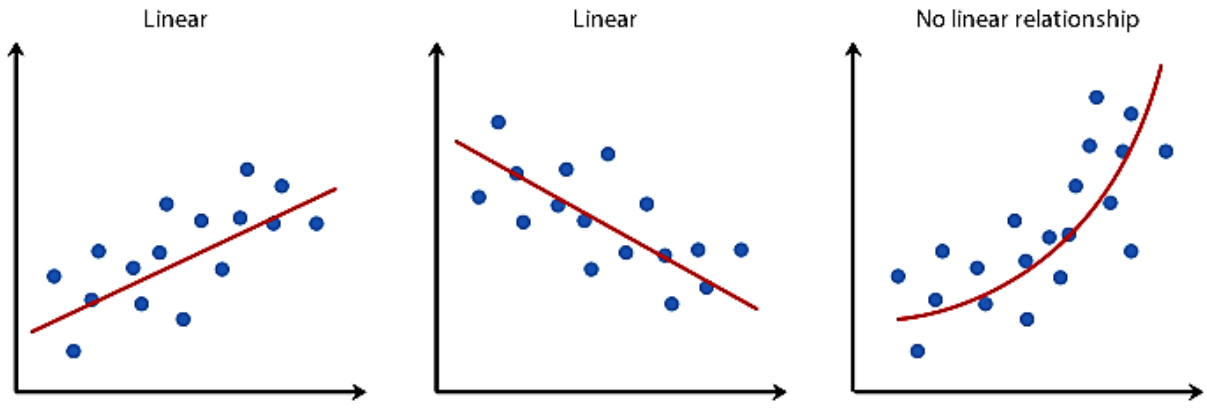



Figure 2.21 Linear and nonlinear regression

### 2.4.3.3 Model performance score

It is important to accurately assess a model's performance after its training in a supervised learning scenario. This is typically the case in a supervised or even semi-supervised learning context, as labels are required to evaluate a model's performance. Well-known metrics are used to measure model performance, tailored to each type of model, whether classification or regression.

### (a) Classification

Here, we will limit ourselves to presenting metrics within the framework of binary classification. For all binary predictions made by a model, we define TP = True Positives, TN = True Negatives, FP = False Positives, and FN = False Negatives. Below is a non-exhaustive list of performance metrics for such models:

- *Accuracy*

Can be calculated in terms of positives and negatives as follows:

$$Accuracy = \frac{TP + TN}{TP + TN + FP + FN} \tag{2.28}$$

- *Precision* :

It allows knowing the proportion of the positive identifications that were correct

$$\text{Precision} = \frac{TP}{TP + FP} \tag{2.29}$$

- *Recall* :

Recall or sensitivity, it allows us to define the proportion of real positive results that were correctly identified.

$$Recall = \frac{TP}{TP + FN} \tag{2.30}$$

- F1-Score

It measures the balance between recall and precision metrics

$$F1\ Score = 2 \times \frac{Precision\ \times Recall}{Precision + Recall} \tag{2.31}$$

- Receiver Operating Characteristic ROC

AUC ROC is the numerical measure between 0 and 1 of the area under the ROC curve (receiver operating characteristic) (BRADLEY 1997). This curve was initially known as a statistical tool derived from signal detection theory. It was later used in various fields (biology, medicine, psychology, etc.) whenever there was a need to quantify the performance of a test. Naturally, it is now used to measure the effectiveness of a classifier. It represents the performance of a classification model across all classification thresholds, where the threshold value determines class membership (typically 0.5 if the classifier output ranges between 0 and 1). This curve plots the true positive rate (TPR) against the false positive rate (FPR).

$$TPR = \frac{TP}{TP + FN} \tag{2.32}$$

$$FPR = \frac{FP}{FP + TN} \tag{2.33}$$

**(b) Regression**

In a regression context, the outputs are continuous numerical values. Below is a non-exhaustive list of metrics used to evaluate the predictions of such models:

- *Mean Squared Error*

Mean Squared Error (MSE) calculates the average squared discrepancy between the actual and forecasted values within a dataset. Essentially, it quantifies the variability or dispersion of the residuals.

$$\text{MSE} = \frac{1}{n}\sum_{i=1}^{n}(y_i - \hat{y}_i)^2 \qquad (2.34)$$

$n$ : number of observations;
$y_i$: actual value;
$\hat{y}_i$: predicted value.

- *Root Mean Square Error*

It is derived by taking the square root of the Mean Squared Error. It serves as a metric for the standard deviation of the residuals.

$$\text{RMSE} = \sqrt{\frac{1}{n}\sum_{i=1}^{n}(y_i - \hat{y}_i)^2} \qquad (2.35)$$

- *Mean Absolute Error*

It calculates the average absolute variance between the real and forecasted values within a dataset. It quantifies the average magnitude of the residuals in the dataset.

$$\text{MAE} = \frac{1}{n}\sum_{i=1}^{n}|y_i - \hat{y}_i| \qquad (2.36)$$

**2.4.3.4 overfitting**

Overfitting is a common problem in machine learning. During the training phase, the model will improve on the data provided to it until it "overlearns," meaning it becomes "specialized" for that specific dataset.

Generalization is a very important principle in machine learning because the goal is to ensure that our model performs well on all data, both the training and validation data (test set). Thus, a model that generalizes well is one that helps to better reduce what is called the "true" risk, the risk associated with the entire dataset, including data the model has not yet encountered.

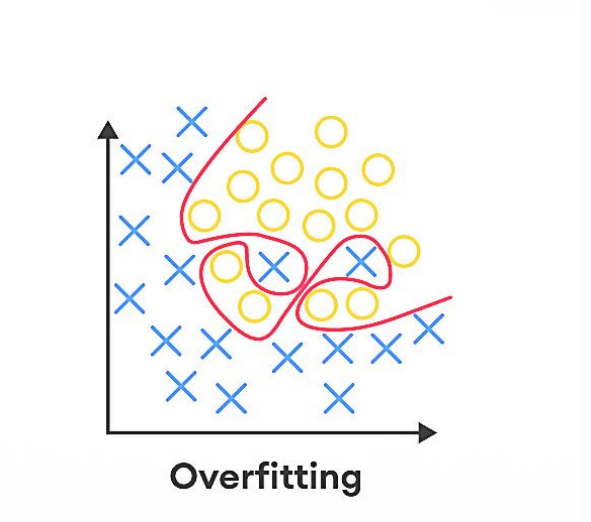



Figure 2.22 Example of overfitting against unseen data.

- *Cross Validation*

Cross-validation is a process used to detect overfitting; the data is split into $k$ subsets, where $k - 1$ subsets are used for training, and the remaining subset is used to validate the model's performance. The validation set is used to assess the relevance of the model and its parameters. This process is repeated $k$ times, each time changing the validation set. This allows for the selection of a model's parameters that perform better overall on average across the $k$ iterations.

## 2.5 Conclusion

We have discussed in this chapter, two important approaches of Non Model Based technique, which are Signal processing starting by frequency-domain analysis by applying Fourier Transform and its different variants since it's heavily used in the diagnosis process and then we passed to Frequency-Time domain analysis techniques by presenting Wavelet Transform and its various types, then we have introduced the limitation of each approach.

In the second part of the chapter, we have introduced AI techniques and machine learning with a focus on supervised learning and classification task and its different models since we focus on this type of technique, we have defined in detail the mostly used classifiers such as Boosting based algorithms, Trees based and Artificial Neural Network. And then we have defined model performance score for both classification and regression tasks and how to detect overfitting while performing and how to prevent it.

In the next chapter we will define the multi winding model that we have used to simulate the induction machine for both healthy and faulty condition.

# Chapter 3

# Squirrel cage induction machine modelling dedicated to fault diagnosis

## 3.1 Introduction

The modelling and simulation of electrical machines constitute a crucial step in diagnostics. They enable the understanding of faulty operation and the validation of fault detection algorithms. Additionally, they allow the construction of databases on the electrical and magnetic manifestations of these faults. It is therefore important to synthesize a model tailored to the problem at hand, describing the machine's behavior not in an average manner, as is done for control, but as precisely as possible. Thus, the modeling of electrical machines is essential both for designers allowing them to observe and analyze the various evolutions of the machine's electromechanical quantities and for the development of diagnostic processes.

Classical methods for studying this type of machine often use simple models in the (d, q) reference frame, neglecting several phenomena. These models are often affected by transformations and changes in reference axes, leading to theoretical interpretations that cannot be used to analyze localized effects, such as rotor bar breakages, while distinguishing them from effects caused by other incidents. Thus, it became necessary to turn to more sophisticated models (multi-winding models) for a description better suited to faults.

The objective of this chapter lies in an appropriate reformulation of the general model of the three-phase squirrel cage induction machine based on the multi-winding representation. Currently, the use of this configuration in modeling dedicated to diagnostics is customary. However, approaches that incorporate faults and calculate the corresponding inductances remain limited. In this context, several solutions are proposed. Nevertheless, few arguments and details about the calculation procedure can be found. Here, we aim to address this gap by extending formalism to a level that allows interested parties to replicate the same steps, use them, and undertake their modeling tasks starting from the latest developments in this work, instead of spending time exploring earlier stages.

And later on we will present the results of the simulated system, the variables of the machine which include speed, torque and stator current will be presented including various operational conditions of the machine.

## 3.2 State model of the machine

### 3.2.1 Multi-winding model

Figure 3.1 represents the rotor of a squirrel cage induction machine, modeled as a polyphase winding where each loop consists of two adjacent bars and two portions of the short-circuit ring. The stator circuit is composed of a three-phase winding, which can be placed in the stator

slots in various ways, thereby defining the type of winding adopted [141,142]. Based on this structure, it is possible to establish the general equations governing its operation by relying on simplifying assumptions, the most important of which are:

1. No saturation in the magnetic circuit. In the final phase, only tooth saturation will be considered.
2. Hysteresis and eddy currents are negligible.
3. No skin effect phenomena.
4. The permeability of the iron is assumed to be infinite.
5. The slotting effect is neglected in the calculation of the air gap permeance.

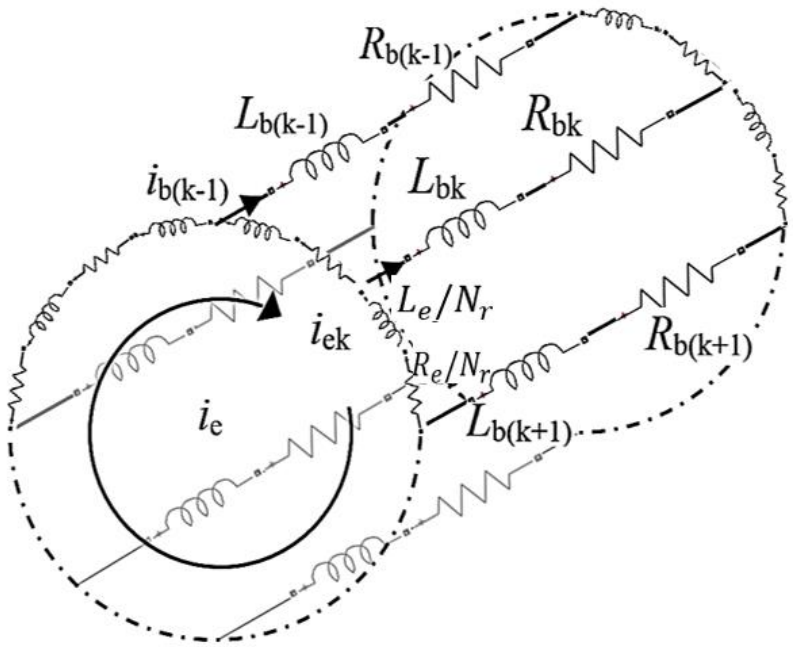



Figure 3.1 Equivalent electrical circuit of the squirrel cage rotor based on the multi-winding structure.

**1.2 Voltage equations**

Figure 3.2 depicts a segment of the equivalent electrical circuit of a rotor mesh, showcasing the rotor bars and short-circuit ring segments through their respective resistances and leakage inductances. Based on this illustration, the equations for the voltages of the three stator phases and the ($N_r$+1) rotor meshes can be derived.

$$[V_s] = [R_s][I_s] + \frac{d[\psi_s]}{dt} \tag{3.1}$$

$$[V_r] = [R_r][I_r] + \frac{d[\psi_r]}{dt} \tag{3.2}$$

where $[\psi_s]$ and $[\psi_r]$ denote the vectors encapsulating the total fluxes through the stator and rotor windings, respectively. Meanwhile, $[I_s]$and $[I_r]$ represent the respective current vectors associated with these windings, as follows:

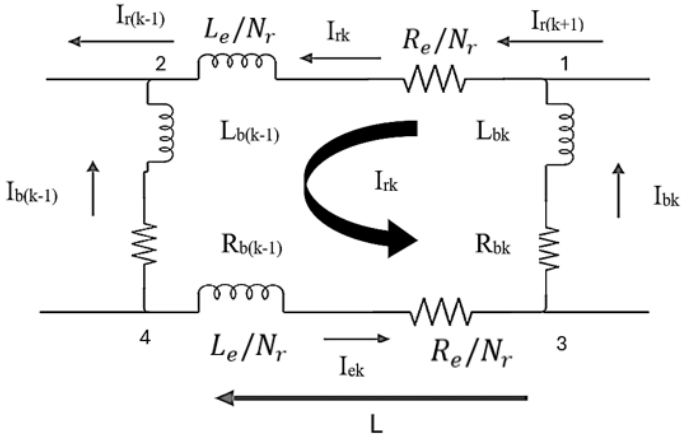



Figure 3.2 Equivalent circuit for the rotor mesh

$$[\psi_s] = [L_{ss}][I_s] + [L_{sr}][I_r] \tag{3.3}$$

$$[\psi_r] = [L_{rs}][I_s] + [L_{rr}][I_r] \tag{3.4}$$

$$[V_s] = [V_{sA} \quad V_{sB} \quad V_{sC}] \tag{3.5}$$

$$[V_r] = \left[V_{r1}V_{r2} \dots \dots V_{rN_b}V_{re}\right]^T \tag{3.6}$$

$$[I_s] = [i_{sA} \quad i_{sB} \quad i_{sC}]^T \tag{3.7}$$

$$[I_r] = \left[i_{r1}i_{r2} \dots \dots \dots i_{rN_r}i_{re}\right]^T \tag{3.8}$$

Where $i_{rj}$ and $i_{re}$ are respectively the currents of the $j^{th}$ rotor mesh and of the short-circuit ring. $V_{rj}$ and $V_{re}$ are the corresponding voltages with, for a cage rotor (short-circuited mesh), $V_{rj}$ = 0 and $V_{re} = 0$; j=1.2,….. $N_b$ .The resistor matrices are symmetric matrices. $[R_s]$ is a 3×3 matrix, while $[R_r]$ has $(N_r + 1) \times (N_r + 1)$ elements that can be reconstructed from the laws relating to electrical circuits.

By joining both of equations (1) and (2) into the same matrix equation, we arrive at:

$$[V] = [R][I] + \frac{d([L],[I])}{dt} \tag{3.9}$$

$$[R_r] = \begin{bmatrix} R_{r1}+R_{rN_b}+2R_c & -R_{r1} & 0 & \cdots & -R_{rN_b} & \vdots & -R_c \\ \ddots & \ddots & \ddots & \ddots & \ddots & \vdots & \vdots \\ 0 & -R_{r(j-1)} & R_{rj}+R_{r(j-1)}+2R_e & -R_{rj} & 0 & \vdots & \vdots \\ \ddots & \ddots & \ddots & \ddots & \ddots & \vdots & \vdots \\ -R_{rN_b} & 0 & \cdots & \cdots & R_{r(N_r-1)}+R_{rN_r}+2R_e & \vdots & -R_e \\ \cdots & \cdots & \cdots & \cdots & \cdots\cdots & \cdots & \cdots \\ -R_e & \cdots & \cdots & \cdots & -R_e & \vdots & N_bR_e \end{bmatrix} \quad (3.10)$$

With:

- $[I]$ as the current vector,
- $S_r$ as the resistance of a stator phase,
- $R_{rj}$ as the resistance of the *j-th* rotor bar,
- $R_e$ as the resistance of a segment of the short-circuit ring.

As shown in expressions (3.11) and (3.12), the stator and rotor inductance matrices are 3×3 and ($N_r$+1)×($N_r$ + 1) matrices, respectively, expressed diagonally by the self-inductances of each winding, and off-diagonally by the mutual inductances between windings (stator phases or rotor loops). The detailed expressions of the elements of each matrix can be found in [143,144].

$$[L_{ss}] = \begin{bmatrix} L_A & L_{AB} & L_{AC} \\ L_{BA} & L_B & L_{BC} \\ L_{CA} & L_{CB} & L_C \end{bmatrix} \quad (3.11)$$

$$[L_{rr}] = \begin{bmatrix} L_{mr}+2(L_b+L_e) & L_{r122}-L_b & \cdots & L_{r1r(N_s-1)} & L_{r12V_b}-L_b & \vdots & -L_e \\ L_{r2r1}-L_b & L_{mur}+2(L_b+L_e) & \cdots & L_{r2r(Nb-1)} & L_{r2rN_s} & \vdots & -L_e \\ \vdots & \vdots & \vdots & \vdots & \vdots & \vdots & \vdots \\ L_{r(N_s-1)r1} & L_{r(N_r-1)r2} & \cdots & L_{mrr}+2(L_b+L_e) & L_{r(N_r-1)rN_s}-L_b & \vdots & -L_e \\ L_{rV_br1}-L_b & L_{rN_br2} & \cdots & L_{rN_rr(N_r-1)}-L_b & L_{mpr}+2(L_b+L_e) & \vdots & -L_e \\ \cdots & \cdots & \cdots & \cdots & \cdots & \cdots & \cdots \\ -L_e & -L_e & -L_e & -L_e & -L_e & \vdots & N_bL_e \end{bmatrix} \quad (3.12)$$

As for $[L_{sr}]$, it contains 3×($N_b$+1) elements that represent the mutual inductances between the stator phases and the rotor loops. $[L_{sr}]$ is given by:

$$[L_{sr}] = \begin{bmatrix} L_{Ar1} & L_{Ar2} & \cdots\cdots & L_{Ar(N_r-1)} & L_{ArN_b} & 0 \\ L_{Br1} & L_{Br2} & \cdots\cdots & L_{Br(N_r-1)} & L_{BrN_b} & 0 \\ L_{Cr1} & L_{Cr2} & \cdots\cdots & L_{Cr(N_r-1)} & L_{CrN_b} & 0 \end{bmatrix}, \quad (3.13)$$

Here, $L_{Arj}$ represents the mutual inductance between stator phase *A* and the *j-th* rotor loop. As for $[L_{rs}]$, it is a ($N_r$+1)×3 matrix obtained in the same way, by replacing $L_{Arj}$ with the mutual inductances $L_{rjA}$. The same applies to phases *B* and *C*. The mutual inductances between each

stator phase and the short-circuit ring are neglected, as they can be considered as coils with perpendicular axes.

By joining both of equations (3.1) and (3.2) into the same matrix equation, we arrive at:

$$[V] = [R][I] + \frac{d([L],[I])}{dt} \tag{3.14}$$

Which gives ,

$$[V] = [R][I] + [I] \cdot \frac{d\theta_r}{dt} \cdot \frac{d[L]}{d\theta_r} + [L] \cdot \frac{d[I]}{dt} \tag{3.15}$$

$$[V] = [R][I] + [I]\Omega_r \cdot \frac{d[L]}{d\theta_r} + [L]\frac{d[I]}{dt} \tag{3.16}$$

While,

$$[V] = \begin{bmatrix}[V_s]\\ [V_r]\end{bmatrix} \tag{3.17}$$

$$[U] = [V_{sA} \quad V_{sB} \quad V_{sC} \quad 0 \quad 0 \quad 0 \quad \cdots \quad 0 \quad 0]^T \tag{3.18}$$

$$[I] = \begin{bmatrix}[I_s]\\ [I_r]\end{bmatrix} \tag{3.19}$$

$$[I] = [i_{sA} \quad i_{sB} \quad i_{sC} \quad i_{r1} \quad i_{r2} \quad \cdots \quad i_{rN_r} \quad i_{re}], \tag{3.20}$$

And,

$$[R] = \begin{bmatrix}[R_s] & 0\\ 0 & [R_r]\end{bmatrix} \tag{3.21}$$

$$[R] = \begin{bmatrix} r_{sA} & 0 & 0 & 0 & 0 & 0 & \cdots & 0 & 0 \\ 0 & r_{sB} & 0 & 0 & 0 & 0 & \cdots & 0 & 0 \\ 0 & 0 & r_{sc} & 0 & 0 & 0 & \cdots & 0 & 0 \\ 0 & 0 & 0 & r_r & -r_b & 0 & \cdots & -r_b & r_e \\ 0 & 0 & 0 & -r_b & r_r & -r_b & \cdots & 0 & r_e \\ 0 & 0 & 0 & 0 & -r_b & r_r & \cdots & 0 & r_e \\ \vdots & \vdots & \vdots & \vdots & \vdots & \vdots & \cdots & \vdots & \vdots \\ 0 & 0 & 0 & -r_b & 0 & 0 & \cdots & r_r & r_e \\ 0 & 0 & 0 & r_e & r_e & r_e & \cdots & r_e & N_r \cdot r_e \end{bmatrix} \tag{3.22}$$

On the other hand,

$$[L] = \begin{bmatrix}[L_{ss}] & [L_{sr}]\\ [L_{rs}] & [L_{rr}]\end{bmatrix} \tag{3.23}$$

Or in general

$$[L] = \begin{bmatrix} L_A & L_{AB} & L_{AC} & L_{Ar1} & L_{Ar2} & . & . & L_{ArN_r} & L_{Are} \\ L_{BA} & L_B & L_{BC} & L_{Ar1} & L_{Br2} & . & . & L_{BrN_r} & L_{Bre} \\ L_{CA} & L_{CB} & L_C & L_{Ar1} & L_{Cr2} & . & . & L_{CrN_r} & L_{Cre} \\ L_{r1A} & L_{r1B} & L_{r1C} & L_{r1} & L_{r1r2} & . & . & L_{r1rN_r} & L_{r1re} \\ L_{r2A} & L_{r2B} & L_{r2C} & L_{r2r1} & L_{r2} & . & . & L_{r2rN_r} & L_{r2re} \\ L_{r3A} & L_{r3B} & L_{r3C} & L_{r3r1} & L_{r3r1} & . & . & L_{r3rN_r} & L_{r3re} \\ \vdots & \vdots & \vdots & \vdots & \vdots & . & . & \vdots & \vdots \\ L_{rN_bA} & L_{rN_bB} & L_{rN_bC} & L_{rN_br1} & L_{rN_br2} & . & . & L_{rN_r} & L_{rN_rre} \\ L_{reA} & L_{reB} & L_{reC} & L_{rer1} & L_{rer2} & . & . & L_{rerN_r} & N_r \cdot L_{re} \end{bmatrix}. \quad (3.24)$$

The details regarding the components of $[L]$ can be derived from equations (3.11), (3.12), and (3.13). $\theta_r$ is the angular position of the rotor, or the mechanical angle measured relative to a fixed reference phase in the stator. $\Omega_r = d\,\theta_r/dt$ represents the mechanical speed of the machine's shaft.

In the case of a star connection with a connected neutral (Figure 3.3), the system must be rearranged to ensure the condition that the sum of the phase currents is zero. Instead of considering line-to-neutral voltages in the state system, the equations are written in terms of line-to-line voltages, which remain unchanged regardless of the connection type [145,146]. This can be achieved as follows:

- Subtract the elements of the second row from those of the first row in the matrices $[U]$, $[R]$, and $[L]$.
- Subtract the elements of the third row from those of the second row in the matrices $[U]$, $[R]$, and $[L]$;
- Assign the value 0 to the third row of the column matrix $[U]$;
- Assign the value 1 to the elements of the first through third columns in the third row of the matrices $[R]$ and $[L]$, and 0 to all other elements.

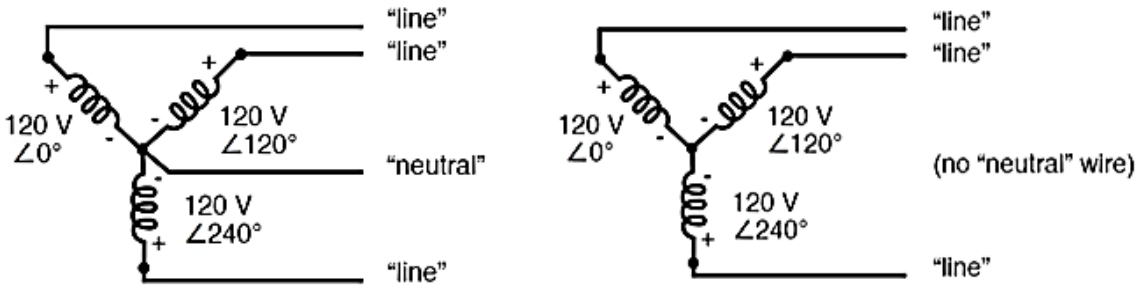



Figure 3.3 Star connection with connected neutral (left) and floating neutral (right).

### 3.2.3 Mechanical equations

Depending on the specific application for which the motor is intended, the mechanical equation of motion can be formulated as follows:

$$J_T \cdot \frac{d\Omega_r}{dt} + f_V \Omega_r = T_e - T_r \quad (3.25)$$

Where :
$J_T$ : total moment of inertia ;
$f_V$ : viscous friction coefficient ;
$T_e$ : electromagnetic torque ;
$T_r$ : load torque.
For a linear magnetic circuit, the co-energy equals the stored magnetic energy, which leads to :

$$T_e = \left[\frac{\partial W_{co}}{\partial \theta_r}\right]_{(I_s, I_r \text{ constant})} \quad (3.26)$$

With

$$W_{co} = \frac{1}{2} \cdot [I]^T \cdot [L] \cdot [I] \quad (3.27)$$

Which gives eventually the electromagnetic torque expression :

$$T_e = \frac{1}{2} \cdot [I]^T \cdot \frac{d[L]}{d\theta_r} \cdot [I] \quad (3.28)$$

If $[L_{ss}]$ and $[L_{rr}]$ are constants, we obtain the following torque equation;

$$T_e = \frac{1}{2} \cdot [I_s]^T \cdot \frac{d[L_{sr}]}{d\theta_r} \cdot [I_r] \quad (3.29)$$

### 3.2.4 System of state equations

We can group the voltage equations and the mechanical equation into a single matrix representation to arrive at a condensed form [147]:

$$\begin{bmatrix} [V] \\ -T_r \\ 0 \end{bmatrix} = \begin{bmatrix} \left([R] + \Omega_r \frac{d[L]}{d\theta_r}\right) & 0 & 0 \\ -\frac{1}{2}[I]^T \frac{d[L]}{d\theta_r} & f_V & 0 \\ 0 & -1 & 0 \end{bmatrix} \cdot \begin{bmatrix} [I] \\ \Omega_r \\ \theta_r \end{bmatrix} + \begin{bmatrix} [L] & 0 & 0 \\ 0 & J_T & 0 \\ 0 & 0 & 1 \end{bmatrix} \cdot \begin{bmatrix} [\dot{I}] \\ \dot{\Omega}_r \\ \dot{\theta}_r \end{bmatrix}, \quad (3.30)$$

And a condensed form :

$$[U] = [B] \cdot [X] + [A] \cdot [\dot{X}] \quad (3.31)$$

The vector $[\dot{X}]$ is written as follows :

$$[\dot{X}] = [\mathrm{A}]^{-1} \cdot [U] - [\mathrm{A}]^{-1} \cdot [\mathrm{B}] \cdot [X] \quad (3.32)$$

We thus reveal the state vector $[X]$ and the vector $[U]$ containing the external quantities to the machine such as:

$$[U] = \begin{bmatrix} [V] \\ -T_r \\ 0 \end{bmatrix} \tag{3.33}$$

$$[X] = \begin{bmatrix} [I] \\ \Omega_r \\ \theta_r \end{bmatrix} \tag{3.34}$$

With the definition of matrices A and B given by:

$$[\mathrm{A}] = \begin{bmatrix} \left([R] + \Omega_r \frac{d[L]}{d\theta_r}\right) & 0 & 0 \\ -\frac{1}{2}[I]^T \frac{d[L]}{d\theta_r} & f_{\mathrm{V}} & 0 \\ 0 & -1 & 0 \end{bmatrix} \tag{3.35}$$

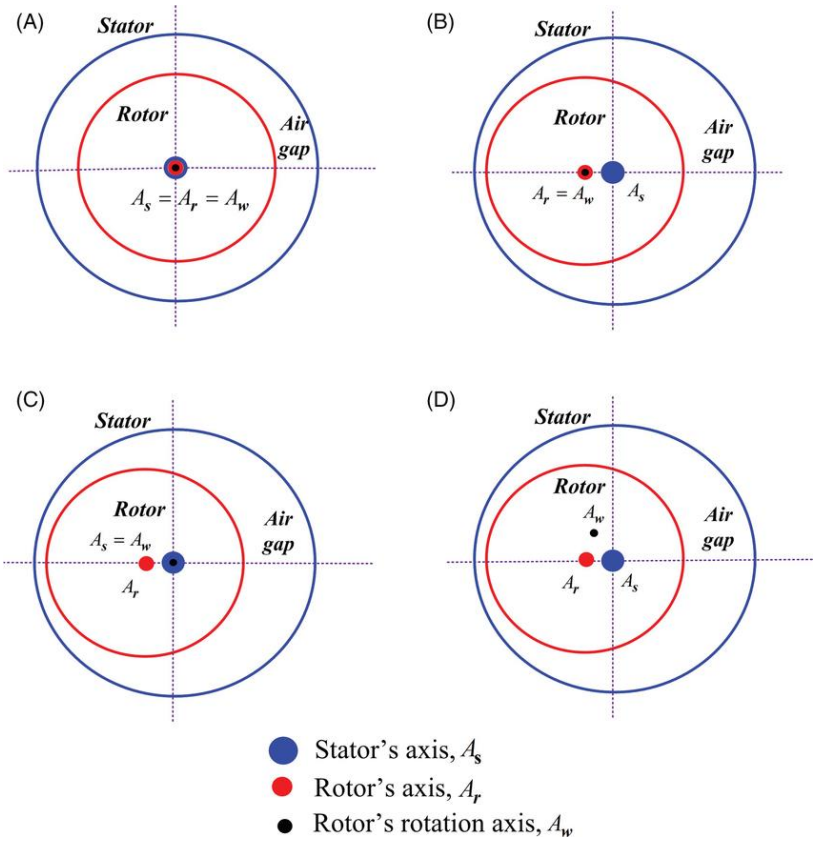
$$[\mathrm{B}] = \begin{bmatrix} [L] & 0 & 0 \\ 0 & J_T & 0 \\ 0 & 0 & 1 \end{bmatrix}. \tag{3.36}$$

We are thus faced with a system of nonlinear and parametric differential equations governing the operation of the machine. To solve it, a numerical method must be implemented. The explicit Runge-Kutta method is the most commonly used in such cases. Before that, we must define the matrices A and B to represent the structure and internal state of the machine. This leads to the challenging task of modeling.

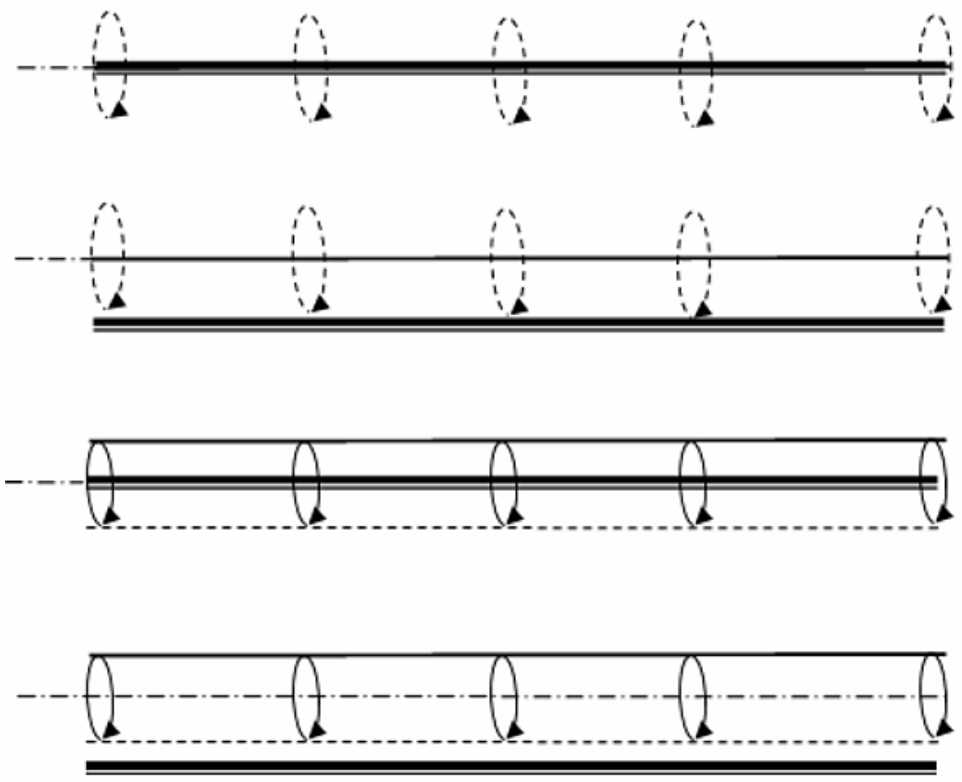
## 3.3 Faulty machine modelling

### 3.1.1 Eccentricity types

Figures 3.4, 3.5, 3.6, and 3.7 illustrate two significant and common cases of air gap eccentricity distributed according to the direction of variation: radial eccentricity and axial eccentricity. In Figures 3.4 and 3.6, the two types of eccentricity are distinguished at any given moment by the position of the rotor relative to the stator, either parallel or inclined. Meanwhile, Figures 3.5 and 3.7 attempt to explain these eccentricities in terms of the relative motion of the axes, ultimately identifying the presumed cases. This representation is considered superior both for understanding the phenomenon and identifying the various possible modes, as well as for modeling the fault.




3.4 Relative motion of rotation centers in the case of eccentricity: A- healthy, B- static, C- Dynamic, D- Mixed.



3.5 Illustration of radial eccentricity. From top to bottom: symmetric case, static eccentricity, dynamic eccentricity, and mixed eccentricity.

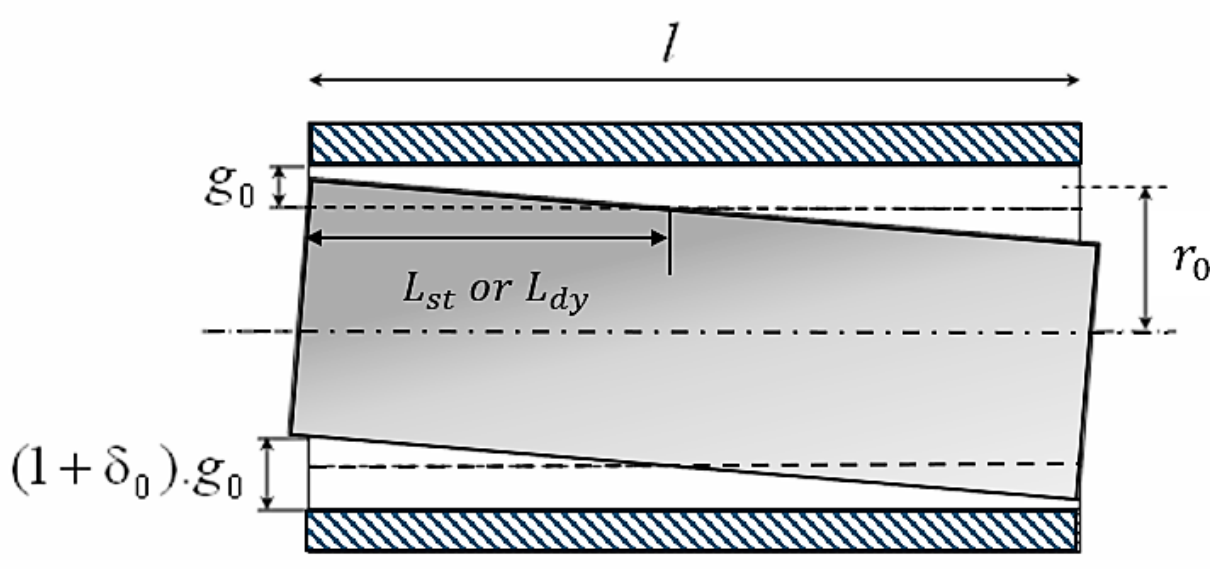



Figure 3.6 terms illustration of *Lst* and *Ldy* that characterize axial eccentricity

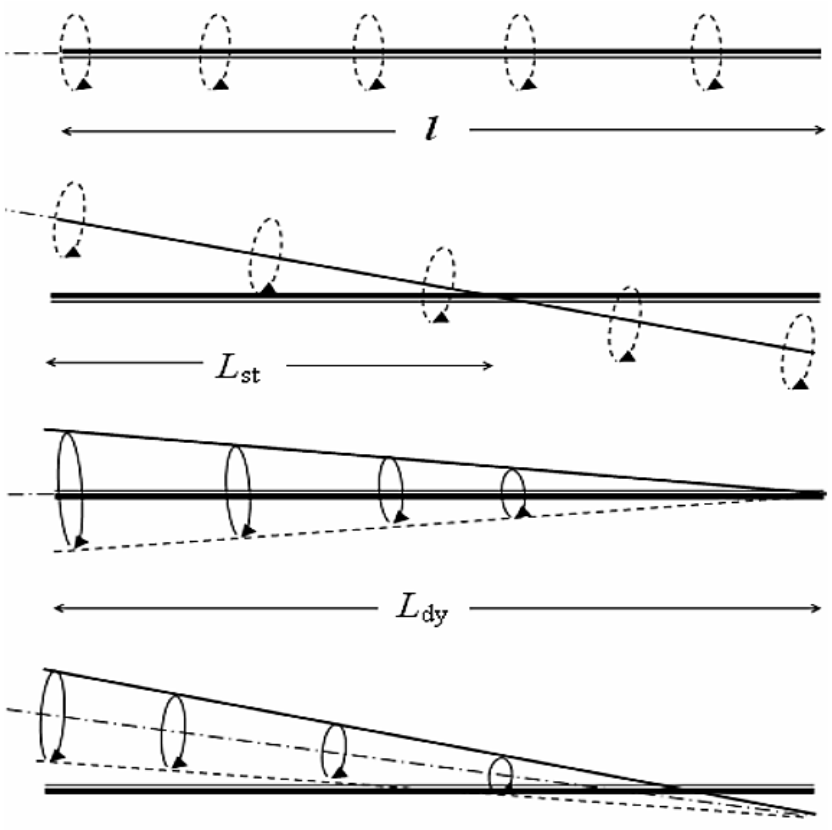



Figure 3.7 axial eccentricity illustration, from top to bottom: healthy, static eccentricity (Lst<1), dynamic eccentricity (Ldy=1) and a variant mixed axial eccentricity.

Radial eccentricity is well explained in several studies. The most likely practical scenario is that this non-uniformity of the air gap depends on the axial length of the machine, meaning it varies

along the length of the machine's shaft. An important step in modeling axial eccentricity is to conceptualize how it can occur. To achieve this, the parameters Lst and Ldy are introduced, defined as the positions of the concentric section of the rotor along the shaft in cases of static and dynamic axial eccentricity, respectively (Figure 3.6). These two parameters, combined with the degree of frontal (or final) eccentricity corresponding to z=0, sufficiently characterize the type of axial eccentricity in question.

Illustratively, Figure 3.7 shows that in the case of static axial eccentricity, the rotor's natural axis always coincides with the axis of rotation and is inclined relative to the stator's axis. In dynamic axial eccentricity, the rotor's axis of symmetry is inclined relative to the stator's axis, which this time coincides with the axis of rotation. It is also possible to imagine combinations of all these modes (radial and axial), resulting in variations of mixed axial eccentricity.

#### 3.3.1.1 Air gap eccentricity model

Rotor eccentricity is accounted for in a modeling task by assigning a sinusoidal variation to the air gap thickness function, often referred to as the air gap function. This variation is related to both the nature of the movement of the rotor's axis of symmetry and its relative position in the direction of evolution.

Eccentricity can be expressed in the following way :

$$g(\varphi, z, \theta_r) = g_0\left[1 - \delta(z) \cdot \cos\left(\varphi - \rho(\theta_r)\right)\right] \tag{3.37}$$

Where $\delta(z)$ represents total eccentricity degree and expressed by

$$\delta(z) = \sqrt{\delta_s(z)^2 + \delta_d(z)^2 + 2\delta_s(z)\delta_d(z) \cdot \cos\left(\rho(\theta_r)\right)} \tag{3.38}$$

Where $\delta_s$, $\delta_d$ represent static and dynamic eccentricity degree respectively, $g_0$ is the air gap thickness in the symmetrical machine, $\varphi$ is the angular opening to a fixed stator reference, $\theta_r$ is the rotor position to a fixed stator reference.

And $\rho(\theta_r)$ is the inverse function of the air gap

$$\rho(\theta_r) = \arctan\left(\frac{\delta_d(z)\sin(\theta_r)}{\delta_s(z)+\delta_d(z)\cos(\theta_r)}\right) \tag{3.39}$$

As will be shown later, expression (3.38) does not directly contribute to the calculation of the flux and, consequently, the inductance. Instead, its inverse is required, which largely defines the air gap permeance. A constraint in the analytical resolution of the integrals necessitates the use of an appropriate expansion to achieve this goal. To this end, in the case of radial eccentricity, the inverse function of the air gap can be modeled using *p* harmonics derived from its Fourier series expansion [148].

$$\begin{cases} g^{-1}(\varphi, \theta_r) = P_0 + \sum_{k=1}^{p} P_k \cdot \cos[k \cdot \{\varphi - \rho(\theta_r)\}] \\ P_0 = \langle g^{-1} \rangle = \left(\frac{1}{g_0\sqrt{1-\delta^2}}\right), P_k = 2 \cdot P_0 \cdot \left(\frac{1-\sqrt{1-\delta^2}}{\delta}\right) \text{ et } k = 1,2..p. \end{cases} \tag{3.40}$$

### 3.3.2 Broken rotor bars

It is quite challenging to accurately describe the sequence of physical phenomena involved in the breaking of a bar.

The breakage of a bar can be modeled by nullifying the current flowing through that bar [149]. The inductance and resistance matrices are modified in such a way that if bar kk is broken, the current $I_{bk}$ must be zero. In this case, the current in loop (k+1) becomes equal to the current in loop $k$, i.e., $I_{r(k+1)} = I_{rk}$.

This is reflected in the inductance and resistance matrices by adding the two columns and rows corresponding to the currents $I_{r(k+1)}$and $I_{rk}$ . The current $I_{r(k+1)}$ is thus removed from the current vector, effectively reducing the system's order (Figure 3.9)

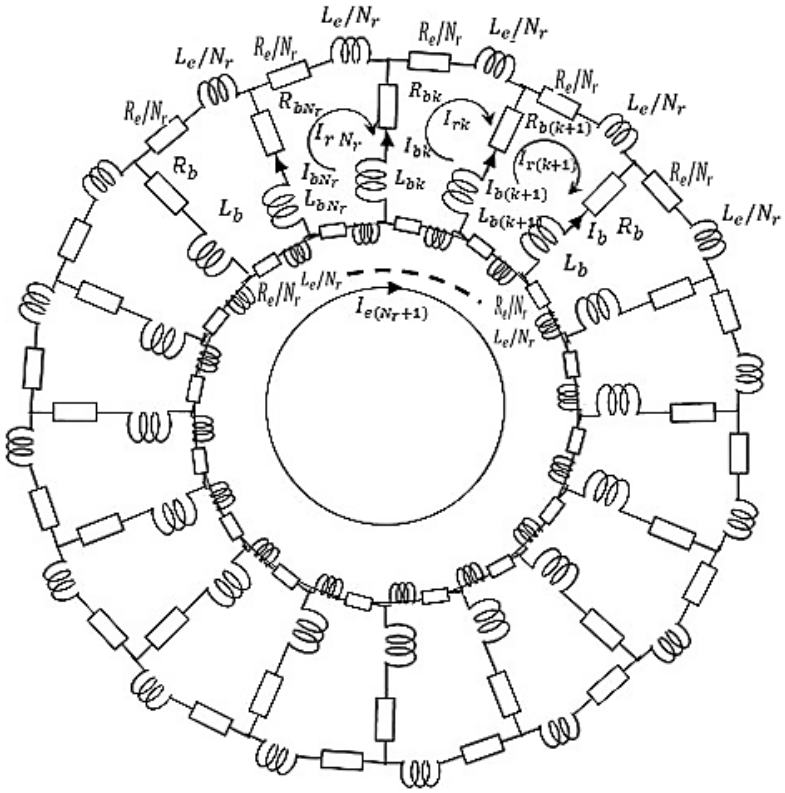



Figure 3.8 Equivalent circuit of a healthy rotor cage

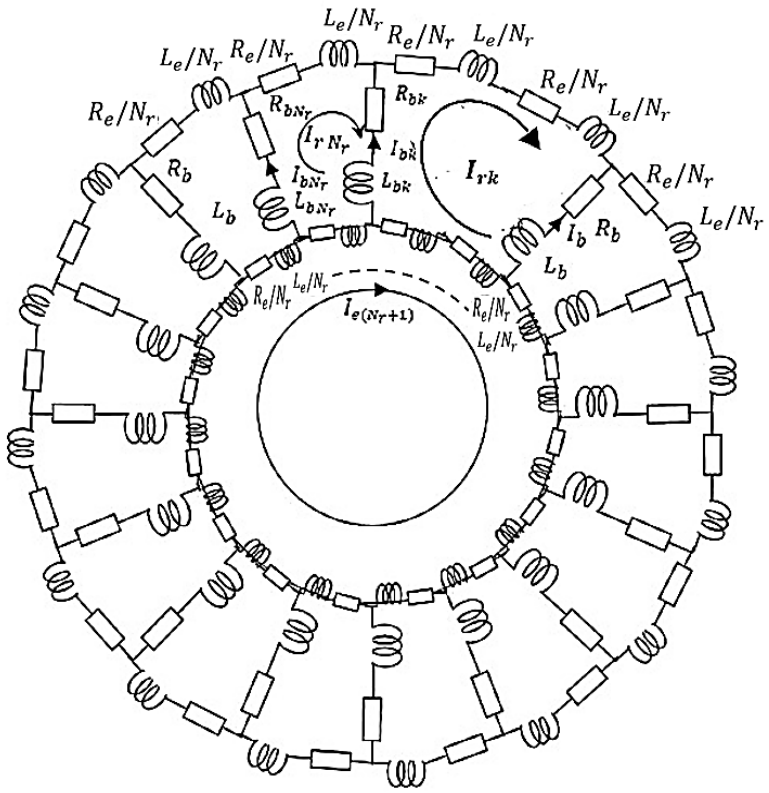



Figure 3.9 equivalent circuit of a rotor cage in case of one broken rotor bar.

### 3.4 Calculation of Inductances

#### 3.4.1 Stator part

By applying Ampere's theorem to a closed loop, the circulation of the magnetic field *H* created by an *i-th* stator phase at any given point can be calculated [150-151]

according to Ampere's theorem:

$$\oint \mathrm{Hdl} = \frac{\mathrm{N_s I_s}}{\mathrm{p}} \tag{3.41}$$

$\mathrm{N_s}$ : number of stator windings per phase;

$\mathrm{I_s}$ : the current of one stator phase;

p : number of pole pairs.

Starting from the expression (3.41), the maximum induction in the air gap equals:

$$\mathrm{B}_{max} = \mu_0 \frac{\mathrm{N_s I_s}}{2 \cdot \mathrm{p} \cdot \mathrm{e}} \tag{3.42}$$

Where

e : is the air gap [mm];

$\mu_0 = 4\pi 10^{-7}$ : void magnetic permeability [H.m$^{-1}$].

The decomposition of the induction into a Fourier series provides the fundamental:

$$B_s(\theta) = \frac{2\mu_0 N_s I_s}{ep\pi}\cos(p \cdot \theta) \qquad (3.43)$$

Consequently, the magnetic flux in the air gap, per pole, is obtained by integrating expression (3.43) over a polar interval along the machine. It is expressed as:

$$\Phi_s = \iint_s B_s ds = \int_0^t dz \int_{-\frac{\pi}{2p}}^{\frac{\pi}{2p}} B_s R \cdot 1 \cdot d\theta \qquad (3.44)$$

We get

$$\Phi_s = \frac{4}{\pi}\mu_0 \frac{N_s^2}{e \cdot p^2} \text{ R.l.I. } I_s \qquad (3.45)$$

Hence, the main flux of the stator winding is:

$$\psi_{sp} = N_s \cdot \Phi_s = N_s \cdot I_s \frac{2\mu_0 \cdot N_s \cdot R \cdot 1}{e \cdot p\pi} \int_{-\frac{\pi}{2p}}^{\frac{\pi}{2p}} \cos(p \cdot \theta) \cdot d\theta \qquad (3.46)$$

So

$$\psi_{sp} = L_s * I_s \qquad (3.47)$$

The main (magnetizing) inductance of the stator phase "n," according to (3.47), is therefore given by [152,153]:

$$L_{sp} = 4\mu_0 \frac{N_s^2}{e \cdot p^2 \pi} R \cdot 1 \qquad (3.48)$$

Leakage flux is given by:

$$\psi_{fs} = L_{fs} * I_s \qquad (3.49)$$

Cyclic inductance $L_{sc}$

$$L_{sc} = \frac{3}{2}L_{sp} + L_{sf} = \frac{6\mu_0 N_s^2 \cdot R \cdot 1}{e \cdot p^2 \cdot \pi} + L_{sf} \qquad (3.50)$$

Due to the symmetry of the stator windings (shifted by an angle of $\frac{2\pi}{3}$), the mutual inductances between the three phases are expressed as:

$$\begin{cases} L_{ab} = L_{sp}\cos\left(\frac{2\Pi}{3}\right) = -\frac{L_{sp}}{2} \\ L_{ac} = L_{sp}\cos\left(\frac{4\Pi}{3}\right) = -\frac{L_{sp}}{2} \\ L_{bc} = L_{sp}\cos\left(\frac{2\Pi}{3}\right) = -\frac{L_{sp}}{2} \end{cases}$$

With

$$\left.\begin{matrix} L_{ab} = L_{ba} \\ L_{ac} = L_{ca} \\ L_{bc} = L_{cb} \end{matrix}\right\} = M_s = -\frac{L_{sp}}{2}$$

### 3.4.2 Rotor part

Figure 3.10 shows the profile of the magnetic induction, assumed to be radial, produced by a rotor loop *k* in the air gap as a function of *θ*\theta.

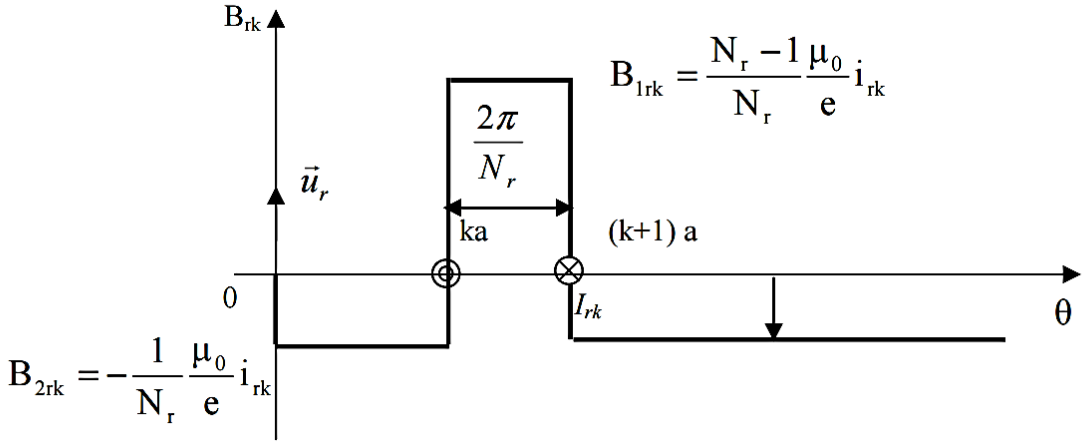



Figure 3.10 Magnetic induction produced by a rotor loop.

$I_{rk}$: current with the loop;

$N_r$ : number of rotor bars;

$B_k$ : magnetic induction in the air gap produced by a rotor loop "k".

Considering each rotor loop as a coil with a single turn, carrying a current $I_{rk}$, it is the seat of a main flux expressed by:

$$\psi_{rpk} = \int_0^{\frac{2\pi}{N_r}} B_{2rk} R \cdot l \cdot d\theta$$

$$\psi_{rpk} = \frac{(N_r - 1)}{N_r^2}\mu_0 \frac{2 \cdot \pi \cdot R \cdot 1}{e} i_{rk} \qquad (3.51)$$

Subsequently, the main inductance of a rotor loop is:

$$L_{rp} = \frac{N_r - 1}{N_r{}^2} \frac{\mu_0}{e} 2\pi \cdot R \cdot 1 \qquad (3.52)$$

The total inductance of the *k-th* rotor loop is equal to the sum of its main inductance, the leakage inductances of the two bars, and the leakage inductances of the two portions of the short-circuit rings closing the loop *k*. Therefore, the expression is given by:

$$L_{rr} = L_{rp} + 2.L_b + 2.L_e \qquad (3.53)$$

The rotor loops are magnetically coupled through the rotor flux in the air gap. The flux passing through the *j-th* loop, produced by the current $i_{rk}$ circulating in the *k-th* loop, is given by:

$$\Phi_{rjrk} = \int_0^t dz \int_{ja}^{(j+1)a} B_{2rk} R \cdot l \cdot d\theta$$

$$\Phi_{rjjk} = \int_0^t dz \int \left(-\frac{1}{N_r} \frac{\mu_0}{e} R \cdot 1 \cdot i_{rk}\right) d\theta \qquad (3.54)$$

Thus, the mutual inductance between non-adjacent (disjoint) rotor loops is expressed by the following relation:

$$M_{rr} = -\frac{1}{N_r^2} \frac{\mu_0}{e} 2 \cdot \pi \cdot 1 \cdot R \qquad (3.55)$$

The mutual inductance between the *k-th* loop and the adjacent loops is given by:

$$\begin{aligned} L_{(k+1)k} &= -\frac{1}{N_r^2} \frac{\mu_0}{e} 2 \cdot \pi \cdot 1 \cdot R - L_{b(k+1)} \\ L_{r(k-1)k} &= -\frac{1}{N_r^2} \frac{\mu_0}{e} 2 \cdot \pi \cdot 1 \cdot R - L_{b(k-1)} \end{aligned} \qquad (3.56)$$

### 3.4.3 Mutual inductance between statror and rotor

Figure 3.11 shows the geometric bases of the expression for the mutual flux between the winding of a phase "n" on the stator and an elementary circuit "k" on the rotor. The transformation in the reference frame attached to the rotor of equation (3.43) gives:

$$B_{mst} = \frac{2\mu_0 N_s \cdot i_s}{e \cdot p \cdot \pi} \cos\left(p\theta - n\frac{\pi}{3}\right) \qquad (3.57)$$

With n= 1, 2, 3

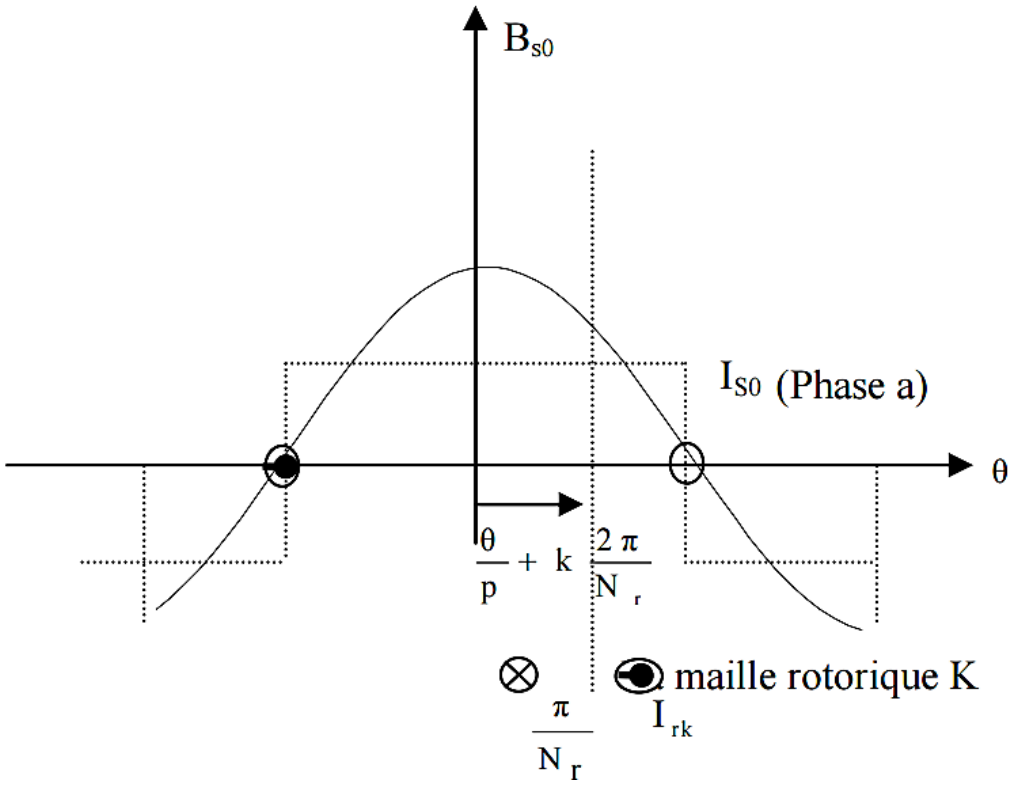



Figure 3.11 mutual flux (stator phase- rotor loop)

The induction produced by the stator coil of phase n induces in the rotor loop k the flux:

$$\Phi_{srlk} = -\frac{2\mu_0}{\pi \cdot e \cdot p} N_s R \cdot 1 \cdot i_{sm} \frac{1}{p}\left[\sin\left(p\theta - n\frac{2\pi}{3}\right)\right]_{\frac{\theta}{\pi}+k\frac{2\pi}{N_r}+\frac{\pi}{N_r}}^{\frac{\theta}{\pi}+\frac{2\pi}{N_r}+\frac{\pi}{N_r}} \qquad (3.58)$$

The mutual inductance between phase "n" of the stator and the *k-th* rotor loop is therefore given by:

$$M_{rkm} = -M_{sr}\cos\left(p\theta - n\frac{2\pi}{3} + ka\right) \qquad (3.59)$$

With

$$M_{sr} = \frac{4\mu_0 N_s R \cdot 1}{\pi \cdot e \cdot p^2}\sin\left(\frac{a}{2}\right)$$

a : electric angle between two rotor loops ( $a = p\frac{2\pi}{N_r}$ ).

Similarly, the mutual inductances between the kk-th loop and phases "b" and "c" are expressed by:

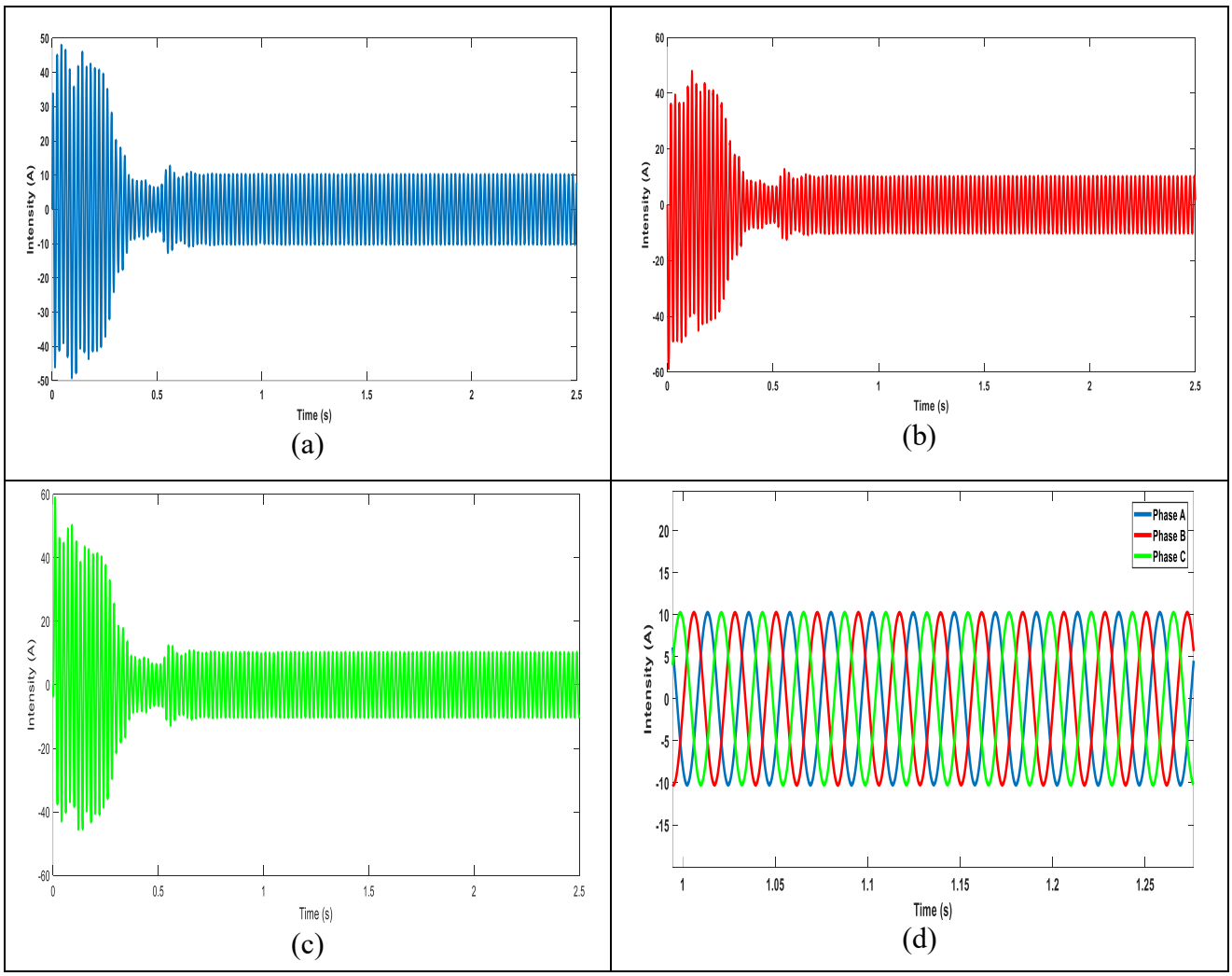
$$\begin{cases} M_{\mathrm{rka}} = \mathrm{M_{sr}}\cos(\mathrm{p}\theta + \mathrm{ka}) \\ \mathrm{M_{rkb}} = \mathrm{M_{sr}}\cos\left(\mathrm{p}\theta + \mathrm{ka} - \dfrac{2\Pi}{3}\right) \\ \mathrm{M_{rkc}} = \mathrm{M_{sr}}\cos\left(\mathrm{p}\theta + \mathrm{ka} + \dfrac{2\Pi}{3}\right) \end{cases}$$

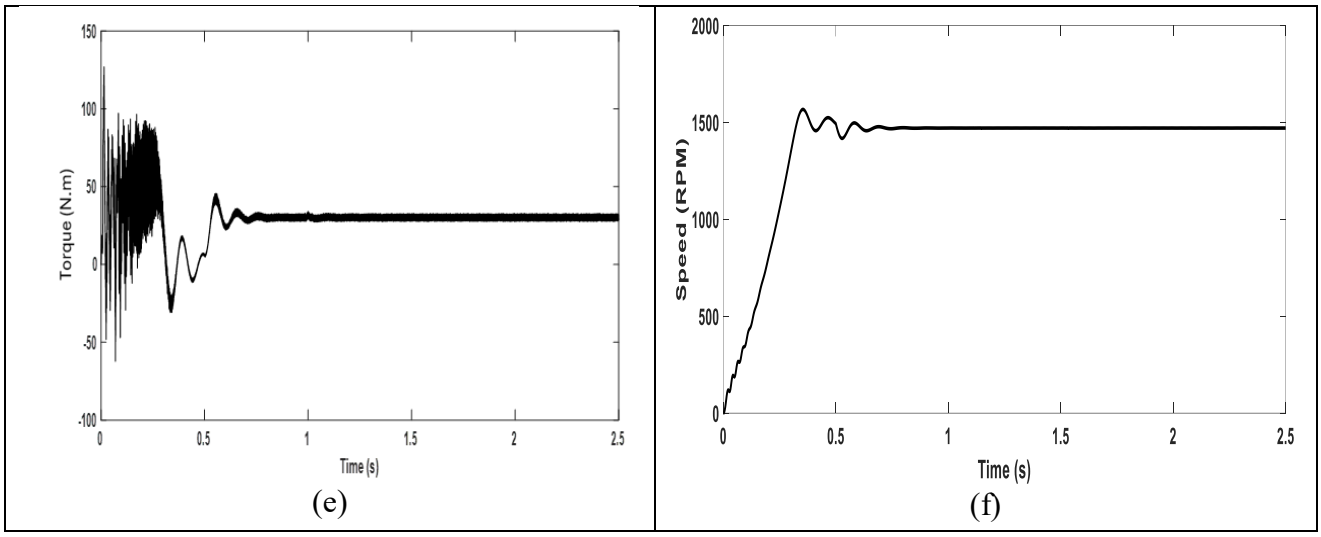
### 3.5 Simulation Results

The data was collected by simulating a quadripolar three-phase squirrel cage induction machine using the multi-winding model with floating neutral for 2.5 *seconds* under both fault-free and faulty scenarios, including air gap eccentricity and broken rotor bars, in the obtained results in the first phase of the simulation, a torque of 30 *N.m* was applied. The simulation results allowed us to obtain various machine variables, such as stator current, speed, electromagnetic torque, and rotor current for each bar.

Some of these variables will be presented in the following section. However, in the diagnosis process, we focus only on the stator current signal, as we employ a non-invasive online approach to diagnose the aforementioned defects. The stator current is the most suitable variables for this task.

#### 3.5.1 Healthy machine variables



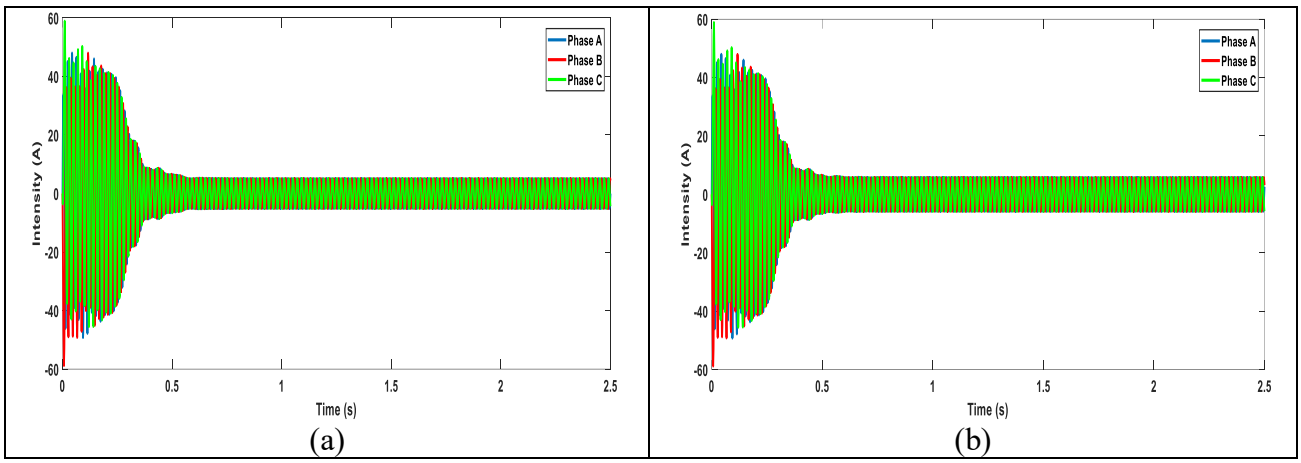



(e) (f)

Figure 3.12: healthy machine variables : a- stator current phaseA, b- stator current phaseB, c- stator current phaseC, d- three phase current signal, e- Electromagnetic torque, f- rotational speed.

### 3.5.1.1 Healthy machine variables by varying load conditions

After obtaining the variables of the machine in healthy state as was showcased in (figure 3.12), another key factor will take place, which is simulating the model under various operational conditions to exhsibit the state of the current signal under the changes of the load, and to achieve this, various torques were applied ( no load, weak load, medium load and heavy load) which were attributed the following torques respectively 0 *N.m*, 10 *N.m*, 30 *N.m*, 40 *N.m.* as mentioned before we are interested in this study of obtaining the current signal which will be used for fault diagnosis, therefore, we will observe the evolution of its signal throughout various operational conditions.




(a) (b)

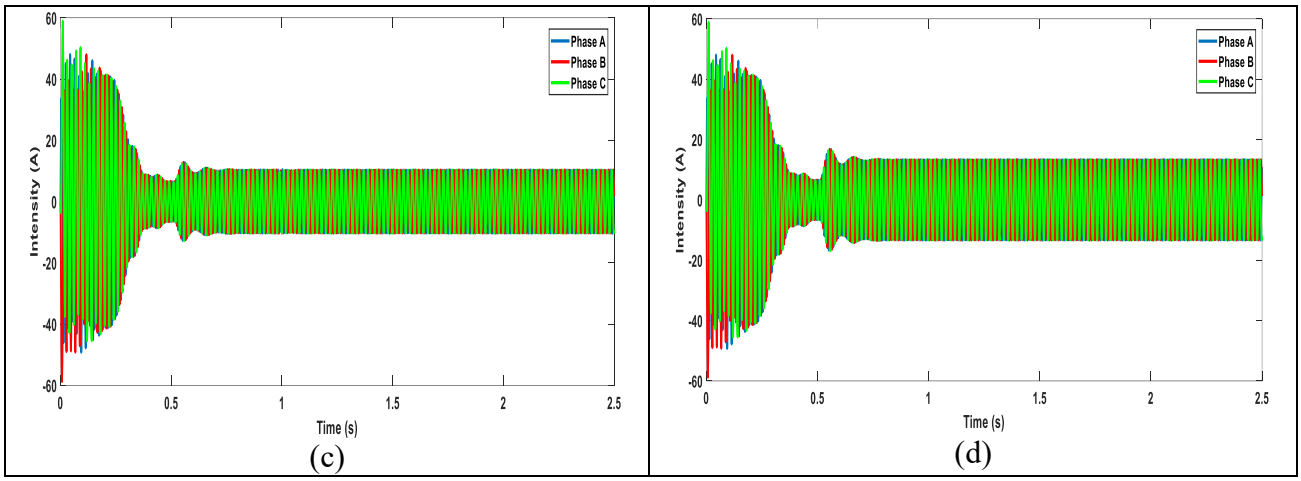
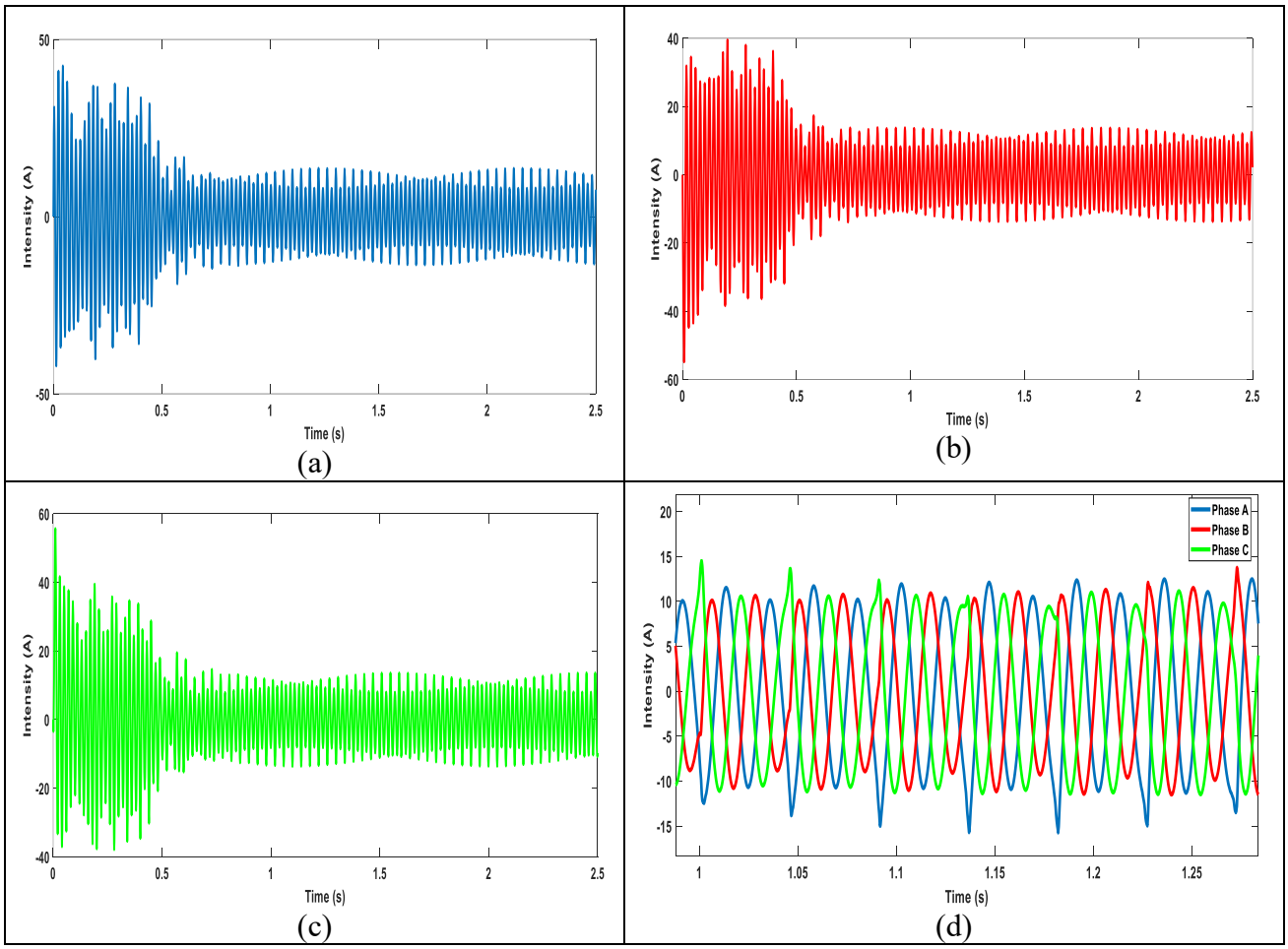


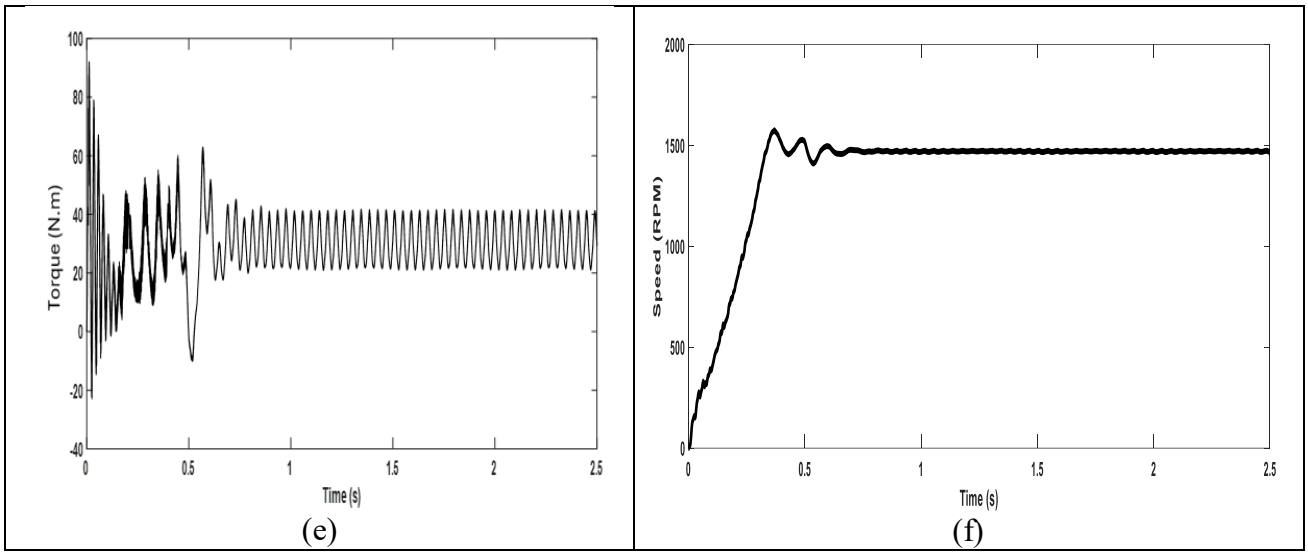

Figure 3.13 Healthy machine stator current: a-No load, b- Weak load, c-Medium load, d-Heavy load

### 3.5.2 Faulty machine variables

The next phase concerns obtaining the results of the simulation for a machine that suffers from eccentricity defect under medium load condition, the results of the simulation are illustrated in (Figure 3.14).

#### 3.5.2.1 Eccentricity fault



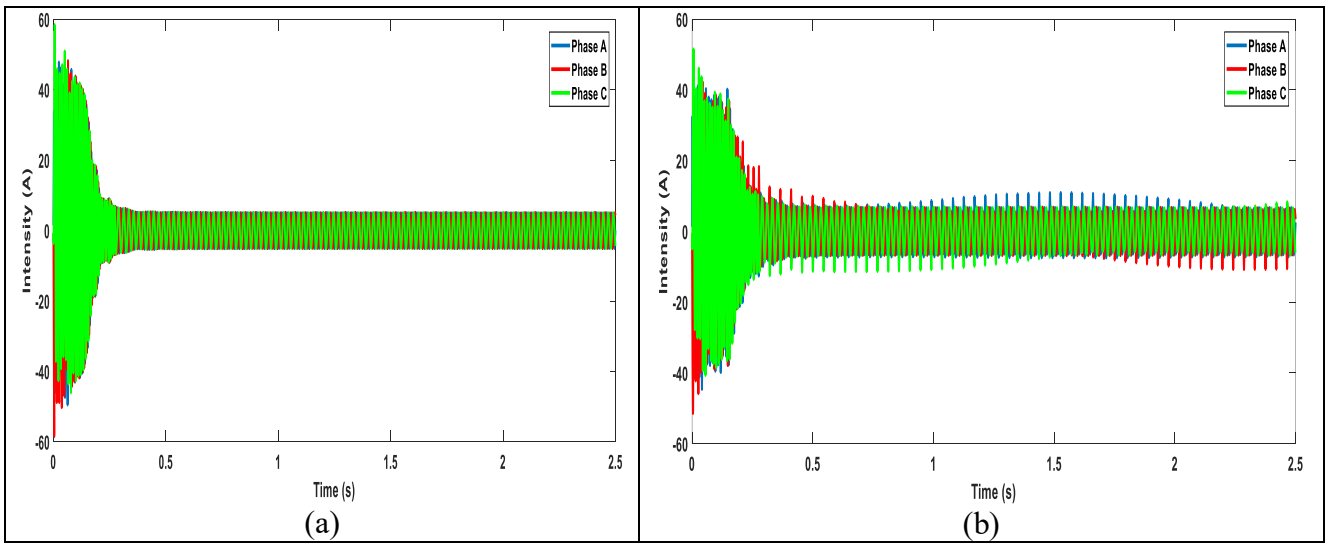



(e) (f)

Figure 3.14 faulty machine variables: a-stator phase A, b- stator phase B, c-stator phase C, d-stator current zoomed part, e- electromagnetic torque, f- rotational speed.

### 3.5.2.2 Eccentricity fault by varying load conditions

As mentioned in chapter 1, eccentricity fault has various types and each defect has its own signature and influence on the machine, therefore, in this section we have chosen one type of eccentricity to showcase its evolution under various load conditions which is dynamic eccentricity (for reasons that we'll explain in the following section) so we can compare it with the results obtained from simulating healthy machine. The results are shown in Figure 3.15 below




(a) (b)

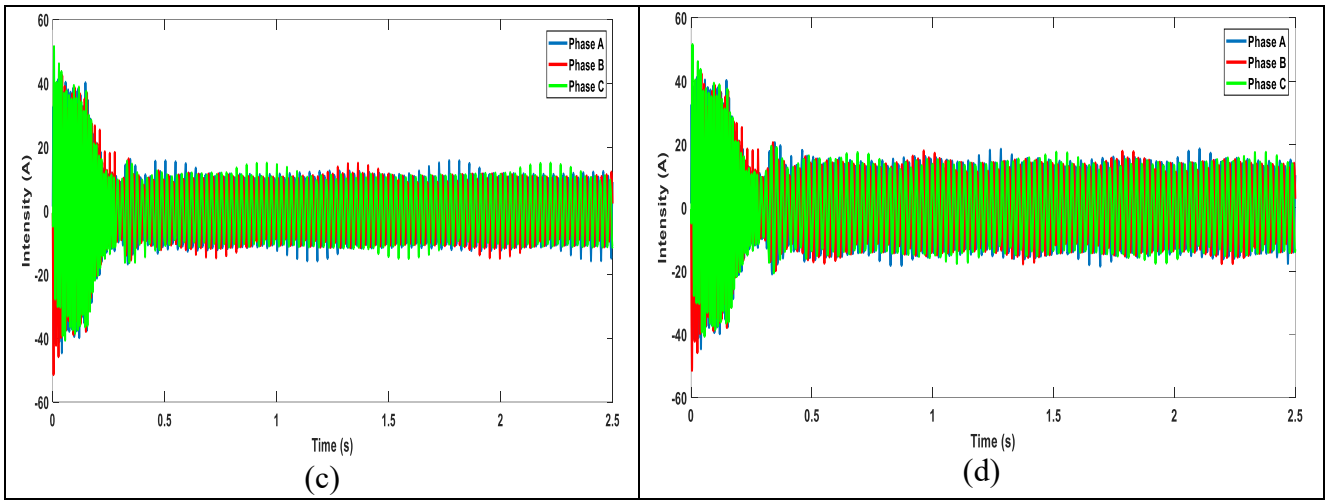
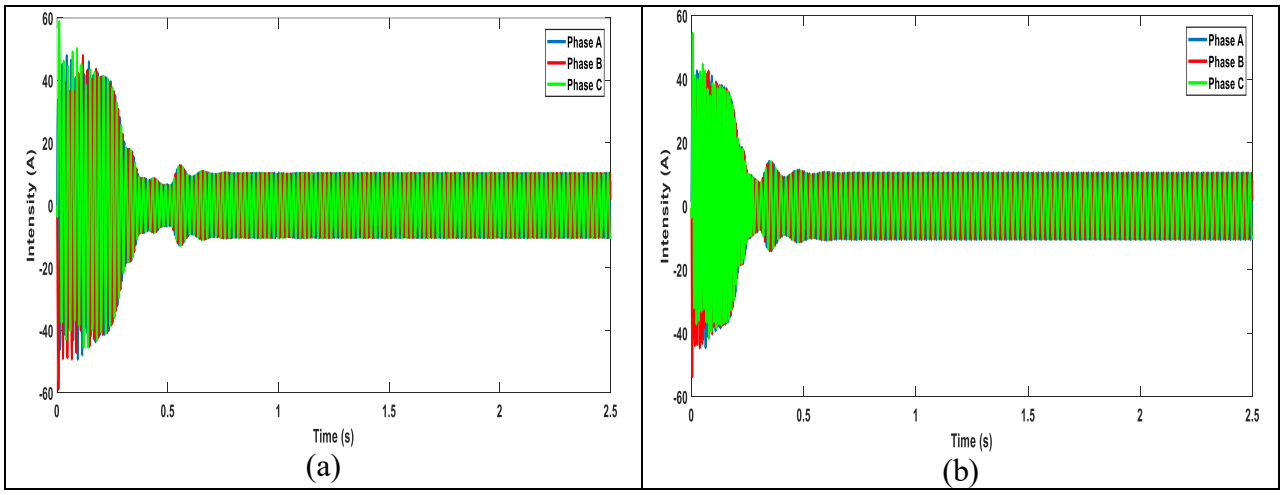



Figure 3.15 Faulty machine stator current: a-No load, b- Weak load, c-Medium load, d-Heavy load.

Figure 3.15 illustrates the influence of eccentricity on stator current which can not be apparent on weak load conditions which is a crucial information to include in the diagnosis process, when the load conditions increase the fault signature also increases by deforming the sinusoidal form of the current which would lead to catastrophic impacts on the machine ( low efficiency, excessive heating, irregular rotational speed,..etc) .

### 3.5.2.3 Eccentricity fault types

As clearly mentioned in chapter 2, eccentricity fault has multiple types and forms. In this section, we will showcase the types of eccentricity by simulating the machine and acquiring stator current signals, the obtained results are acquired through simulating the machine under medium load condition, the results are shown in Figure 3.16 below



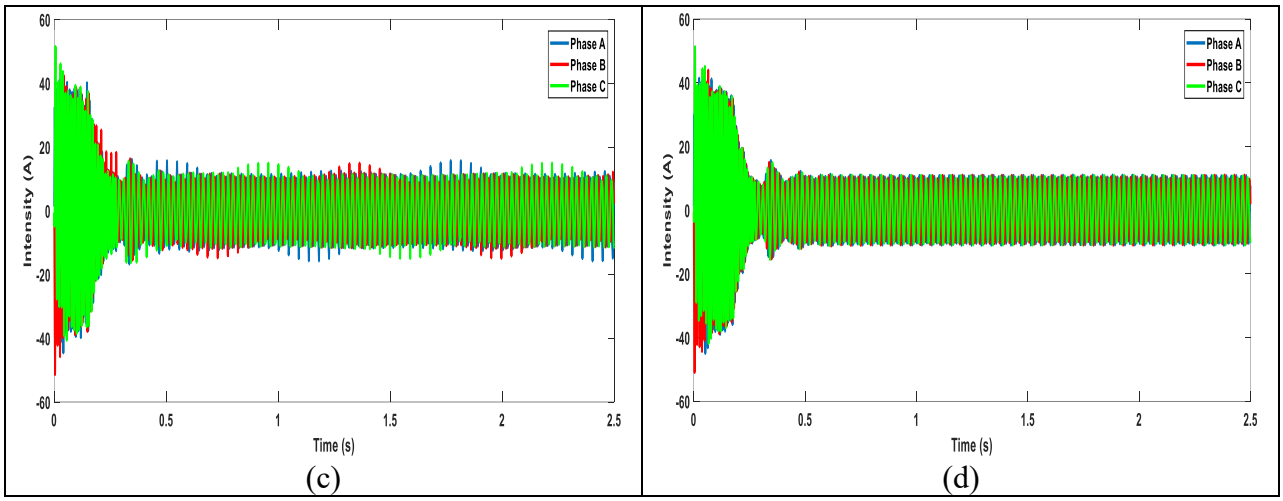



Figure 3.16 Eccentricity fault types: a- healthy machine, b- static eccentricity, c- dynamic eccentricity and d- mixed eccentricity.

After analyzing the results of each type of eccentricity, it became evident that each type of eccentricity has its own influence on the stator current and some of them are not easy to detect, another important point which would determine the course of our research, which is the fact that eccentricity has an impact on all of the phases of the current, that indicates that all of them must be included for fault detection.

### 3.5.2.4 Eccentricity fault under various fault severity degrees

This section is dedicated to illustrating the severity degree of each type of defect, the simulation is obtained by fixing the load condition at *30N.m*. The importance of these results resides in tracing the defect evolution at several severity degrees from early to extreme stages to have a better understanding of its influence on the stator current, which is a crucial step towards a proper diagnosis of the machine's condition.

The chosen degrees of eccentricity for each type are set from healthy to early stage to extreme to critical, in this case 10% is considered a healthy degree, since eccentricity fault is omnipresent even in newly manufactured machines ( mentioned in state-of-the-art section), 20% is considered early stage, 30% is considered extreme stage and above that is critical stage.

The following results concern signals of the stator current under static eccentricity with various severity degrees compared to the one obtained from healthy signal.

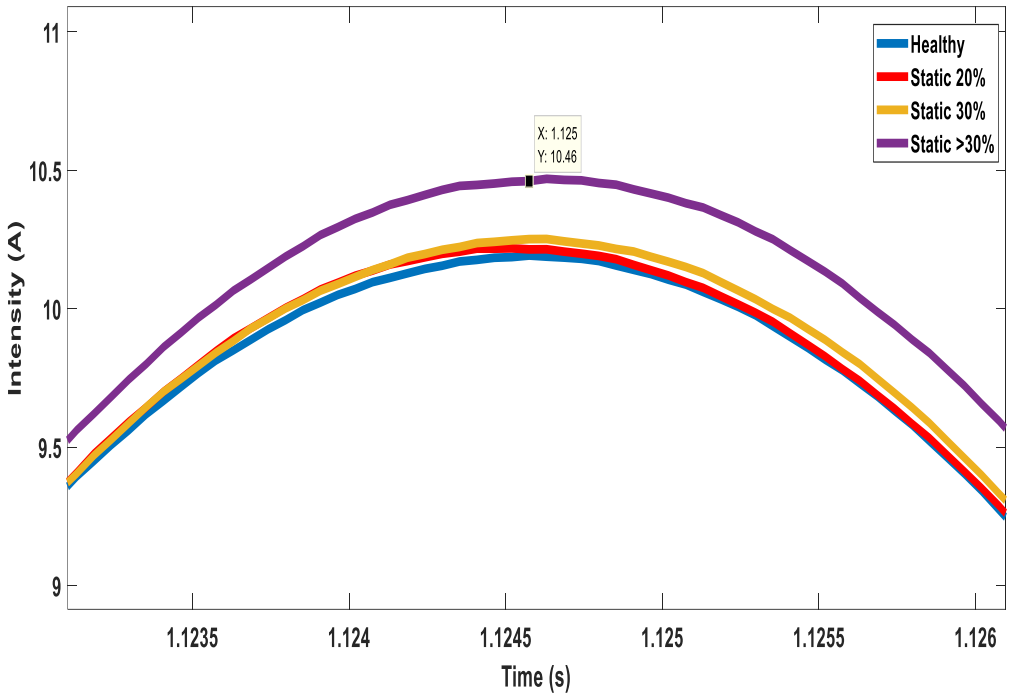
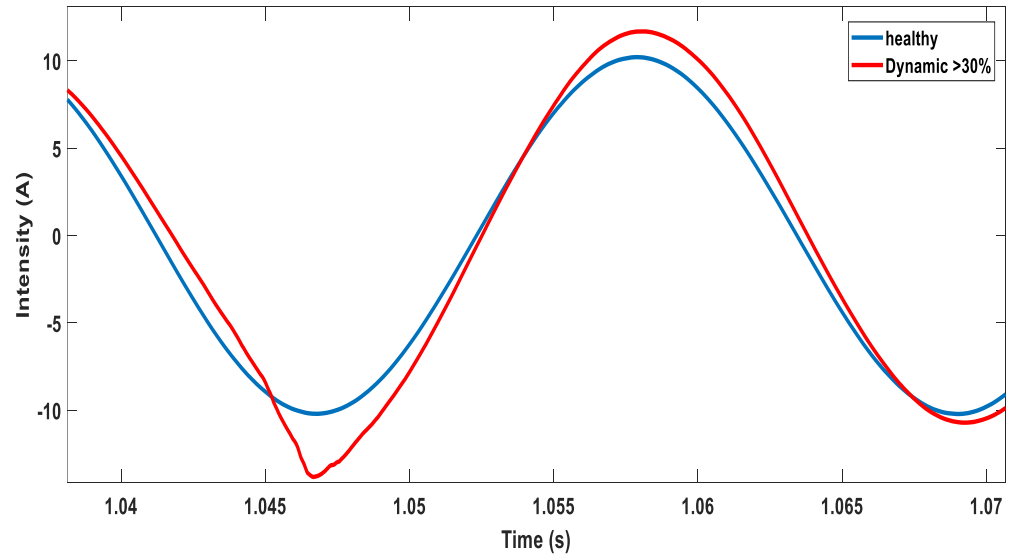



Figure 3.17 static eccentricity influence on stator current : a-healthy, b-20% eccentricity, c-30% eccentricity, d- critical static eccentricity.

By inspecting the results obtained from simulating the model under various degrees of static eccentricity, one can notice that static eccentricity has a subtle influence on the stator current especially on its early stages, where hardly any harmonics are visible on the sinusoidal form of the current, which makes the detection by the naked eye hard in this case and requires more advanced techniques for fault detection.

Figure 3.18 illustrates the results of dynamic eccentricity impact on the stator current under various severity degrees compared to the healthy signal.



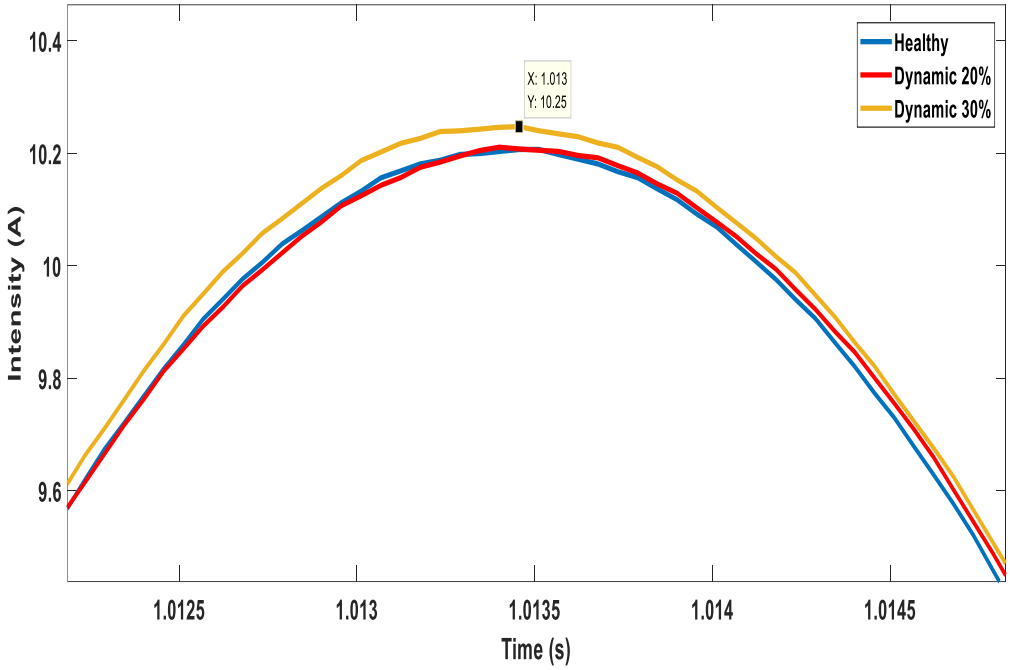



Figure 3.18 Dynamic eccentricity influence on stator current

By investigating the results obtained from simulating the model for dynamic eccentricity, like the previous type of eccentricity, the early stage of defect can be barely visible or easy to detect and the evolution of the defect can exacerbate the fault condition causing more critical harmonics if the problem persists with extreme degrees of severity.

Figure 3.19 shows the results of mixed eccentricity with various severity degrees compared to the obtained healthy signal.

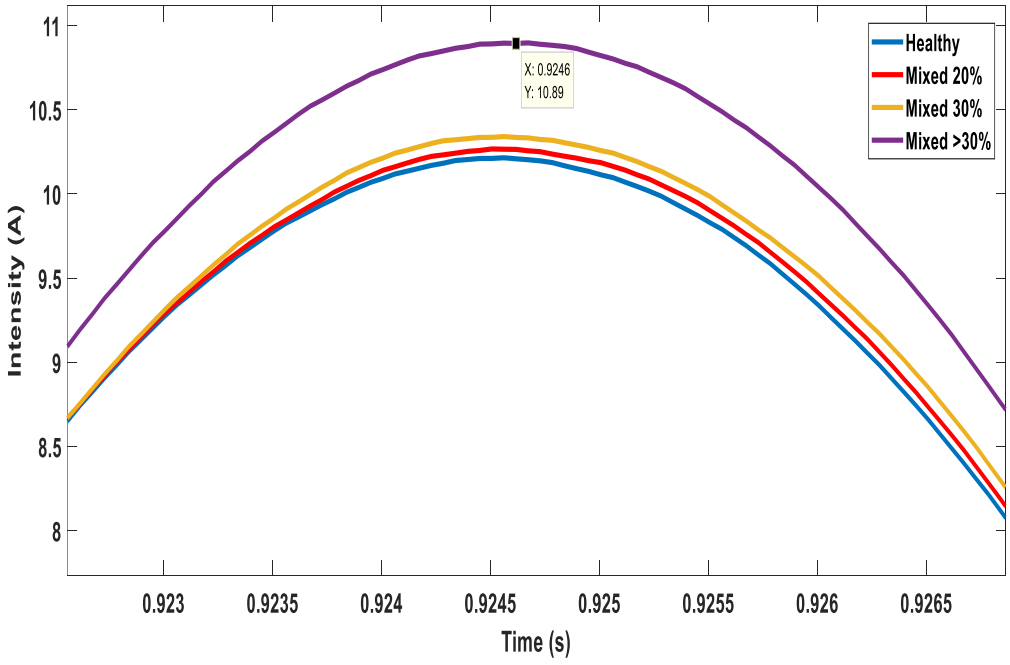



Figure 3.19 Mixed eccentricity influence on stator current

The same observation can be extracted from the visual analysis of this result and the previous results, leading to a conclusion that the fault at its early stages is hard to detect and requires more sophisticated approaches to distinguish between each case to be able to make the right decision about the machine's condition.

Now after analyzing the results, we can extract some vital information about the air gap eccentricity, which is the fact that relying only on visual analysis by itself for fault detection is not useful especially for early stage of the defect and also at no to weak load conditions, where the defect doesn't manifest on the current signal, which is a downside for this approach and may lead to misdiagnosis or ignoring the presence of the defect from the first place. The problem can only be visible at extreme stages of the defect which is not ideal for fault detection, since these degrees are critical to the machine's health state and will lead to sudden breakdowns of the machine, which means that preserving the machine's health impractical, therefore, for the upcoming results we will focus on these key factors in our diagnosis :

- **10%** severity degree is considered a healthy state for the previously mentioned reasons.
- **20%** is considered as an early stage, and since it's hard to detect, this case will be considered as faulty condition and will be included in fault detection.
- **30%** is considered as an extreme stage since its effects are more visible and can lead to undesirable consequences.
- Degrees above **30%** were used such as **40%**, **50%** and **60%** of air gap eccentricity and their impact is more apparent on the current signature, therefore, they will be considered as critical cases.

#### 3.5.2.5 Broken rotor bars fault

Now the model is simulated for broken rotor bars, it is notable that the used model has 40 rotor bars in total, and in this section we'll focus on applying the defect at ***1 second*** to showcase the reaction of the stator current with this type of defects, and as the previous approach we will extract all of the stator phases to observe whether the fault's impact manifests on a particular phase or all the phases combined, speed and electromagnetic torque results are also gathered to showcase the faults impact on other variables of the machine and its ability to influence the machines performance.

In this study we will study 5 cases of broken rotor bars, which are the following:

- One broken rotor bar (1BRB).
- Two broken rotor bars (2BRB) adjacent to each other.
- Two broken rotor bars (2BRB) apart from each other.
- Three broken rotor bars (3BRB) adjacent to each other.
- Three broken rotor bars (3BRB) apart from each other.

The results obtained in Figure 3.20 concern broken rotor bars, we have chosen the case of two broken rotor bars specifically at ***1 second*** , it is notable that we will not use combined faults in this study, rather we will study each defect independently, to have a better understanding of the fault's signature and influence on the current signal .

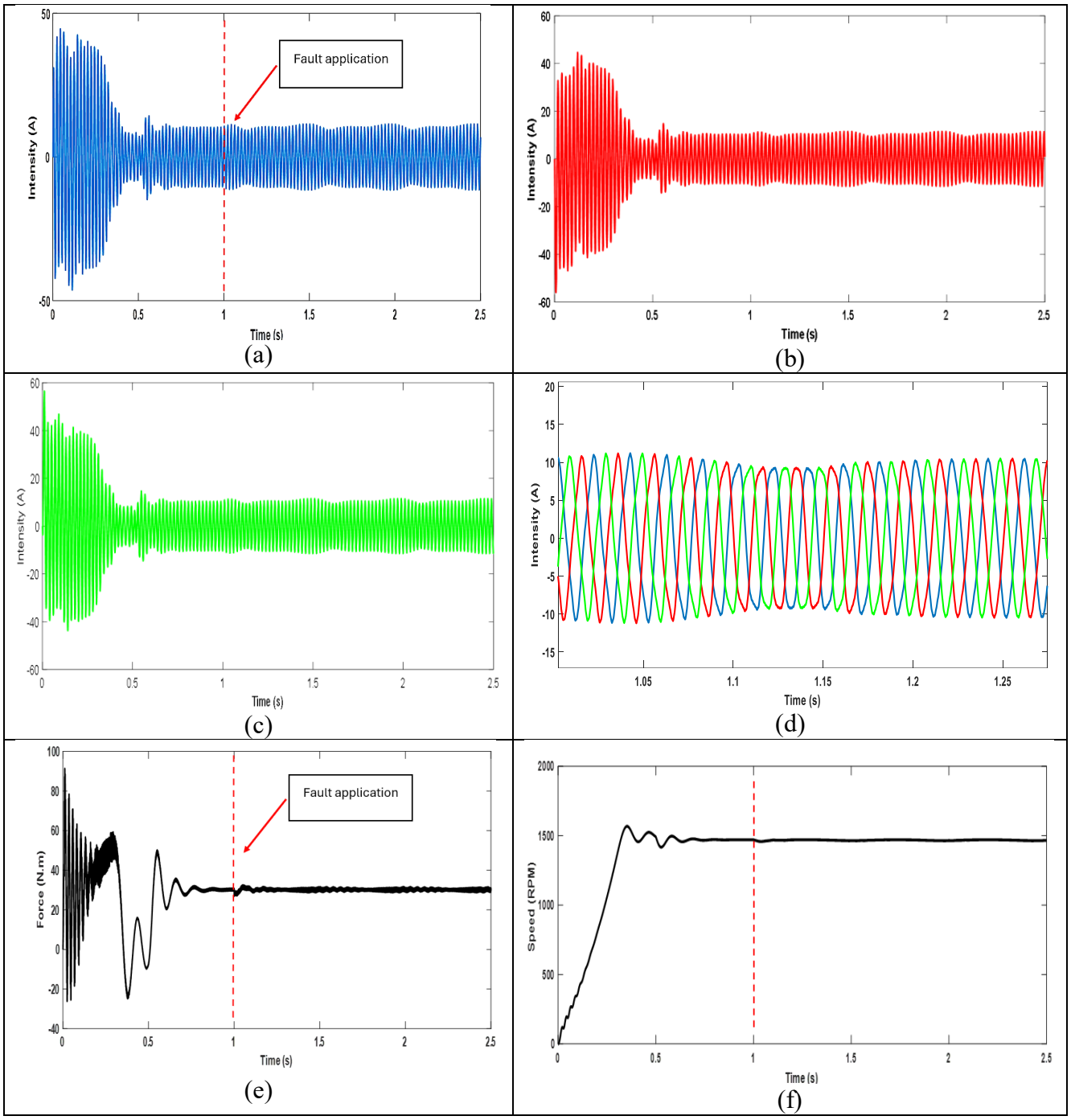



Figure 3.20 faulty machine variables: a-stator phase A, b- stator phase B, c-stator phase C, d-stator current zoomed part, e- electromagnetic torque, f- rotational speed.

After analyzing the obtained results, it is clear that broken rotor bars fault has its impact on the current signal by creating oscillations on all of the current phases and in the general sinusoidal form of the current, also the impact extends to effect electromagnetic toque by causing ripples after applying the fault at ***1 second*** and its impact persists after that, same thing could be said about the angular rotational speed.

### 3.5.2.6 Broken rotor bars fault by varying load conditions

In this section we obtained the results of applying multiple load conditions with the presence of BRB fault, the loads considered for this simulation are no load, weak load, medium load and heavy load which were attributed the following torques respectively 0 *N.m*, 10 *N.m*, 30 *N.m*, 40 *N.m*.

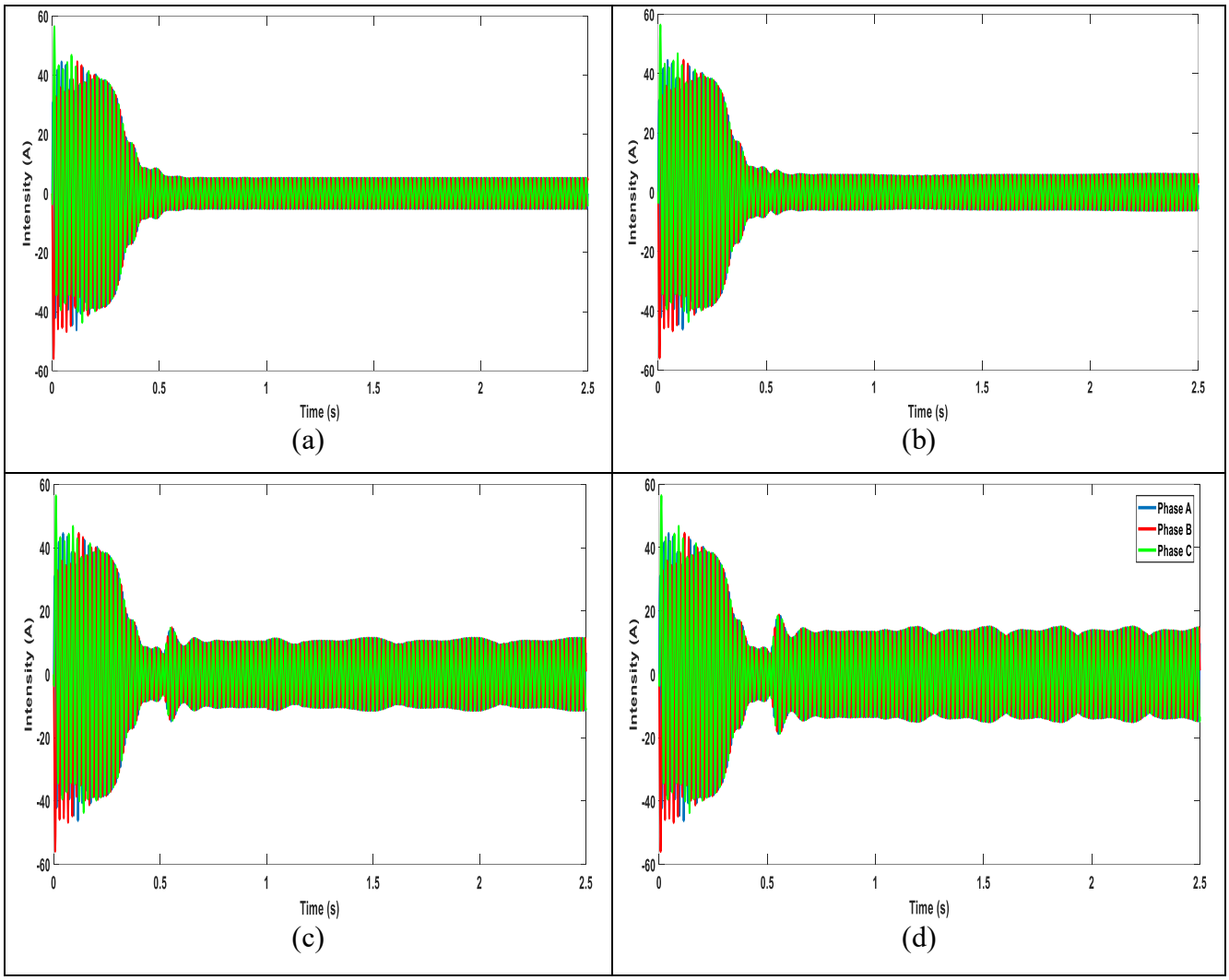



Figure 3.21 Faulty machine stator current: a-No load, b- Weak load, c-Medium load, d-Heavy load.

After analyzing the obtained results, one can notice that the defect is apparent that at no load and weak load conditions the defect's influence is less apparent, which is not ideal for practical fault conditions in these scenarios.

### 3.5.2.7 Broken rotor bars fault under various fault severity scenarios

In this section we will simulate broken rotor bars defect under various fault severity degrees and type, to showcase properly the signature of the defect on the stator current we have fixed the load condition at ***30N.m*** (medium load), the results are illustrated in Figure 3.22.

For the case of two adjacent broken rotor bars we have chosen bar number **1 and 2**, and for the ones apart from each other we have chosen bars number **1 and 15.**

For the case of three adjacent broken rotor bars we have chosen bar number **1, 2 and 3**, and for the ones apart from each other we have chosen bars number **1, 20 and 30.**

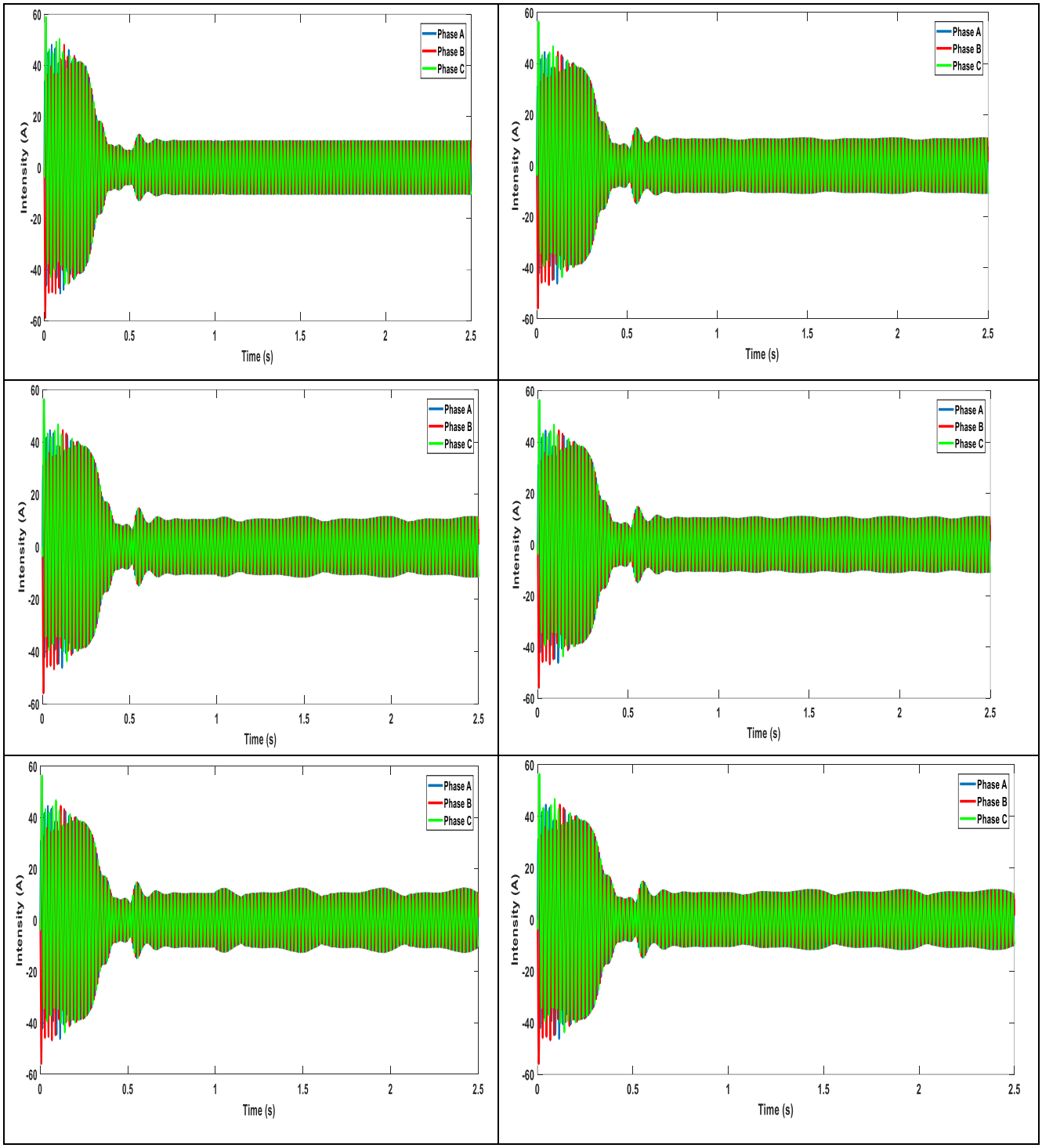



Figure 3.22 broken rotor bars fault signature : a- healthy machine, b- 1 BRB, c- 2 BRB adjacent, d- 2 BRB apart, d- 3 BRB adjacent, e- 3 BRB apart.

After analyzing the results, we can notice that the defect at its early stages has a modest impact on the current signal and as it evolves it becomes greater in the image of 2 BRB, however, in the case of 2 BRB when the bars are apart from each other, we can notice that the harmonics have less amplitude but more frequency in the current signal in comparison to the adjacent bars

case. However, in 3 BRB case we can notice that, when the fault is consecutive within the bars the harmonics are more frequent and have great amplitude in comparison to the case where they are apart from each other.

As a summary to the results that we have presented, it became clear that both eccentricity and broken rotor bars faults possess some similarities with each other, we can sum them up in these points :

- Fault signature on the stator signal can be reliable as a fault indicator.
- In lower load conditions, fault signature is less apparent and hard to detect even in extreme severity degrees of the defect.
- Each type of defect has its own signature on the current signal, which requires a reliable approach to study each case individually because relying only on visual analysis may lead to misdiagnosis of the actual defect within the machine.

### 3.6 Conclusion

In this chapter, we have introduced the mathematical model of the three-phase squirrel cage induction machine, which will be used for the simulation in order to generate variables related to air gap eccentricity and broken rotor bar faults.

First, we adapted the model for the simulation of the previously mentioned faults by presenting the simplifying assumptions on which the multi-winding model is based. Subsequently, we calculated the various stator and rotor self and mutual inductances.

This model helps us better understand the physical properties related to these types of defects.

# Chapter 4

# Proposed Diagnostic Methodology and Artificial intelligence techniques application

## 4.1 Introduction

In this chapter, we will discuss the adopted methodology for diagnosing the induction machine using the current stator variables to assess its health condition under both healthy and faulty states. The latter encompasses the machine's condition under air gap eccentricity and broken rotor bar faults, as well as various fault types and operational conditions.

The first phase of this chapter will be dedicated to traditional MCSA techniques for diagnosis, such as signal processing using FFT and wavelet decomposition. Here, the current signal will undergo processing for feature extraction to determine the machine's health condition.

The second phase will focus on proposing a flowchart based on the AI algorithm and showcasing preliminary results of gradually employing the collected dataset in the AI model. Eventually, we will determine which type of supervised learning task is most suitable for the diagnostic process.

In the following section of this chapter, we will introduce more sophisticated techniques to diagnose defects leveraging the current signal to overcome the limitations of the simple visual analysis.

## 4.2 Classic MCSA approaches

It was mentioned in the state of art chapter that signal processing techniques are considered as a non-model-based approaches used frequently for various domains including fault detection encompassing image processing, audio processing and signal processing.

In this section we will use two most frequently used techniques used in Motor Current Signature Analysis (MCSA), which are FFT and WT techniques, to showcase their ability to extract vital information about the machine’s health state, and to trace the fault signature within the signal.

### 4.2.1 Frequency domain analysis

#### 4.2.1.1 Frequency domain analysis under variable load conditions for eccentricity

The following analysis is conducted using one phase of the stator current, the chosen load profiles are weak and heavy load conditions *10 N.m* and *40 N.m* respectively for healthy and faulty machines see (Figure 4.1, 4.2):

The frequency of the air gap eccentricity is given by :

$$f_{ecc} = |f_s \pm k \cdot f_r| \tag{4.1}$$

Which gives a specific harmonic components on the stator current spectrum.

Where :

$f_s$: supply frequency;

$f_r$: mechanical rotation frequency; ( $f_r = \frac{f_s(1-s)}{p}$ )

s: is the slip ; ( $s = \frac{N_s - N_r}{N_s}$ )

$k$: integer (1,2,3..);

$p$: number of pole pairs.

Static eccentricity : $$f_{se} = f_s \left[ (kR \pm n_d) \frac{1-s}{p} \pm v \right] \tag{4.2}$$

Where :

$R$: number of rotor slots;

$n_d$: order of the eccentricity ( for static eccentricity $n_d = 0$ because we have a static rotational speed where the rotor turns on itself ) and for dynamic eccentricity $n_d = 1,2,3 \ldots$;

$v$: stator harmonic order.

Dynamic eccentricity

$$f_{de} = f_s \pm f_r \tag{4.3}$$

Mixed eccentricity

$$f_{me} = |f_s \pm k \cdot f_r| \tag{4.4}$$

#### 4.2.1.2 Frequency domain analysis under weak loads

Three current samples of the same type (static air gap eccentricity) have been chosen for the spectral analysis, to showcase the frequency domain analysis ability to detect frequencies related to the defect under weak loads, these samples are healthy, early stage and extreme stage the results of the spectral analysis are illustrated in Figure 4.1 below :

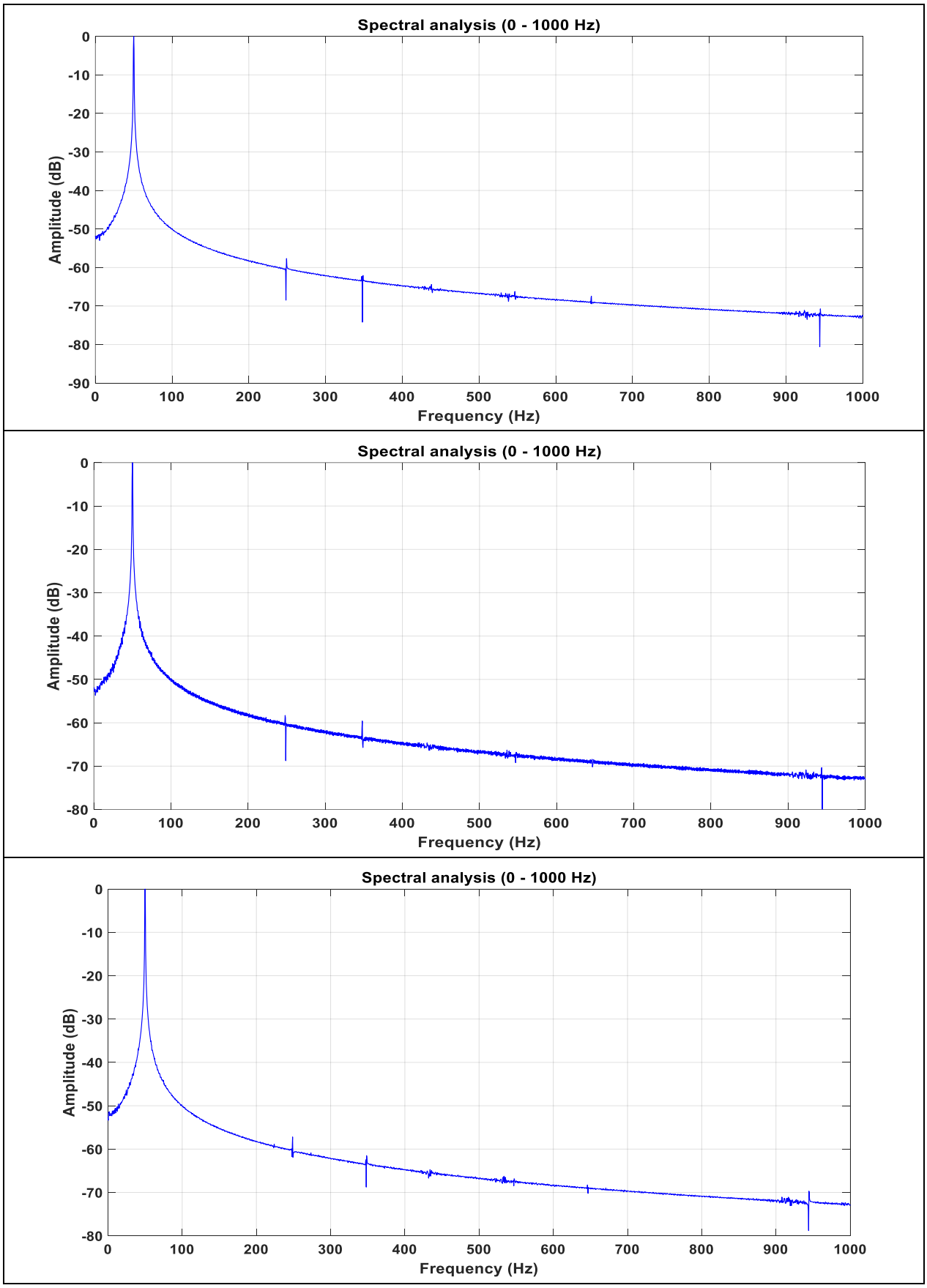
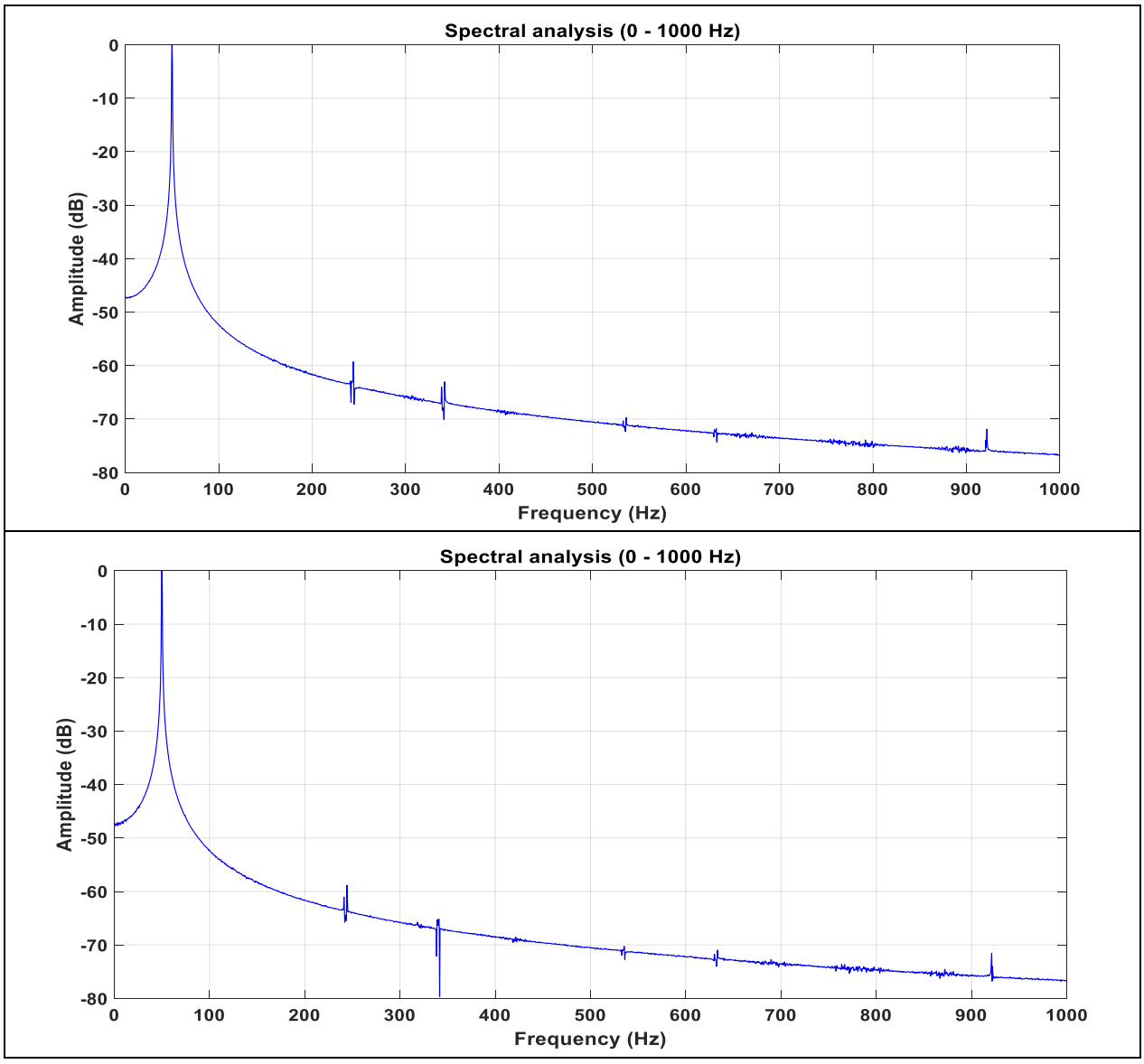



Figure 4.1 Current spectral analysis: a-Healthy machine, b- Early stage, c- Extreme stage.

The spectral analysis of the current shows that the frequencies related to the defect at early stage and extreme stage are not apparent especially around the fundamental $f_s$ because static eccentricity has no modulation in the magnetic flux due to constant air gap and the frequencies related to the defect only appear at high frequencies [200-400 Hz] with small amplitudes, which indicates that the approach struggles at this level of load condition.

#### 4.2.1.3 Frequency domain analysis under heavy loads

The same analysis was conducted using same profiles but under heavy loads, the results are illustrated in Figure 4.2 :



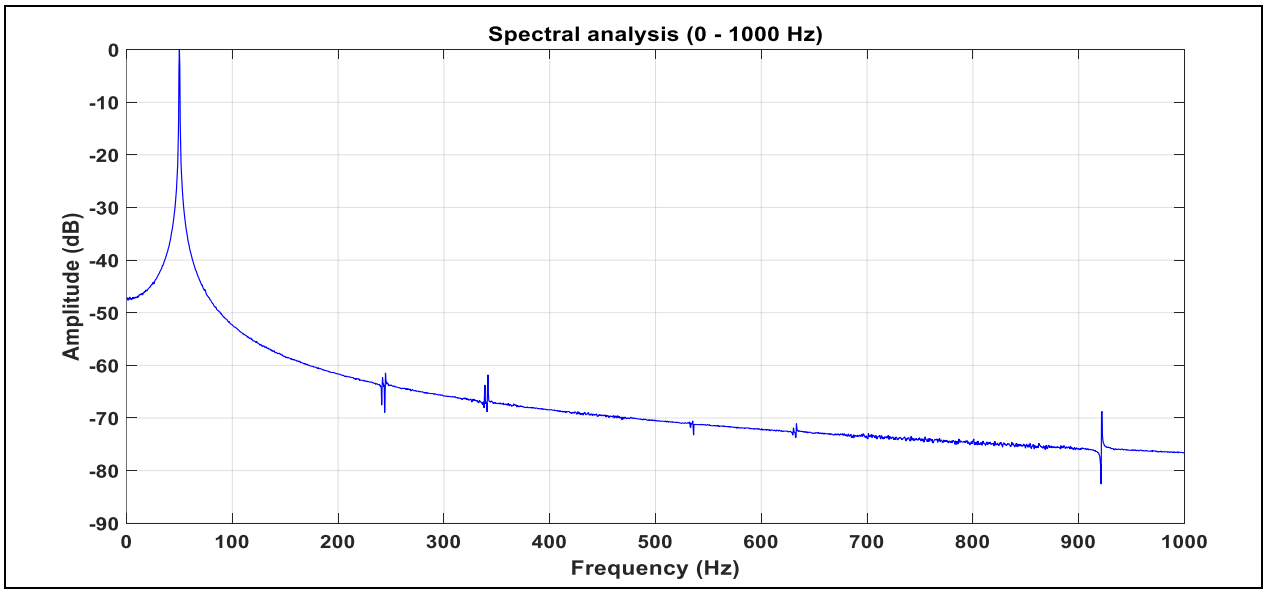



Figure 4.2 Current spectral analysis: a-Healthy machine, b- Early stage, c- Extreme stage.

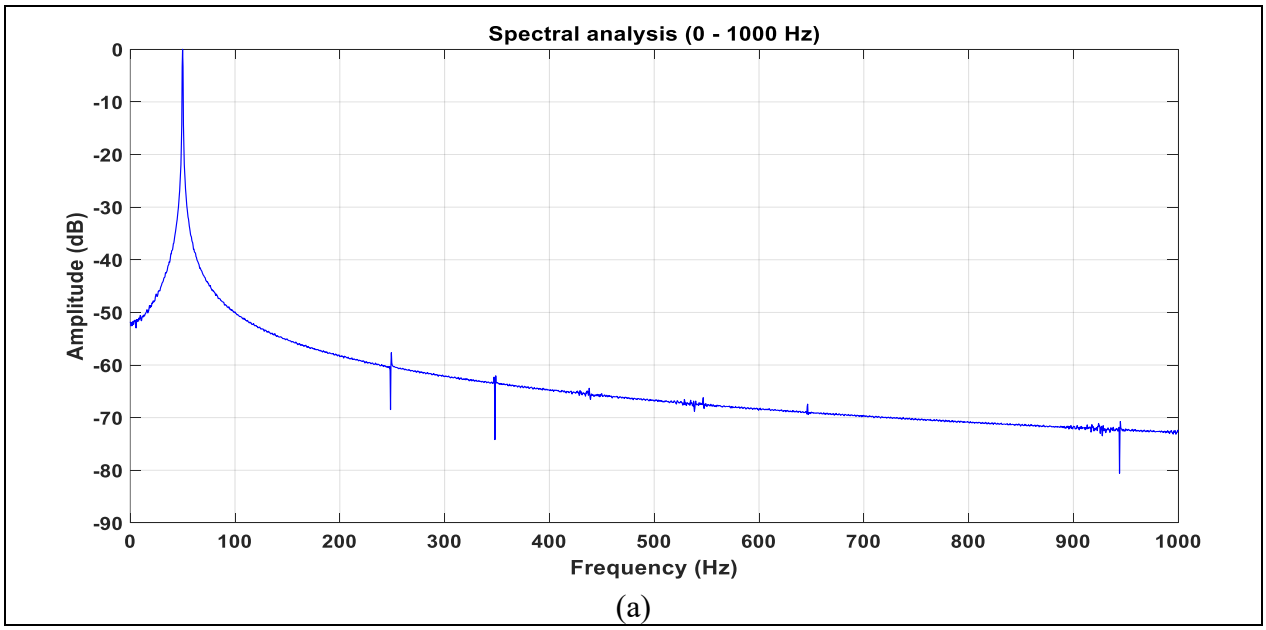
Under heavy load conditions, multiple frequencies can be shown especially at [200-400 Hz], [500-700 Hz] and [900-1000 Hz] that can be used to identify fault existence, that means that the spectral analysis provides vital information about the frequencies related to the defect and its severity.

#### 4.2.1.4 Frequency domain analysis under various fault types

the following section consists of using the spectral analysis on multiple types of air gap eccentricity ( static, dynamic and mixed) and under multiple load conditions (weak and heavy loads) the results are shown in Figures (4.3 and 4.4)

#### 4.2.1.5 Frequency domain analysis under various fault types at weak loads

The next step consists of using the technique to identify fault type,




(a)

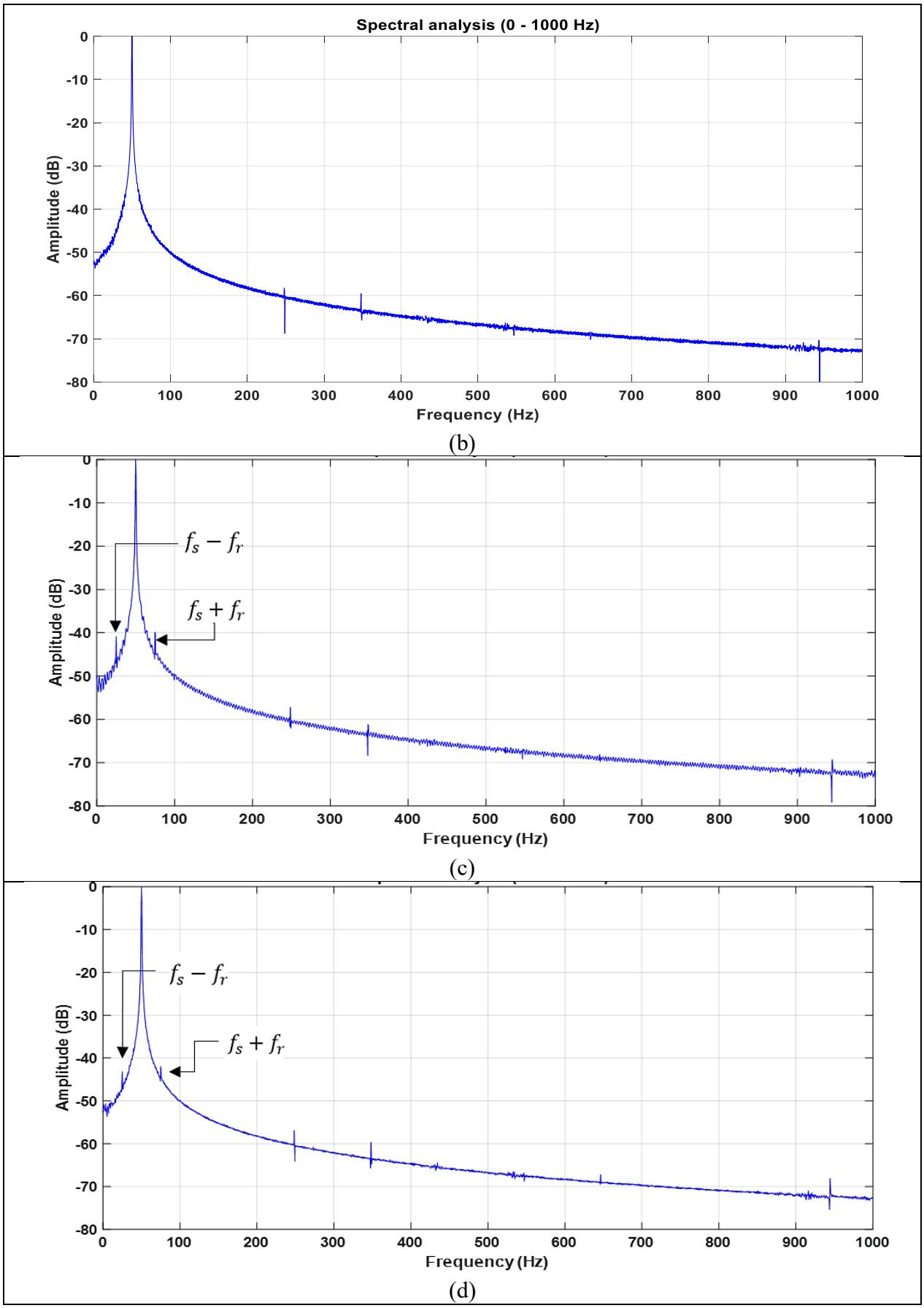
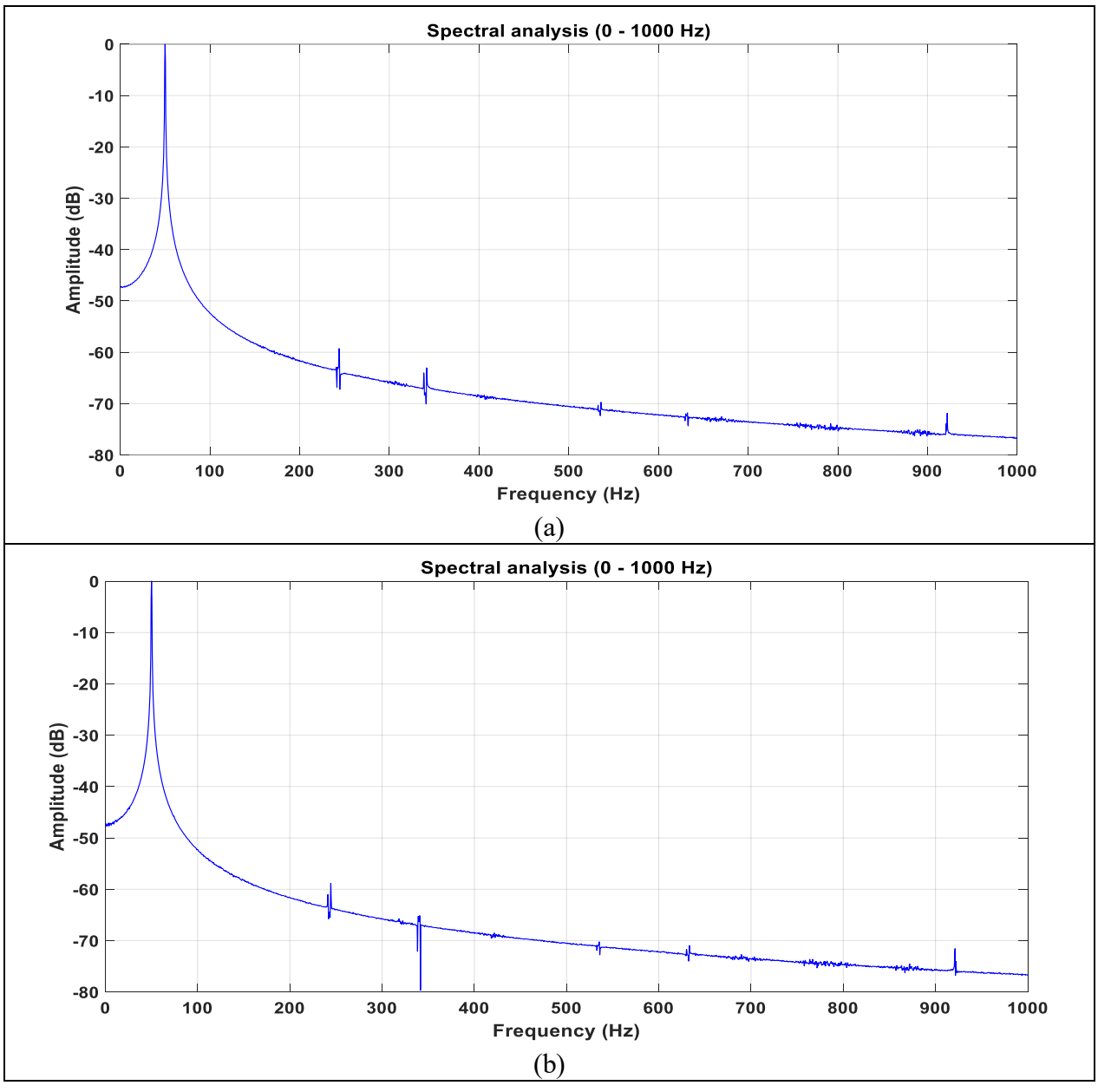



Figure 4.3 Current spectral analysis: a-Healthy machine, b- Static eccentricity, c- Dynamic eccentricity, d- Mixed eccentricity.

We can notice that at weak loads, static eccentricity is the type has no apparent frequencies around the fundamental unlike dynamic and mixed which they have small amplitudes around the fundamental frequency in the order of ( $f_s \pm f_r$ ) because this type of defect has a modulation on the magnetic flux due to uniform air gap, since the rotor has a variation of rotational axis over time.

#### 4.2.1.6 Frequency domain analysis under various fault types at heavy loads



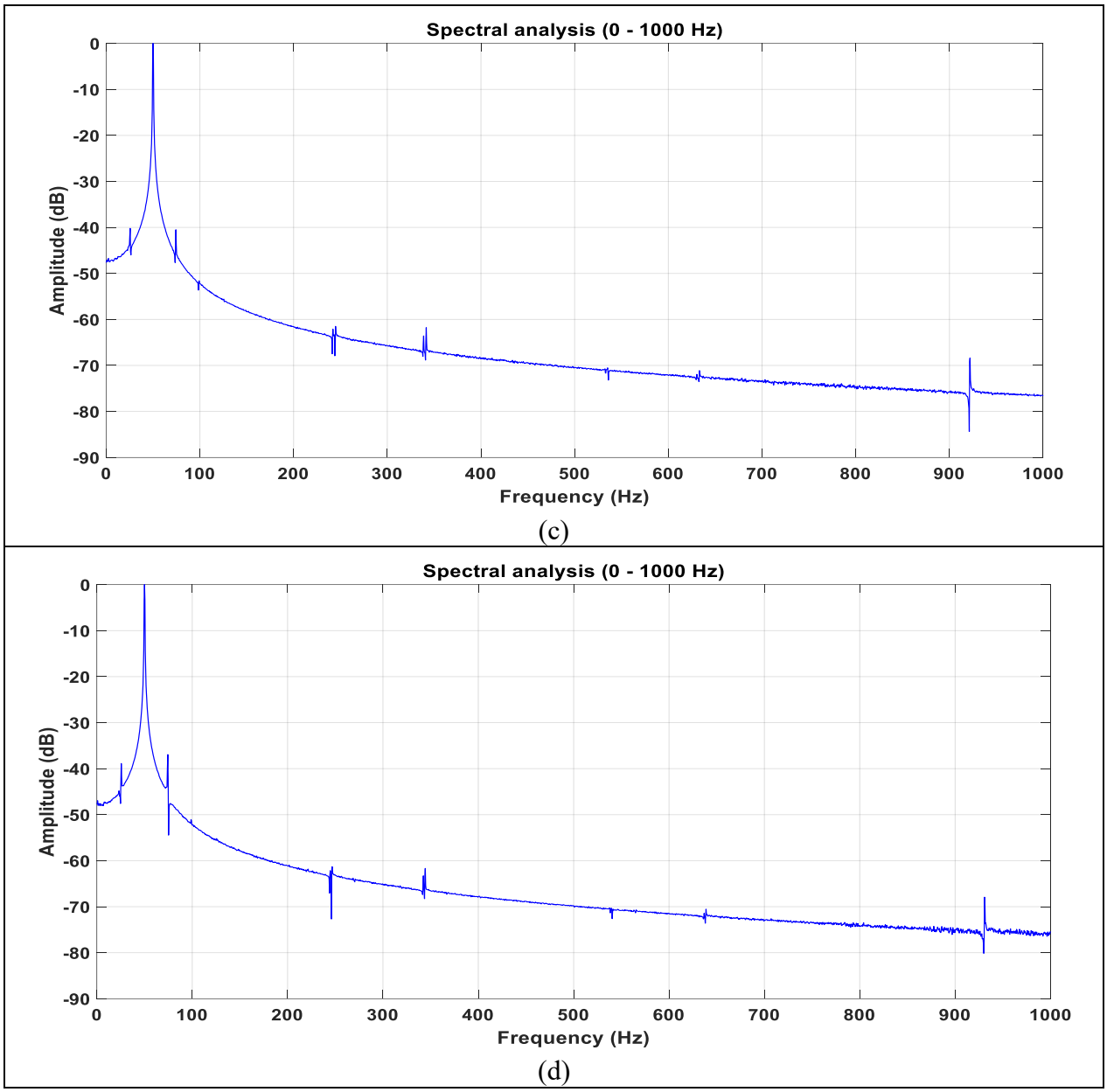



Figure 4.4 Current spectral analysis: a-Healthy machine, b- Static eccentricity, c- Dynamic eccentricity, d- Mixed eccentricity.

In summary, after conducting the frequency domain analysis on eccentricity faults, we have reached the following conclusion:

- The approach struggles at weak loads, which renders it impractical for fault detection.
- The approach can't identify certain types of eccentricity (Static) even at extreme stages of the defect, this can be critical in fault detection.
- The spectral analysis can identify frequencies related to the defect at heavy load conditions, that makes the technique reliable at certain scenarios.

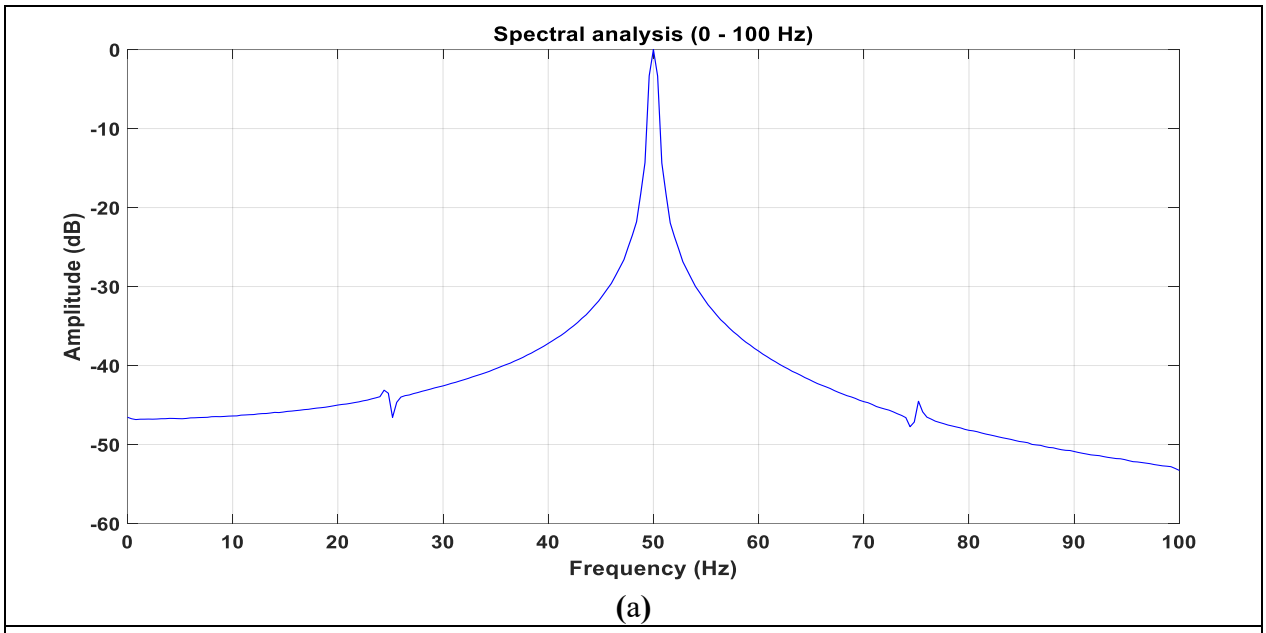
#### 4.2.1.7 Frequency domain analysis under variable load conditions for broken rotor bars

The general frequency that caracterizes a broken rotor bar fault is given by :

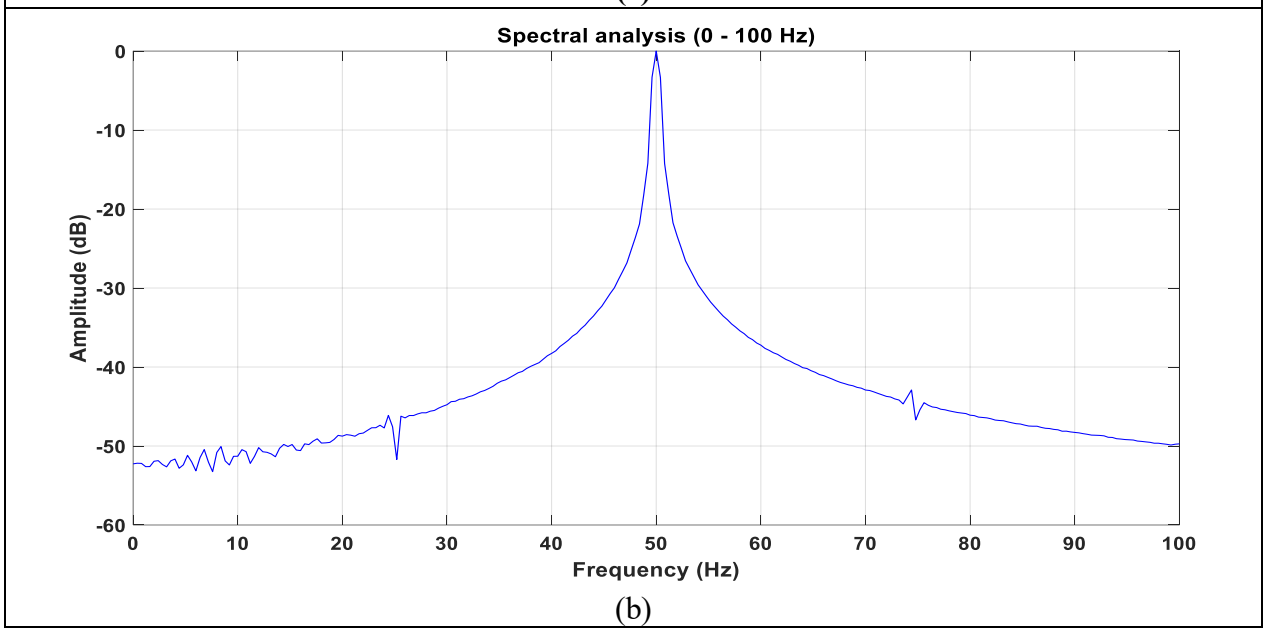
$$f_{BRB} = f_s(1 \pm 2ks) \quad (4.5)$$

For this analysis we have used a bandwidth from 0-100Hz for better frequencial resolution.

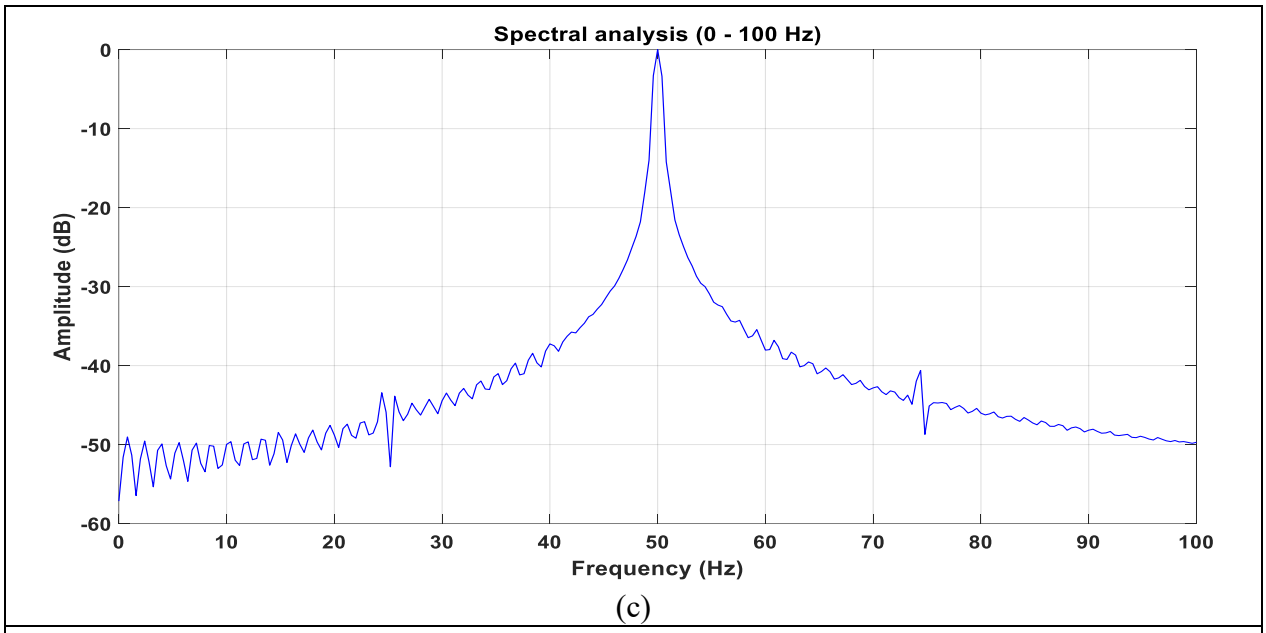
### 4.2.1.8 under weak load conditions



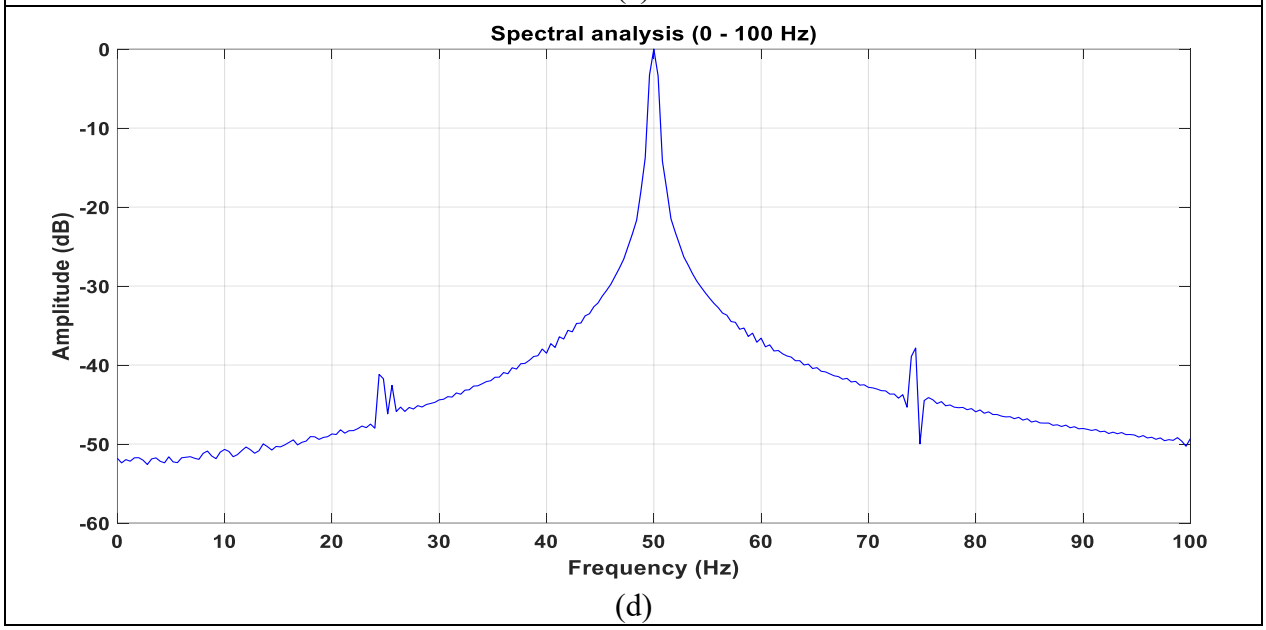

(a)




(b)




(c)



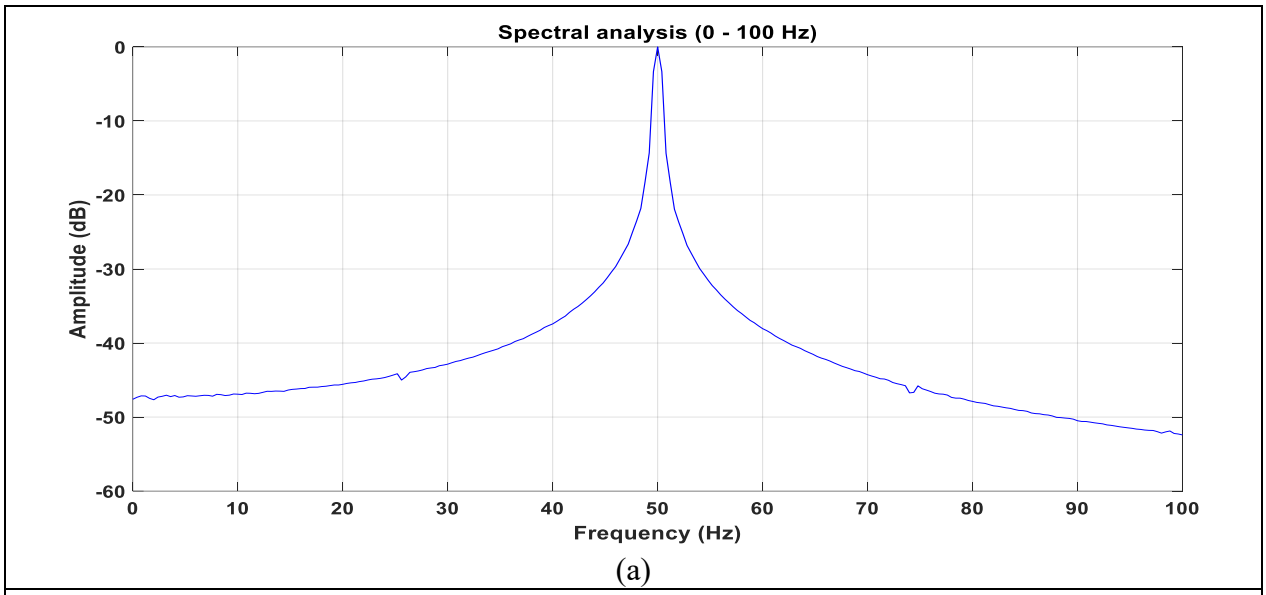

(d)

Figure 4.5 Current spectral analysis at weak load: a-Healthy machine, b- 1 BRB, c- 2 BRB, d- 3 BRB.

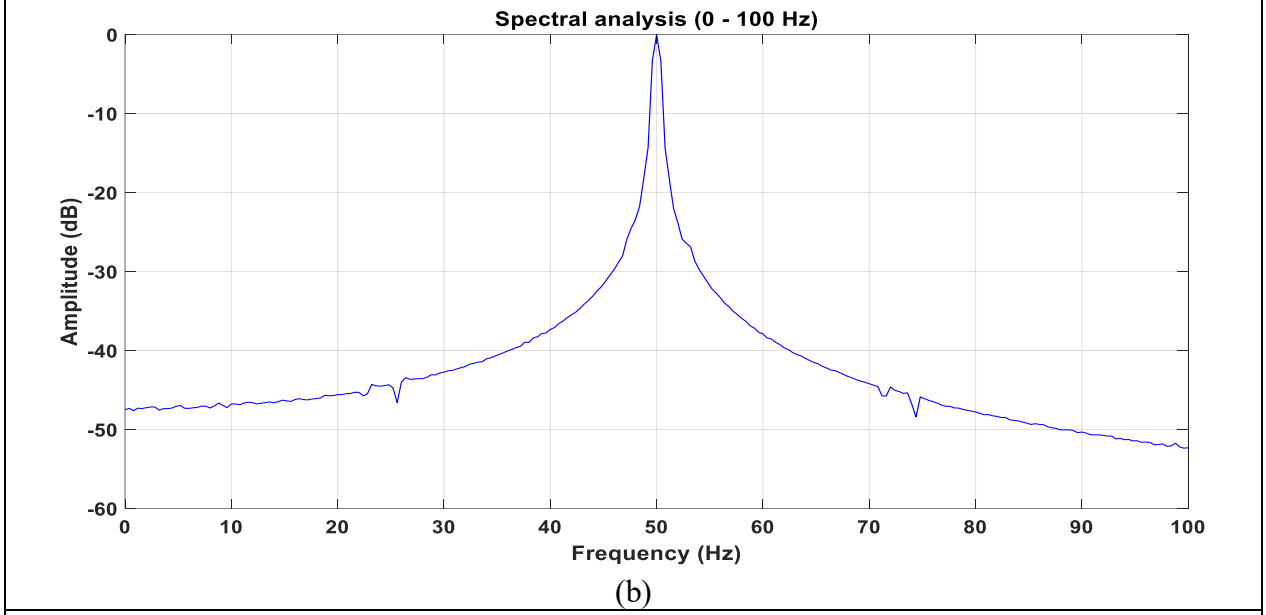
After analysis we can notice that broken rotor bars fault as eccentricity has its own signature on the current signal

The more the fault develops the more the frequencies related to the defect increase, especially in the bandwidth around the fundamental and [20-30 Hz] and [70-80 Hz] where the frequencies are more visible and significant.

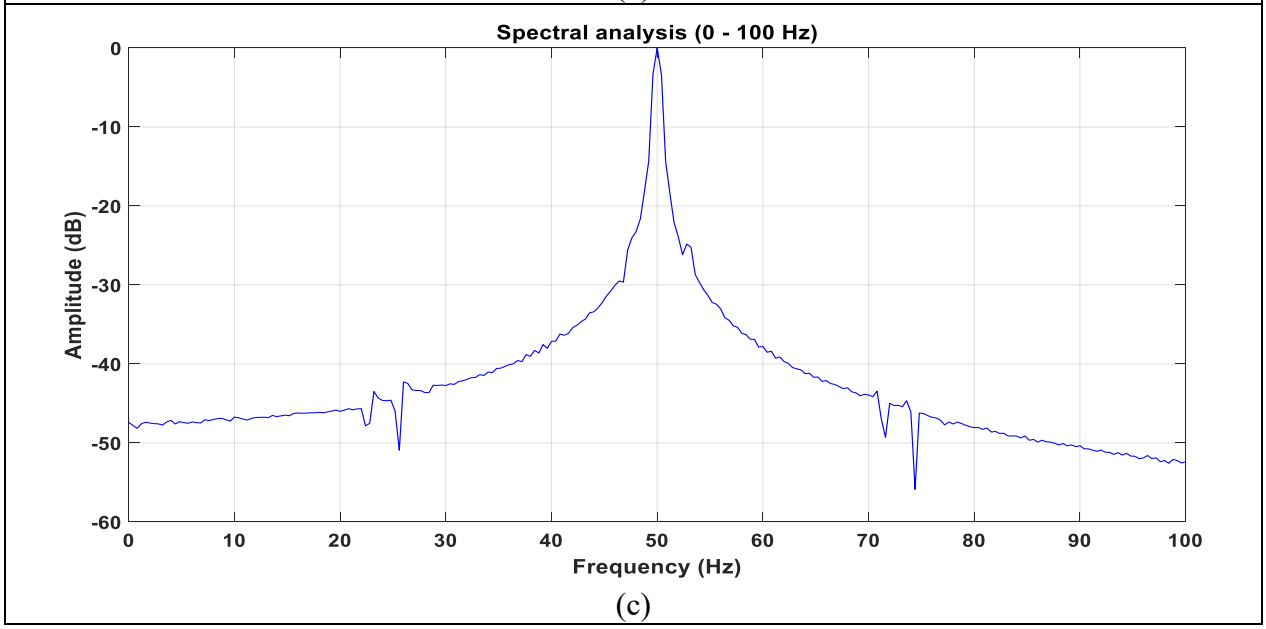
#### 4.2.1.9 under heavy load conditions


Spectral analysis (0 - 100 Hz)
Amplitude (dB)
Frequency (Hz)
0
-10
-20
-30
-40
-50
-60
0
10
20
30
40
50
60
70
80
90
100

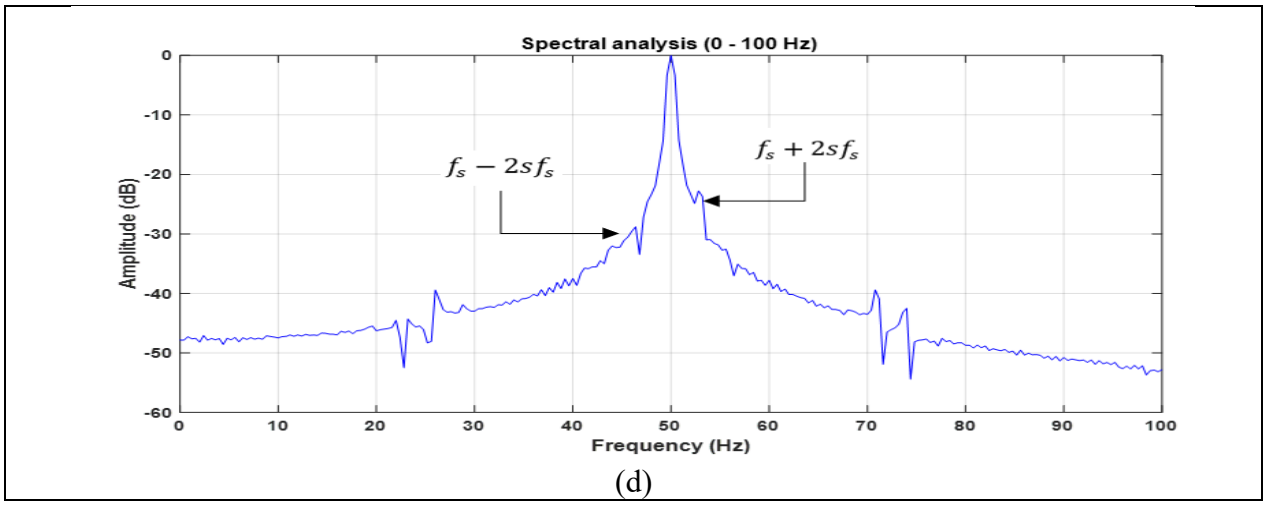
(a)


Spectral analysis (0 - 100 Hz)
Amplitude (dB)
Frequency (Hz)
0
-10
-20
-30
-40
-50
-60
0
10
20
30
40
50
60
70
80
90
100

(b)


Spectral analysis (0 - 100 Hz)
Amplitude (dB)
Frequency (Hz)
0
-10
-20
-30
-40
-50
-60
0
10
20
30
40
50
60
70
80
90
100

(c)




(d)

Figure 4.6 Current spectral analysis at heavy load: a-Healthy machine, b- 1 BRB, c- 2 BRB, d- 3 BRB.

Under heavy load conditions, the frequencies related to the defect the order of $f_s \pm 2ksf_s$ become aparent the more the severity of the defect increases, which could be in this case a good broken bar fault indicator using this technique, but struggles when there's only one broken rotor bar which makes frequency extraction hard.

After applying FFT on the provided current signal of both air gap eccentricity and broken rotor bars under various operating conditions and types and severity degrees, the technique proved reliable in some cases by applying a spectral analysis in order to extract the frequential identity related to each fault, the technique struggled with some types of defect and under certain conditions especially at weak load conditions which renders the approach unreliable for a decisive fault detection and requires enhancements of the spectral resolution which means more modifications on the root code and extensive study.

### 4.2.2 time-frequency domain analysis

To mitigate the limitation of FFT technique when dealing with non-stationary signal, WT delivers a robust time-frequency domain analysis for both stationary and non-stationary signals, and among its tools DWT is the most efficient technique in terms of computational capabilities which gives more accuracy when dealing with non-stationary signal and especially at low frequency.

The first step of the research is to perform a full decomposition of the stator raw current signal, and to achieve this 1-D DWT decomposition was used up to 12 levels to cover all the ranges of frequency bands of both approximations and details by using debauchees -24 as the mother wavelet function and the sampling frequency was set to 10KHz. Full decomposition results for both healthy and air gap irregularity current signals were collected to be compared later on.

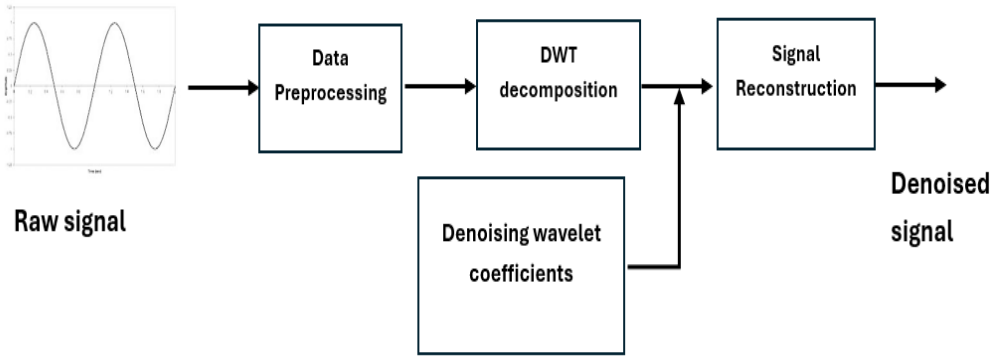
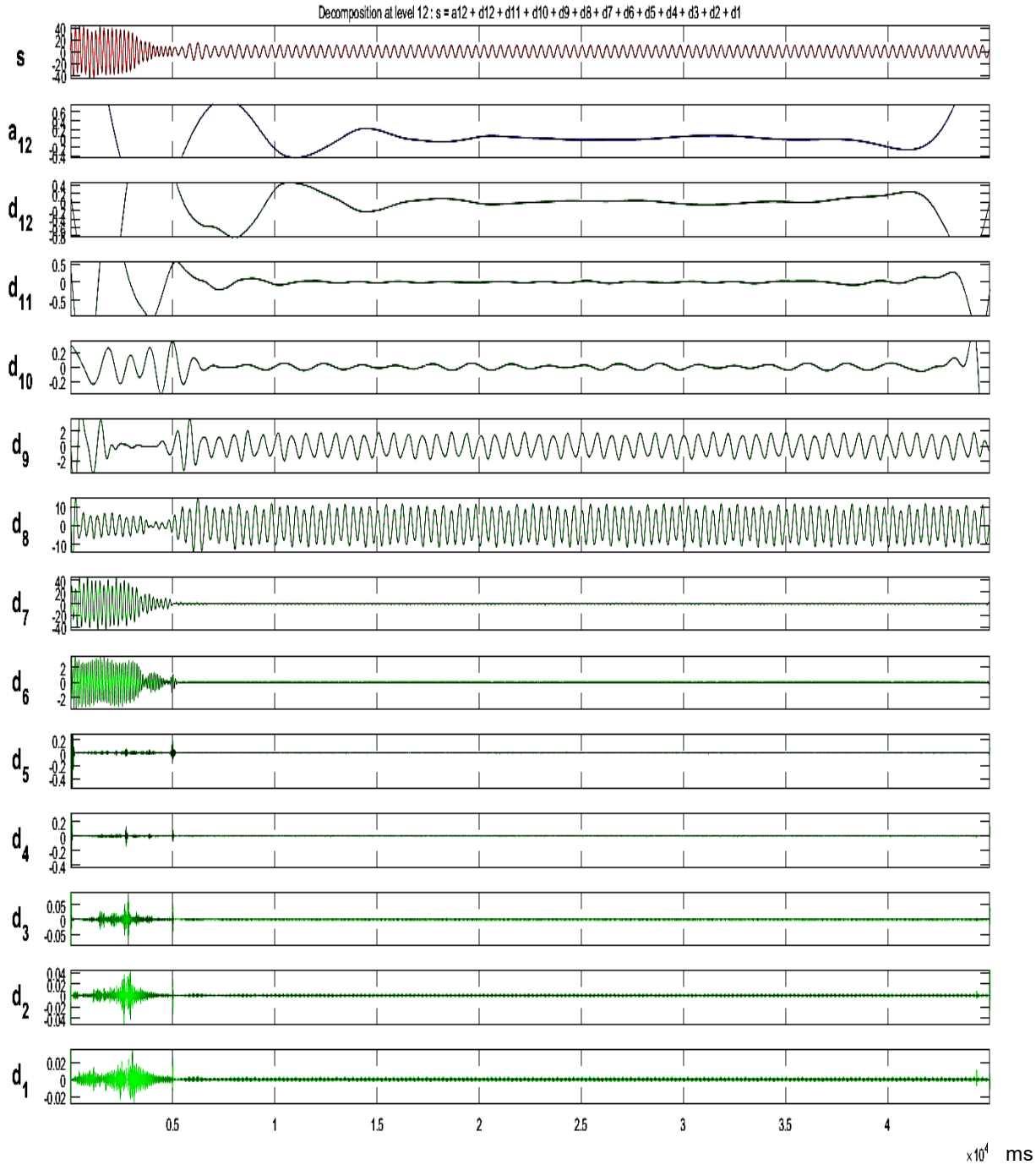
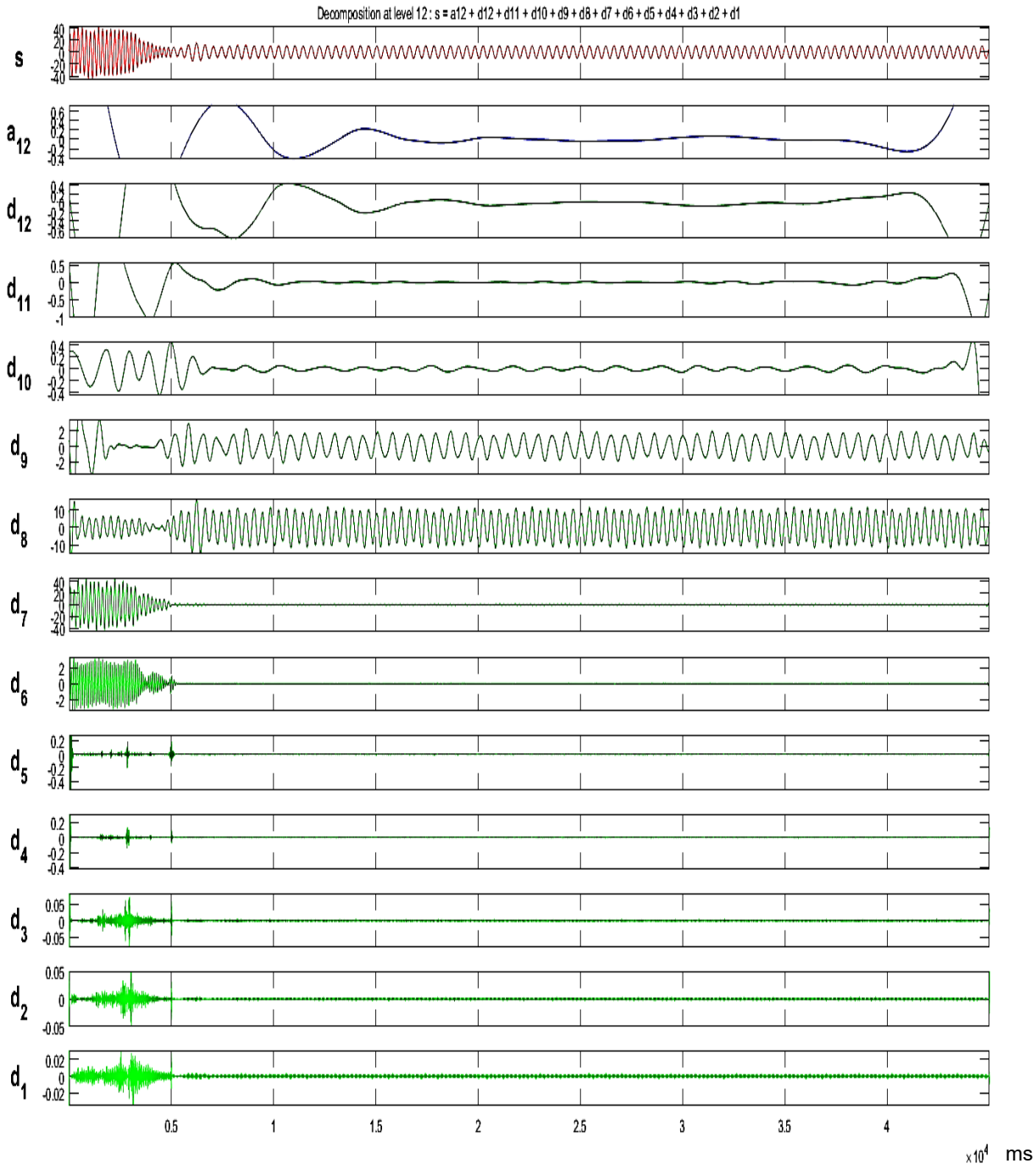



Figure 4.7 DWT signal decomposition and reconstruction.

Till the present day, there's no specific rule that dictates the choice of a specific mother wavelet. However, through various deep studies it was noticed that Debauchees mother wavelet provides more stability and a robust reconstruction of the original signal with maintaining information since it locates less in time with less oscillation due to its dilation nature, which makes it practical for the diagnosis of induction machine[154]. Figure 4.8 shows the complete decomposition using DWT of raw current signal for healthy and faulty machines




(a) Decomposition levels of a healthy signal




(b) Decomposition levels of a faulty signal

Figure 4.8 Full decomposition of stator current

It can be shown in figure 4.8 that a full decomposition using (WT) was performed for both a healthy and faulty machine as a solution to mitigate the limitation of FFT technique by employing time and frequency domain analysis in order to have a better understanding of the signal's condition. However, when not treated with a proper investigation and extensive study, WT is limited while choosing the right mother wavelet to be implemented in the decomposition process, it can be computationally too extensive, WT has many variants and each has its own advantage and drawback which requires a prior knowledge on the specified technique to be used. Figure 4.9 illustrates clearly the disadvantages of WT energy distribution technique, while performing feature extraction it requires a careful choice of decomposition level through all of

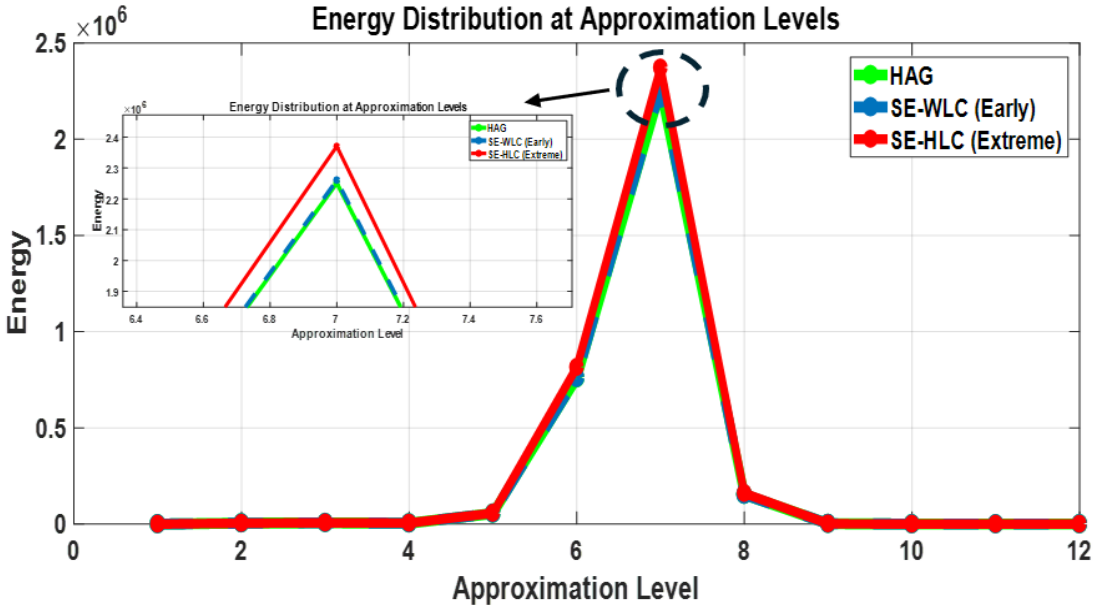
the signals conditions (fault type, health condition and load's condition) so it can be suitable for the diagnosis task ( in (b) it can be shown that a faulty machine dissipates more energy than the healthy model which is illogical and may lead to misinterpretation that can render this technique unsuitable for this case.

HAG: Healthy Air Gap

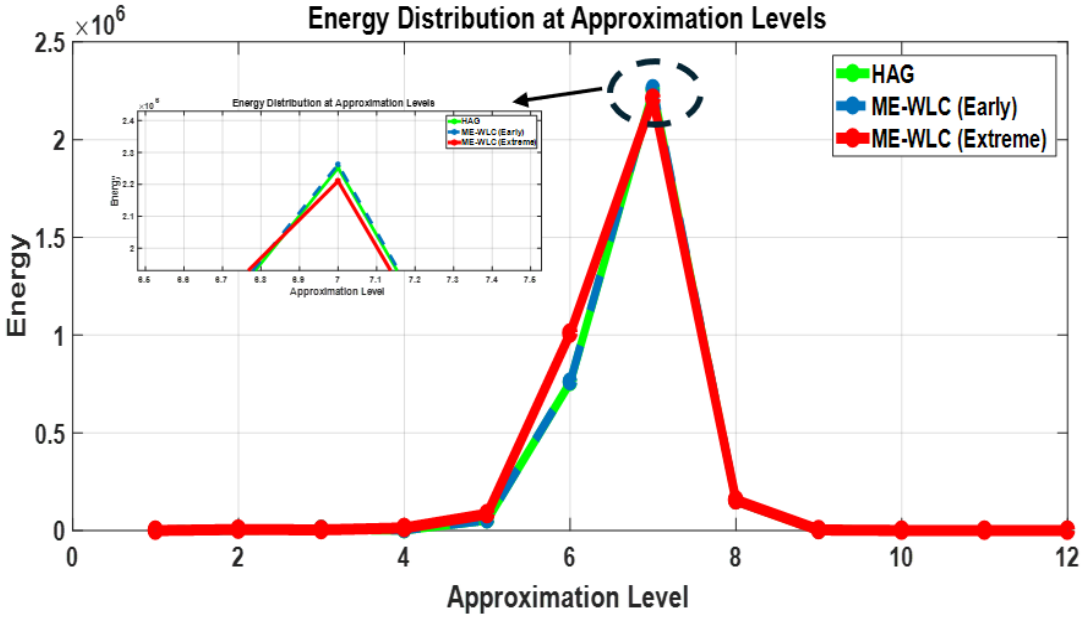
SE: Static Eccentricity

WLC: Weak Load Condition

HLC: Heavy Load Condition




(a)




(b)

Figure 4.9 Energy distribution analysis

After conducting the aforementioned diagnostic techniques, it becomes evident that the MBMs exhibit limitations, particularly when the IM is operating without a load or under weak load conditions. Additionally, these methods face challenges in detecting defects at early stages, where subtle fluctuations in the current pose difficulties. Moreover, their inadequacy extends to the identification of the nature of the defect, and also given that certain faults, such as bearing defects, broken rotor bars, and air gap eccentricity, manifest similar symptoms under weak load conditions, leading to potential misdiagnosis.
In scenarios where the IM operates with a small slip and rotational speed is in close proximity to synchronization, the frequencies associated with defects become challenging to discern due to their proximity to the fundamental frequency, coupled with their small amplitudes, which are situated in the side bands.
Furthermore, the limitations of MBMs extend to transient mode conditions, where spectral leakage becomes a significant issue. In situations where abrupt load fluctuations occur during operational conditions (e.g., in mills, wind turbines), these methods encounter challenges. The sudden changes in load cause distortion in the spectral image of the current, resulting in ambiguous frequencies. This distortion leads to a loss of information, as fault frequencies become obscured behind the frequency of load fluctuation. To address this issue and improve spectral resolution, longer measurement times are required, necessitating additional storage and sophisticated equipment.

## 4.3 AI-based approaches

In the following section, two AI-based approaches will be used namely one without signal processing and the other is by leveraging signal processing tools for feature selection and extraction.

The idea relies on using raw data signal (stator current signal), and employ it as input for the chosen algorithm, the methodology flowchart will be explained below.

### 4.3.1 without signal processing

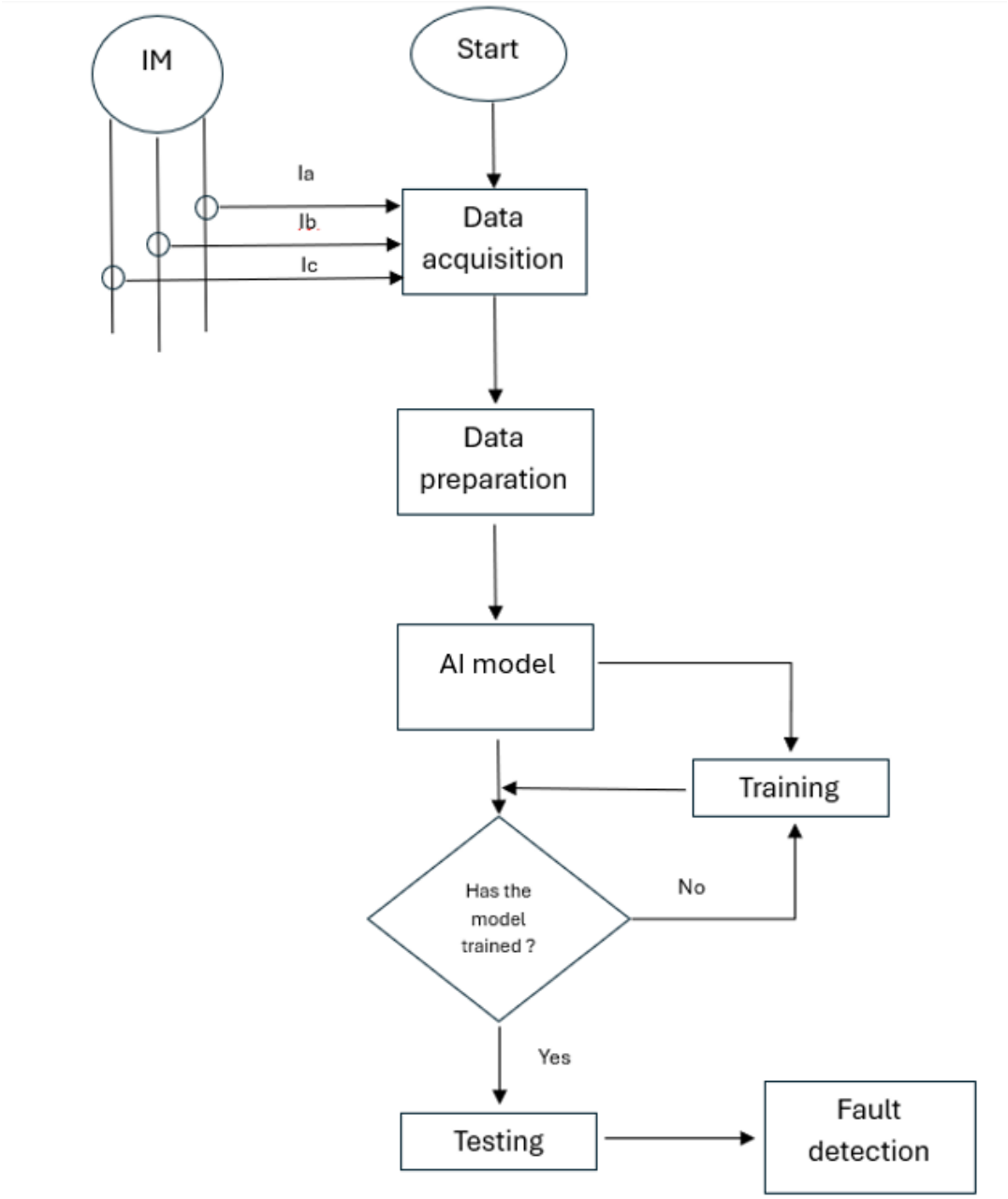



Figure 4.10 AI algorithm integration in fault detection

Figure 4.10 illustrates employing an AI model by feeding inputs coming from the IM, AI models has an embedded signal processing tools, which means it relies on itself for signal cleaning, normalizing and transforming, which would help the model to overcome noise and data complexity.

When applying neural networks to address the diagnosis of failures in an electromechanical system, two primary steps need to be implemented [155]:

• The initial step involves examining the problem at hand to confirm its suitability for neural network-based solutions. This includes defining the objectives that need to be met to ensure the quality and effectiveness of the selected solution.

• The second step centers on the neural network technique. This involves selecting the appropriate network type and its configuration, such as determining the learning method and specifying the number of hidden layers. These choices are made based on the specific characteristics of the problem under investigation and the defined objectives.

The neural network was designed and trained to perform characterizations based on a database consisting of 216 samples. Each sample in the database contained 45,000 points representing the current signature, and the network aimed to predict four outputs related to the health state of the induction machine, the condition of the loads, and the designated stator current phase. For this phase the following tasks have been realized:

• The IM was simulated in ordinary operational conditions (healthy state) ;
• The IM has been simulated in abnormal operational conditions (in the presence of defects of air gap eccentricity in both types static and mixed) ;
• The IM has been simulated for both normal and abnormal for different working modes : low load torque (10N.m), medium load torque (30N.m) and high load torque (40N.m).

**Table 4.1** shows the designated output for supervised machine learning, as a first attempt to use the AI model, we have chosen the machine signals to detect the fault and to identify it (two types of eccentricity SE and ME) and to determine which phase (phase A,B and C) and to be able to identify each operational condition (WLC,MLC and HLC)
We end up by having 4 outputs containing 4 variables describing the machine parameters as follows:

S1: machine's health state.
S2 : nature of air gap eccentricity (static or mixed).
S3: load's condition.
S4: stator current Phase.

Table 4.1 output dataset denotation

| Machine condition | Load condition | Phase | Code | | | |
|---|---|---|---|---|---|---|
| | | | S1 | S2 | S3 | S4 |
| HAG | WLC | IIA | 0 | 0 | 0 | 0 |
| | | IIB | 0 | 0 | 0 | 0.5 |
| | | IIC | 0 | 0 | 0 | 1 |
| | MLC | IIA | 0 | 0 | 0.5 | 0 |
| | | IIB | 0 | 0 | 0.5 | 0.5 |
| | | IIC | 0 | 0 | 0.5 | 1 |
| | HLC | IIA | 0 | 0 | 1 | 0 |
| | | IIB | 0 | 0 | 1 | 0.5 |
| | | IIC | 0 | 0 | 1 | 1 |
| SE | WLC | IIA | 1 | 0 | 0 | 0 |
| | | IIB | 1 | 0 | 0 | 0.5 |

| | | | | | | |
|---|---|---|---|---|---|---|
| | | I I C | 1 1 | 0 0 | 0 | 1 |
| | MLC | I I A | 1 1 | 0 0 | 0.5 | 0 |
| | | I I B | 1 1 | 0 0 | 0.5 | 0.5 |
| | | I I C | 1 1 | 0 0 | 0.5 | 1 |
| | HLC | I I A | 1 1 | 0 0 | 1 | 0 |
| | | I I B | 1 1 | 0 0 | 1 | 0.5 |
| | | I I C | 1 1 | 0 0 | 1 | 1 |
| ME | WLC | I I A | 1 1 | 1 0 | 0 | 0 |
| | | I I B | 1 1 | 1 0 | 0 | 0.5 |
| | | I I C | 1 1 | 1 0 | 0 | 1 |
| | MLC | I I A | 1 1 | 1 0 | 0.5 | 0 |
| | | I I B | 1 1 | 1 0 | 0.5 | 0.5 |
| | | I I C | 1 1 | 1 0 | 0.5 | 1 |
| | HLC | I I A | 1 1 | 1 0 | 1 | 0 |
| | | I I B | 1 1 | 1 0 | 1 | 0.5 |
| | | I I C | 1 1 | 1 0 | 1 | 1 |

### 4.3.2 with signal processing

The proposed method is based on two steps, in the first section of the paper, a signal processing was employed using DWT full decomposition, in order to denoise our raw current signal for the purpose of extracting the most suitable feature from the obtained signal, then an energy distribution analysis was conducted in order to choose the best frequency band sensitive to the variations of current signal for both healthy and faulty machines, root mean square (RMS) was backed as a fault indicator to reinforce the learning process in the upcoming section. Later, an AI-based diagnosis was performed using machine learning algorithms in hope to classify the chosen dataset into 3 classes: fault type, fault localization and severity degree as shown in Figure 4.11 :

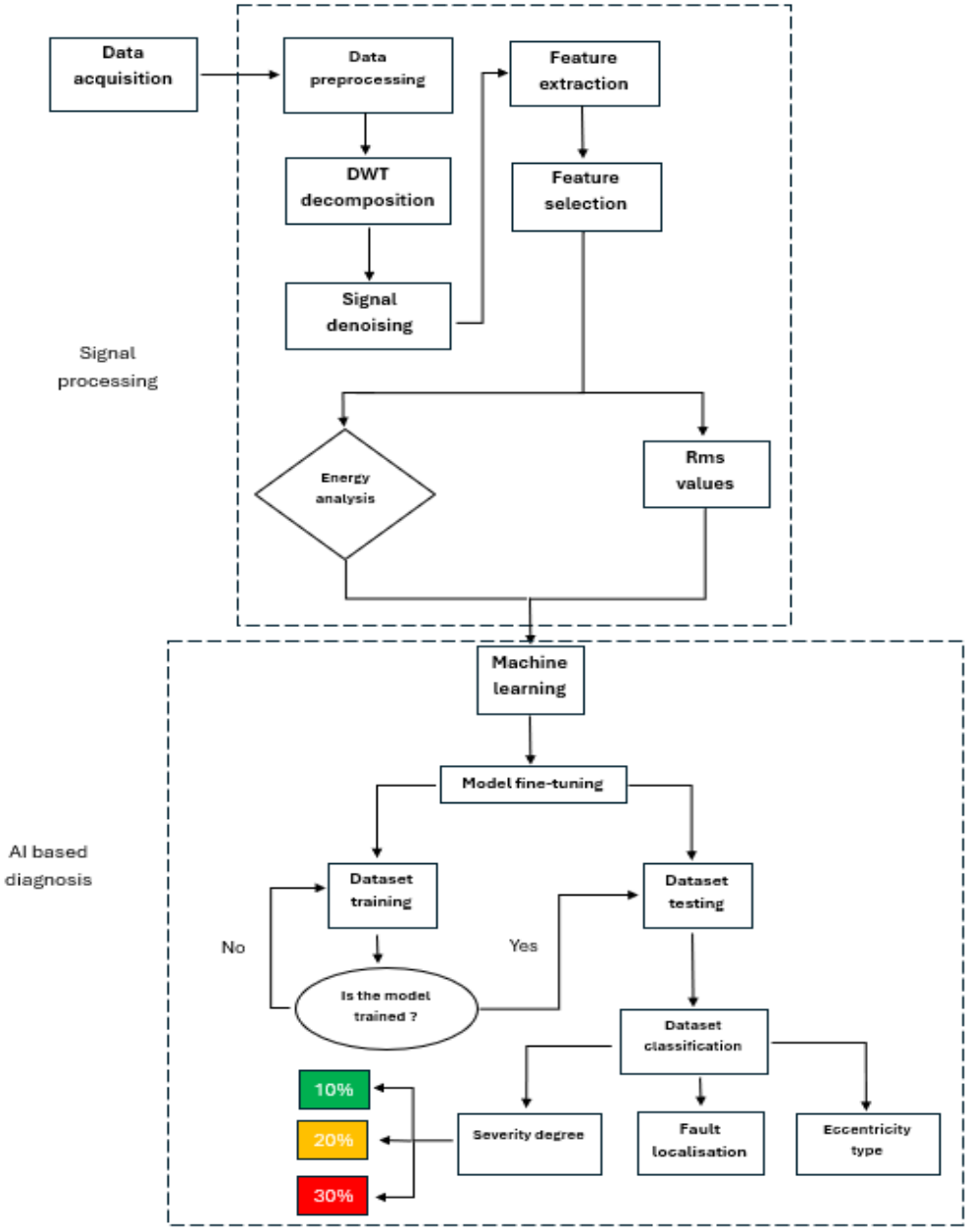
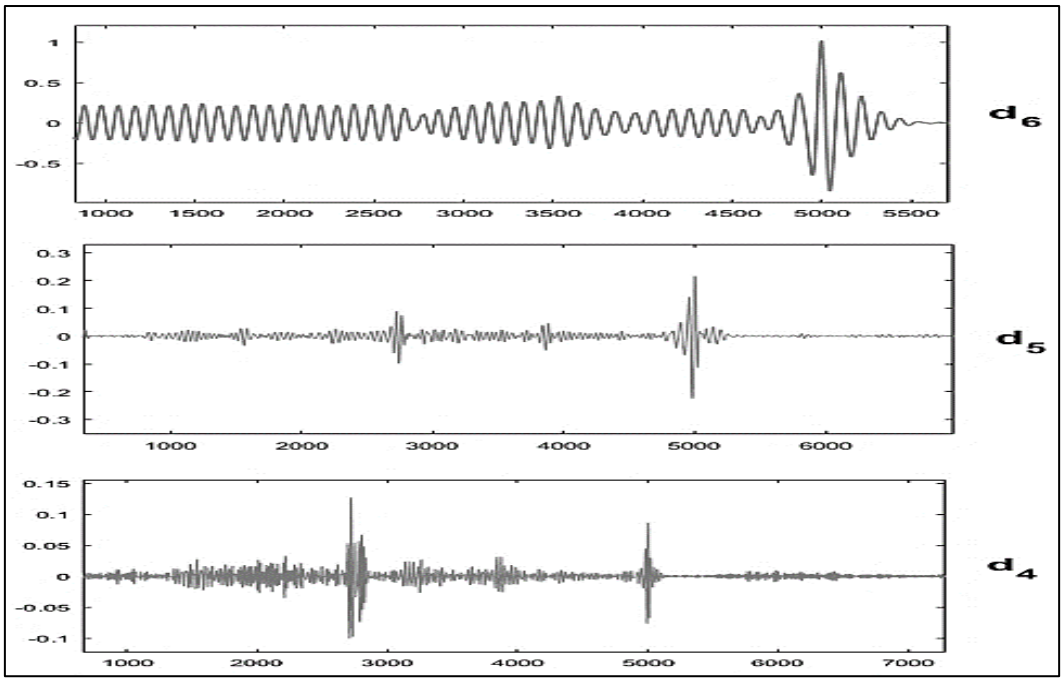


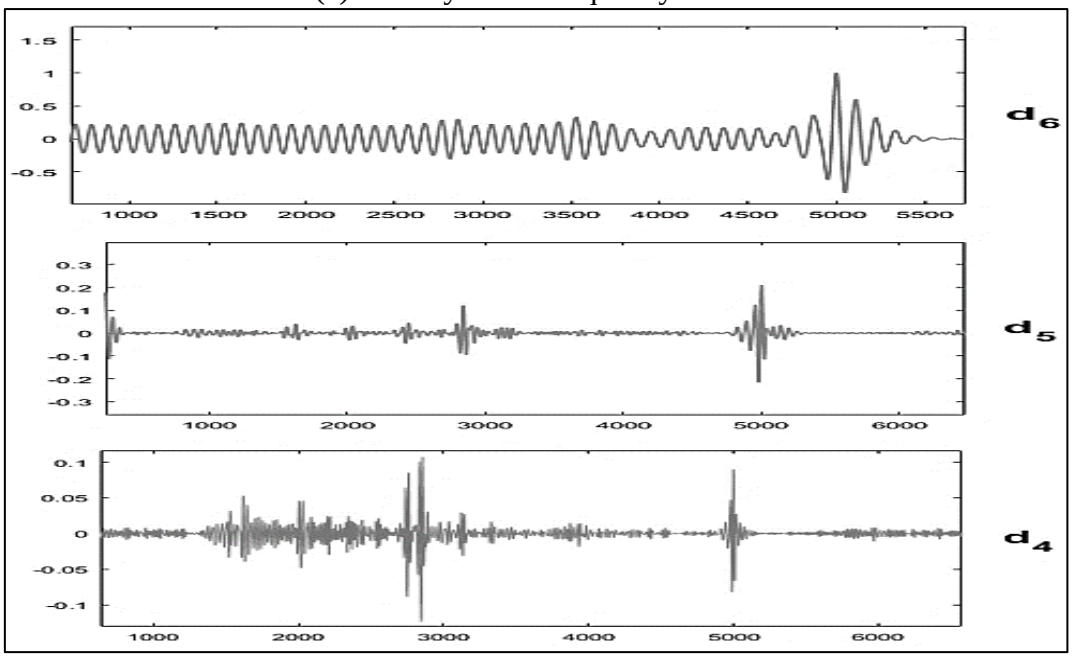

Figure 4.11 AI algorithm combination with signal processing in fault detection

After analyzing the obtained results of the full decomposition for both approximation and detail frequencies in healthy and faulty condition, we can notice that air gap irregularity manifests some changes in high frequency (detail frequency) band [1000-5500Hz] and they're more visible in levels 4,5 and 6, which can deliver a promising comparison opportunity, further results are discussed thoroughly in the next section.

Three decomposition levels were selected since they show promising characteristics comparison and contain inherent frequency that characterize air gap defect which are Levels 4, 5 and 6th level of detail decomposition illustrated in Figure 4.12



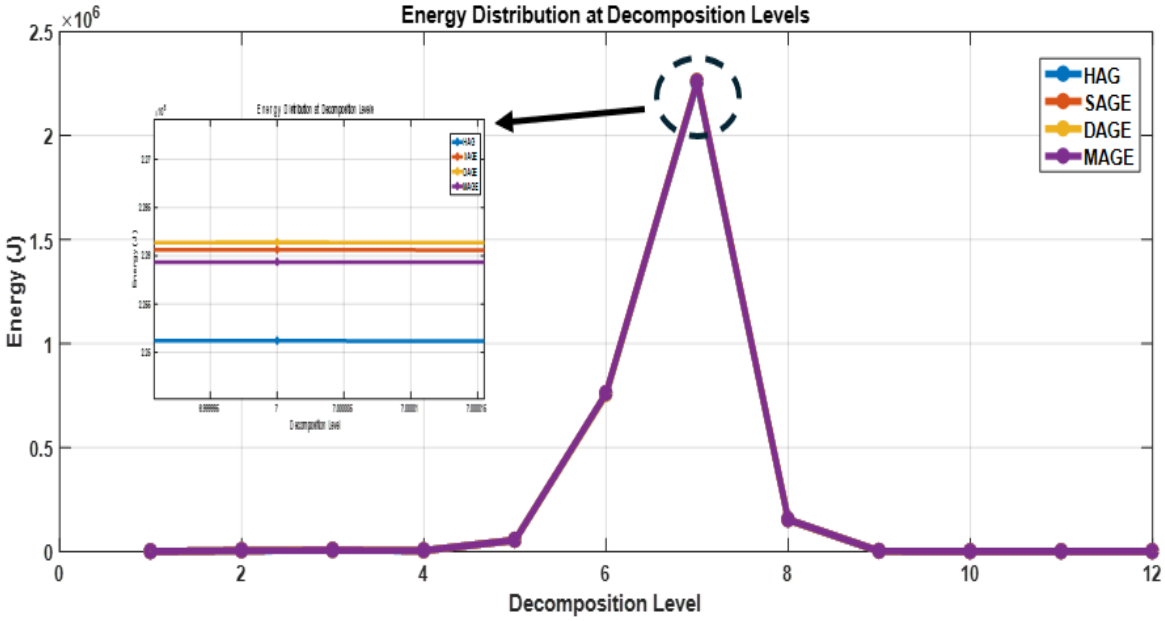

(a) Healthy detail frequency levels



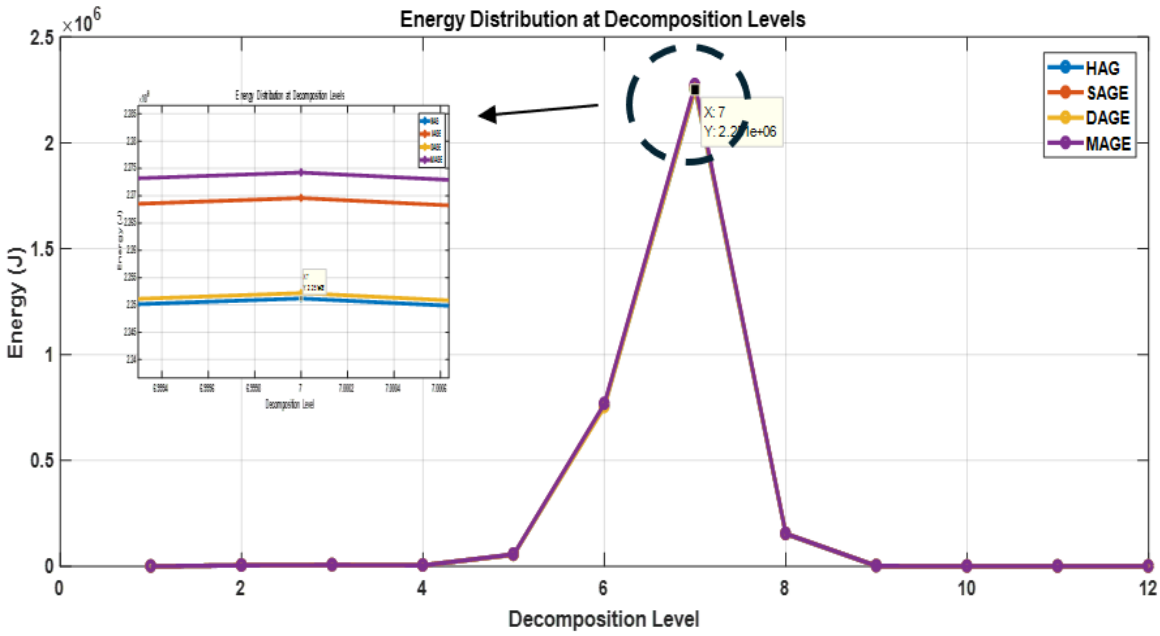

(b) Faulty detail frequency levels

Figure 4.12 Detail decomposition levels 4, 5 and 6.

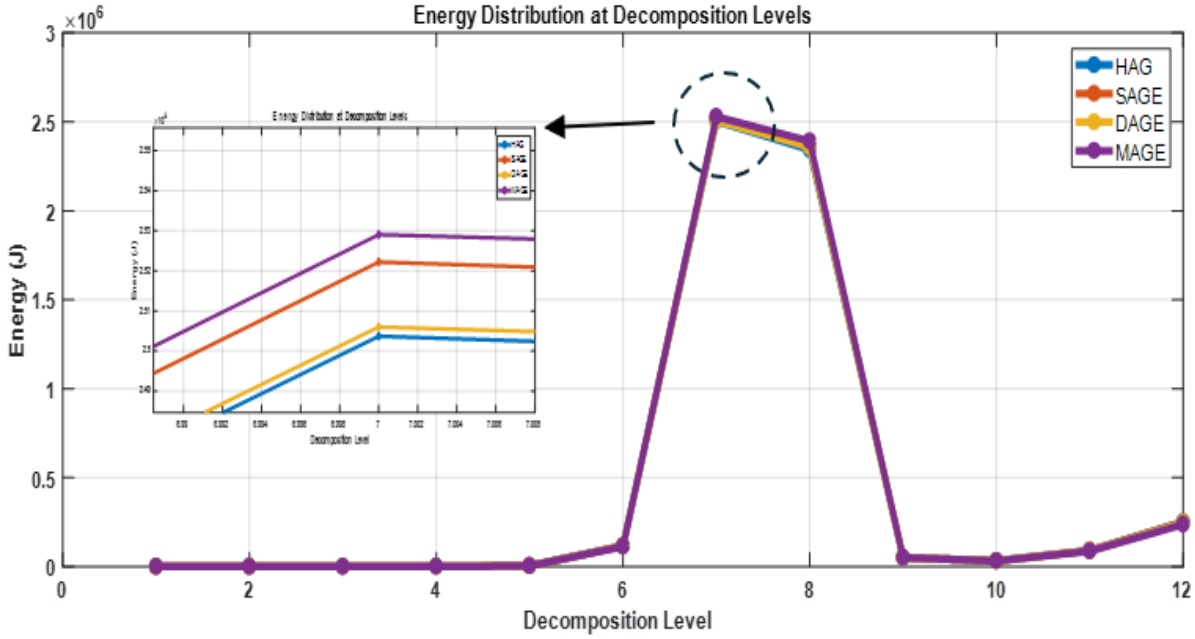
An energy distribution analysis was performed in order to determine the most suitable and pertinent detail levels that dissipate more energy under various operating conditions and for various severity degrees of the defect for each type of air gap eccentricity, the results are shown in Figure 4.13:




a) Energy distribution analysis of the decomposition levels at early stage of air gap irregularity weak load




b) Energy distribution analysis of the decomposition levels at 30% air gap irregularity weak load




c) Energy distribution analysis of the decomposition levels at 30% air gap irregularity medium load

Figure 4.13 Energy distribution analysis under various conditions for air gap types

It became evident that the most pertinent results for energy distribution reside in levels 6,7 and 8 with a prominent advantage for level 7, that exhibits the peak of energy dissipation for all the operating conditions and under various fault types and severity degrees.

Detailed results of dissipated energy levels are shown in Table 4.2 below:

Table 4.2: Energy levels of decomposition levels.

| Machine Condition | Decomposition Level | Dissipated Energy (J) |
|---|---|---|
| **HAG** | D6 | $1.173\times10^5$ |
| | D7 | $2.504\times10^6$ |
| | D8 | $2.344\times10^6$ |
| **SAGE** | D6 | $1.164\times10^5$ |
| | D7 | $2.522\times10^6$ |
| | D8 | $2.363\times10^6$ |
| **DAGE** | D6 | $1.155\times10^5$ |
| | D7 | $2.206\times10^6$ |
| | D8 | $2.359\times10^6$ |
| **MAGE** | D6 | $1.126\times10^5$ |
| | D7 | $2.529\times10^6$ |
| | D8 | $2.392\times10^6$ |

in this section, we will apply the proposed methodology by integrating various standalone AI techniques in one hand such as neural networks, ensemble methods and decision trees and in the other hand, we will combine these techniques with another non model based method in the image of signal processing by using a suitable wavelet decomposition as mentioned earlier.

The application of AI techniques aims to determine the best AI algorithm to be used for fault detection and to choose the most suitable method under supervised machine learning by feeding the current signal as an input and designating the desired output to classify each sample according to the machine's health condition, fault type, load condition and phase location.

The proposed AI models will undergo various phases such as feature scaling and engineering, hyperparameter fine tuning, model evaluating and testing such as splitting train/test data and using cross validation approaches for potential overfitting performance and finally used the most common evaluation metrics to test the model's performance.

Passing through all these phases will allow us to pick the best approach to be used for fault detection for both air gap eccentricity and broken rotor bars, putting into consideration the model's accuracy and speed of prediction.

### 4.4 Artificial neural networks

The dedicated work in this paper aims to use artificial intelligence (ANN) to be able to detect and identify air gap eccentricity (static and mixed) in the induction machine and gives the modeling details of a three-phase induction motor suffering from static and mixed air gap eccentricity condition. To achieve this, we adopted the multi winding model because it is crucial in fault detection for electrical machines as it improves fault localization, identification, sensitivity, monitoring capabilities, and provides diagnostic insights.

The learning process of the neural network aims to provide the ANN with clean and accurate information to learn from using a database containing raw data, which would make the model able to distinguish between the healthy model from the faulty one, and the second phase would allow us to conduct a thorough diagnosis able to identify the nature of the problem and also locate which phase of the stator current and the related load's condition of the analyzed machine.

After many trials and experiments with different topologies and parameters, the network's architecture employed for this task was a feed forward multi-layered neural network with two hidden layers, where each layer consists of 64 neurons and uses the sigmoid activation function to capture complex relationships within the input data. These layers are followed by an output layer that consists of several neurons that matches the dimensionality of the output which in our case 4 outputs.

The results of the classification are shown in figures (4.14-4.17)

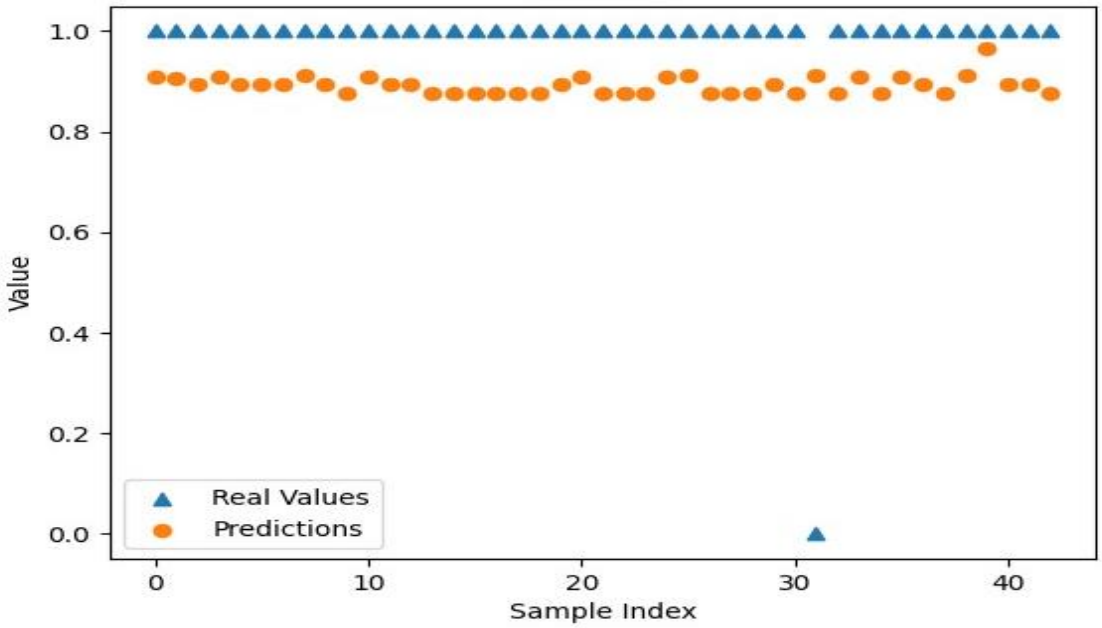



Figure 4.14 Results of the machine's health condition classification.

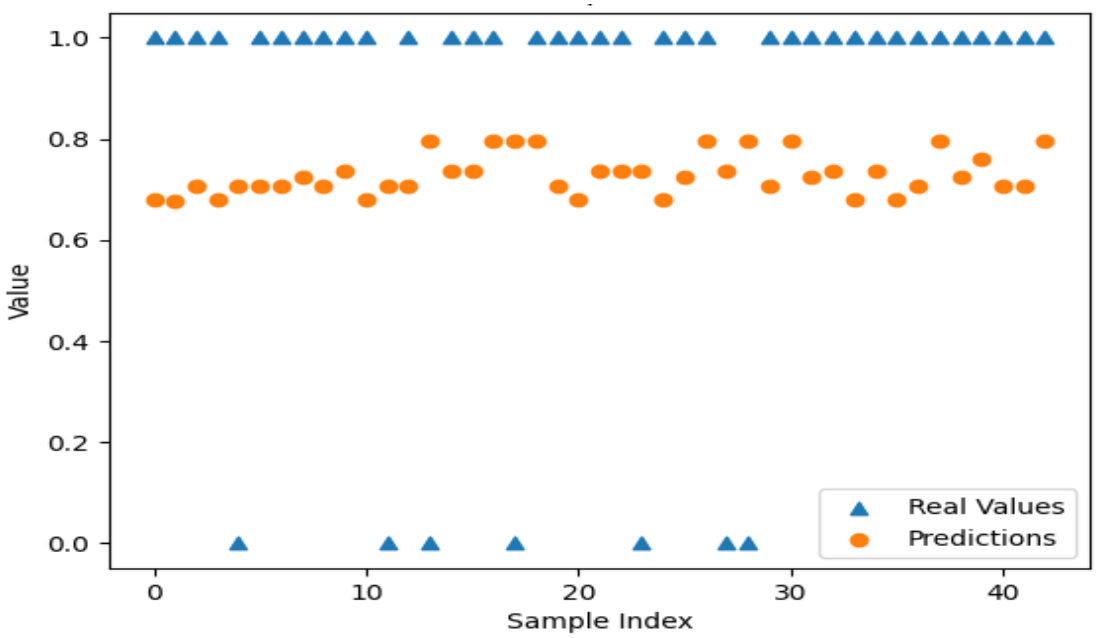



Figure 4.15 Results of the machine's fault nature classification.

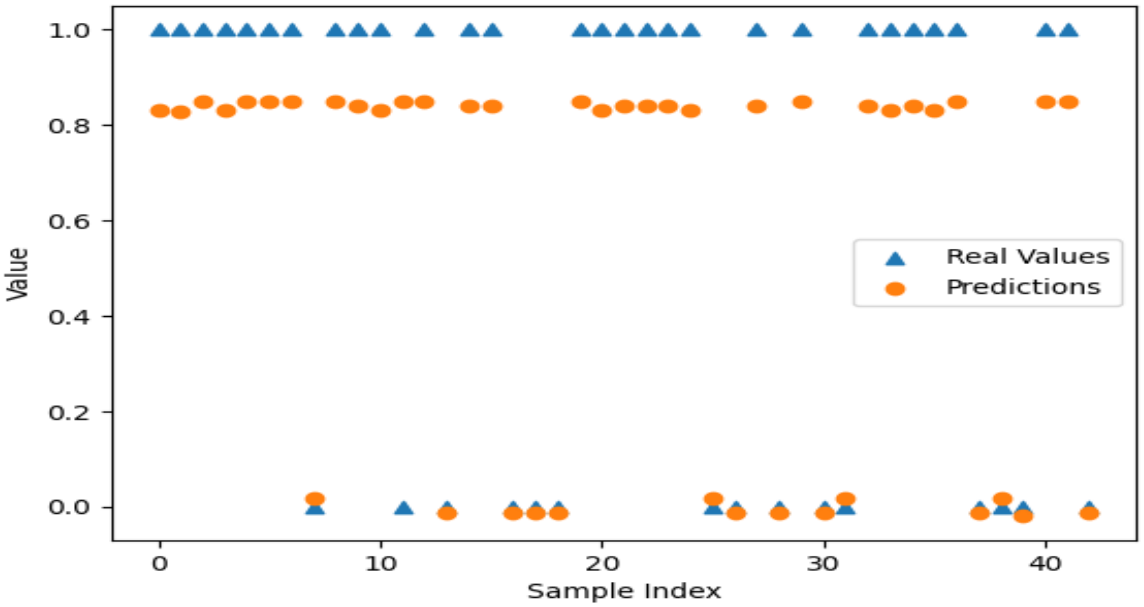



Figure 4.16 Results of the machine's load condition classification.

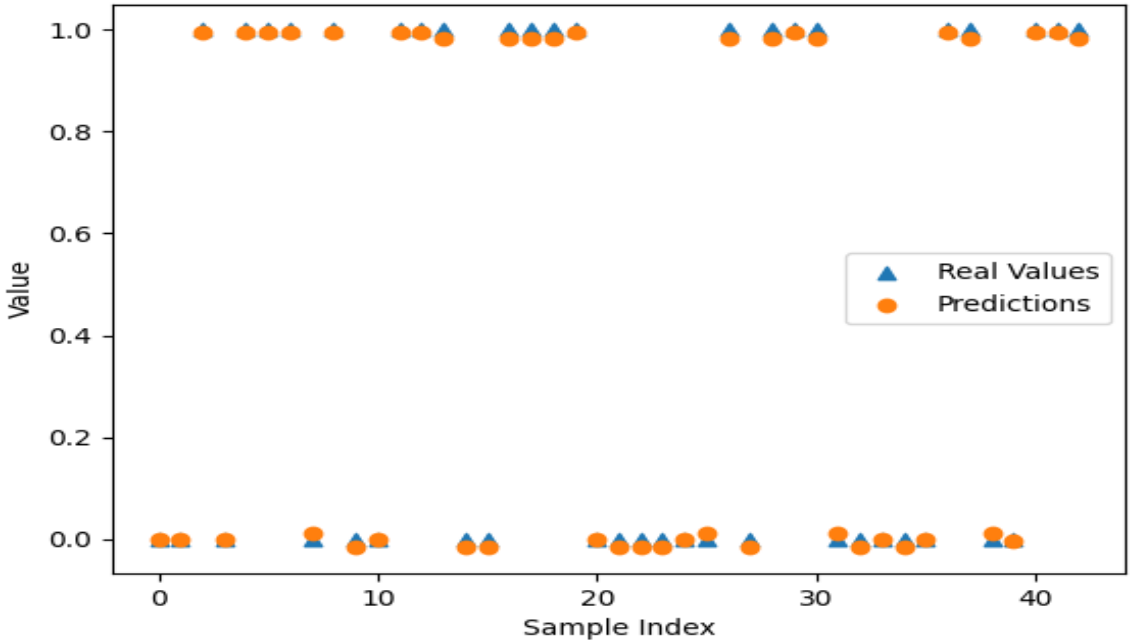



Figure 4.17 Results of the machine's current phase classification.

After investigation, we can notice that ANN handeled most of the tasks in a good way, however, it struggled with data imbalance which is a significant issue in machine learning this issue is clearly visible in figure 1, where the model failed to predict healthy samples labeld as 0 due to data imbalance (healthy vs faulty) and (static vs mixed) , but it perfomred good with other classification,this analysis provides insights of the model's reaction and ability in fault detection

### 4.4.2 Model evaluation

To evaluate the network, three evaluation metrics were used, Mean Squared Error (MSE), Root Mean Squared Error (RMSE), and Mean Absolut Error (MAE). As for the optimizer, we used

the Adam optimizer. The model was trained for 100 epochs with a batch size of 32, allowing the network to learn and refine its weights and biases through iterative updates.

The evaluation of the network's performance was carried out using multiple error optimization metrics, which quantifies the average difference between the predicted and actual values. The lower the error, the closer the predictions were to the true values. Additionally, the loss curve was plotted to visualize the training progress and ensure that the model was converging and improving over the epochs., figures (4.18) and table 1 below.

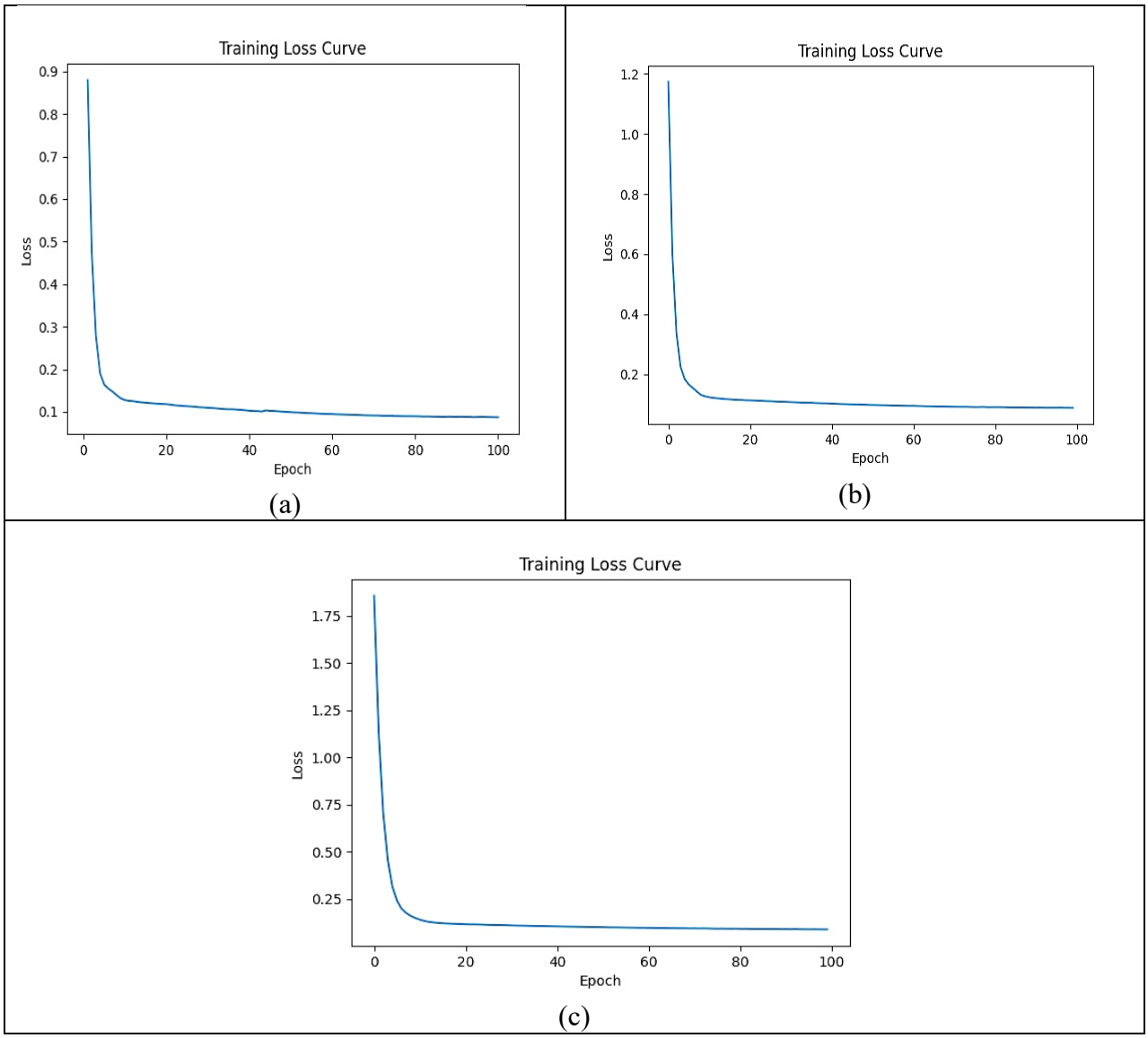



Figure 4.18 loss curve results after 100 epochs : a- MSE, b- MAE and RMSE

the train/test set of loss curve values are summarized in the table below.

Table 4.3: Train/test loss curve values

| Metric | Train set | Test set |
|---|---|---|
| ***MSE*** | 0.0865 | 0.0643 |
| ***RMSE*** | 0.0877 | 0.0664 |
| ***MAE*** | 0.1732 | 0.1395 |

We can clearly notice that MSE technique scored the best results in terms of error optimisation in comparison to other tchniques for both train/test datasets, which makes it a better solution for our example and a strong candidate for model evaluation in the upcoming trials.

### 4.5 Classification and multi-class classification

The dedicated work in this paper aims to use the artificial intelligence techniques through applying multiple machine learning algorithms to be able to detect, identify and localize air gap eccentricity (static and mixed) in the induction machine and gives the modelling details of a three-phase induction motor suffering from static and mixed air gap eccentricity condition under different load conditions. The premise of adopting this proposed technique is to perform a multiclassification process using classification.

#### 4.5.1 Classification

Classification techniques are employed for the identification and categorization of specific fault classes or operational states of the induction machine. Using historical data that includes normal and faulty machine behavior, a classification model is trained to recognize patterns associated with different fault types. This enables the system to classify the current state of the machine into predefined categories, indicating the presence or absence of specific faults. Commonly used classification algorithms include neural networks, logistic regression, decision trees and support vector machines.

In the process of conducting the classification diagnosis, it is essential to note that alterations were made to the dataset's nature. Specifically, dataset transitioned from a set of continuous points representing the current sinusoidal signature to exclusive Root Mean Square (RMS) values. This modification aimed to enhance the suitability of utilizing labels crucial for this specific classification, ensuring that the dataset aligns optimally with the requirements of the classification task.

The classification process involved selecting RMS current values as predictors. To determine key attributes such as health state, fault type, load condition, and phase , they were chosen as response values , a 5-fold cross-validation method was applied. This technique partitions the dataset into five subsets for iterative training and validation, effectively avoiding overfitting risks.

As for the results, they are as follows :

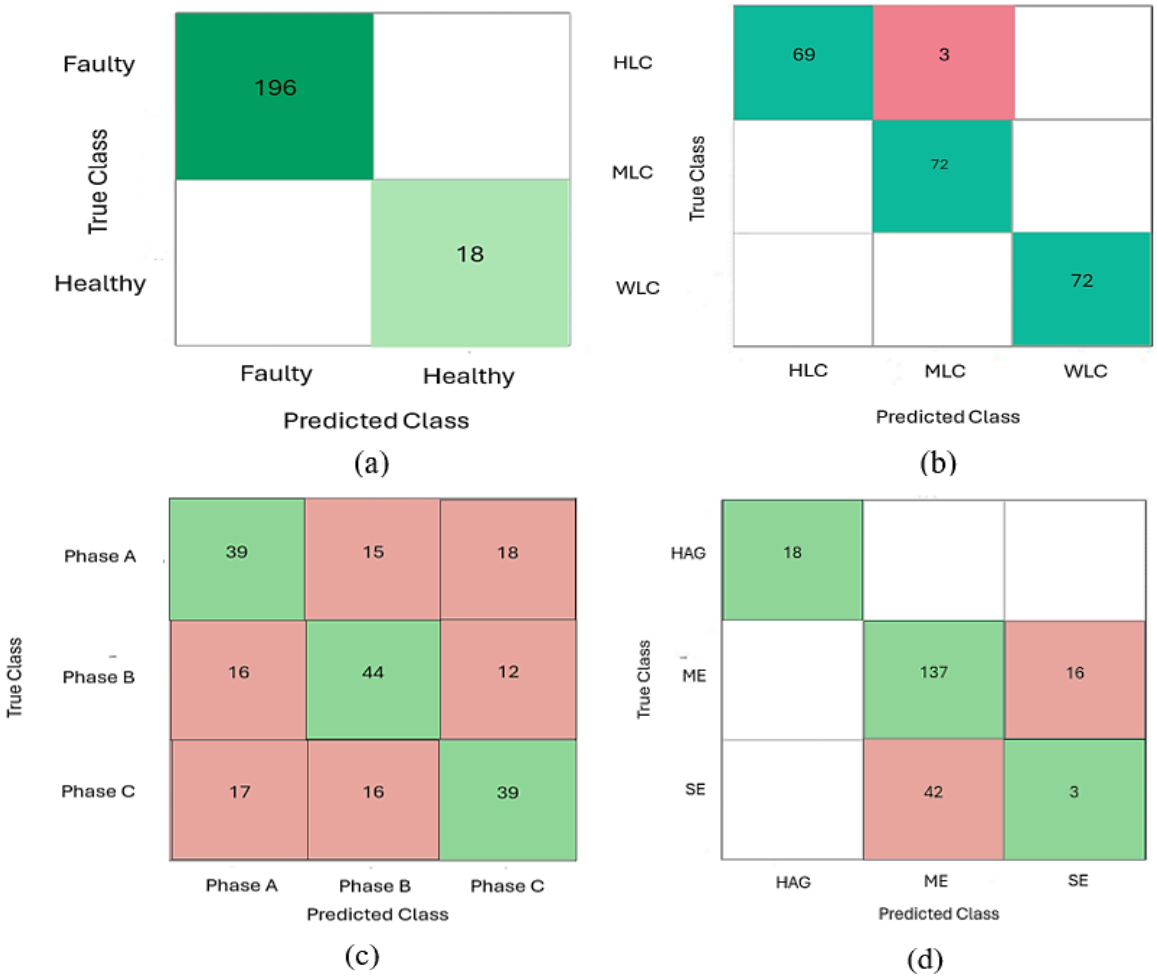



Figure 4.19 Confusion matrix results : a-health state ;b-load's condition ;c-phase localization ;d-fault's type.

The above-mentioned results of DT confusion matrix indicate that the model performed moderetly by distinguishing each class simultaneously but had some difficulties in phase localization by confusing some samples with others.

The detailed results of the classification technique are shown below in table 4.4

Table 4.4: different classifier models of the classification task.

| | Complex tree | Medium tree | Cubic SVM | Fine Gaussian SVM | Boosted trees | RUSboosted trees |
|---|---|---|---|---|---|---|
| | 100% | **100%** | 100% | 98.1% | 91.7% | 91.7% |
| | 69.9% | **72.7%** | 62.5% | 75.5% | 69.9% | 42.6% |
| | 97.7% | **97.7%** | 98.6% | 96.8% | 95.8% | 94.4% |
| | 53.2% | **53.2%** | 35.6% | 20.4% | 52.8% | 49.1% |
| | 80.2% | **80.9%** | 74.1% | 72.7% | 77.5% | 69.4% |

| **Preset** | Fault detection | Fault identification | Load condition | Phase localization | Overall accuracy |
|---|---|---|---|---|---|

Upon completing the classification task, it becomes evident that the Decision Trees classifier excels compared to the other selected classifiers, boasting an overall accuracy surpassing 80%. Specifically, by opting for the medium tree as its preset, it attained a commendable accuracy rate of 80.9%. This performance effectively enhances fault detection, fault identification, load condition assessment, and phase localization predictions.

### 4.5.2 Multi-class classification technique

The second phase, we used multi-class classification approach was tested on raw dataset (a matrix of 216×45000) since It proves valuable in forecasting, hypothesis testing, and controlling for confounding variables, the interpretability of regression models also aids in pinpointing specific variables contributing to faults.

The chosen program utilizes the Random Forest classifier from the scikit-learn framework to develop a multi-class prediction model. It begins by importing data from the raw data set provided as inputs for features and the output from Table 1 as the target data. The dataset is then divided into training and test subsets in an 80:20 ratio (80% for training and 20% for test) to assess the model's efficiency on new data. Standardization of input features is performed using the StandardScaler to optimize the model training process. Following this, the Random Forest , comprised of 100 decision trees, is instantiated and trained on the standardized training dataset. Subsequent predictions are made for both the training and test sets.

When assessing the effectiveness of the multi-class claasification methods, measures like Root Mean Square Error (RMSE), Mean Squared Error (MSE), and Mean Absolute Error (MAE) are extensively used to measure how closely predictions align with actual data. These measures offer a perspective on the suitability of a classification model to the dataset and the dependability of its forecasts.

Table 4.5 Multi-class classification models performance

| ML algorithm | Multi-class Model | MSE | RMSE | MAE |
|---|---|---|---|---|
| Supervised learning | Decision Trees | 0.05813 | 0.24112 | 0.05813 |
| | ElasticNet | 0.1322 | 0.36359 | 0.31994 |
| | KernelRidge | 0.05365 | 0.23163 | 0.15355 |
| | K-Nearest Neighbors (KNN) | 0.05720 | 0.23918 | 0.10775 |
| | Support Vector Machine (SVM) | 0.04370 | 0.20906 | 0.13230 |
| Ensemble Methods | Random Forest | 0.01431 | 0.11962 | 0.16926 |
| NEURAL Networks | Artificial neural Networks (ANN) | 0.07595 | 0.27559 | 0.19438 |
| | Long Short-Term Memory (LSTM) | 0.2001 | 0.44742 | 0.39508 |

In contrast to various classification algorithms such as Artificial Neural Network (ANN), K-Nearest Neighbors (KNN), Support Vector Machine (SVM), Kernel Ridge, ElasticNet, Long Short-Term Memory (LSTM), and Decision Tree, Random Forest consistently demonstrated superior performance across key evaluation metrics. The thorough assessment highlighted Random Forest's proficiency in minimizing prediction errors, demonstrating its efficiency in capturing inherent patterns and relationships within the dataset. This finding emphasizes the reliability and effectiveness of the Random Forest algorithm in classification applications, establishing it as a compelling choice for accurate and dependable predictive modelling.

The Random Forest technique prediction results are as follows:

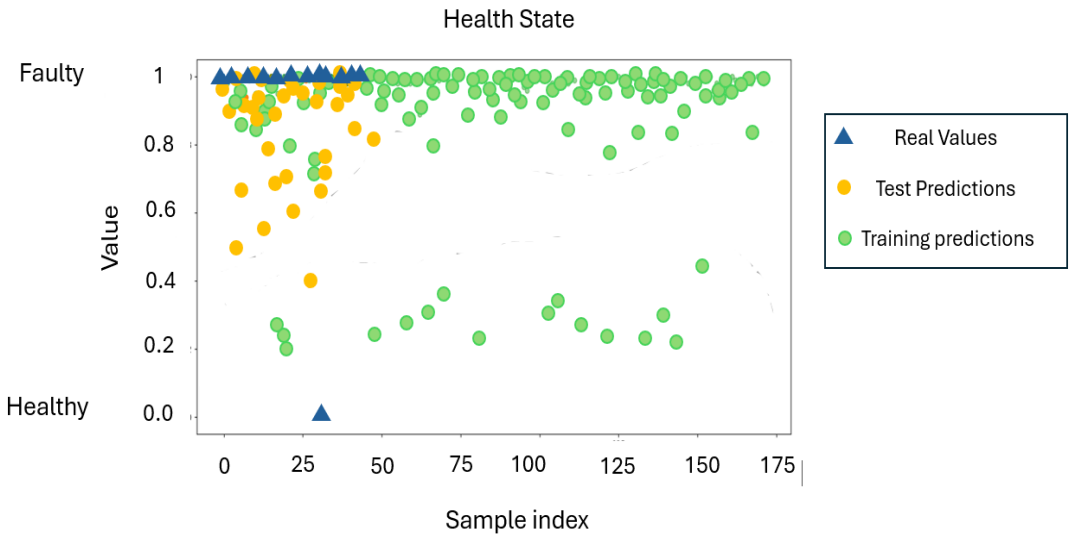



Figure 4.20 results of the machine's health prediction

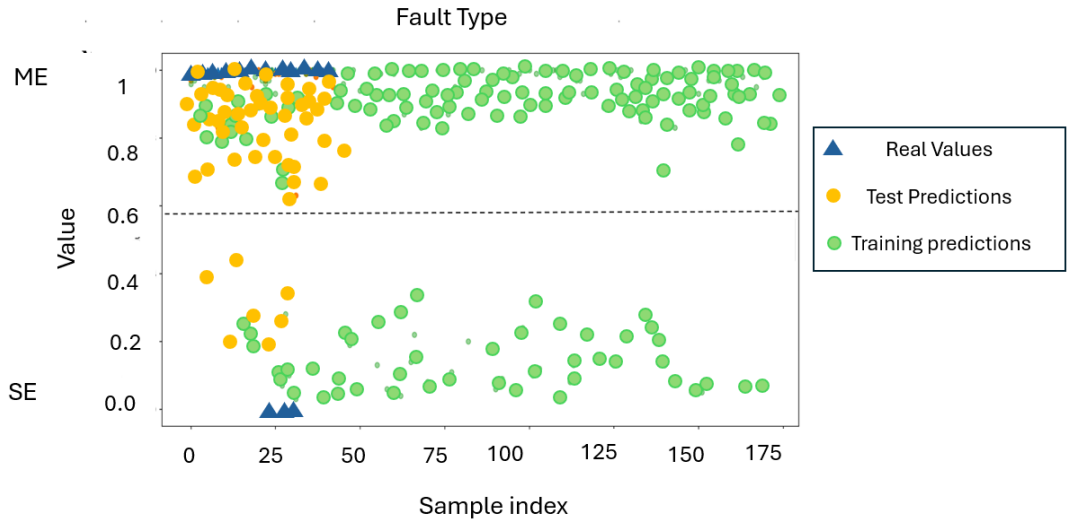



Figure 4.21 results of the machine's fault type

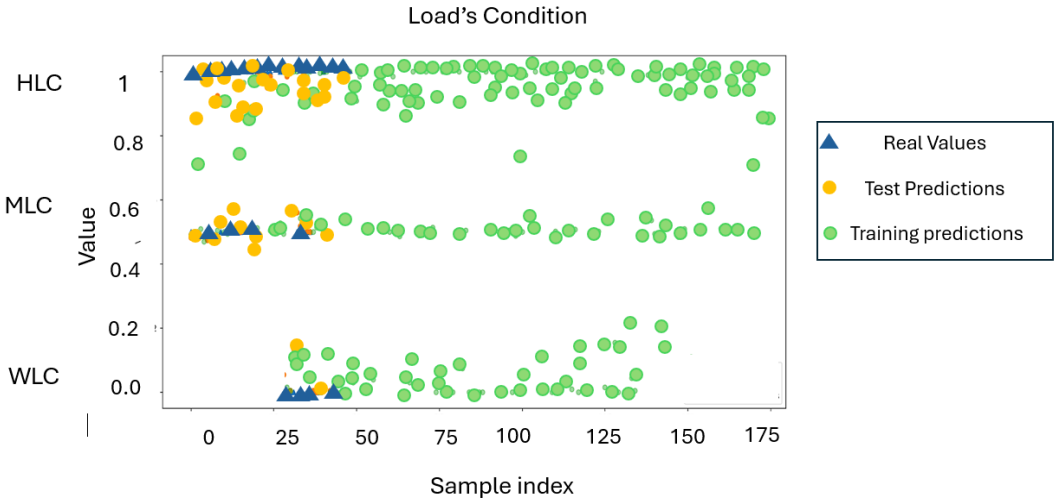



Figure 4.22 results of the machine's load condition

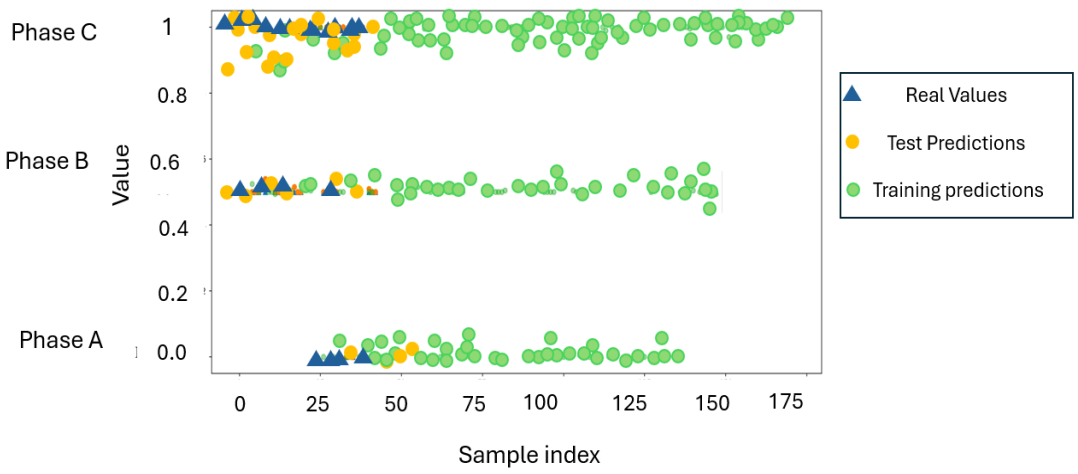



Figure 4.23 results of the machine's phase localization

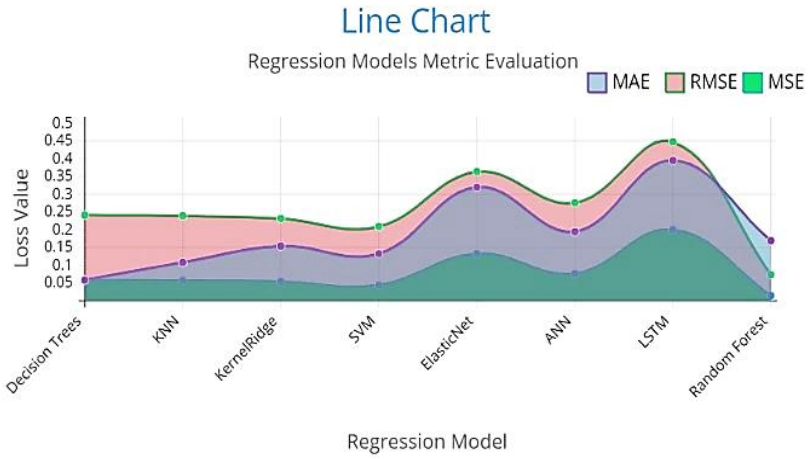



Figure 4.24 overall comparison of classification models.

After a thorough comparison of the classification task preset model and the regression task models for identifying air gap eccentricity faults in induction machines, both methods exhibit considerable potential. Yet, when using stator current raw data as inputs, the regression task model slightly outperforms in accuracy and precision. This slight advantage implies that regression methods might provide deeper understanding of the machine's health condition, pinpointing the exact type and location of faults, and assessing operational load conditions. Nonetheless, both strategies offer valid choices, and the selection should align with particular application needs and goals.

### 4.6 Ensemble Methods in fault detection

The next step of our work will focus on developing an algorithm capable of recognizing and predicting the degree of air gap eccentricity, considering its various types and load conditions. The primary objective is to enable effective monitoring at early stages of the defect of the machine's health status and prevent imminent dangers that could provoke undesirable breakdowns. In order to apply the classification algorithm for monitoring and fault detection task, supervised learning technique was used on a dataset that contains 288 samples and each sample contains the raw current signal with 45000 points, these signals were collected under various operational conditions 0N.m, 10N.M, 30N.M and 40 N.M which describe no load, weak load, medium load and heavy load respectively, under various severity degrees 10% (tolerable in real operational conditions), 20% which requires caution and notification, and above 20% which is considered a dangerous state of AGE, in order to train the classification algorithm, a multi-classification task, this type of tasks will allow the algorithm to distinguish between data samples and properly classify them based on : health condition (healthy, faulty), defect type: (static, mixed) and defect severity, will be discussed and presented in the following sections.

The dataset was divided into training and testing sets to facilitate the learning process, with features carefully selected for model training. Additionally, a validation phase was conducted to assess the model's predictive capabilities against real values. Based on these evaluations, hyperparameters were fine-tuned to optimize the choice of loss function and algorithm architecture, aiming to enhance prediction accuracy.The chosen XGBoost classifier model has scored satisfying accuracy and performed mderetly better for the chosen classes (Fault

Detection, Fault type and Fault severity); to evaluate the model several performance evaluation techniques were chosen like F1-score, recall, precision and accuracy.

Table 4.6 XGBoost model architecture.

| **Hyperparameter** | **Parameter value** |
|---|---|
| **Number of estimators** | 100 |
| **Learning rate** | 0.1 |
| **Max depth** | 6 |
| **Objective function** | Binary logistic |
| **Booster** | Gbtree |
| **Subsample** | 1 |

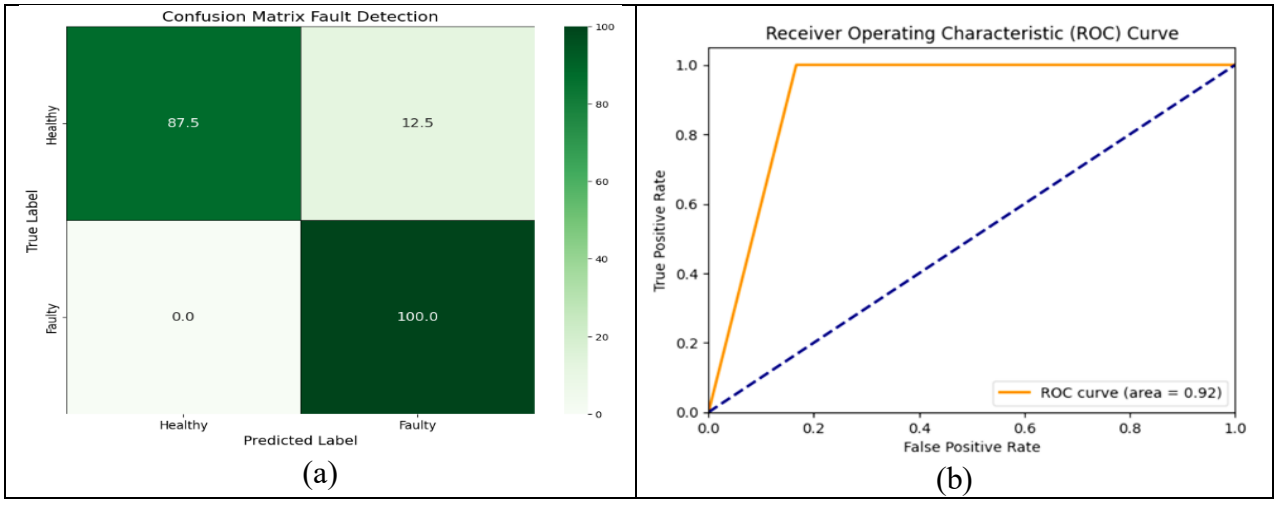
The chosen XGBoost classifier model has scored a satisfying accuracy and performed moderetly better for the chosen classes (Fault Detection, Fault type and Fault severity), in order to evaluate the model several performance evaluation techniques were chosen like F1-score, recall, precision and accuracy.

Table 4.7 Performance evaluation of xgboost

| **Task** | **Precision** | **Recall** | **F1-Score** | **Accuracy** | **Overall accuracy** |
|---|---|---|---|---|---|
| **Fault detection** | 0.99 | 0.94 | 0.96 | 0.98 | 0.9683 |
| **Fault type** | 0.97 | 0.937 | 0.957 | 0.965 | |
| **Severity** | 0.84 | 0.895 | 0.865 | 0.96 | |

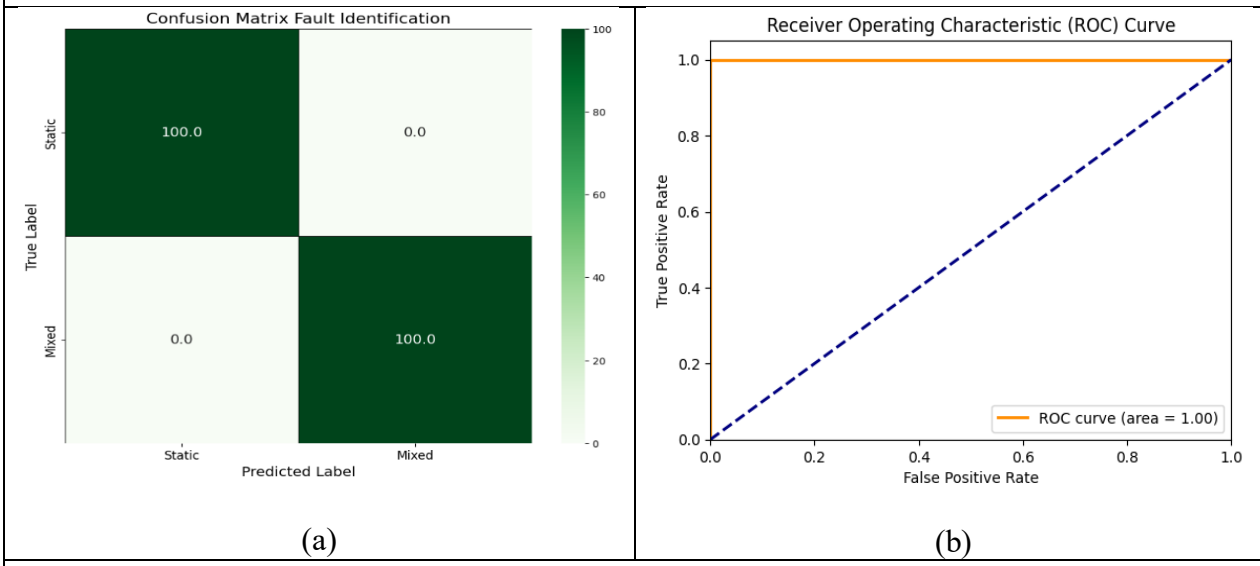
Giving that the model has delivered promising results under Ensemble Methods family and with the task of early-stage fault detection, next we will exhibit a detailed analysis of the model's performance and against other classifiers from the same family and other family algorithms.

Figure 4.25-27 illustrate the model's performance evaluation with more detailed visualization like confusion matrix and ROC curve.



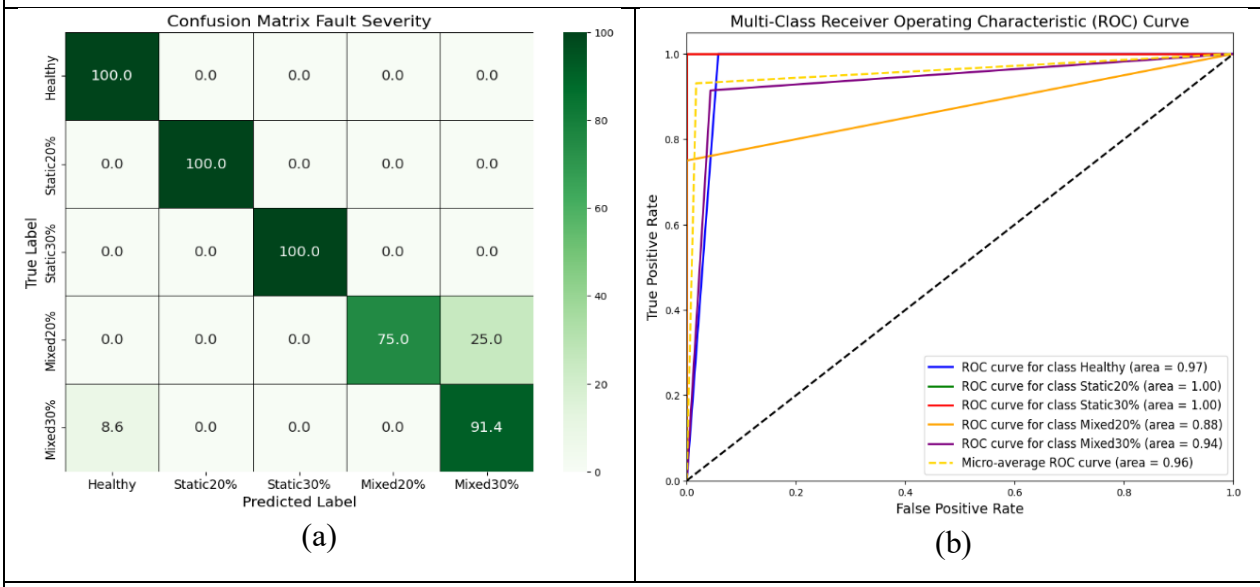

(a) (b)

Figure 4.25. Performance results for fault detection **:** a- Confusion matrix, b- ROC curve




(a) (b)

. Figure 4.26 Performance results of fault type : a- Confusion matrix, b- ROC curve




(a) (b)

Figure 4.27 Performance results of fault severity : a- Confusion matrix, b- ROC curve

By investigating the results of the confusion matrix, it is evident that the model was accurate in predicting each sample with its true label, committing only a few minor errors. This indicates a reduced rate of confusion and a strong, reliable prediction performance.

Next, we will showcase the model's performance against other classifiers:

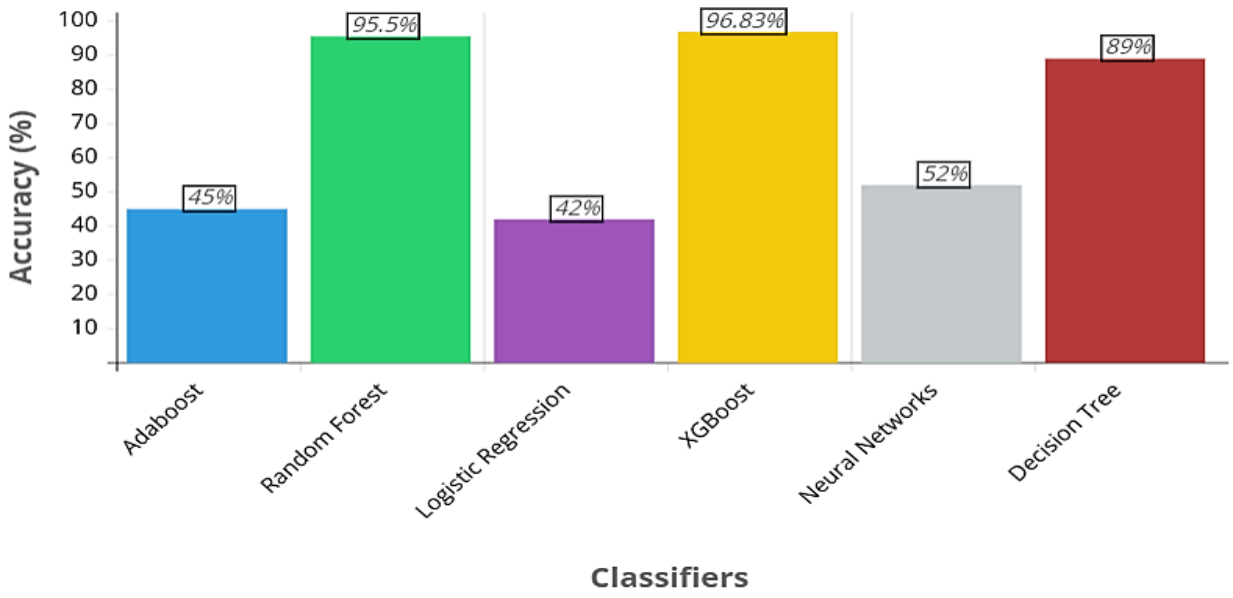



Figure. 4.28 Classifiers accuracy results comparison

Ensemble Methods like XGBoost and RF significantly outperformed traditional models and single learners. This implies the classification problem benefits from models that handle feature interaction and reduce variance/bias effectively.

### 4.6.1 Ensemble Methods: boosting

After analyzing the results obtained, it becomes clear that Ensemble Methods using boosting techniques are suitable for our type of data and for the specific task of fault evolution monitoring.

The next step of our research will focus on developing the model's ability to perform accurate and rapid fault detection on all types of air gap eccentricity including its various degrees. With a focus on the ensemble methods, as was previously mentioned in the literature and based on the results of machine learning, both decision trees and ensemble methods outperformed against other AI techniques, so for this particular reason, we will propose a model that combines between the strong points of each technique in order to develop a strong and reliable algorithm capable of handling all of the designated tasks with accuracy and speed.

### 4.6.2 LightGBM

This section states the architecture of LightGBM model and the used hyperparameters (see Table 4.8), it is worth noting that the model underwent hyperparameter tuning. This configuration was adopted for both classification tasks ( Binary and multi-class).

Table 4.8 LightGBM hyperparameters.

| Hyperparameter | Value |
|---|---|
| Number of trees | 100 |
| Learning rate | 0.1 |
| Maximum number of bins | 255 |

| | |
|---|---|
| Minimum number of samples required in each leaf node. | 20 |
| Number of data points used to construct histogram bins. | 200000 |
| Drop rate | 0.1 |
| Maximum number of leaves | 31 |

Next we trained the model alongside its original algorithms that it derived from to test the speed, accuracy and overfitting possibilities.

The next step consists of applying a 10 folds cross-validation approach to test the model's performance and potential overfitting or underfitting, one can notice in Figure 4.29 that the model starts with a small training score and then sharply increases in the next iteration with a small provided subset of the actual training dataset thanks to the model's ability to successfully employing weak learners, at the end of training there's a small gap between training accuracy and validation accuracy which suggests that the model has a good generalization capability against new data allowing it to have a good prediction.

Keeping in mind that the model went through optimization techniques such as Particle Swarm Optimization (PSO) where the hyperparameters of the model were fine tuned in order to meet our expectations.

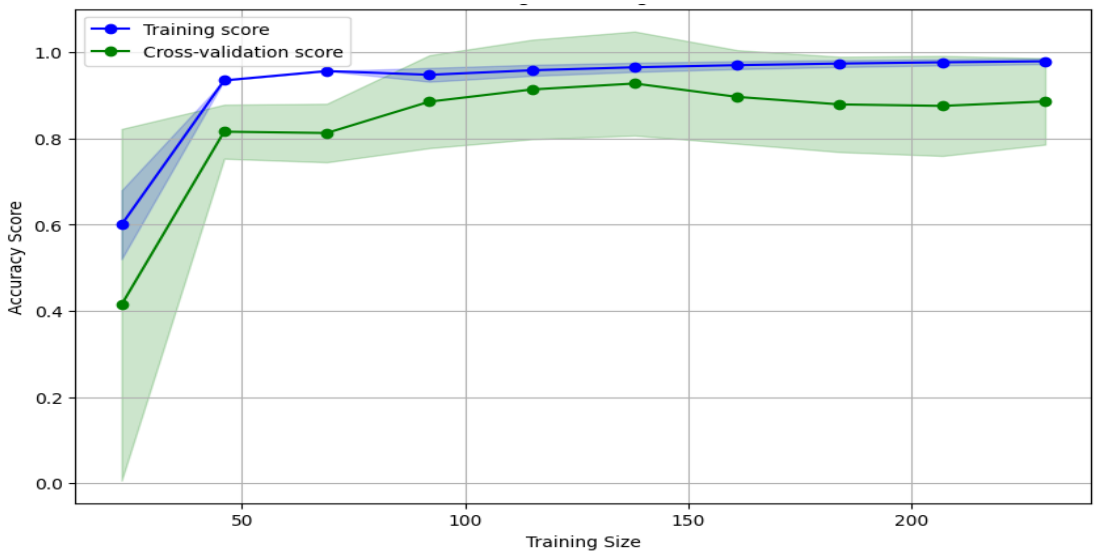



Figure 4.29 LightGBM learning curve for overfitting evaluation

Next overfitting test is against original models.

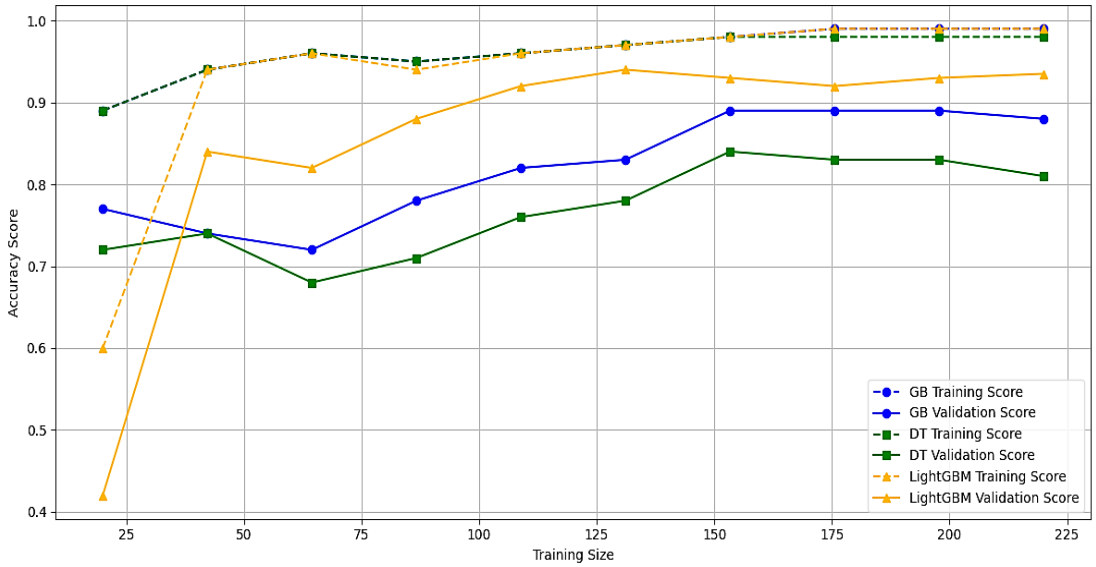



Figure 4.30 Comparative Learning curve for overfitting evaluation for GB, DT and LightGBM

The comparative analysis of the learning curves for each classifier suggests that in terms of training performance both LightGBM and GB surpassed DT by reaching 99% against 97%, as for the validation performance DT performed moderately scoring 81% while GB scored 88% and once again LightGBM outperformed by achieving the highest score of 94%, one can notice also the existence of large gap between training and validation that indicates the possibility of overfitting while training of DT model which makes the model not good enough in generalization, this problem is slightly noticed in GB learning curve which delivers relatively better generalization and again LightGBM excels in performance where convergence can be clearly noticed between training and validation suggesting that the model has excellent generalization and can deliver a promising great prediction against unseen and new data

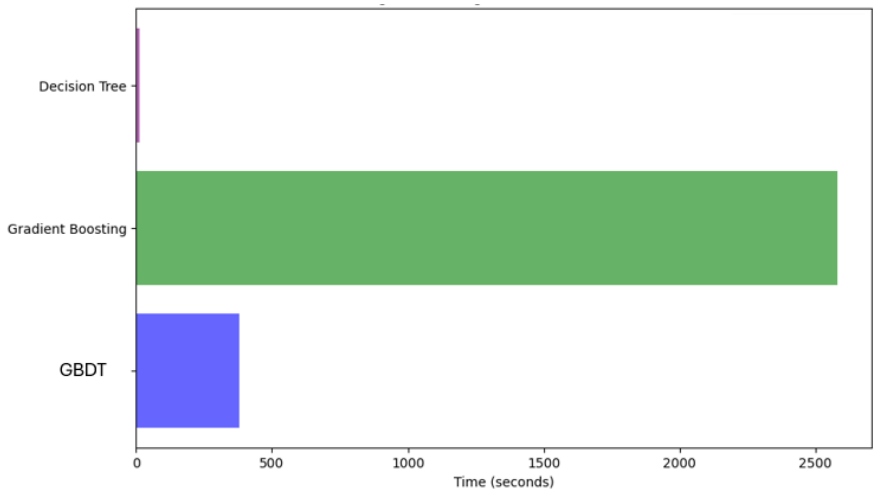



Figure 4.31 Speed prediction test

The training time of GBDT comes next after GB. GBDT leverages the boosting technique to combine multiple decision trees, improving performance over a single decision tree. While

it is faster than GB, GBDT still involves multiple iterations and calculations, leading to moderate training times. The DT model has the fastest training time among the three. This is because decision trees are straightforward algorithms that partition the data space and build a tree in a single pass. However, this simplicity comes at a cost. Although DTs are quick to train, they often lack the precision of more sophisticated models like GBDT and GB.
This section is dedicated to comparing the model's performance against the traditional models which it derives from.

Table 4.9 lightGBM model evaluation against original models.

| Classifier | Task | Prediction Time (sec) | F1-Score | Recall | Precision | Accuracy |
|---|---|---|---|---|---|---|
| **DT** | Binary | 0.1564 | 0.94 | 0.95 | 0.95 | 94% |
| | Multi-class | 0.2224 | 0.84 | 0.84 | 0.85 | 84% |
| **GB** | Binary | 0.2374 | 0.98 | 0.98 | 0.98 | 98% |
| | Multi-class | 0.1612 | 0.96 | 0.97 | 0.95 | 96.5% |
| **LightGBM** | Binary | **0.071** | 0.98 | 0.98 | 0.98 | **98.23%** |
| | Multi-class | **0.069** | 0.98 | 0.98 | 0.98 | **98%** |

We can notice that LightGBM outperformed in both binary and multi-class classifications accuracy and also marking remarkable prediction times faster than its original algorithms x2 and x3 faster rates against DT and GB respectively.

Figure 4.32 showcase the results of multi-class classification of the model encompassing the three types of air gap eccentricity alongside their sevrity degree.

We can notice that lightGBM does not necessarily need a numerical format for target data encoding instead the model does that automatically by changing the category classes into numerical ones.

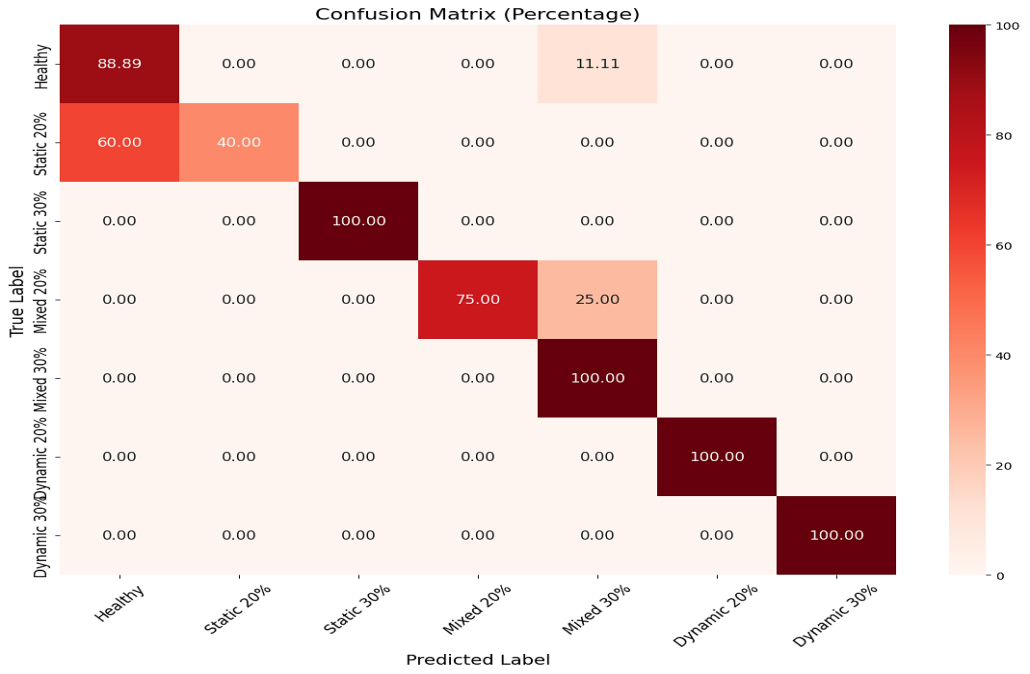



Figure 4.32 Confusion matrix results of multi-class classification.

After insuring the model's ability to detect air gap eccentricity with all its types and severity degrees, we trained the model on another dataset containing raw current signal of broken rotor bars of 1,2 and broken bars and in two different case scenarios where the bars were adjacent to each other, meaning we collected signals from the bars 1,2 and 3 and 1, 20 and 30 for adjacent and far from each other bars respectively.

The results of the classification are evaluated through confusion matrix in figures 4.33 and 4.34

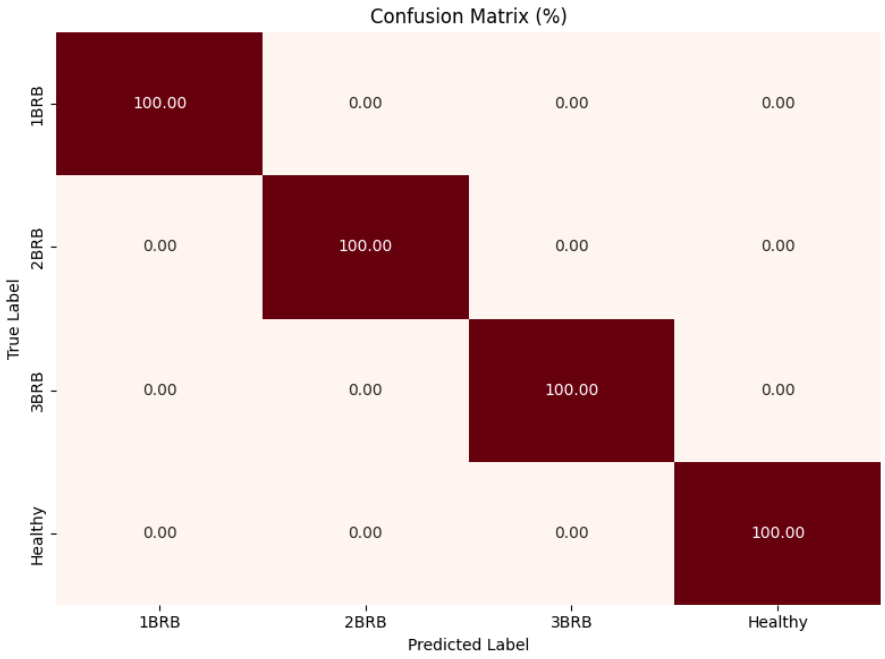



Figure 4.33 classification of adjacent broken rotor bars

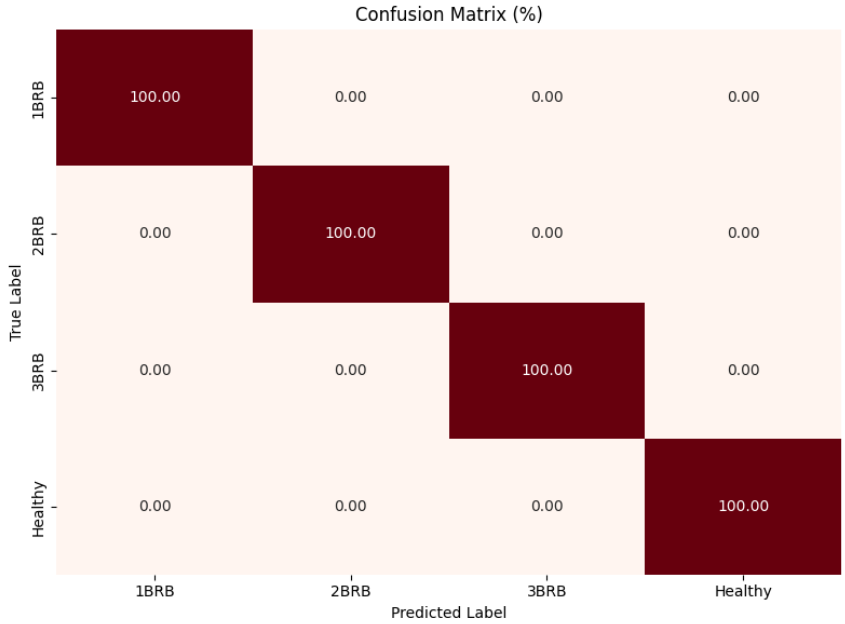



Figure 4.34 classification of seperated borken rotor bars

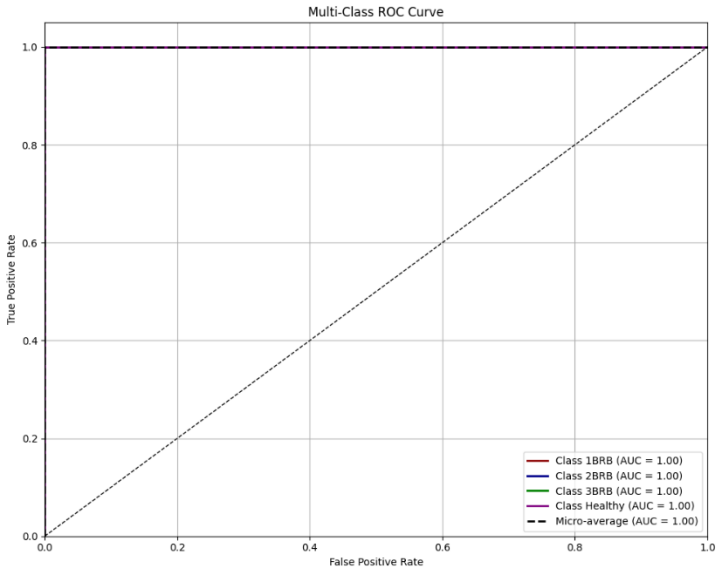



Figure 4.35 ROC values one vs rest

LightGBM classifier was employed for the multi-class classification task involving four distinct fault classes. The model was configured using the default hyperparameters, with class weight 'balanced' enabled to compensate for class imbalance in the dataset. To address the limited size of the dataset, data augmentation was applied, effectively increasing the training volume. The model was trained on 80% of the augmented dataset and tested on the remaining 20%.

The LightGBM classifier achieved 100% accuracy on the test set, demonstrating perfect classification across all fault categories. Furthermore, the Receiver Operating Characteristic (ROC) analysis was conducted in a one-vs-rest manner for the multi-class scenario. The results yielded an AUC value of 1.00 for each class as well as for the micro-averaged ROC, confirming the model's high ability to distinguish between all classes with no overlap or misclassification.

Now we will test the model's performance against other classifiers from Ensemble Methods:

Table 4.10 lightGBM performance evaluation against Ensemble Methods models

| Classifier | Task | Prediction Time | F1-Score | Recall | Precision | Accuracy |
|---|---|---|---|---|---|---|
| **AdaBoost** | Binary | 0.256 | 0.98 | 0.98 | 0.98 | 98% |
| | Multi-class | 0.24 | 0.25 | 0.29 | 0.38 | 29% |
| **XGBoost** | Binary | 8.8719 | 0.98 | 0.98 | 0.98 | 98.27% |
| | Multi-class | 8.2224 | 0.96 | 0.97 | 0.95 | 96.5% |
| **RF** | Binary | 0.1468 | 0.94 | 0.95 | 0.950 | 94% |
| | Multi-class | 0.6948 | 0.94 | 0.95 | 0.94 | 94.82% |
| **LightGBM** | Binary | **0.071** | 0.98 | 0.98 | 0.98 | **98.23%** |
| | Multi-class | **0.069** | 0.98 | 0.98 | 0.98 | **98%** |

After analyzing the results obtained from testing the models' predictions, we can summarize that lightGBM delivered outstanding results against its peers from Ensemble Methods that had different performances against the attributed tasks and also in prediction speed, where XGBoost

performed great in terms of accuracy in the previous test, however, it delivered poorly in prediction times scoring much slower speed than most of the classifiers which is a crucial point for fault detection, furthermore, other ensemble methods have an unsteady performance when handling both binary and multi-class classifications unlike LightGBM that gives a steady and high performance.

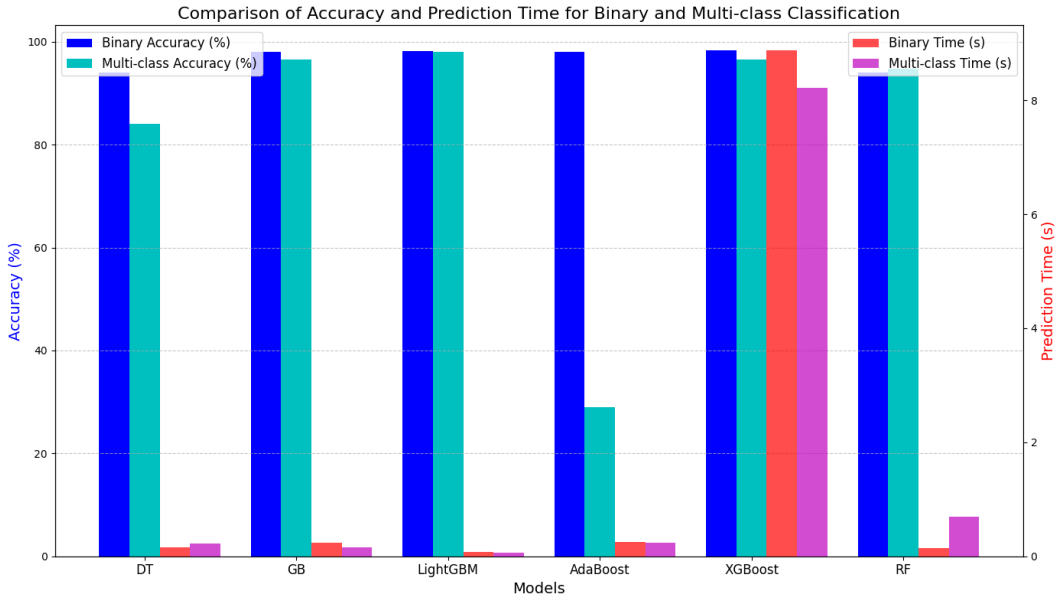



Figure 4.36 Performance comparison of LightGBM vs Ensemble Methods

### 4.7 Machine learning-signal processing combination

In this section, two machine learning algorithms were employed for the diagnosis of air gap eccentricity, the first algorithm is SVM, after training our model using energy levels and RMS values as inputs the results of testing the model's precision is shown in the confusion matrix.

SVM model exhibited some satisfying results when classifying early stage degrees for both static and dynamic air gap eccentricity which served the purpose of monitoring of this defect with an overall accuracy above 70% and also the detection of the fault itself by successfully distinguishing healthy samples from the faulty ones with an accuracy of 79%.

The chosen architecture for SVM model is shown in the following Table 4.11

Table 4.11 SVM architecture

| Classifier | Parameter | Chosen Setting |
|---|---|---|
| SVM | Kernel Function | Linear kernel |
| | Standardization | Input features are standardized |
| | Box Constraint | 1 |
| | Kernel Scale | Not used |
| | Multiclass Scheme | One-vs-one |

The following results of the training using a multi-class classification of the seven classes delivered mixed performances, where SVM scored high results with some classes it performed poorly with others, evaluation results are shown in Table 4.12:

Table 4.12 SVM multi-class classification performance.

| Condition | Precision | Recall | F1score |
|---|---|---|---|
| DAGE-20%- | 100% | 75% | 85% |
| DAGE-30%- | 80% | 66% | 72% |
| HAG | 84% | 87.5% | 85.7% |
| MAGE-20%- | 100% | 75% | 85.7% |
| MAGE-30%- | 47% | 66% | 55% |
| SAGE-20%- | 69% | 75% | 72% |
| SAGE-30%- | 53% | 58% | 56% |

The results shown in table 4.11 illustrate various performances of SVM when dealing with diffrenet classes, where the model struggled with higher degrees of the defect due to the confusion that it made, for better visualization we can see the results of the confusion matrix in Figure 4.37

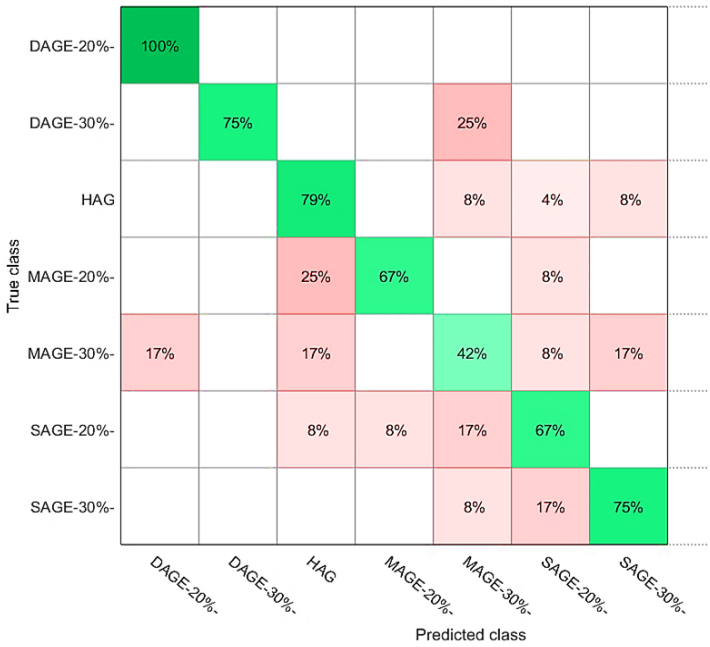



Figure 4.38 SVM confusion matrix results

The second machine learning algorithm chosen is DT algorithm, which delivered outstanding results in comparison to SVM model by successfully classifying the defected samples and the healthy ones and each type of the defect alongside its severity degree.

The chosen architecture for DT model is shown in Table 4.13:

Table 4.13 DT architecture

| Classifier | Parameter | Chosen Setting |
|---|---|---|
| DT | Splitting Criterion | Gini's diversity index |
| | Max Splits | 100 |
| | Minimum Leaf Size | 1 |
| | Maximum Tree Depth | No strict cap |
| | Pruning | Post-pruning |
| | Surrogate Splits | Not used |

Confusion matrix results are illustrated in Figure 4.39, that shows outstanding performance results and classification capabilities:

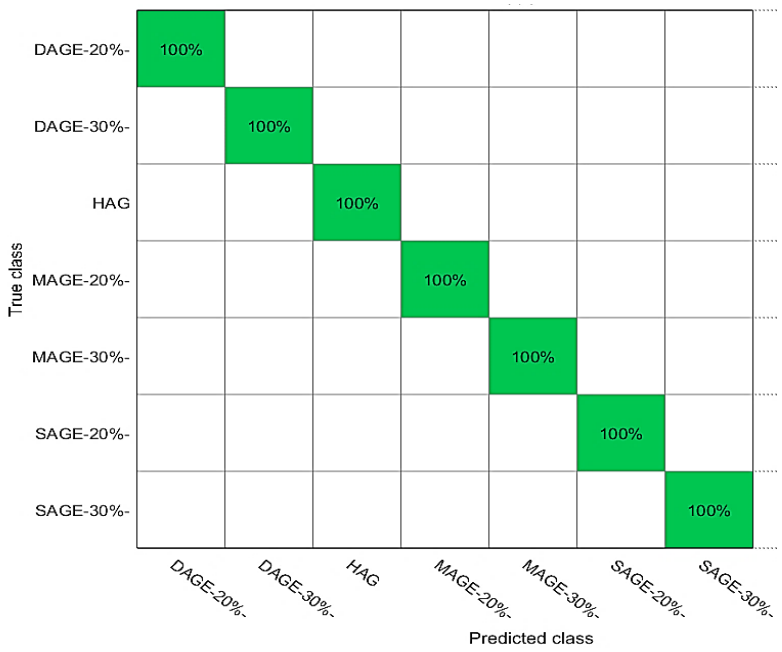



Figure 4.39 DT multi-class classification

We can notice that using DT model combined with preprocessing tools gave great results with the provided clean dataset, however achieving 100% of accuracy in the field of machine learning is usually not a promosing thing, since the model is too accurate with predicting the test dataset with the actual real values, which makes the model too "specialized" with the provided dataset and prone to face difficulties with newer dataset which makes it less "generalized".

### 4.7.1 Models evaluation

To generalize the overview that we had by training multiple models under various scenarios to detect air gap eccentricity and broken rotor bars, we have summerized our findings through four categories based on accuracy, task handling, prediction speed and overfitting, in order to extract the best model suitable for our type of fault detection.

The results of the comparative analysis are gathered in table 4.14

Table 4.14 Global approachs evaluation

| Approach | model | Accuracy | Prediction speed | Task handling | overfitting |
|---|---|---|---|---|---|
| Stand-alone AI | ANN | Moderate | Bad | Bad | possible |
| | DT | Good | Moderate | Moderate | possible |
| | Ensemble Methods | Good | Good | Good | Rare |
| AI+signal processing | SVM+DT | Good | Bad | Moderate | possible |

Best overall performer: Ensemble Methods they provide good accuracy, fast prediction, robust task handling, and low risk of overfitting, making them highly suitable for diagnosing air gap eccentricity and broken rotor bars.

ANNs, while powerful, underperform here due to low speed, bad task handling, and high overfitting risk, because the dataset or feature space doesn't favor deep learning without enhancements.

AI with signal processing (SVM+DT) maintains good accuracy, but suffers from bad speed and moderate generalization, likely due to increased complexity and computation time.

**4.8 Conclusion**

The results obtained in this study clearly demonstrate the effectiveness of artificial intelligence (AI) models—particularly classification algorithms—in the detection and diagnosis of faults such as air gap eccentricity and broken rotor bars in induction machines. The high accuracy and perfect ROC values achieved highlight not only the precision of these models but also their robustness and adaptability to complex fault scenarios.

Compared to traditional model-based and non-model-based approaches like Fast Fourier Transform (FFT) and wavelet transforms, which require extensive preprocessing, domain-specific expertise, and careful signal interpretation, AI models provide a more autonomous and streamlined solution. Even when compared to hybrid techniques that combine signal processing with AI, standalone AI models have proven to be more efficient. This is primarily due to their built-in capabilities for data preprocessing, automatic feature extraction, and selection, which reduce the need for manual intervention and mitigate the risk of introducing bias or errors during feature engineering and this is what we found out using Ensemble Methods in the image of LightGBM with autonomous feature extraction and swift learning rate, it proved reliable in fault detection.

Moreover, this efficiency mitigates the need for developing complex dynamical models of the machine and bypasses the urge to construct mathematical replicas to estimate system parameters. By relying solely on raw or minimally processed data, AI models offer a data-driven approach that simplifies implementation while maintaining exceptional diagnostic performance.

In summary, the findings confirm that AI-based classification models offer a superior alternative for fault detection in induction machines. Their ability to deliver high performance without the complexity of traditional modeling pipelines positions them as powerful tools for real-time, scalable, and reliable condition monitoring systems.

# General Conclusion

In conclusion, artificial intelligence has demonstrated promising effectiveness in the field of fault diagnosis for induction machines. By adopting data-driven analysis techniques—particularly ensemble learning methods—AI enables the detection and classification of faults with high accuracy and reliability, without the need for a dynamic model of the real system. This not only simplifies the diagnostic process but also significantly reduces the complexity, time, and computational cost typically associated with traditional model-based techniques.

The strength of AI lies in its ability to learn from historical and real-time data, capturing subtle and complex patterns that may not be easily observable or modelable through analytical equations. Furthermore, its flexibility extends beyond mere fault classification to include severity estimation under various operational conditions. This capability provides a robust and adaptive monitoring framework, which is essential for predictive maintenance strategies.

As demonstrated throughout this thesis, AI-based methods have not only outperformed classical non-model-based approaches but have also shown superiority over model-based signal processing techniques such as Fast Fourier Transform (FFT) and Wavelet Transform. While these traditional techniques offer valuable insights into signal characteristics, they often suffer from limitations such as sensitivity to noise, reduced performance in non-stationary environments, and the need for expert-driven feature extraction. In contrast, AI models—particularly those based on ensemble strategies like Random Forest, Gradient Boosting, and LightGBM—can automatically learn optimal representations from raw data, adapt to changing operating conditions, and deliver more consistent and scalable results.

The advantages of AI techniques extend to their ability to perform an autonomous signal processing by filtering the provided data signal which was the stator current in our study, and leave only the harmonics which designate each condition of the machine, which would be later on used for feature extraction, to perform a strong reliable training with good prediction capabilities.

Ultimately, artificial intelligence stands out as a transformative approach for machine fault diagnosis, offering improved diagnostic precision, reduced dependency on physical modeling, and enhanced decision-making capabilities that are crucial for modern industrial monitoring systems.

Refrences

References


[1]. Cummings, P.G.; Kerr, R.H.; Dunki-Jacobs, J.R. Protection of induction motors against unbalanced voltage operation. In Proceedings of the 1984 Annual Meeting Industry Applications Society, Chicago, IL, USA, 30 September–4 October 1984; IEEE: New York, NY, USA, 1984; pp. 143–158.

[2]. Bento, F.; Adouni, A.; Muxiri, A.C.P.; Fonseca, D.S.B.; Cardoso, A.J.M. On the risk of failure to prevent induction motors permanent damage, due to the short available time-to-diagnosis of inter-turn short-circuit faults. IET Electr. Power Appl. 2021, 15, 51–62.

[3]. Adouni, A.; Cardoso, A.J.M. Thermal Analysis of Low-Power Three-Phase Induction Motors Operating under Voltage Unbalance and Inter-Turn Short Circuit Faults. Machines 2021, 9, 2.

[4]. Kurt, M.S.; Balci, M.E.; Aleem, S.H.E.A. Algorithm for estimating derating of induction motors supplied with under/over unbalanced voltages using response surface methodology. J. Eng. 2017, 2017, 627–633.

[5]. S. Chen and R. Zivanovic, "A novel high-resolution technique for induction machine broken bar detection," in Power Engineering Conference, 2007. AUPEC 2007. Australasian Universities. IEEE, 2007, pp. 1–5.

[6]. O. Ondel, E. Boutleux, and G. Clerc, "A method to detect broken bars in induction machine using pattern recognition techniques," Industry Applications, IEEE Transactions on, vol. 42, no. 4, pp. 916–923, 2006.

[7]. S. Ahamed, S. Karmakar, M. Mitra, and S. Sengupta, "Diagnosis of induction motor faults due to broken rotor bar and rotor mass unbalance through discrete wavelet trans form of starting current at no-load," J. Electrical Systems, vol. 6, no. 3, pp. 442–456, 2010.

[8]. S.Nandi,H.Toliyat,S.Nandi,andH.Toliyat,"Condition Monitoring And Fault Diagnosis of electrical machines-a review," IEEE Transactions on Energy Conversion, vol. 20, no. 4, pp. 719–729, 2005.

[9]. Seera, M., Lim, C.P., Nahavandi, S., et al.Ś 'Condition monitoring of induction motorsŚ a review and an application of an ensemble of hybrid intelligent models', Expert Syst. Appl., 2014, 41, pp. 4891–4903

[10]. Ghorbanian, V., Faiz, J.Ś 'A survey on time and frequency characteristics of induction motors with broken rotor bars in line-start and inverter-fed modes', Mech. Syst. Signal Process., 2015, 54, pp. 427–456

[11]. Marcello, C., Fossatti, J.P., Terra, J.I.Ś 'Fault diagnosis on induction motors based on FFT', in Salih, S. (Ed.)Ś 'Fourier transform signal processing' (InTech, USA, 2012), pp. 157–182.

[12]. Hassan, O.E., Amer, M., Abdelsalam, A.K., et al.Ś 'Induction motor broken rotor bar fault detection techniques based on fault signature analysis – a review', IET Electr. Power Appl., 2018, 12, (7), pp. 895–907

Refrences


[13]. Nandi, S., Toliyat, H.A., Li, X.Ś 'Condition monitoring and fault diagnosis of electrical motors – a review', IEEE Trans. Energy Convers., 2005, 20, (4), pp. 719–729.

[14]. AFNOR. (1986a). *Comment réussir votre maintenance*. Paris: Association Française de Normalisation, Collection "Guides de l'utilisateur", 163 p. (14 p).

[15]. AFNOR (1986 b), "Recueil de normes françaises. Fiabilité, maintenabilité, disponibilité", Paris, Association Française de Normalisation, (2° édition), 567 p.

[16]. Heng, J. (2011). *Practice of Preventive Maintenance* (2nd ed.). Dunod Publishing.

[17]. Villemeur, A., "Sûreté de fonctionnement des systèmes industriels, Fiabilité - Facteurs Humains - Informatisation", Collection de la Direction des Études et Recherches d"Électricité de France, Édition Eyrolles, n° 67, Paris, (1988).

[18]. M. R. Zemouri, "Contribution to the Monitoring of Production Systems Using Dynamic Neural Networks: Application to e-Maintenance," Doctoral Thesis, University of Franche-Comté, 2003.

[19]. Sherif Fakher, Abdelaziz Khlaifat, Hashim Nameer, Improving electric submersible pumps efficiency and mean time between failure using permanent magnet motor, Upstream Oil and Gas Technology, Volume 9, 2022, 100074, ISSN 2666-2604,

[20]. E. Schaeffer, « Diagnostic des machines asynchrones modèles et outils paramétriques dédiés à la simulation et à la détection des défauts », thèse de doctorat, université de Nantes, France,1999.

[21]. T. Boumegoura, «Recherche de signature électromagnétique des défauts dans une machine asynchrone et synthèse d'observateurs en vue de diagnostic », thèse de doctorat, école centrale de Lyon, France,2001.

[22]. A. Menacer, Identification of Parameters and States of an Induction Machine: Diagnosis and Development of Robust Control, Saarbrucken: European University Editions, 2010.

[23]. Adamou, A. A., & Alaoui, C. (2024). Efficiency-Centered Fault Diagnosis of In-Service Induction Motors for Digital Twin Applications: A Case Study on Broken Rotor Bars. *Machines*, *12*(9), 604. https://doi.org/10.3390/machines12090604.

[24]. X. Jin, M. H. Azarian, C. Lau, L. Cheng, and M. Pecht, ''Physics-of-failure analysis of cooling fans,'' in Proc. Prognostics Syst. Health Manage. Conf., May 2011, pp. 1–8

[25]. K. Kudelina, T. Vaimann, B. Asad, A. Rassõlkin, A. Kallaste, and G. Demidova, ''Trends and challenges in intelligent condition monitoring of electrical machines using machine learning,'' Appl. Sci., vol. 11, no. 6,p. 2761, Mar. 2021.

[26]. Bonnett, A.H. and. Soukup, G..,C., "Cause and Analysis of Stator and Rotor Failures in Three-phase Squirrel-Cage Induction Motors", IEEE Transactions On Industry Applications, V. 28, n°. 4, (July / August 1992), 921-936.

[27]. BIANCHI Bolognani S., Pré M.D., « Strategies for the fault-tolerant current control of a five-phase permanent-magnet motor", IEEE Transaction on industry Applications, vol.43, no.4, p. 960-970, July August 2007.

[28]. Valtierra-Rodriguez, M.; Rivera-Guillen, J.R.; Basurto-Hurtado, J.A.; De-Santiago-Perez, J.J.; Granados-Lieberman, D.; Amezquita-Sanchez, J.P. Convolutional Neural Network and Motor Current Signature Analysis during the Transient State for Detection of Broken Rotor Bars in Induction Motors. *Sensors* **2020**, *20*, 3721. https://doi.org/10.3390/s20133721.

Refrences


[29]. ONNETT A.H., YUNG C., “Increased efficiency versus increased reliability”, IEEE Industry Applications Magazine, p.1077-2618, January-February 2008.

[30]. Cameron JR, Thomson WT, Dow AB. Vibration and current monitoring for detecting air gap eccentricity in large induction motors. In: Proceedings of IEE Electric Power Applications; 1986. pp. 155–163.

[31]. Nandi S, Toliyat HA, Li X. Condition monitoring and fault diagnosis of electrical motors – a review. IEEE Transactions on Energy Conversion. 2005; 20.4: 719–729.

[32]. Faiz J, Ojaghi M. Different indexes for eccentricity faults diagnosis in three-phase squirrel-cage induction motors: a review. Mechatronics. 2009; b19: 2–13.

[33]. Thomson WT, Gilmore RJ. Motor current signature analysis to detect faults in induction motor drives–fundamentals, data interpretation and industrial case histories. In: Proceedings of the 32nd Turbomachinery Symposium, Houston, TX, USA; 2003. pp.145–156.

[34]. Karami M, Mariun N, Mehrjou MR, Ab Kadir MZA, Misron N, Mohd Radzi MA. Static eccentricity fault recognition in three-phase line start permanent magnet synchronous motor using finite element method. Mathematical Problems in Engineering. 2014; 1–12.

[35]. Torkaman H, Afjei E. Sensorless method for eccentricity fault monitoring and diagnosis in switched reluctance machines based on stator voltage signature. IEEE Transactions on Magnetics. 2013; 49.2: 912–920

[36]. Hong J, Park S, Hyun D, Kang T, Lee SB, Kral C, Haumer A. Detection and classification of rotor demagnetization and eccentricity faults for PM synchronous motors. IEEE Transactions on Industry Applications. 2012; 48.3: 923–932.

[37]. Wiedenbrug EJ, Teska M, Nandi S, Chelvan IT. Automated monitoring of air gap eccentricity for inverter-fed induction motors under standstill conditions. IEEE Transactions on Industry Applications. 2011; 47.3: 1257–1266.

[38]. Dorrell DG, Cossar C. A vibration-based condition monitoring system for switched reluctance machine rotor eccentricity detection. IEEE Transactions on Magnetics. 2008; 44.9: 2204–2214.

[39]. Bonnett AH, Soukup GC. Cause and analysis of stator and rotor failures in three-phase squirrel-cage induction motors. IEEE Transactions on Industry Applications. 1992; 28.4: 921–937.

[40]. [40]Pennacchi P, Bachschmid N, Vania A, Zanetta GA, Gregori L. Use of modal representation for the supporting structure in model-based fault identification of large rotating machinery : Part 1- theoretical remarks. Mechanical Systems and Signal Processing. 2006; 20.3: 662–681.

[41]. Bachschmid N, Pennacchi P, Tanzi E. Cracked rotors: a survey on static and dynamic behavior including modeling and diagnosis. Springer Science & Business Media, 2010. ISBN 978-3-642-01484-0.

[42]. Issa, R.; Clerc, G.; Hologne-Carpentier, M.; Michaud, R.; Lorca, E.; Magnette, C.; Messadi, A. Review of Fault Diagnosis Methods for Induction Machines in Railway Traction Applications. Energies 2024, 17, 2728. https://doi.org/10.3390/en17112728.

Refrences


[43]. Goyal, Deepam & Choudhary, Anurag & Pabla, Bs & Dhami, Sukhdeep. (2020). Support vector machines based non-contact fault diagnosis system for bearings. Journal of Intelligent Manufacturing. 31. 1-15. 10.1007/s10845-019-01511-x.

[44]. Didier G, Ternisien E, Caspary O, Razik H. A new approach to detect broken rotor bars in induction machines by current spectrum analysis. Mechanical Systems and Signal Processing. 2007; 21: 1127–1142.

[45]. Andrew JK, Lin D, Dragan B. A review on machinery diagnostics and prognostics implementing condition-based maintenance. Mechanical Systems and Signal Processing. 2006; 20: 1483–1510.

[46]. Chow MY. Guest editorial special section on motor fault detection and diagnosis. IEEE Transactions on Industrial Electronics. 2000; 47.5: 982–983.

[47]. Bin GF, Gao JJ, Li XJ, Dhillon BS. Early fault diagnosis of rotating machinery based on wavelet packets – Empirical mode decomposition feature extraction and neural network. Mechanical Systems and Signal Processing. 2012; 27: 696–711.

[48]. Burnett R, Watson J, Elder S. The application of modern signal processing techniques to rotor fault detection and location within three phase induction motors. Signal processing. 1996; 49.1: 57–70.

[49]. Bonnett AH, Yung C. Increased efficiency versus increased reliability. IEEE Industry Applications Magazine. 2008; 14.1: 29–36.

[50]. Mehrjou MR, Mariun N, Hamiruce Marhaban M, Misron N. Rotor fault condition monitoring techniques for squirrel-cage induction machine – a review. Mechanical Systems and Signal Processing. 2011; 25.8: 2827–2848.

[51]. A. Bouzida and M.A. Boumaza. `` Diagnostic de défauts au rotor par l'approche de l'estimation paramétrique ``. PFE, Ecole Nationale Polytechnique d'Alger, 2005.

[52]. Boumegoura. `` Recherche de signature électromagnétique des défauts dans une machine asynchrone et synthèse d'observateurs en vue du diagnostic » Thèse, Ecole centrale de Lyon, France, 2001.

[53]. D. Ichalal. `` Estimation et diagnostic de systèmes non linéaires `` Thèse de doctorat, INPL Nancy, 2009.

[54]. S. Moreau. `` Contribution à la modélisation et l'estimation paramétrique des machines électriques à courant alternatif : Application au diagnostic `` Thèse de doctorat ENSIP Poitiers, 1999.

[55]. Beard R. V., "failure accommodation in linear systems through selfreorganization", PhD thesis, department of aeronautics and astronautics, MIT, Cambridge, Massachusetts, USA, (1971).

[56]. Combastel, C. „Méthodes d'aide à la décision pour la détection et la localisation de défauts dans les entraînements électriques", PhD thesis Automatique / Robotique. Institut National Polytechnique de Grenoble -INPG, (2000).

[57]. De Persis, C. and Isidori, A., "A geometric approach to nonlinear fault detection and isolation", IEEE Trans. on Automatic Control, V. 46. n°6, (June 2001), 853-865.

[58]. Djemaï, M., Barbot, J.P. and Bethoux, O., "On the problem of fault detection and residual generation". Proceedings of the 39" IEEE Conference on Decision and Control Sydney, Australia (December, 2000), 4335-4340.

Refrences


[59]. Alcorta, G. E. et Frank, P. M., « A novel design of structured observerbased residual for FDI ", Proc. Of American Control Conference, California, USA, June (1999), 1341-1345.

[60]. Chen J., Patton R.J. and Zhang H.Y., " Deign of unknown input observer and robust fault detection filters", International Journal of Control, V63, n°1, (1996), 85-105.

[61]. Porrill, John & Dean, Paul & Anderson, Sean. (2012). Adaptive filters and internal models: Multilevel description of cerebellar function. Neural networks : the official journal of the International Neural Network Society. 47. 10.1016/j.neunet.2012.12.005.

[62]. Isermann, R., "Model-based fault detection and diagnosis-Status and applications" Annual Reviews in Control, V. 29, n°1, (2005), 71–85.

[63]. Bouattour, J., Gertler, J. and Hu, Y., "Diagnosis parametric faults in induction motor with nonlinear parity relations", Proceeding of IFAC Safe process, Budapest, Hungary, (2000), 992-997.

[64]. Cocquempot V., "Contribution à la surveillance des systèmes industriels complexes", HDR, UST Lille, France, (2004).

[65]. Benbouzid M.E.H., "A review of induction motors signature analysis as a medium of faults detection", IEEE Trans. On Industrial electronics, V.47, n°5, (2000), 984-993.

[66]. Alcorta, G. E. and Frank, P. M., "Fault detection and isolation in nonlinear systems", Proc. Of ECC"99, Karlsruhe, Germany, (31 August-3 September 1999), 609-614.

[67]. Alger, P.L., "Induction Machines: Their Behavior and Used", ed. Gordon and Breach, (1970).

[68]. Ferdjouni, A., Salhi, H., Djemaï, M., Bussawon, K., "Observer-Based Detection Of Inter-Turn Short Circuit In Three-Phase-Induction Motor Stator Windings", Mediterranean Journal of Measurement and Control, V.2, n°3, (2006), 132-143.

[69]. Benbouzid, M.E.H. A review of induction motors signature analysis as a medium for faults detection. IEEE Trans. Ind. Electron.2000, 47, 984–993.

[70]. Bellini, A. ; Filippetti, F. ; Tassoni, C. ; Capolino, G.-A. Advances in Diagnostic Techniques for Induction Machines. IEEE Trans. Ind. Electron. 2008, 55, 142–149

[71]. Lang, W. ; Hu, Y. ; Gong, C. ; Zhang, X. ; Xu, H. ; Deng, J. Artificial Intelligence-Based Technique for Fault Detection and Diagnosis of EV Motors : A Review. IEEE Trans. Transp. Electr. 2022, 8, 384–406.

[72]. Kumar, R.R. ; Andriollo, M. ; Cirrincione, G.; Cirrincione, M.; Tortella, A. A Comprehensive Review of Conventional and Intelligence-Based Approaches for the Fault Diagnosis and Condition Monitoring of Induction Motors. Energies 2022, 15, 8938.

[73]. Benbouzid, M.E.H.; Kliman, G.B. What stator current processing-based technique to use for induction motor rotor faults diagnosis. IEEE Trans. Energy Convers. 2003, 18, 238–244.

[74]. Henao, H.; Capolino, G.-A.; Fernandez-Cabanas, M.; Filippetti, F.; Bruzzese, C.; Strangas, E.; Pusca, R.; Estima, J.; Riera-Guasp, M.;Hedayati-Kia, S. Trends in Fault Diagnosis for Electrical Machines: A Review of Diagnostic Techniques. IEEE Ind. Electron. Mag. 2014, 8, 31–42.

Refrences


[75]. Dorrell, D.G.; Thomson, W.T.; Roach, S. Analysis of airgap flux, current, and vibration signals as a function of the combination of static and dynamic airgap eccentricity in 3-phase induction motors. IEEE Trans. Ind. Appl. 1997, 33, 24–34. [CrossRef]

[76]. Immovilli, F.; Bellini, A.; Rubini, R.; Tassoni, C. Diagnosis of Bearing Faults in Induction Machines by Vibration or Current Signals: A Critical Comparison. IEEE Trans. Ind. Appl. 2010, 46, 1350–1359. [CrossRef]

[77]. Henao, H.; Demian, C.; Capolino, G.-A. A frequency-domain detection of stator winding faults in induction machines using an external flux sensor. IEEE Trans. Ind. Appl. 2003, 39, 1272–1279.

[78]. Zamudio-Ramírez, I.; Osornio-Rios, R.A.; Antonino-Daviu, J.A. Smart Sensor for Fault Detection in Induction Motors Based on the Combined Analysis of Stray-Flux and Current Signals: A Flexible, Robust Approach. IEEE Ind. Appl. Mag. 2022, 28, 56–66.

[79]. Choudhary, A.; Goyal, D.; Letha, S.S. Infrared Thermography-Based Fault Diagnosis of Induction Motor Bearings Using Machine Learning. IEEE Sens. J. 2021, 21, 1727–1734.

[80]. Choudhary, A.; Mian, T.; Fatima, S.; Panigrahi, B.K. Passive Thermography Based Bearing Fault Diagnosis Using Transfer Learning with Varying Working Conditions. IEEE Sens. J. 2023, 23, 4628–4637.

[81]. Garcia-Perez, A.; Romero-Troncoso, R.J.; Cabal-Yepez, E.; Osornio-Rios, R.A.; Lucio-Martinez J.A. Application of high-resolution spectral analysis for identifying faults in induction motors by means of sound. J. Vib. Control 2012, 18, 1585–1594.

[82]. Esfahani, E.T.; Wang, S.; Sundararajan, V. Multisensor Wireless System for Eccentricity and Bearing Fault Detection in Induction Motors. IEEE/ASME Trans. Mechatron. 2014, 19, 818–826.

[83]. Gao, Z.; Cecati, C.; Ding, S.X. A Survey of Fault Diagnosis and Fault-Tolerant Techniques—Part I: Fault Diagnosis with Model-Based and Signal-Based Approaches. IEEE Trans. Ind. Electron. 2015, 62, 3757–3767.

[84]. Kreischer, C.; Gołebiowski, L. Detection of broken bars and rings in induction machines. In Proceedings of the 2012 International Conference and Exposition on Electrical and Power Engineering, Iasi, Romania, 25–27 October 2012; pp. 355–359.

[85]. Trujillo-Guajardo, L.A.; Rodriguez-Maldonado, J.; Moonem, M.A.; Platas-Garza, M.A. A Multiresolution Taylor–Kalman Approach for Broken Rotor Bar Detection in Cage Induction Motors. IEEE Trans. Instrum. Meas. 2018, 67, 1317–1328.

[86]. Krause, P.C. Method of Multiple Reference Frames Applied to the Analysis of Symmetrical Induction Machinery. IEEE Trans. Power Appar. Syst. 1968, PAS-87, 218–227.

[87]. Gyftakis, K.N.; Cardoso, A.J.M. Reliable Detection of Stator Interturn Faults of Very Low Severity Level in Induction Motors. IEEE Trans. Ind. Electron. 2021, 68, 3475–3484.

[88]. Toliyat, H.A.; Lipo, T.A. Transient analysis of cage induction machines under stator, rotor bar and end ring faults. IEEE Trans. Energy Convers. 1995, 10, 241–247.

[89]. Tang, J.; Chen, J.; Dong, K.; Yang, Y.; Lv, H.; Liu, Z. Modeling and Evaluation of Stator and Rotor Faults for Induction Motors. Energies 2020, 13, 133.

Refrences


[90]. Nandi, S.; Bharadwaj, R.; Toliyat, H. Performance analysis of a three-phase induction motor under mixed eccentricity condition. IEEE Trans. Energy Convers. 2002, 17, 392–399.

[91]. Lubin, T.; Hamiti, T.; Razik, H.; Rezzoug, A. Comparison between finite-element analysis and winding function theory for inductances and torque calculation of a synchronous reluctance machine. IEEE Trans. Magn. 2007, 43, 3406–3410.

[92]. Thomson, W.T.; Fenger, M. Current signature analysis to detect induction motor faults. IEEE Ind. Appl. Mag. 2001, 7, 26–34.

[93]. Jung, J.-H.; Lee, J.-J.; Kwon, B.-H. Online Diagnosis of Induction Motors Using MCSA. IEEE Trans. Ind. Electron. 2006, 53, 1842–1852.

[94]. Cusido, J.; Romeral, L.; Ortega, J.A.; Rosero, J.A.; Garcia Espinosa, A. Fault Detection in Induction Machines Using Power Spectral Density in Wavelet Decomposition. IEEE Trans. Ind. Electron. 2008, 55, 633–643.

[95]. Bouzida, A.; Touhami, O.; Ibtiouen, R.; Belouchrani, A.; Fadel, M.; Rezzoug, A. Fault Diagnosis in Industrial Induction Machines Through Discrete Wavelet Transform. IEEE Trans. Ind. Electron. 2001, 37, 1227–1233.

[96]. Soualhi, A.; Medjaher, K.; Zerhouni, N. Bearing health monitoring based on hilbert huang transform, support vector machine, and regression. IEEE Trans. Instrum. Meas. 2015, 64, 52–62.

[97]. Climente-Alarcon, V.; Antonino-Daviu, J.A.; Riera-Guasp, M.; Puche-Panadero, R.; Escobar, L. Application of the Wigner–Ville distribution for the detection of rotor asymmetries and eccentricity through high-order harmonics. Electr. Power Syst. Res. 2012, 91, 28–36.

[98]. Delgado-Prieto, M.; Cariño, J.A.; Saucedo-Dorantes, J.J.; Osornio-Rios, R.A.; Romeral, L.; Romero Troncoso, R.J. Novelty detection based condition monitoring scheme applied to electromechanical systems. In Proceedings of the 2018 IEEE 23rd International Conference on Emerging Technologies and Factory Automation (ETFA), Turin, Italy, 4–7 September 2018; Volume 1, pp. 1213–1216.

[99]. Edomwandekhoe, K.; Liang, X. Advanced feature selection for broken rotor bar faults in induction motors. In Proceedings of the 2018 IEEE/IAS 54th Industrial and Commercial Power Systems Technical Conference (ICPS), Niagara Falls, ON, Canada, 7–10 May 2018; pp. 1–10.

[100]. Ali, M.Z.; Shabbir, M.N.S.K.; Liang, X.; Zhang, Y.; Hu, T. Machine learning-based fault diagnosis for single- and multi-faults in induction motors using measured stator currents and vibration signals. IEEE Trans. Ind. Appl. 2019, 55, 2378–2391.

[101]. Ramírez Chavez, M.; Ruíz Soto, L.; Arellano Espitia, F.; Saucedo, J.J.; Delgado Prieto, M.; Romeral, L. Evaluation of multiclass novelty detection algorithms for electric machine monitoring. In Proceedings of the 2019 IEEE 12th International Symposium on Diagnostics for Electrical Machines, Power Electronics and Drives (SDEMPED), Toulouse, France, 27–30 August 2019; pp. 330–337.

[102]. Su, H.; Chong, K.T. Induction machine condition monitoring using neural network modeling. IEEE Trans. Ind. Electron. 2007, 54, 241–249.

Refrences


[103]. Schoen, R.R.; Lin, B.K.; Habetler, T.G.; Schlag, J.H.; Farag, S. An unsupervised, on-line system for induction motor fault detection using stator current monitoring. IEEE Trans. Ind. Appl. 1995, 31, 1280–1286.

[104]. Martins, J.F.; Ferno Pires, V.; Pires, A.J. Unsupervised neural-network-based algorithm for an on-line diagnosis of three-phase induction motor stator fault. IEEE Trans. Ind. Electron. 2007, 54, 259–264.

[105]. Shifat, T.A.; Hur, J.-W. ANN Assisted Multi Sensor Information Fusion for BLDC Motor Fault Diagnosis. IEEE Access 2021, 9, 9429–9441.

[106]. 38. Martinez-Herrera, A.L.; Ferrucho-Alvarez, E.R.; Ledesma-Carrillo, L.M.; Mata-Chavez, R.I.; Lopez-Ramirez, M.; Cabal-Yepez,

[107]. E. Multiple Fault Detection in Induction Motors through Homogeneity and Kurtosis Computation. Energies 2022, 15, 1541.

[108]. 39. Zhao, R.; Wang, D.; Yan, R.; Mao, K.; Shen, F.; Wang, J. Machine Health Monitoring Using Local Feature-Based Gated Recurrent Unit Networks. IEEE Trans. Ind. Electron. 2018, 65, 1539–1548.

[109]. 40. Zhao, R.; Wang, J.; Yan, R.; Mao, K. Machine health monitoring with lstm networks. In Proceedings of the 2016 10th International Conference on Sensing Technology (ICST), Nanjing, China, 11–13 November 2016; pp. 1–6.

[110]. Tran, M.-Q.; Liu, M.-K.; Tran, Q.-V.; Nguyen, T.-K. Effective Fault Diagnosis Based on Wavelet and Convolutional Attention Neural Network for Induction Motors. IEEE Trans. Instrum. Meas. 2022, 71, 3501613.

[111]. Nishat Toma, R.; Kim, C.-H.; Kim, J.-M. Bearing Fault Classification Using Ensemble Empirical Mode Decomposition and Convolutional Neural Network. Electronics 2021, 10, 1248.

[112]. Chen, Z.; Li, W. Multisensor Feature Fusion for Bearing Fault Diagnosis Using Sparse Autoencoder and Deep Belief Network. IEEE Trans. Instrum. Meas. 2017, 66, 1693–1702.

[113]. Saucedo-Dorantes, J.J.; Delgado-Prieto, M.; Osornio-Rios, R.A.; Romero-Troncoso, R.d.J. Industrial Data-Driven Monitoring Based on Incremental Learning Applied to the Detection of Novel Faults. IEEE Trans. Ind. Inform. 2017, 66, 1693–1702.

[114]. Sun, J.; Yan, C.; Wen, J. Intelligent bearing fault diagnosis method combining compressed data acquisition and deep learning. IEEE Trans. Instrum. Meas. 2018, 67, 185–195.

[115]. Toma, R.N.; Piltan, F.; Kim, J.-M. A Deep Autoencoder-Based Convolution Neural Network Framework for Bearing Fault Classification in Induction Motors. Sensors 2021, 21, 8453.

[116]. S. Hamnane :"De l'analyse de Fourier traditionnelle aux ondelettes : une approche par le signal musical ", Université Paris VI – Pierre et Marie Curie, 2005.

[117]. L. Amandine, G. Maëlys :"Les ondelettes ", Université Claude Bernard de Lyon 1, 2014.

[118]. R. Frazier, S. Samsam, L. Braida and A. V. Oppenheim :"Enhancement of speech by adaptative filtering", Proceedings of the IEEE International Conférence on Acoustics, Speech, and Signal Processing, Philadelphia, Vol. 1, 1976.

Refrences


[119]. A. Lallouani :"Débruitage d'un signal de la parole corrompu par un bruit colorée en utilisant la transformée en ondelette et implantation sur un processeur de traitement numérique des signaux ", Université du Québec, 2004.

[120]. O. Soltani :"Restauration d'images satellites via la transformée en ondelette ", Thèse de Magister, Université de Batna, 2011.

[121]. D. Gabor :"Theory of communication ", J Inst Elect. Eng, 93 :429-457, London, 1946.

[122]. J. P. Ovarlez :"Distributions temps-fréquence ", 92322 Châtillon, France.

[123]. N. Hamdad :"Transformée de Huang-Hilbert : Application à la détection des défauts ", Mémoire de Magister, Université Mouloud Mammeri de Tizi-Ouzou, 2013.

[124]. J. C. Goswami : "Fundamental of wavelet : theory, algorithms and applications", Inc Canada, J. Wiley & Sons, 1999.

[125]. Y. Meyer :"Ondelettes, fonctions splines et analyses graduées, lectures données", Université de Torino, Italie, 1986.

[126]. S.G. Mallat :"A theory for multiresolution signal decomposition : the wavelet representation", IEEE Transaction on Pattern Analysis and Machines Intelligences, 11(7) : 674-693, July 1989.

[127]. M. O. Macaulay and M. Shafiee, "Machine learning techniques for robotic and autonomous inspection of mechanical systems and civil infrastructure," Auton. Intell. Syst., vol. 2, no. 1, Apr. 2022, doi: https://doi.org/10.1007/s43684-022-00025-3.

[128]. RISH, I. (2001). An empirical study of the naive bayes classifier

[129]. WATKINS, C. J. C. H. & DAYAN, P. (1992). Q-learning. Machine Learning, 8(3), 279-292. https://doi.org/10.1007/BF00992698

[130]. https://datascientest.com/algorithme-de-classification-definition-et-principaux-modeles

[131]. O. Maimon and L. Rokach, "Introduction to Supervised Methods," in Data Mining and Knowledge Discovery Handbook, O. Maimon and L. Rokach, Eds., New York: Springer-Verlag, 2005, pp. 149–164. doi: 10.1007/0-387-25465-X_8.

[132]. HEARST, M., DUMAIS, S., OSUNA, E., PLATT, J. & SCHOLKOPF, B. (1998). Support vector machines. IEEE Intelligent Systems and their Applications, 13(4), 18-28. https://doi.org/10.1109/5254.708428

[133]. S. Kang, "k-Nearest Neighbor Learning with Graph Neural Networks," Mathematics, vol. 9, no. 8, p. 830, Apr. 2021, doi: https://doi.org/10.3390/math9080830.

[134]. L. D. S. Pacifico, V. Macario, and J. F. L. Oliveira, "Plant Classification Using Artificial Neural Networks," in 2018 International Joint Conference on Neural Networks (IJCNN), Rio de Janeiro : IEEE, Jul. 2018, pp. 1–6. doi: 10.1109/IJCNN.2018.8489701.

[135]. V. Lemaire, C. Salperwyck, and A. Bondu, "A Survey on Supervised Classification on Data Streams," in Business Intelligence, vol. 205, E. Zimányi and R.-D. Kutsche, Eds., in Lecture Notes in Business Information Processing, vol. 205., Cham : Springer International Publishing, 2015, pp. 88–125. doi: 10.1007/978-3-319-17551-5_4.

[136]. L. Kuncheva. Combining Pattern Classifiers : Methods and Algorithms. Wiley, 2004.

[137]. T. Chen, C. Guestrin. XGBoost : A scalable tree boosting system. Proceedings of the ACM International Conference on Knowledge Discovery and Data Mining (SIGKDD), 2016.

Refrences


[138]. ROSENBLATT, F. (1958). The Perceptron : A Probabilistic Model for Information Storage and Organization in The Brain. Psychological Review, 65-386.

[139]. Hopfield, John J. "Artificial neural networks." IEEE Circuits and Devices Magazine 4, no. 5 (1988) : 3-10.

[140]. Janiesch, Christian, Patrick Zschech, and Kai Heinrich. "Machine learning and deep learning." Electronic Markets 31, no. 3 (2021) : 685-695.

[141]. Y. LeCun, B. Boser, J. S. Denker, D. Henderson, R. E. Howard, W. Hubbard, and L. D. Jackel. Backpropagation applied to handwritten zip code recognition. Neural Computation, 1(4) :541551, Dec 1989.

[142]. F. Scarselli, M. Gori, Ah Chung Tsoi, M. Hagenbuchner, and G. Monfardini. The graph neural network model. IEEE Transactions on Neural Networks, 20(1) :6180, January 2009.

[143]. L. Heming, S. Liling, X. Boqiang. “Research on transient behaviors and detection methods of stator winding inter-turn short circuit fault in induction motors based on multi-loop mathematical model”, In: Proceeding of IEEE ICEMS, 27-29 September 2005; 3: pp: 1951 – 1955.

[144]. X. Luo, Y. Liao, H.A. Toliyat, A. El-Antably, and T.A. Lipo, “Multiple coupled circuit modelling of induction machines,” IEEE Trans. Indust. Appl., vol. 31, March/April 1995, pp: 311-318.

[145]. A. Ghoggal, “ Diagnostic de la machine asynchrone triphasée- Modèle dédié à la détection des défauts ”, Mémoire de Magistère de l’université de Batna, 05/2005.

[146]. D. Gaïtan, “Modélisation et diagnostic de la machine asynchrone en presence de défaillance,” Phd dissertation, Université Henri poincaré, Nancy-I, France, Oct. 2004.

[147]. L. Heming, S. Liling, X. Boqiang. “Research on transient behaviors and detection methods of stator winding inter-turn short circuit fault in induction motors based on multi-loop mathematical model”, In: Proceeding of IEEE ICEMS, 27-29 September 2005; 3: pp: 1951 – 1955.

[148]. X. Luo, Y. Liao, H.A. Toliyat, A. El-Antably, and T.A. Lipo, “Multiple coupled circuit modelling of induction machines,” IEEE Trans. Indust. Appl., vol. 31, March/April 1995, pp: 311-318.

[149]. H. Razik, G. Didier, "Notes de cours sur le diagnostic de la machine asynchrone," Notes de cours, I.U.F.M. de Lorraine, Maxeville, 7 Janvier 2003.

[150]. J. Faiz, I.T. Ardekanei, “Extension of winding function theory for nonuniform air-gap in electric machinery”, IEEE Trans. Magn. Vol. 38, no.6, 2002, pp: 3654-3657.

[151]. A. Toliyat, T. A. Lipo, " Transient Analysis of Cage Induction Machines Under Stator, rotor bars and end – ring Faults", IEEE Transactions on Energy Conversion, Vol 10, N°6, June 1995, pp. 241-247.

[152]. Belhamdi. S « Prise en compte d’un défaut rotorique dans la commande d’un moteur asynchrone », thèse de magister, Université de Biskra ,2005.

[153]. Abed. A « Contribution à l’étude et au diagnostic de la machine asynchrone », thèse de doctorat, Université Henri Poincaré Nancy, 2002.

Refrences

[154]. Baghli. L, Contribution à la commande de la machine asynchrone utilisations de la logique floue, des réseaux de neurones et des algorithmes génétiques»,thèse de doctorat Université Henri Poincaré Nancy, 99.

[155]. E.Ritchie and X.Deng « Dynamic model of three-phase squirrel cage induction motor with rotor faults , Conference Proceedings of the International Conference on Electrical Machine 8,ICEM,pp694498.1994.

# Appendix

The simulation database was generated using the multi-winding model on Matlab 2017 platform.

AI models were used on both Matlab 2017 and Python (Pycharm platform)

The parameters of the used model for 3 phase induction machine are as follows:

| **Parameter** | **Identification** |
|---|---|
| Machine type | 3-phase squirrel cage with inclined bar |
| Number of bars | 40 |
| Frequency | 50 Hz |
| Rated Voltage | 415 V |
| Rated Power | 11 KW |
| Rated torque | 40 N.m |
| Winding number | 28 |
| Air gap radius | 82 mm |
| Air gap thickness | 0.8 mm |
| Rotor length | 0.11 m |
| Rotor leakage inductance | 6.1 mH |
| Rotoric bar resistance | $31\times10^{-6}$ Ω |
| Rotoric bar leakage inductance | $0.095\times10^{-6}$ H |
| Stator phase resistance | 1.75 Ω |
| Short circuit ring resistance | $2.2\times10^{-6}$ Ω |
| Short circuit ring segment leakage inductance | $0.018\times10^{-6}$ H |
| Permeability | $12.56\times10^{-7}$ H/m |

Appendix